AGARD-AR-344

AGARD

ADVISORY GROUP FOR AEROSPACE RESEARCH & DEVELOPMENT
7 RUE ANCELLE, 92200 NEUILLY-SUR-SEINE, FRANCE

AGARD ADVISORY REPORT 344

Ice Accretion Simulation

(la Simulation de l'accumulation de glace)

Report of the Fluid Dynamics Panel Working Group 20.

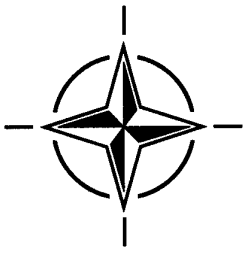

NORTH ATLANTIC TREATY ORGANIZATION

Published December 1997

Distribution and Availability on Back Cover

AGARD

ADVISORY GROUP FOR AEROSPACE RESEARCH & DEVELOPMENT

7 RUE ANCELLE, 92200 NEUILLY-SUR-SEINE, FRANCE

AGARD ADVISORY REPORT 344

Ice Accretion Simulation

(la Simulation de l'accumulation de glace)

Report of the Fluid Dynamics Panel Working Group 20.

North Atlantic Treaty Organization
Organisation du Traité de l'Atlantique Nord

The Mission of AGARD

According to its Charter, the mission of AGARD is to bring together the leading personalities of the NATO nations in the fields of science and technology relating to aerospace for the following purposes:

- Recommending effective ways for the member nations to use their research and development capabilities for the common benefit of the NATO community;
- Providing scientific and technical advice and assistance to the Military Committee in the field of aerospace research and development (with particular regard to its military application);
- Continuously stimulating advances in the aerospace sciences relevant to strengthening the common defence posture;
- Improving the co-operation among member nations in aerospace research and development;
- Exchange of scientific and technical information;
- Providing assistance to member nations for the purpose of increasing their scientific and technical potential;
- Rendering scientific and technical assistance, as requested, to other NATO bodies and to member nations in connection with research and development problems in the aerospace field.

The highest authority within AGARD is the National Delegates Board consisting of officially appointed senior representatives from each member nation. The mission of AGARD is carried out through the Panels which are composed of experts appointed by the National Delegates, the Consultant and Exchange Programme and the Aerospace Applications Studies Programme. The results of AGARD work are reported to the member nations and the NATO Authorities through the AGARD series of publications of which this is one.

Participation in AGARD activities is by invitation only and is normally limited to citizens of the NATO nations.

Printed on recycled paper

Published December 1997

ISBN 92-836-1067-9

Printed by Canada Communication Group Inc.
(A St. Joseph Corporation Company)
45 Sacré-Cœur Blvd., Hull (Québec), Canada K1A 0S7

Ice Accretion Simulation

(AGARD AR-344)

Executive Summary

Ice Accretion Simulation is an important issue for flight safety. Every year several incidents happen which can be associated with severe icing problems. Although the bulk of them may be due to human mistakes during flight in icing conditions, some cases remain which are consequences of icing conditions never observed before or of failures not foreseen. Therefore, icing has always attracted great interest from aircraft manufacturers, authorities responsible for certification, and many researchers.

The overall goal of the work presented in this report is to improve reliability, to reduce efforts and costs in civil and military aircraft certification/qualification procedures, and to improve civil and military aircraft flight safety. This report covers the effects of ice accretion on wings, tail surfaces, engine inlets, and rotary wings. Experimentally, besides the capability of icing wind tunnel facilities, the problems of spray tanker aircraft experiments are considered, the related similarity laws are examined, and the techniques for measuring droplet size and distribution are reviewed. The basic factors influencing computational predictions are discussed in detail, especially factors such as surface roughness and surface heat transfer. In addition to the 2D prediction methodology, the status of extensions to 3D is presented. An essential aim of a planned follow-on activity should be to establish some well-documented reference cases by suitable in-flight experiments, and to calibrate prediction tools and experimental facilities and techniques for those reference cases.

La simulation de l'accumulation de glace

(AGARD AR-344)

Synthèse

La simulation de l'accumulation de glace est une question importante pour la sécurité des vols. Des incidents liés à des problèmes majeurs de givrage se produisent chaque année. Bien que la plupart de ces incidents soient, certes, dûs à des erreurs de pilotage dans des conditions de givrage, il reste néanmoins certains cas qui ont pour origine soit des conditions de givrage inconnues jusqu'à présent, soit des défaillances imprévues. Par conséquent, le givrage a toujours suscité beaucoup d'intérêt de la part des avionneurs, des services officiels et des chercheurs.

Le but de l'ouvrage présenté dans ce rapport est de permettre une meilleure fiabilité, de réduire les efforts et les coûts des procédures d'homologation/qualification des avions civils et militaires et d'améliorer leur sécurité de vol. Ce rapport couvre les effets de l'accumulation de glace sur les voilures, les gouvernes, les entrées d'air moteur et les voilures tournantes. Du point de vue expérimentale, en plus des possibilités offertes par les souffleries de givrage, les problèmes posés par les expériences réalisées sur les avions-citernes à épandage d'eau sont étudiés, les lois de similitude sont examinées et les techniques employées pour le calibrage et la répartition des gouttelettes sont résumées. Les facteurs de base ayant une influence sur les prévisions informatiques sont discutés dans le détail, et en particulier la rugosité de surface et l'échange thermique en surface. En plus de la méthodologie de la prévision à deux dimensions, les possibilités d'extension vers la prévision en trois dimensions sont présentées.

L'un des objectifs principaux du projet de suivi doit être l'établissement d'un certain nombre de cas de référence bien documentés, par le biais d'expériences conduites en vol, ainsi que le calibrage des outils de prévision, des installations expérimentales et des techniques demandés pour ce projet.

Contents

Preface

Ice Accretion Simulation is an important issue for flight safety. Every year several incidents happen which can be associated with severe icing problems. Although the bulk of them may be due to human mistakes during flight in icing conditions, some cases remain which are consequences of icing conditions never observed before or of failures not foreseen. Therefore icing has always attracted great interest from aircraft manufacturers, authorities responsible for certification and many researchers.

Since aircraft icing is important for both civil and military aircraft, it has been the subject of many AGARD publications. In particular the Fluid Dynamics Panel (FDP) is engaged in the fluid mechanics aspects of ice accretion that include the fluid flow and thermal mechanisms of accreting ice as well as the flow around aircraft components contaminated by ice. Both perspectives are addressed in this report and the primary aim of the work is to present the guidance that fluid mechanics can contribute towards attainment of safe flight under icing conditions and for corresponding certification and qualification efforts.

In the FDP, icing problems were last addressed in a Specialists Meeting on 'Effects of Adverse Weather on Aerodynamics' in Toulouse, 1991. Following that meeting a Working Group on 'Ice Accretion Simulation' was proposed in the same year and was approved in 1993 as FDP Working Group 20. It started working in Spring 1994. The scope of the work has mainly been restricted to the above mentioned fluid dynamic aspects of the topic and therefore the objectives are:

(i) Critical evaluation of aircraft performance degradation and of certification demands, including design recommendations

(ii) Enhancements and verification of experimental techniques, ice test facilities and similarity laws

(iii) Review, validations, and progress of ice accretion prediction codes

(iv) New look at the data base of critical atmospheric conditions

The report covers the effects of ice accretion on wings, tail surfaces, engine inlets, and rotary wings. Experimentally, besides the capability of icing wind tunnel facilities, the problems of spray tanker aircraft experiments are considered, the related similarity laws are examined and the techniques for measuring droplet size and distribution are reviewed. The basic factors influencing computational predictions are discussed in detail, especially those not completely known up to now as for example surface roughness and surface head transfer. In addition to the 2D prediction methodology, the status of extensions to 3D is presented. An essential aim of a planned follow-on activity should be to establish some well-documented reference cases by suitable in-flight experiments and to calibrate prediction tools and also experimental facilities and techniques for those reference cases. The overall goal is to improve reliability and to reduce efforts and costs in the aircraft certification/qualification procedure.

The members of FDP Working Group 20 who contributed to the present report were:

Prof. Dr. Nafez ALEMDAROGLU, Middle East Technical University, Ankara, Turkey
Dr. Alejandro FEO, INTA, Madrid, Spain
Roger W. GENT, DRA, Farnborough, UK
Prof. Dr. Carmine GOLIA, CIRA, Capua, Italy (FDP-member)
Dr. Didier P. GUFFOND, ONERA, Châtillon, France
Dr. David W. HAMMOND, BAe Sowerby Research Centre, Filton, UK
Jack van HENGST, Fokker Aircraft B.V., Amsterdam, Netherlands
Dr. Richard JECK, FAA Technical Center, Atlantic City NJ, USA
Prof. Dr. Richard J. KIND, Carleton University, Ottawa, Canada (FDP-member)
Staffan MEIJER, FFA, Bromma, Sweden (invited by Norway)

Dr. Mark G. POTAPCZUK, NASA Lewis Research Center, Cleveland OH, USA
Rainer SEUBERT, DLR, Braunschweig, Germany
Anil SHAH, Boeing Commercial Airplane Group, Seattle WA, USA
Prof. Dr. Bernhard WAGNER, Dornier Luftfahrt GmbH, Munich, Germany (Chairman, FDP-member)

The above members of FDP WG20 thank for co-operation their following colleagues, who were prevented, for various reasons, from contributing after they had been nominated as WG20 members:

Prof. Dr. Mario CARBONARO, VKI, Brussels, Belgium
Manrico de LEO, ALENIA, Naples, Italy
Prof. Dr. Helge NORSTRUD, Norwegian University of Science and Technology (NTNU), Trondheim, Norway (FDP-member)

Furthermore, the Group members want to express their warmest thanks to JAA for support and especially to the JAA representative

Mme. BOUILLOUD, Services Techniques des Programmes Aéronautiques (STPA/NIT), Paris, France

who attended the third meeting contributing to a very constructive discussion on the certification aspects, and critically reviewed our work. Also the FDP WG20 is indebted to

Prof. Dr. K. BROICHHAUSEN, Dasa-MTU, Munich, Germany (AGARD PEP-member)

who had the kindness to re-examine our work from the viewpoint of an engine expert on behalf of the AGARD Propulsion and Energetics Panel (PEP).

The AGARD Working Group 20 of the Fluid Dynamics Panel needed five meetings at approximately half-yearly intervals scheduled as in the following table in timely relation to meetings of the Fluid Dynamics Panel:

Time Schedule of AGARD FDP Working Group 20 on "Ice Accretion Simulation"

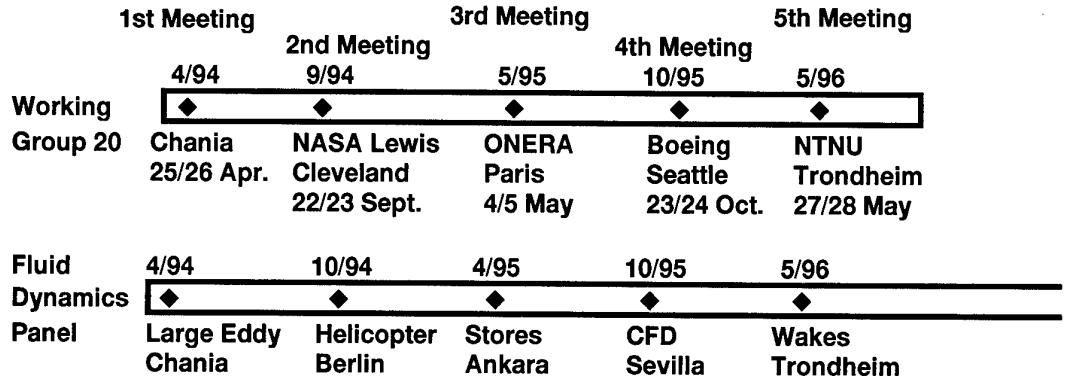

The material of the present report has been presented and pre-printed in the course notes for the AGARD-VKI Special Course on "Effect of Icing, De-Icing, and Heavy Rain on Aircraft Performance", February 24-26 1997, held at the von Kármán Institute, Brussels, Belgium. For this AGARD-FDP-VKI course supplements to the WG20 topics had been agreed which were to include the effects of de-icing fluids and of heavy rain on aircraft performance. Both topics have also been prepared and presented by two members of WG20, Prof. Carbonaro and Dr. Feo, respectively. The corresponding Papers have been included as appendices to the present report.

July 1997

Recent Publications of the Fluid Dynamics Panel

AGARDOGRAPHS (AG)

Turbulent Boundary Layers in Subsonic and Supersonic Flow
AGARD AG-335 July 1996

Computational Aerodynamics Based on the Euler Equations
AGARD AG-325, September 1994

Scale Effects on Aircraft and Weapon Aerodynamics
AGARD AG-323 (E), July 1994

Design and Testing of High-Performance Parachutes
AGARD AG-319, November 1991

Experimental Techniques in the Field of Low Density Aerodynamics
AGARD AG-318 (E), April 1991

Techniques Expérimentales Liées à l'Aérodynamique à Basse Densité
AGARD AG-318 (FR), April 1990

A Survey of Measurements and Measuring Techniques in Rapidly Distorted Compressible Turbulent Boundary Layers
AGARD AG-315, May 1989

REPORTS (R)

Turbulence in Compressible Flows
AGARD R-819, Special Course Notes, June 1997

Advances in Cryogenic Wind Tunnel Technology
AGARD R-812, Special Course Notes, January 1997

Aerothermodynamics and Propulsion Integration for Hypersonic Vehicles
AGARD R-813, Special Course Notes, October 1996

Parallel Computing in CFD
AGARD R-807, Special Course Notes, October 1995

Optimum Design Methods for Aerodynamics
AGARD R-803, Special Course Notes, November 1994

Missile Aerodynamics
AGARD R-804, Special Course Notes, May 1994

Progress in Transition Modelling
AGARD R-793, Special Course Notes, April 1994

Shock-Wave/Boundary-Layer Interactions in Supersonic and Hypersonic Flows
AGARD R-792, Special Course Notes, August 1993

Unstructured Grid Methods for Advection Dominated Flows
AGARD R-787, Special Course Notes, May 1992

Skin Friction Drag Reduction
AGARD R-786, Special Course Notes, March 1992

Engineering Methods in Aerodynamic Analysis and Design of Aircraft
AGARD R-783, Special Course Notes, January 1992

ADVISORY REPORTS (AR)

Sonic Nozzles for Mass Flow Measurement and Reference Nozzles for Thrust Verification
AGARD AR-321, Report of WG-19, June 1997

Cooperative Programme on Dynamic Wind Tunnel Experiments for Manoeuvring Aircraft
AGARD AR-305, Report of WG-16, October 1996

Hypersonic Experimental and Computational Capability, Improvement and Validation
AGARD AR-319, Vol. I, Report of WG-18, May 1996

Aerodynamics of 3-D Aircraft Afterbodies
AGARD AR-318, Report of WG-17, September 1995

A Selection of Experimental Test Cases for the Validation of CFD Codes
AGARD AR-303, Vols. I and II, Report of WG-14, August 1994

Quality Assessment for Wind Tunnel Testing
AGARD AR-304, Report of WG-15, July 1994

Air Intakes of High Speed Vehicles
AGARD AR-270, Report of WG-13, September 1991

Appraisal of the Suitability of Turbulence Models in Flow Calculations
AGARD AR-291, Technical Status Review, July 1991

Rotary-Balance Testing for Aircraft Dynamics
AGARD AR-265, Report of WG11, December 1990

Calculation of 3D Separated Turbulent Flows in Boundary Layer Limit
AGARD AR-255, Report of WG10, May 1990

CONFERENCE PROCEEDINGS (CP)

Aerodynamics of Wind Tunnel Circuits and Their Components
AGARD CP-585, June 1997

The Characterization & Modification of Wakes from Lifting Vehicles in Fluids
AGARD CP-584, November 1996

Progress and Challenges in CFD Methods and Algorithms
AGARD CP-578, April 1996

Aerodynamics of Store Integration and Separation
AGARD CP-570, February 1996

Aerodynamics and Aeroacoustics of Rotorcraft
AGARD CP-552, August 1995

Application of Direct and Large Eddy Simulation to Transition and Turbulence
AGARD CP-551, December 1994

Wall Interference, Support Interference, and Flow Field Measurements
AGARD CP-535, July 1994

Computational and Experimental Assessment of Jets in Cross Flow
AGARD CP-534, November 1993

High-Lift System Aerodynamics
AGARD CP-515, September 1993

Theoretical and Experimental Methods in Hypersonic Flows
AGARD CP-514, April 1993

Aerodynamic Engine/Airframe Integration for High Performance Aircraft and Missiles
AGARD CP-498, September 1992

Effects of Adverse Weather on Aerodynamics
AGARD CP-496, December 1991

Manoeuvring Aerodynamics
AGARD CP-497, November 1991

Vortex Flow Aerodynamics
AGARD CP-494, July 1991

Missile Aerodynamics
AGARD CP-493, October 1990

Aerodynamics of Combat Aircraft Controls and of Ground Effects
AGARD CP-465, April 1990

Computational Methods for Aerodynamic Design (Inverse) and Optimization
AGARD CP-463, March 1990

Applications of Mesh Generation to Complex 3-D Configurations
AGARD CP-464, March 1990

Fluid Dynamics of Three-Dimensional Turbulent Shear Flows and Transition
AGARD CP-438, April 1989

Members of Fluid Dynamics Panel Working Group 20 on "Ice Accretion Simulation"

BELGIUM -

Prof. Mario CARBONARO
von Kármán Institute for Fluid Dynamics
Chaussée de Waterloo, 72
1640 Rhode-Saint-Genèse

CANADA -

Prof. Richard J. KIND
Dept of Mechanical & Aerospace Engineering
Carleton University
1125 Colonel By Drive
Ottawa, Ontario K1S 5B6

FRANCE -

Mr. Didier GUFFOND
ONERA -Physics Dept OP/L3c
8, rue des Vertugadins
92190 MEUDON

GERMANY -

Dr. B. WAGNER **(Chairman)**
Dornier Luftfahrt GmbH (DASA-LR)
Aerodynamics, TE 42
P.O. Box 1103, Building 318
82230 WESSLING

Mr. Rainer SEUBERT
DLR SM-EA
Flughafen
38022 BRAUNSCHWEIG

ITALY -

Prof. Carmine GOLIA
CIRA
Via Maiorise
81043 CAPUA (CE)

Mr. Manrico de LEO
ALENIA
Viale dell Aeronautica
80038 POMIGLIANO D'ARCO (NAPOLI)

NETHERLANDS -

Mr. Jack van HENGST
Fokker Services B.V.
Engineering Technical support
M/S S055-11
P.O. Box 75047
1117 ZN SCHIPHOL

NORWAY -

Prof. Dr. H. NORSTRUD
Dept. of Mechanics, Thermo-and Fluid
Dynamics - Norwegian Inst. of Technology
The University of Trondheim
7034 Trondheim-NTH

SPAIN -

Dr. Alejandro FEO
INTA-Experimental Aerodynamics Lab.
Ctra de Ajalvir, Km 4.5
28850 Torrejon de Ardoz MADRID

SWEDEN -

Dr. Staffan MEIJER
FFA / P.O. Box 11021
16111 BROMMA

TURKEY -

Prof. Dr. Nafiz ALEMDAROGLU
Aeronautical Engineering Dept.
Middle East Technical University
Inonu Bulvari PK:06531
06531 ANKARA

UNITED KINGDOM -

Mr. Roger W. GENT
Defence Research Agency Farnborough
Structures Dept, X41F Bldg
HAMPSHIRE GU14 6TD

Mr. David W. HAMMOND
British Aerospace (Operations) Ltd
Sowerby Research Centre
FPC 267, P.O. Box 5
FILTON, BRISTOL BS12 7QW

UNITED STATES -

Mr. Richard JECK
Flight Safety Research Branch
ACD-230
FAA Technical Center
ATLANTIC CITY, NJ 08405

Dr. Mark G. POTAPCZUK
NASA Lewis Research Center
MS 77-10
21000 Brookpark Road
CLEVELAND, OHIO 44135

Mr. Anil SHAH
Boeing Commercial Airplane Group
P.O. Box 3707
Mail Stop 6M-KE
SEATTLE, WA 98124-2207

1. INTRODUCTION

1.1 BASIC ASPECTS OF SAFETY, CERTIFICATION/QUALIFICATION, ICE PROTECTION AND DESIGN

Ice accretion is a consequence of certain meteorological conditions - usually connected with the occurrence of supercooled droplets in clouds - and can cause very critical situations with respect to the flight safety of an aircraft. Once ice has accumulated on the aircraft surface, it essentially affects the aerodynamic performance of all types of lifting components. These are the wings, the horizontal tail, the vertical tail, and any rotary wings including propellers. Obviously, not only the aircraft flight performance can become drastically reduced but also the handling qualities. The stability and control properties, in longitudinal as well as in lateral movements, can diminish remarkably. Hence the flight can become quite dangerous if the mission cannot be completed (e.g. the flight range may be cut, or ceiling heights needed for crossing mountains may not be reached), or if safe control is lost (e.g. tail stall effects may occur earlier). Also, engines can become adversely affected, eventually even leading to flame-outs. This could result from ice accretion directly on the air inlets, which may cause inflow problems, or from ice shedding into the inlet. Ice shed from other aircraft surfaces may also fall into the inlet and damage fan or compressor blades.

The hazards resulting from ice accretion are underlined by cases reported by the CAA (Civil Aviation Authority, UK) in document CAP 479. Cole and Sand (1991) provided some icing accident statistics established at NCAR (National Center of Atmospheric Research, Boulder, Col.). They showed that more than one half of all related accidents are due to carburettor icing of general aviation aircraft, mostly not fatal. More than one quarter are due to take-off icing - which should not happen at all because of the 'clean wing concept' (see below). They demonstrated also that roughly one third of the accidents happen in each of the three basic flight phases: take-off, in-flight, and landing. The group of - mostly fatal - accidents in consequence of in-flight airframe icing are presented in Fig. 1.1-1 showing that approximately 30 related accidents happen per year (an accident is defined as an event which implies loss of full control of the aircraft and may involve injuries or fatalities). Of course special circumstances, e.g. the presence of mountains or great lakes, can significantly increase the danger of icing and therefore also the frequency of accidents. The National Transportation Safety Board (NTSB, Washington, D.C.) published statistical data of accidents based on the accident records representing the years 1976 through 1979. More than 50% of all icing accidents involve fatalities. The NTSB statistics reveal that the fatal commercial aircraft icing accidents amount to 5.6% of all icing accidents and to 40% of all commercial aircraft icing accidents.

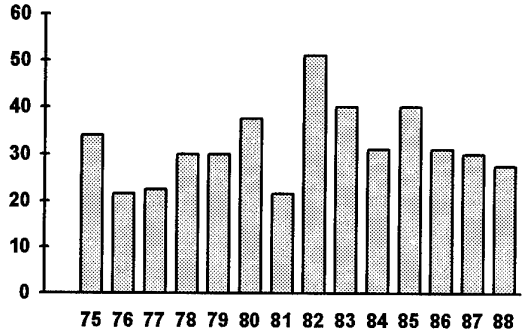

Fig. 1.1-1: Number of In-flight Airframe Icing Accidents per Year (1975-1988)

Of course, in present days all aircraft used by commercial airlines have to be equipped with an effective de-icing (in-flight removal of ice) or anti-icing (prevention of ice accretion) system in order to maintain acceptable aerodynamic performance and safety of the aircraft in flight under icing conditions. A lot of efforts are presently spent to improve ice protection systems in the directions of enhanced safety or of avoiding performance disadvantages of classical de-icing devices. Inflatable rubber boots, for example, are not compatible with maintaining laminar flow on the surface. The ice protection problem does not only concern the wings but also the tail surfaces, engine inlets, ducts, and pitot-probes. For example, ice contaminated tailplane stall (ICTS) is one of the most dangerous icing effects and must be considered thoroughly with respect to tail ice protection and ice plugged pitot-probes (which can give false airspeed readings). Possible engine flame-outs due to icing must be prevented by a suitable ice protection.

Because of the danger of flight in icing conditions the civil certification authorities FAA (Federal Aviation Administration in the United States) and JAA (Joint Airworthiness Authority in Europe) have established some important rules for so-called 'ice-certification'. These are laid down for transport aircraft in JAR/FAR § 25.1419 (Joint Airworthiness Requirements/Federal Aviation Regulations, part 25). Smaller general aviation aircraft have to follow the rules of JAR/FAR part 23 that are similar to part 25 with respect to ice certification. For helicopters the JAR/FAR parts 27 (small rotorcraft) and 29 (transport rotorcraft) are applicable. The military authorities, which of course possess national sovereignty, also have established rules for the ice qualification of their aircraft which usually follow the civilian regulations in many aspects. The basic demand of all these regulations is that safe flight must be maintained in all permitted icing conditions.

More serious icing conditions must be avoided or immediately left; examples are:

- Take-off is not permitted if any ice contamination on the aircraft's surfaces exists.
- Freezing rain must be avoided (conditions which exhibit much larger freezing water droplets than other - more usual - icing environments and contaminate all aircraft surfaces completely).

Furthermore the Federal Aviation Regulations for equipment in icing conditions, § 121.341, lay down that unless an aircraft is certified under transport category airworthiness requirements relating to ice protection, nobody may operate an aircraft in icing conditions unless it is equipped with means for prevention or removal of ice on windshields, wings, empennage, propellers and other parts where ice formation will adversely affect the safety of the aircraft.

While in these times of extensive air traffic ground icing is routinely removed and subsequently prevented by application of de-icing fluids, there now exists also a selection of ice protection systems for in-flight icing. In flight, ice builds up on all forward facing surfaces. Aircraft components that therefore may need some consideration and possibly ice protection are:

— leading edges, lifting and control surfaces
— rotor blades
— propellers and spinners
— engine inlets
— windshields and radomes
— flight sensors
— antennas and drain masts

The classical ice protection systems are as follows:

- On medium sized and large jet aircraft, typically heating is applied in the region of the leading edge using bleed air from the engine compressors, either to evaporate all impinging water droplets (anti-icing) or to melt accreted ice at the surface and thus to cause it to move downstream. In the latter case there is a potential that the ice-water mixture can re-freeze forming further downstream so-called run-back ice. For modern high bypass turbofans the amount of available bleed air is rather limited and therefore the manufacturers try to reduce the extent of the protected regions as far as possible and research on alternate systems is to be encouraged.
- For turboprop aircraft, the most usual de-icing devices are pneumatic boots. These are inflated cyclically and require a very small amount of energy. These systems fracture, debond and expel the ice accretion from the surface. For effective ice removal the ice shapes must have a minimum thickness of about one quarter to one half of an inch and this thickness must be tolerable for safe flight of the aircraft. In extreme icing conditions some residual ice may remain behind the boots and form a nucleus for the growth of possibly dangerous ice ridges.
- On some aircraft anti-icing is done by forcing a freezing point depressant fluid (normally mixture of glycol and water) out of a porous panel at the leading edge, thus either preventing ice accretion or releasing ice already accreted and moving it downstream on a liquid film on the airfoil surface. Such systems can in principal be extended to become, in addition, anti-contamination systems for wings designed to maintain a long laminar flow range.
- Engine inlets for the jet aircraft are usually anti-iced to evaporate all the water impinged on the inlet lip. This prevents any runback ice which can potentially damage the fan blades.
- Helicopter rotors and propellers are mainly protected by electric heating of the leading edge region of the blades. Also, electric heating is sometimes applied for parts of fixed-wing aircraft, usually for smaller, critical components.

An overview of ice protection systems including those principles presently under development are listed in tables 1.1-1 and 1.1-2. More details such as system selection criteria, design guidance and system concerns of ice protection methods listed in these tables can be found in the FAA Aircraft Icing Handbook by Heinrich et al. (1991). An interesting summary of some of early work done in the past on ice prevention or removal can be found in an article of Geer (1939).

Generally, certification and qualification procedures for the ice protection system and for the aircraft itself in icing conditions are very time-consuming and costly. Besides the normal flight situations when the ice protection system is in action, a failure of the ice protection system under special circumstances must also be taken into account. Safe flight must be demonstrated during certification even for extreme flight situations that may not be encountered intentionally (e.g. maximum rudder deflection with ice accretion, although this is normally used only during one engine failure).

The steadily increasing demands for all-weather-flight capabilities and a significant number of severe accidents have recently stressed the interest in aircraft icing again. Considerable research has been performed during the last decade and a large number of publications produced. The meteorological prerequisites, details of ice accretion, and the effects of performance degradation have been investigated in detail. Also, AGARD has arranged quite a number of meetings in different panels comprising many important presentations on this subject. The Fluid Dynamics Panel treated the subject 'Effects of Adverse Weather on Aerodynamics' with some emphasis on icing at last in a Specialists' Meeting (AGARD, 1991a). The former Flight Mechanics Panel had a Symposium on 'Flight in Adverse Environmental Conditions' touching of course

also on ice accretion (AGARD, 1989). The Propulsion and Energetics Panel had a Symposium on 'Low Temperature Environment Operations of Turboengines (Design and User's Problems)', (AGARD, 1991b). Furthermore the AGARD Report 166 on 'Rotorcraft Icing - Status and Review' should be mentioned (AGARD, 1986). Most recently Reinmann (1994) published a survey on the icing subject within an AGARD Lecture Series. Although AGARD is principally directed to military aspects of aeronautics, the corresponding papers were often concerned with civil aircraft applications or they were of dual, i.e. civil and military, use. On the other hand, qualification of military aircraft and certification of civil airplanes are similar in many senses, and are both aimed at flight safety. Therefore the present report is also directed to both, to military qualification as well as to civil certification aspects.

Civil transport aircraft are either fast and jet powered or slower, usually smaller and turbine/propeller (turboprop) powered. The turboprops have almost straight wings and fly more often at lower altitudes, especially during hold. Both factors increase the danger of icing and of corresponding performance degradation compared with swept wing jets cruising at higher altitudes. Both types of aircraft are also in military use and their qualification usually adapts the same rules as prescribed for civil certification. Fighter aircraft fly only for short times in icing conditions and as a consequence of their high speeds with corresponding surface heating, larger wing sweep, and sharp leading edges, the danger of ice accretion and the respective attention to it concentrates mainly on the engine inlet. Helicopters are equally in use for military and civil purposes but the development of full ice protection systems still poses a difficult problem to manufacturers and to date only the AS332 Super Puma has achieved FAA icing certification. While full UK military clearance is a contractual requirement for the new Merlin helicopter under development for the British Royal Navy, in practice, most military and some civil helicopters have more frequently been cleared to a limited envelope for flight in icing. These 'limited clearances' have been based on requirements specified by the appropriate national certification authority (see AGARD, 1986) and are not therefore to the same standard of icing envelope.

This report is mainly an ***aerodynamic*** compendium of icing effects, due to its origin from the Fluid Dynamics Panel, but it covers some other fields wherever needed. From the aerodynamic point of view the problems of the certification or qualification procedure are characterised by the performance degradation of various components of an aircraft due to ice accretion. It is not however easy to identify and locate the most critical cloud conditions, as prescribed by qualification/ certification authorities, in the natural environment. Therefore, qualification and certification are extremely time consuming and very costly. Fortunately, it has been shown that in almost all interesting situations it is possible to replace the natural ice accretion shapes by artificially modelled ones. Recent developments in computational methods for predicting ice accumulations, and classical means for reproducing ice shapes observed in ice tunnel experiments, allow fabricated ice shapes to be used in dry air for most of the necessary measurements to determine performance degradation in icing. These 'dry air' experiments can be done either in windtunnels or in flight tests. Only a few flight tests must then be performed after sufficient ice contamination has been achieved flying in natural icing conditions. It must however be shown by these tests that the selected artificial ice shapes represent an envelope of worst cases which will not be exceeded by natural ice cases, with respect to performance degradation.

These considerations lead to the final question: "What can an aircraft engineer do with respect to aerodynamic design in order to avoid safety problems in icing conditions, and how can problems with respect to ice accretion be avoided as far as possible during certification and qualification procedures?" Many aircraft companies have had similar experiences when certifying and qualifying new aircraft in recent times. Some of these observations are contained to some extent in the following report and may, hopefully, become a starting point for enhancing guidelines for aircraft design in this respect.

1.2 ICE ACCRETION PHYSICS

It is worth noting that whilst ice can have many different crystallographic forms, ice formed in the conditions present on aircraft in clouds is crystalline and has hexagonal crystal symmetry. This is often referred to as Ice 1h. Whilst the basic crystal structure is fixed, the variety of different ways of arranging ice crystallites, air and water gives us the familiar diversity of ices. Good general texts on ice include Hobbs (1974), now out of print, and Pruppacher and Klett (1978).

Before progressing further defining some ***types of water particles*** is helpful:

Droplet	liquid- any size, often used for particles less than 0.1 mm
Drizzle	liquid- diameter in range of approximately 0.1 to 1.0 mm (Sometimes taken to refer only to droplets formed by coalescence.)
Rain	liquid- drop diameter of approximately 1.0 mm or greater
Ice Crystal	solid- any size, often taken to mean less than 0.1 mm in clouds
Snow Crystal	solid- ice crystal with dendritic growths (forms from the vapour)
Snow Flake	solid- aggregation of snow crystals (by clumping)
Graupel	solid- forms by riming of an *ice crystal*. Contains significant volume of air. (Sometimes referred to as sleet.)

Hail	solid- formed by riming of ice crystals. Contains little air.
Sleet	solid + liquid, e.g. melting ice particles or mixed phase precipitation (The word is also used in place of Graupel.)

Other ***widely used words***:

Riming	Growth of ice by collection of water droplets
Clumping	Growth of ice by collection of ice particles.
Coalescence	Growth of liquid by collection of liquid

Liquid water may easily be cooled to well below freezing point in the absence of a freezing nucleus. The energy barrier nuclei which are sufficient to nucleate the growth of a water droplet (condensation nuclei) often will not promote the freezing of that droplet (act as freezing nuclei) until it is supercooled by tens of degrees centigrade (Vali and Stansbury 1966). In this way clouds may contain liquid water contents of several grams per cubic meter of air in the form of supercooled droplets for prolonged periods. Soluble particles in the air can act as very effective condensation nuclei. Supercooled droplets will tend to freeze when they encounter ice particles or solid structures such as aircraft. This process (riming) is responsible for the rapid growth of ice formations which cause aerodynamic and control problems for aircraft and generate graupel and hail particles in the atmosphere.

Differences in the particulate contents of air in terrestrial and maritime weather systems can affect condensation and subsequent freezing processes. Insoluble aerosols form much better freezing nuclei than soluble ones. Therefore, it is sometimes relevant to consider different weather systems, which produce the similar temperature and liquid water content, as other factors such as altitude, uniformity of conditions and the presence of ice particles with water will influence the aircraft.

The distribution of water droplet sizes can be important as it influences the extent to which a given part of the aircraft collects ice. Droplets of drizzle size and greater tend to be little affected by the air flow for many aircraft components. Droplets of a few microns diameter, however, tend to follow the stream lines. The most frequent and extensive conditions in nature seldom have median volume droplet diameters of more than approximately 20 microns. This droplet size has become a widely used standard for experimental, analytical and numerical work on aircraft components. However, some critical phenomena (e.g. possible accretion of ridges behind the boots of turboprop aircraft) depend strongly on the droplet size and therefore other droplet diameters or the complete spectra of droplet sizes must be considered, too.

Most usually ice formations on unheated aircraft structures, in flight, form by riming (mentioned above). Such ice is called 'Impact Ice'. Two words are often used to describe the character of impact ice, namely 'rime' and 'glaze'. A brief description of the corresponding processes when ice accretes on aircraft components, as currently understood, may be useful. This description is based mainly on papers by Messinger (1953), Hansman and Turnock (1989), Bilanin (1991), Hansman et al. (1991) and Hansman et al. (1993).

In-flight icing by droplets of supercooled liquid water of course requires an ambient air temperature below freezing, i.e. below 0 C. At steady state these surfaces can be assumed to be adiabatic. Immediately upon impact the droplets striking upstream-facing surfaces freeze either partially or completely. The latent heat of fusion is released from the water which freezes and this tends to warm the accreted ice and the underlying solid surface towards 0 C. This warming tendency is counteracted by convective heat loss to the ambient air. The temperature in the impact region is thus mainly the result of a balance between the rate of latent heat release and the convective heat transfer to the ambient air. In cold temperatures with low liquid water content (LWC) the temperature of the accreted ice remains below 0 C and the impacting droplets freeze completely. On the other hand, with high LWC and/or air temperatures only slightly below 0 C the temperature of the accreted ice is 0 C and only a part of the liquid water freezes upon impact; that is, the freezing fraction, n, is less than unity. The unfrozen water tends to run back along the surface and it too may eventually freeze. In addition to the effect of temperature the LWC of the clouds plays a crucial role in determining the value of the freezing fraction and the shape and other characteristics of the ice deposit. With high LWC the freezing fraction tends to be less than one because the rate of convective heat loss is insufficient to remove all of the latent heat that would be released if all of the liquid water were to freeze. With low LWC, on the other hand, convection has the capacity to remove the latent heat released by freezing of all of the impinging liquid water so that the freezing fraction is unity and the temperature of the accreted ice can be less than 0 C.

Ice particles that may be suspended in the air have little effect on ice accretion; it appears that they simply bounce off the accreted ice or aircraft surfaces.

Conditions in which the freezing fraction is unity (cold air, low LWC) are known as rime icing conditions. The rime ice accretion process is relatively simple because the impacting droplets freeze and remain where they strike the surface. In experiments it is only necessary to correctly simulate droplet trajectories and to ensure that the temperature of the accreting ice remains below 0 C. Rime ice deposits are relatively simple in shape (see Fig. 1.2-1a); they have an opaque milky appearance because of air inclusions and their surface is typically somewhat rough.

When the freezing fraction is less than unity, glaze icing conditions are said to prevail. Glaze icing is much more complex than rime icing because of the unfrozen water which is present in the impingement zone. As already mentioned, this water runs back and tends to freeze somewhat downstream of where it impinged on the surface. Complex shapes tend to develop, often with large double-horns (Fig. 1.2-1b) in two-dimensional cases and complex three-dimensional 'lobster-tail' shapes on swept surfaces including some rime ice feathers (see below) at the same time. Glaze ice deposits are normally clear because there are relatively few air inclusions.

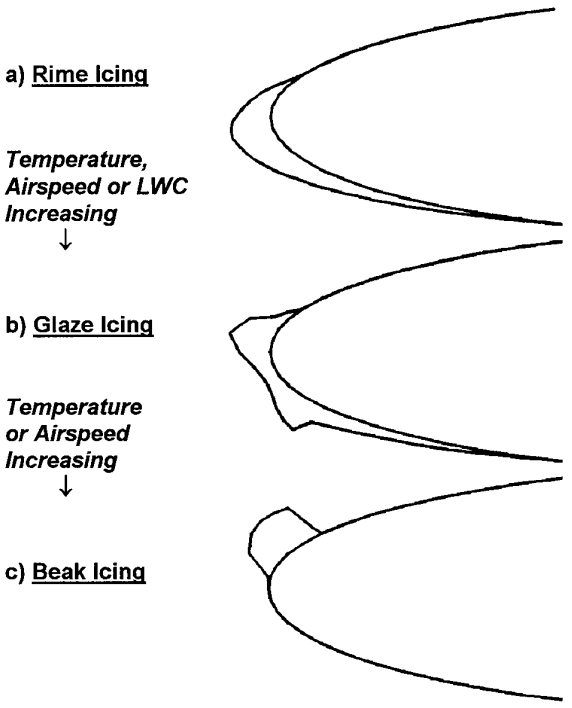

Fig. 1.2-1: Types of Ice Accretion

Recent research by Olsen and Walker (1986), Hansman and Turnock (1989), Hansman et al. (1991) and Yamaguchi and Hansman (1992) indicates that in glaze icing the detailed behaviour of the runback water has a very important influence on the shapes of the ice deposits. The runback water appears to exercise this influence through its effects on the rate of convective heat transfer from the surface to the ambient air. More freezing will occur where this heat transfer rate is high. Close-up video observations (Hansman et al., 1991) show that the liquid water forms an approximately uniform film on the accreted ice layer near the flow stagnation point but that farther back the liquid film breaks down and the water collects into discrete droplets on the surface. Olsen and Walker (1986) first observed these discrete droplets and recognised their probable significance. These droplets appear to act as aerodynamic roughness which is well known to substantially increase convective heat transfer coefficients (Achenbach, 1977, Kirchner, 1983). The observations show relatively rapid growth of ice thickness just downstream of the discrete-droplet zone. Indeed ice horns were found to develop here. The breakup of the liquid film into discrete droplets appears to be associated with transition from laminar to turbulent flow in the air boundary layer. Of course roughness would tend to influence the transition location. The discrete-droplet zone is observed to migrate slowly upstream as icing runs progress. Hansman et al. (1991) have also noted that the runback water sometimes forms into rivulets and that rivulet behaviour may have an important influence on ice accretion for reasons similar to those outlined in the preceding paragraph. Bilanin (1991) suggests that splashing in the impingement region and perhaps aerodynamic stripping of liquid water from the surface may be important.

In the light of the two preceding paragraphs it appears that surface tension plays an important role in glaze icing and must be included in similarity considerations. Indeed Hansman and Turnock (1989) observed a substantial change in ice deposit shape when a surfactant was added to the spray water during an icing tunnel test. The surfactant reduced surface tension by a factor of approximately two.

Hansman et al. (1993) and Hansman (1993) have also observed growth of 'feathers' in parts of the ice accretion region under certain 'mixed ice' conditions (i.e. intermediate between rime and glaze). Feather development appears to be initiated by small protuberances which locally enhance both the convective heat transfer rate and the capture efficiency. Locally the freezing fraction is unity and the feathers are rime ice formations even though glaze ice icing prevails elsewhere. The protuberances which initiate feathers can be either roughness on the aircraft surface or a small bump that develops on the surface of the accreting ice. This phenomenon illustrates the great importance of factors which change the rate of convective heat transfer to the ambient air.

Besides runback ice, which is often associated with melt water from thermal ice protection of the leading edge region, the interaction of the icing process with mechanical de-icing systems may lead to special residual ice forms. Even for well designed inflatable rubber boots of normal chordwise extent, some ice can be built up behind the boots under extreme meteorological conditions (especially large droplets). In this case during the ice removal cycles some ice may remain behind the boots which forms an upstream facing step changing the airfoil geometry. On this (at first rather small) barrier more ice can accumulate between cycles and may not be removed during the following cycles. Thus ridges of noticeable height (1-2 cm) have been observed. The point at which the barrier may break by the aerodynamic forces depends on the (unknown) mechanical properties of the ice, but the maximum size seems to be generally limited. This ice type has recently attracted much attention of aircraft manufacturers, certification authorities and researchers because of

related accidents. The few existing publications on this problem do not yet provide a conclusive picture.

For helicopter blades a special ice shape is referenced (see Gent, 1991). At combinations of high speed and warm ambient temperature, close to 0 C, the only place where ice can form is in the region of low pressure on the upper surface near the leading edge. Under these circumstances a 'slushy' ridge of ice forms, termed 'beak ice' (Fig. 1.2-1c).

Finally, a type of ice contamination has to be mentioned which just represents increased surface roughness. Such contamination results from frost, freezing rain and snow freezing on the aircraft surface. This ice type mostly occurs in ground operation before take-off, e.g. if hoar-frost precipitates overnight (see e.g. van Hengst and Boer, 1991, and Kind and Lawrysyn, 1991). Although take-off must be prevented in these cases due to the 'clean wing concept' prescribed by FAA and JAA, and freezing rain is always to be avoided, such contamination can also happen in-flight as an initial ice accretion (Lynch et al., 1991) and must be considered for certification.

1.3 DEGRADATION OF AIRCRAFT PERFORMANCE AND HANDLING WITH RESPECT TO CERTIFICATION/QUALIFICATION

Aircraft in operation can encounter a very broad range of icing conditions. There is some evidence that pilots are sometimes aware that they are likely to have ice on their aircraft but, possibly through confidence gained in previous icing encounters, they do not correctly anticipate the behaviour of the aircraft. Many differences in conditions can affect the distribution and amount of ice on the aircraft, making it difficult for the pilot to develop a reliable feel for the aircraft with ice. Most critical are situations when the pilot does not recognise or not correctly judge how severe the encountered icing contamination of the aircraft already is. On the other hand, the certification authorities give the clear advice written in FAR/JAR § 25.1419: "The aeroplane must be able to safely operate in the continuous maximum and intermittent icing conditions determined under Appendix C". Therefore thorough investigations of the performance/stability and control degradation are needed during the certification process of an aircraft and design enhancements may even be necessary. Also the above remarks reveal the importance of early and reliable detection of ice accretion.

Brumby (1991) provided an excellent and impressive survey on the degradation effects from aircraft manufacturers point of view and some of these effects are also demonstrated here. The most striking effect of ice contamination on lifting surfaces concerns the lifting characteristic of a wing. Due to the fact that the nose shapes of wing sections are essentially sharpened by the usual ice forms or become rough due to icing phenomena, the maximum lift will drastically be reduced and even the gradient of lift with respect to angle of attack may be smaller (Fig. 1.3-1). In consequence also the stall angle, i.e. the angle of attack at which maximum lift is reached and beyond of which the lift decreases, moves to lower values. At the same time the drag polars (C_L versus C_D) change (Fig. 1.3-2) in the sense that the drag will remarkably increase at constant lift.

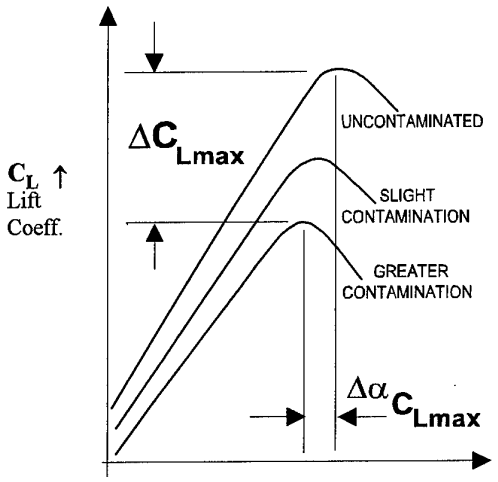

Fig. 1.3-1: Effect of Ice Contamination on Lift

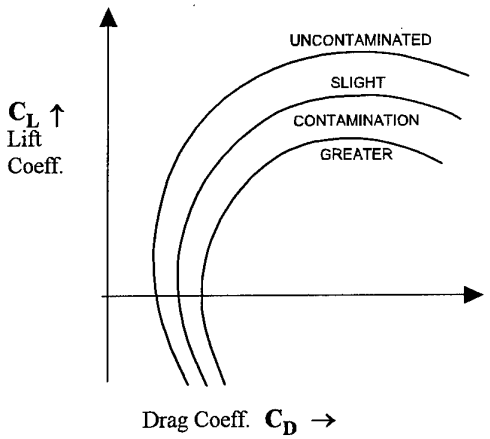

Fig. 1.3-2: Effect of Ice Contamination on Drag

The wing ice contamination can also strongly affect the longitudinal stability behaviour. While the aircraft is trimmed at approximately zero stick force without ice accretion, this balance is upset due to ice contamination, particularly on contemporary jet aircraft with tapered, swept wings. With increasing ice ridge size the aircraft will become mistrimmed in the nose-up direction. Thus the aircraft will, for instance, pitch up more rapidly during take-off and will require an abnormal push force to maintain the desired airspeed during climb. Of course this behaviour causes some danger if the pilot does not recognise the ice contamination early and does not react properly. At the same time the stick force may be reduced by the ice accretion tempting the

pilot to pull adversely while the lateral control needs more attention and eventually fast reactions to keep the aircraft from rolling off. On a typical transport aircraft this happens within a few seconds and it demands a well trained flight crew to detect the situation and to counteract promptly in the correct sense. If a stick pusher is implemented it must be fired sufficiently early to prevent stalling also under icing conditions.

The consequences of ice accretion can be severe in all flight phases. During take-off, for example, the aircraft's climb capability is lowered or even lost leading to extremely hazardous situations, e.g., inability to clear obstacles, especially in the case of an additional engine failure. Also in other flight phases the ice effects severely reduce the performance, e.g. the ceiling height with engine failure may become insufficient for many missions. The most difficult problem with respect to handling characteristics often arises from the demand to demonstrate safe flight in icing conditions even under extreme circumstances, e.g. full control surface deflections and one engine failure. This is especially critical in cruise and landing conditions where large ice horns may be present. Hence, the possibility of ice accretion must always thoroughly be considered and has become a decisive factor in aircraft design with respect to performance as well as with respect to stability and control.

Lift losses can even be caused by rather small roughness effects on the entire upper surface of the wing due to frost, snow or freezing drizzle. Such roughening can sometimes accumulate while the aircraft is on the ground and may remain on the surface although the 'clean wing concept' should prevent take-off with contamination. A surprisingly large degradation even for small contamination can be observed which sometimes can be partially recovered by slat extension. There is some strong sensitivity to the exact chordwise position of smaller roughness bands and to roughness height. The stall speed also changes correspondingly and it becomes readily apparent that a small amount of roughness on the wing upper surface may cause a large increase in stall speed, even with slats extended. This reveals the importance of the 'clean wing concept' for take-off as already mentioned.

The basic demands for ice certification are fixed in JAR/ FAR § 25.1419 and the meteorological conditions are defined in appendix C of that document. The content of ACJ (Advisory Circular Joint) 25.1419 of JAA and various AC (Advisory Circular) of FAA provide 'Interpretative Material and Acceptable Means of Compliance'. Furthermore the proposal AMJ (Advisory Material Joint) 25.1419 of JAA contains quite detailed and more concrete guidance on how safe flight in icing shall be proved during certification. Military certification/qualification procedures often are based on these civil regulations, especially in case of military transports. Special regulations for helicopters may be found in AGARD (1986).

1.4 ICE ACCRETION SIMULATION

As already shown in the previous sections of this introduction, icing simulation is necessary if we look on aircraft safety and certification/qualification from a commercially realistic viewpoint. Therefore, the aircraft manufacturers and the certification/qualification authorities alike have a strong interest in this subject. Besides this general view the following aspects have recently increased the corresponding activities considerably:

- Increases of air traffic lead to higher risks and more incidents, especially with respect to icing flights since severe icing situations cannot always be avoided (e.g. increased holding times).
- High performance aerodynamic shapes of modern aircraft should not be degraded by ice accretion or by a non-appropriate ice protection system. Therefore a lot of development activities for new protection systems have been pushed in recent years.
- New military aircraft are under development which require adverse weather capability.
- Some existing military aircraft experienced foreign object damage (FOD) due to shed ice.
- The modern high bypass ratio engines for jet transport and advanced turboprop engines of tomorrow do not allow for much bleed air or much other energy extraction for ice protection.
- Only one civilian helicopter has currently achieved full ice certification by the authorities up to now.

For the certification of a new aircraft, safe flight under icing conditions and the effectiveness of the ice protection system must clearly be demonstrated. Of course, some full scale flight tests in real icing conditions are indispensable for fulfilling this objective. However, to minimise the hazard of these tests and to save money and time as much as possible, simulation has proved extremely valuable. Potapczuk and Reinmann (1991) give hints that initial efforts for icing simulation took place in the late 1920's and early 30's. In the early 40's NACA built the icing research tunnel (IRT) at the Lewis Research Center. Since then systematic research in ice accretion has become easier, focusing on the formation of ice shapes and on aerodynamic performance degradation. Icing simulation activities have increased dramatically from the late 70's to today. The advent of high speed computer systems has allowed the development of sophisticated computer simulations of ice accretion processes and also to begin simulations of performance degradation. A new task has arisen, namely to built a validation data base for ice accretion calculations.

Despite this long history of icing research, there still remains a significant number of unresolved issues in the process of icing simulation. These issues range from

the fundamental physics of the icing process to the mechanisms underlying the ice removal process. For example the importance of the surface roughness effects created by ice accretion is recognised with regard to their strong influence on the heat exchange at the surface; however, the roughness influence in theoretical icing models is not quantitatively understood since the ice roughness usually exceeds the boundary layer thickness in contradiction to the de facto-situation in the underlying classical boundary layer tests. Therefore the motivation of the present working group activity was to review the simulation possibilities and to provide guidance for - or at least emphasis on - future developments in order to make certification/qualification processes safer, faster and cheaper.

The AGARD FDP Working Group 20 on 'Ice Accretion Simulation' concentrated its work on the possibilities and perspectives in the prediction of in-flight ice accretion since further improvement in this area is urgent from the aircraft manufacturers' and from the certification/qualification authorities' points of view. The corresponding parts of the report deal with all types of ice accretion simulation, experimentally through in-flight and ground tests as well as theoretically by computer simulations. Important - especially for experimental simulations in icing tunnels - are, in addition, the similarity and scaling laws for the supercooled droplets in icing environments. In this report information is also provided on suitable instrumentation for icing tests - in-flight and in ground facilities. Improvements in understanding the meteorological presumptions are relevant for most aspects of ice accretion simulation and are therefore included. The report gives also an overview concerning the effects of ice accretions on aircraft performance and handling as these effects are critical for safety and therefore decisive for certification. In consequence, the possible counter measures are also addressed. These can be adapted by aircraft designers for optimising the layout of the ice protection system and for configuration improvements.

Excluded from the scope of this report are the computational simulations of performance degradation. Of course these activities have made reasonable progress during recent years but we are still far from the possibility of simulating a complete aircraft with ice accretions. Thus all aircraft manufacturers rely on experiments for this purpose and calculations have only limited value for the authorities up to now. Detection of accreted ice - although an important aspect for safe flight in icing conditions - is not addressed in detail in this report since it is not a matter of ice accretion simulation. We discussed, but only briefly, the aspects of de-icing before take-off because standard procedures are in use for that purpose and simulation is not expected to provide much additional knowledge on this subject. In addition, the 'clean wing concept' prescribed by the authorities strictly forbids take-off with any ice contamination on the surfaces, thus reducing simulation interests in this respect. The effects caused by fluids for ground de-icing were also beyond our interest. Furthermore, we have not looked into the details of ice accretion affecting the engines since some recent information has been collected by the AGARD Propulsion and Energetics Panel (AGARD 1991b).

In-flight testing in natural icing conditions is the most realistic means for checking effects of icing on aircraft. However, in-flight testing in natural icing conditions is costly, potentially hazardous and it is usually difficult to find in nature the specific performance- and handling-critical atmospheric conditions needed to demonstrate the adequacy of the systems. Even finding a reasonable encounter for a short time period, can require many flight hours. As much as ten percent of the total certification flight program hours are often spent in looking for the proper icing conditions. The elapsed time to certify single engine airplanes and rotorcraft have taken up to 5 years. This perhaps reflects the difficulty that certain types of aircraft, particularly single engine airplanes and rotorcraft, have in finding natural icing conditions. Also, the varying compliance procedures could be a contributing factor in certification efforts.

Nevertheless, in-flight testing in real icing conditions is necessary to some extent in order to demonstrate the ice protection system effectiveness and verify the ice forms for simulations using artificial ice shapes. In addition, the degradation of performance and handling characteristics must be checked for natural ice accretion by investigating some reference cases. However, if the critical ice shapes are determined using ground facilities such as icing tunnels or outdoor spray rigs or prediction codes (those accepted by the authorities), the degraded performance and handling characteristics can be investigated by flight tests in dry air using artificial ice shapes attached to the aircraft surfaces (at least common practise for fixed-wing aircraft, for helicopters see end of this chapter).

Another approach to in-flight testing is to make use of icing spray tankers which fly in front of the aircraft being tested and produce a cloud of water droplets of appropriate size distribution. The spray droplets will be sufficiently supercooled by the ambient air before impinging on the aircraft if a suitable ambient temperature is chosen by flying at appropriate altitude. But, because the diameter of the spray plume is always rather limited, only components of the test aircraft can be investigated. This limitation is severe for fixed wing aircraft and therefore tanker tests cannot generally become accepted by the certification authorities. However, rotorcraft and some military aircraft have successfully been tested using icing tankers for demonstration of airworthiness.

Because of the-limited size capability of ground facilities a full size aircraft can not normally be accommodated and a part, component or model simulation may

be necessary. This may not be adequate to show full compliance of an airplane with the design requirements concerning ice accretion. Also, the similarity rules for scaled testings are limited and many cases perhaps are inadequate to simulate conditions for realistic ice accretion. However, ground facilities are very valuable tools to analyse icing problems in early design phases before a prototype becomes available, to check aircraft components with respect to icing and to generate ice shapes for defining artificial ones being used in dry air tests. Therefore a considerable part of this report is devoted to survey the available ground facilities for icing tests and the similarity laws needed for model experiments.

Experimental ice accretion simulations on the ground cover a wide range of test types. Some intend to simulate natural in-flight icing situations, and others only simulate certain aspects present in the complex ice accretion process. Compromises have to be accepted with respect to the similarity requirements as the only possibility to obtain reliable data in repeatable and controlled environments. To perform tests in prescribed conditions, complex facilities are needed. Usually, they are specifically suited for different groups of tests:

— Fixed-Wing Aircraft
— Rotorcraft and Propellers
— Engines

Of course, for investigating degradation of performance and handling characteristics by applying artificial ice shapes conventional windtunnels are sufficient. Rather few special facilities exist however for generating realistic icing conditions.

Last but not least, the area of computational prediction of ice accretion has progressed greatly during recent years and is now an important and quite reliable simulation tool. The computer models are used for two purposes in the design and certification process of an aircraft:

- On the basis of an aerodynamic flow field calculation the water droplet trajectories can be calculated and from that data the local water collection efficiency on the body surface can be determined. These results are often used to decide the necessary chordwise extent of ice protection systems, e.g. rubber boots, even if contour changes due to the accreted ice have not been taken in account.

- Once the collection efficiency on the body surface is known, the ice growth process can be studied. While this procedure is simple for rime ice accretion (as easily may be understood), it needs a thorough heat and mass balance analysis for glaze ice accretion in order to decide what mass fraction of the impinged water freezes locally and what fraction is evaporated or sublimated by the latent heat released during freezing or runs downstream in a water film. An empirical key input for this calculation is the heat transfer coefficient between the flow around the body and the rough ice surface. The heat balance is sensitive to this parameter but unfortunately the corresponding values are poorly validated since well-proved values for a large parameter range are only available from the classical boundary layer experiments. These experiments exhibit much smaller roughness height that never approaches the boundary layer thickness, or even exceeds it, as frequently observed in icing problems. This calculation procedure is used for predicting the growing glaze ice shapes and hence to determine the corresponding artificial ice shapes for experiments in dry air.

Up to now the first step in the calculation procedure is usually an inviscid calculation of the steady flow field around the body. This result is usually sufficient as the basis for the determination of the droplet trajectories moving through the flow field since the extent of the trajectories influenced by viscous effects is very short (close to the body surface, immediately before impingement). However, this calculation becomes difficult as soon as the ice form grows and the inviscid flow field needs to be determined around the body contour changed by the ice shape. Formally, this causes difficulties with field methods to create suitably smoothed meshes around the ice horns while panel methods can easily deal with them. However, the crucial point in flow physics is that flow separation can be provoked by the ice horns which then demands Navier-Stokes methods for a realistic solution.

Trajectory codes on the above basis are widely and successfully in use for determining the collection efficiency in 2D and 3D problems. Also rime ice accretion can be predicted simply from the corresponding results. The prediction of glaze ice however needs more sophisticated codes as indicated above which are quite rare and which cannot be expected to produce perfect results in all situations. Nevertheless, great progress has been observed in improving glaze ice prediction by advancing the ingredients of these computer programs during recent years and further progress may be anticipated. 2D codes have been introduced into the certification procedures while 3D codes basically are under development but can already provide promising results. The 2D codes of NASA Lewis (Lewice), ONERA and DRA have already been accepted by some of the national European authorities for predicting the forms of artificial ice shapes that may be used in flight tests for certification.

Some special remarks may be necessary concerning helicopters. Many of the problems associated with the clearance of helicopters for flight in icing are similar to the problems faced by airplane manufacturers. In particular, finding an adequate range of natural icing conditions during flight trials is a common problem and may be further compounded for helicopters due to their shorter range and endurance. Technologies developed for the protection of wind screen, air data sensors, tailplane and engines are generally common to both,

helicopters and airplanes, and therefore the helicopter manufacturer can make use of the same range and extent of ice accretion simulation capabilities. The helicopter manufacturer however faces new problems when attempting to clear engine intakes and rotors for flight in icing. To date a combination of in-flight and icing tunnel testing has largely been adopted for the development of engine intake protection systems, although the size and cost of icing tunnel facilities available is a constraint. Testing in natural icing is still considered essential by certification agencies to ensure that no FOD (foreign object damage) hazard results from the ice shed from components mounted on the fuselage upstream of the intakes. It is also required to provide an additional check that run back water or slush will not be collected and freeze within the intakes. Significant progress has been made in recent years in the computer simulation of ice accretion within helicopter intakes and for the external flow about the fuselage/intake combination (Mann and Tan, 1990). These codes will undoubtedly feature more in the future certification of helicopter engine intake protection systems.

For the helicopter rotor systems, the design and development of protection systems has, in recent years, relied heavily on theoretical simulation techniques. These protection system simulation codes require an adequate representation of the thermodynamics of the ice accretion process and therefore rely heavily on analyses developed to predict ice accretion profiles on wings. However, there are significant differences between the ice accretion prediction analysis used for the wing icing and the analysis required for the simulation of an electrothermal protection system. A steady state analysis is normally considered sufficient for wing icing problems and heat conduction in the structure is usually neglected. For the modelisation of electrothermal protection systems however, the ice accretion prediction analysis must necessarily include the heat, both generated and conducted within the structure. The analysis is transient (time dependent) rather than equilibrium (while anti-icing systems may be considered to be an 'equilibrium' problem, they may more readily modelled via the transient approach).

Although in-flight testing with artificial ice has been very successful for fixed wing aircraft and is accepted by the certification authorities, this technique has not proved useful to the clearance process of helicopters after some evaluations in the past. Such tests with correspondingly modified rotor profiles merely serve to confirm the large, and unacceptable, performance degradation that results (primarily a large increase in rotor torque/power). At this time therefore, ice accretion simulation techniques for helicopter applications are essential to the safe and cost-effective design and development of the protection systems required for the engine intakes and for the rotors (AGARD, 1986).

REFERENCES

Achenbach, E. (1977), "The Effect of the Surface roughness on the Heat Transfer from a Circular Cylinder to the Cross Flow of Air", *Int. J. Heat Mass Transfer*, Vol. 20, pp. 359-369.

AGARD (1986), "Rotorcraft Icing - Status and Review", AGARD-AR-223.

AGARD (1989), *Flight in Adverse Environmental Conditions*, Flight Mechanics Panel (edit.), AGARD-CP-470,

AGARD (1991a), *Effects of Adverse Weather on Aerodynamics*, Fluid Dynamics Panel (edit.), AGARD-CP-496.

AGARD (1991b), *Low Temperature Environment Operations of Turboengines (Design and User's Problems)*, Propulsion and Energetics Panel (edit.), AGARD-CP-480.

Bilanin, A. J. (1991), "Proposed Modifications to Ice Accretion/Icing Scaling Theory", *J. Aircraft*, Vol. 28, pp. 353-359.

Brumby, R. E. (1991), "The Effect of Wing Ice Contamination on Essential Flight Characteristics", in: AGARD-CP-496 (1991).

CAA CAP 479 (1976, updated twice a year), Civil Aviation Authority (UK), "World Airline Accident Summary, Volume 2 - 1976 and onward", C.A.A. Document No. CAP 479.

Cole, J. A., and Sand, W. R. (1991), "Statistical Study of Aircraft Icing Accidents", AIAA 91-0558.

Geer, W. C. (1939), "An Analysis of the Problem of Ice on Airplanes", *J. Aeron. Sci.*, Vol. 6, pp. 451-459.

Gent, R. W. (1991), "A Review of Icing Research at the Royal Aerospace Establishment", in: *Effects of Adverse Weather on Aerodynamics*, AGARD-CP-496.

Gerardi, J. J., Ingram, R. B., and Catarella, R. A. (1995), "A Shape Memory Alloy Based De-Icing System for Aircraft", AIAA 95-0454.

Hansman, R. J., Jr. (1993), "Microphysical Factors which Influence Ice Accretion", *Proc. First Bombardier International Workshop: Aircraft Icing, Boundary-Layer Stability and Transition*, Ecole Polytechnique de Montreal, Montreal, Sept. 1993, pp. 86-103.

Hansman, R. J., Jr., and Turnock, S. R. (1989), "Investigation of Surface Water Behavior During Glaze Ice Accretion", *J. Aircraft*, Vol. 26, pp. 140-147.

Hansman, R. J., Jr., Yagamuchi, K., Berkowitz, B., and Potapczuk, M. G. (1991), "Modelling of Surface Roughness Effects on Glaze Ice Accretion", *J. Thermophysics*, Vol. 5, pp. 54-60.

Hansman, R. J., Jr., Breuer, K. S., Hazan, D., Reehorst, A., and Vargas, M. (1993), "Close-up Analysis of Aircraft Ice Accretion", AIAA 93-0029.

Heinrich, A., Ross, R., et al. (1991), "Aircraft Icing Handbook, Vol. 2 of 3", FAA Technical Center, DOT/FAA/CT-88/8-2.

Hobbs, P. V. (1974). "Ice Physics", Oxford University Press. (Out of print)

JAR/FAR 25.1419 (continuously amended), "Ice Protection", including Appendix C and ACJ 25.1419.

JAR AMJ 25-1419 (1992), "Flight in Icing Conditions - Acceptable Handling Characteristics and Performance Aspects", in: NPA 25F-219 Issue 2 (22 Jan. 1992).

Kind, R. J., and Lawrysyn, M. A. (1991), "Effects of Frost on Wing Aerodynamic and Take-off Performance", in: *Effects of Adverse Weather on Aerodynamics*, AGARD-CP-496.

Kirchner, R. D. (1983), "Aircraft Icing Roughness Features and Its Effect on the Icing Process", AIAA 83-0111.

Lynch, F. T., Valarezo, W. O., and McGhee, R. J. (1991), "The Adverse Aerodynamic Impact of Very Small Leading-Edge Ice (Roughness) Buildups on Wings and Tails", in: *Effects of Adverse Weather on Aerodynamics*, AGARD-CP-496.

Mann, D. L., and Tan, S. C. (1990), "Application of a Water Droplet Trajectory Prediction Code to the Design of Inlet Particle Separator Anti-icing Systems", AGARD-CP-480.

Messinger, B. L. (1953), "Equilibrium Temperature of the Unheated Icing Surface as a Function of Air Speed", *J. Aero. Sci.*, Vol. 20, pp. 29-42.

Olsen, W., and Walker, E. (1986), "Experimental Evidence for Modifying the Current Physical Model for Ice Accretion on Aircraft Surfaces", NASA TM-87184.

Potapczuk, M. G., and Reinmann, J. J. (1991), "Icing Simulation: A Survey of Computer Models and Experimental Facilities", in: AGARD-CP-496 (1991).

Pruppacher, H. R. and Klett, J. D. (1978), "Microphysics of Clouds and Precipitation", D. Reidel Publishing. Company, Holland.

Reinmann, J. J. (1994), "Icing: Accretion, Detection, Protection", In: AGARD-LS-197 *Flight in an Adverse Environment.*

Vali, G. and Stansbury, E. J. (1966), "Time-Dependant Characteristics of the Heterogeneous Nucleation of Ice", Can. J. Phys. 44, pp. 477-502.

van Hengst, J., and Boer, J. N. (1991), "The Effect of Hoar-Frosted Wings on the Fokker 50 Take-off Characteristics", in: *Effects of Adverse Weather on Aerodynamics*, AGARD-CP-496.

Yagamuchi, K., and Hansman, R. J., Jr. (1952), "Heat Transfer on Ice Accreting Surfaces", *J. Aircraft*, Vol. 29, pp. 108-113.

Table 1.1-1 : Overview of Conventional Ice Protection Systems

De-icing systems:	Characteristics:	Advantages:	Disadvantages:
Pneumatic Impulse De-icing System	The tubes within the fabric-reinforced synthetic rubber boot are inflated alternately to fracture and to debond the ice accretion on the surface to be protected.	- relatively cheap - relatively light-weight - low bleed air consumption - proven technology	- aerodynamic effects (inflated/deflated boots and ice build-up between cycles) - restrictions concerning transonic speed - limited life due to wear and erosion - low resistance to oil and hydraulic fluids - water ingress through pinholes in rubber - water ingress through air supply - constant suction required when not in use
Fluid Ice Protection System	FPD (Freezing Point Depressant) fluid is pressed through porous skin onto the surface to be protected, to lower freezing point of the impinged supercooled water droplets.	- no bleed air consumption - clean leading edge (dirt) - proven technology	- high weight; reservoir required - logistics (fluid availability and costs) - environmental restrictions - L.E. skin must remain porous (holes open) - drag can be caused by roughness of porous leading edge
Electro Thermal Systems	Heating elements on skin surface area provide heat to melt the build-up ice	- no bleed air required - proven technology	- high energy consumption (typical 12 W/in^2) - weight (additional generator) - FOD (Foreign Object Damage) sensitive - cyclic use (controller or thermostat required) - (over) heating problems when used in combination with composites
Hot Air Systems	Hot air is applied to raise the skin temperature to prevent freezing of the supercooled droplets or to melt the ice.	- aerodynamically clean when it is a fully evaporative system - proven technology - reduction of bleed air consumption can be achieved by changing system into a de-icing system without major re-design/development	- weight of air distribution system, air temperature and airflow control units - aerodynamic degradation in icing conditions when used as de-icing system - significant engine performance penalty (bleedair) for advanced high bypass ratio engines - aerodynamic degradation caused by runback ice when it is a running wet system - structural implications of using hot air, e.g. for composites, adhesives, high strength alloys
Low Adhesion Coating (Kilfrost Comp.) (ICEX)	Reduces considerably the adhesive forces for ice accretions	- simple and inexpensive	-supplement for an usual ice protection system (e.g. for improved pneumatic systems) - not a stand alone ice protection means

Table 1.1-2 : Overview of New De-icing Systems under Development			
De-icing Systems:	**Characteristics:**	**Advantages (according to vendor):**	**Disadvantages:**
Electro-Expulsive Separation System or Electro-Expulsive De-Icing System (EESS, EEDS)	Consists of conductors embedded in elastomeric blanket (boot) covering the ice accreting surfaces. Opposing currents in two legs create opposing magnetic fields causing a repulsive force between the top and bottom conductor layers. The top surface of the blanket is accelerated so as to destroy the ice-blanket bond.	- effective for removing thin ice layer. - minimising aerodynamic penalties. - easy manufacturing retrofitting. - low power consumption.	- typical de-icing penalties (consisting of aerodynamic effects due to residual ice and ice build-up between cycles) - elastomeric boots tend to get pulled away from surface (smoothness) - unknown effects of lightning strike - service life: dependent on ability of elastomeric materials to withstand rain, sand, erosion, oil and hydraulic fluids
Eddy Current Repulsion De-Icing Boot (ECRDIB)	(same as above but use of eddy currents instead of opposing magnetic field).	[see above]	[see above]
Pneumatic Impulse Ice Protection System (B.F.Goodrich) (PIIP)	Pneumatic impulse tubes covered by titanium skin on top of aircraft leading edge skin. High pressure air is supplied to impulse valve which discharges a pulse into the impulse tubes, snapping the surface outward. The surface is stretched more than ice is capable of stretching without fracturing.	- reduced intrusion of inflated de-icer into airstream. - provides a superior weather & erosion resistant surface material. - improves ability of ice protector to remove thin ice (0.03 inch). - low power and low system weight.	- typical de-icing penalties - high pressure air required - cannot be bonded to aluminium skin - fatigue of titanium skin (aerodynamic smoothness and accuracy reduced; service life).
Electromagnetic Impulse De-Icing (EIDI)	Flat-wound coils inside the leading edge induce eddy currents in metal skin, with the result that skin and ice layer are deformed.	- low power consumption and low maintenance costs. - does not alter external surfaces, so no aerodynamic impacts.	- typical de-icing penalties. Does not adapt readily for retro-fitting. - possible fatigue and EMI (Electro-Magnetic Interference) - unproven for transport aircraft - unknown effects of lightning strike - maintenance of active system is a problem (lethal electric power level).

Table 1.1-2 : Overview of New De-icing Systems under Development (Continued)

De-icing Systems:	Characteristics:	Advantages (according to vendor):	Disadvantages:
Shape Memory Alloy Based De-Icing System (SMA). Innovative Dynamics, Inc. developed two De-Icing Systems and IDI patent is pending. For more details see Gerardi et al. (1995).	Shape Memory Alloys (SMA's) exhibit a large temperature induced dimensional change (up to 8% strain for a NiTi-alloy) over a relatively narrow transition temperature range. In addition internal stresses in the SMA generate a force during the shape change. When cooled the shape expands and returns to its original shape when heated and so an ice braking action is created.	- SMA de-icer is designed for application on rotor blades and propellers - substantial power savings over existing electrothermally powered de-icing systems with greater durability and erosion resistance. - results of NASA Lewis IRT test results encourages further developments.	- for fixed wing application an additional system may be required to aid in the shedding of the debonded ice from the surface due to the lack of rotational dynamics that propellers and rotorblades do have to expel the debonded ice. - under development, not yet installed on helicopter or propeller for in-service trials.
Space Age Electro-Thermal System Using Nickel Coated Carbon Fiber Mat (Thermion No-Ice™)	Very Light Very Thin Cloth-like Nickel Coated Carbon Fiber Heater Mat. Can be laid up in E-glass or sandwiched in silicon embedded cloth. Can be layered for increased power density. Used in power applications from 12 V dc to 280 V ac.	- Very close to surface - Reduced power required - Eliminates circuit breakage discontinuities - Very light weight (2 lb. per 500 sqft) - Self regulating (design for temperature) - Easily tested for continuity - Life of airframe reliability	- Lay-up applications must be professionally done and quality controlled - Requires cycling circuitry for efficient power control

2. METEOROLOGICAL DATA FOR USE IN SIMULATING ICING CONDITIONS

Meteorological data on icing conditions is necessary for three main purposes---1) forecasting and reporting icing conditions, 2) designing and testing ice protection systems, and 3) simulating icing conditions (usually for test purposes). The third application is the focus of this chapter.

It is well known that the amount of ice accumulated on an aircraft in flight in icing conditions depends primarily on the collective liquid water content (LWC) of the cloud droplets, the sizes of the droplets, the in-cloud temperature along the flight path, and on the duration of the exposure. The airspeed, shape and temperature of the aircraft surfaces are controlling factors too, but we are concerned in this chapter with only the atmospheric variables.

In order to simulate icing conditions in wet wind tunnels, or with airborne water sprays, or by computer modeling, it is necessary to know what combinations of values of these cloud variables to reproduce. Official guidance for civilian certification work is contained in the design envelopes (FAA, 1994a, 1994b) or specific test conditions (FAA, 1973 for example) issued by the Federal Aviation Administration in the U.S.A. Similar guidance is issued by the Joint Airworthiness Authority (JAA) in Europe. For military aircraft, the civil guidance is used as a starting point, but it may be modified as needed to suit mission or design requirements. Different test conditions may be specified too.

The FAR-25 (JAR-25) envelopes will be briefly reviewed here, but their application to simulating icing conditions is limited. New research has examined other, more useful ways to display and compare icing variables. Since one purpose of this report is to review the latest information available, these new display methods will be described here too, and example applications to icing simulations will be given.

2.1 CURRENT DESIGN ENVELOPES

Figures 2.1-1 through 2.1-4 show some of the civil design criteria for inflight icing conditions (FAA, 1994a, 1994b). These design envelopes have been in use since the mid 1950's. Figures 2.1-1 and 2.1-2 apply to the more-or-less horizontally continuous icing conditions associated with stratiform-like clouds and overcast. Figures 2.1-3 and 2.1-4 apply to the more intermittent icing conditions associated with convective and vertically taller cumuliform clouds. All of the figures are based on an extensive set of cloud physics research flights conducted by researchers from the U.S. Weather Bureau and the National Advisory Committee for Aeronautics (NACA) during the winters of 1946 to 1950 (Lewis, 1947; Lewis and Jones, 1949; Kline, 1949; Lewis and Hoecker, 1949; Hacker and Dorsch, 1951). These flights were dedicated to characterizing the icing environment for the rapidly expanding, postwar, commercial airline industry.

The basic envelopes (Figs. 2.1-1 and 2.1-3) simply give the "probable maximum" value of LWC to be expected over a specific averaging distance, for a given temperature and cloud droplet size distribution represented by the median volume diameter (MVD) of the droplets. (The published figures actually use the older concept of mean effective diameter, MED; but for all practical purposes MED and MVD are the same (Jeck, 1983).) Thus, if one wants to simulate the approximate extreme values of LWC for an MVD and temperature of interest, figures 2.1-1 and 2.1-3 will give the values of LWC to be used. For example, figure 2.1-1 indicates that 0.8 g/m^3 is the largest value of LWC to be expected in supercooled stratiform clouds as an average over 17.4 nautical miles (nm) when the cloud droplets have an MVD of 15 μm and the in-cloud, flight-level temperature is 0 C. "Probable maximum" is understood to mean the 99th percentile value of LWC, as well as the 0.1% probability that *all three* variables (LWC, MVD, and temperature) represented by a point on the envelopes will be exceeded simultaneously in natural icing conditions (Lewis, 1969).

Except for the selection of overall maximum values of LWC, these envelopes are otherwise of no help for icing simulation purposes. For example, they do not indicate which MVD's are more probable, and in fact they do not even show any MVD's smaller than 15 μm.

A major difficulty is that the envelopes, as shown, are valid only for fixed averaging distances of 3 statute miles (2.6 nm) for convective (intermittent) clouds, and 20 statute miles (17.4 nm) for stratiform (continuous) clouds. These are arbitrary reference distances but were convenient for the original NACA researchers because most of their measurements were averages over about 3 and 10 miles. It is known, however, that for both types of clouds, longer averaging distances will result in lower maximum values of LWC as an average over the total exposure distance. To account for this behavior, additional curves (Figs. 2.1-2 and 2.1-4) had to be developed so the envelopes could be adapted to other averaging distances. For example, to find the maximum probable LWC to be expected as an average during flight through a 100 nm -wide expanse of stratiform icing clouds, the appropriate multiplying factor (0.46 in this example) is taken from figure 2.1-2. Thus, for stratiform clouds in which the MVD is 25 μm and the temperature is -10 C (+14 F), the maximum average LWC over 100 nm is 0.46 x $0.3 g/m^3$ = $0.14 g/m^3$. Basically, this procedure amounts to "shrinking" the vertical (LWC)

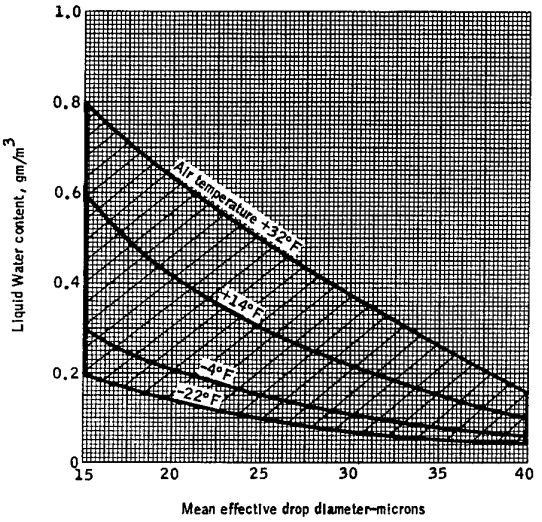

Fig.2.1-1: Conventional LWC vs. MVD Envelopes for Stratiform Icing Clouds (FAA, 1994a).

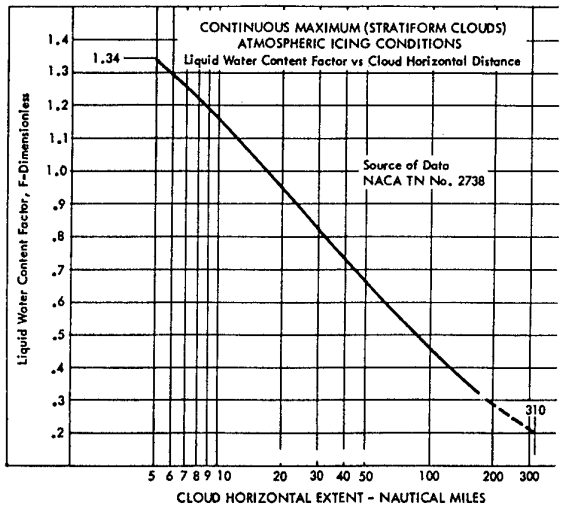

Fig. 2.1-2: LWC Scale-Adjustment Factor for use with Fig. 2.1-1 (FAA, 1994a).

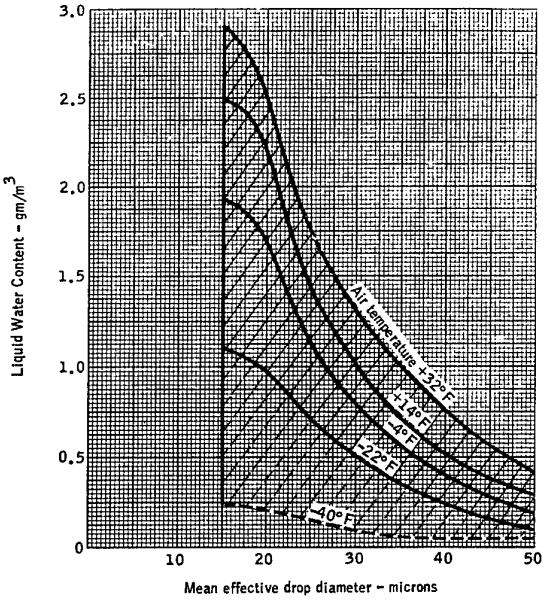

Fig. 2.1-3: Conventional LWC vs. MVD Envelopes for Cumuliform Icing Clouds (FAA, 1994a).

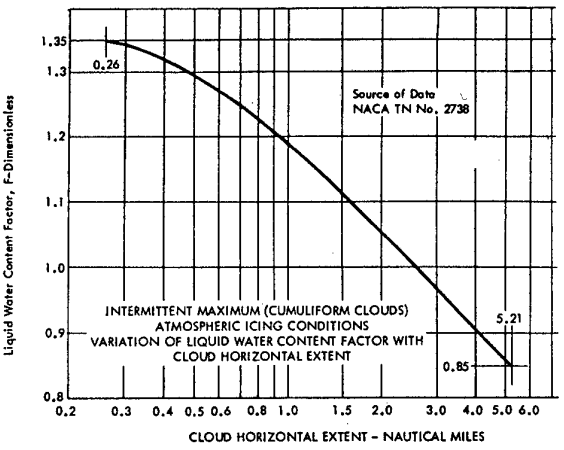

Fig. 2.1-4: LWC Scale-Adjustment Factor for use with Fig. 2.1-3 (FAA, 1994a).

scale in Fig. 2.1-1 or 2.1-3 by the adjustment factor. This is all right, but it prevents plotting test and/or design points with different averaging distances on the same figure.

Another problem is that wind tunnels and computer simulations typically work with timed exposures, not distance-based exposures. It is not practical to convert figures 2.1-1 and 2.1-3 to time-based envelopes, and therefore there is no convenient way to compare variously-timed exposures to fixed-distance envelopes.

2.2 NEW DATA-DISPLAY FORMATS

It has been demonstrated (Jeck, 1994) that plotting LWC against averaging distance (AD) is a much more convenient and versatile format for constructing icing design envelopes and for plotting and comparing design and test points. Some of the advantages are:

- ♦ Envelopes are obtained which are free of the cumbersome constraint of being tied to one particular exposure distance (ED).
- ♦ The LWC adjustment curves (Figs. 2.1-2 and 2.1-4) are no longer necessary and can be eliminated.
- ♦ Design values of ED other than the standard reference distances (2.6 nm and 17.4 nm) can be easily considered, if desirable.
- ♦ The basic LWC vs horizontal extent (HE) envelopes can be easily converted into envelopes of other useful variables too, such as the water impingement rate (LWC x airspeed) and total water exposure (LWC x HE).
- ♦ Test points in any of these variables can be plotted directly on the envelopes without concern for adjusting the envelopes to match variable averaging distances.
- ♦ The distance scale can be easily converted to a time-based scale for easy compatibility with wind tunnel and computer simulations.
- ♦ Overlays of helpful information, such as probability limits to LWC, or MVD, temperature, altitude, seasonal, or even geographical dependences of LWC can be easily added.
- ♦ Equivalent exposures can be defined and conveniently plotted to facilitate the comparison of test points and design points.
- ♦ The HE-based plotting format is compatible with the conventional LWC vs MVD envelopes in figures 2.1-1 and 2.1-3. That is, design values can be picked from the conventional envelopes and transferred to the HE-based format for plotting and for comparison with values from test exposures.

The LWC vs AD plotting format is briefly described here and overlays of helpful information are shown. Sample applications to the simulation of icing conditions are illustrated. The emphasis here will be on the advantages of the LWC vs AD format for plotting and comparing design and test points in simulation applications.

2.2.1 The Basic Display.

Figure 2.2-1 is the starting point. It shows most of the available LWC averages in a recently expanded database of inflight measurements in icing conditions (Jeck, 1983, 1994). There are about 3500 data points (nearly 2500 hidden by others) representing nearly 28,000 nm (data miles) of in-cloud exposures. Each point lies at the recorded average LWC over the corresponding in-cloud averaging distance. In this format, all the data points fall naturally in place on a single graph, no matter what their averaging distance. Dashed, vertical lines at the conventional design distances of 2.6 nm and 17.4 nm are drawn on the figures to serve as familiar reference marks. The plotting symbols are code letters representing the different organizations (Jeck, 1983) which have contributed the data. The asterisks represent measurements in known convective type clouds. These are mostly cumulus, cumulus congestus, and cumulonimbus, but summertime clouds above 3 km (10,000 Ft) are not included in this graph. The asterisk symbol was chosen to easily distinguish between convective and stratiform cloud types in the graph.

The slanted lines drawn on the graph are computed 99th percentile limits to LWC averages as a function of HE. The lines are computed from the recorded data, and the 99th percentile values serve as a practical upper limit to both LWC and HE. For example, over a 100 nm wide cloud the largest LWC to be expected as an average is about 0.4 g/m^3. Or, a LWC of 1 g/m^3, as an average, can be expected to last over a horizontal extent no longer than about 12 nm in natural icing conditions, but only in or among convective clouds.

2.2.2 Some New Advantages.

Figure 2.2-2 shows three other immediate advantages of the new format.

2.2.2.1 ***Conversion to a Time-Based Format.*** The distance axis can be easily converted to exposure time simply by dividing the distance scale by the airspeed of interest. In this figure an airspeed of 200 kt has been chosen for illustration purposes, and an equivalent time scale has been marked along the HE axis. LWC values from computer simulations or wet wind tunnel runs can now be plotted directly on the graph. A 200 kt exposure lasting for 15 minutes would be plotted above the 15

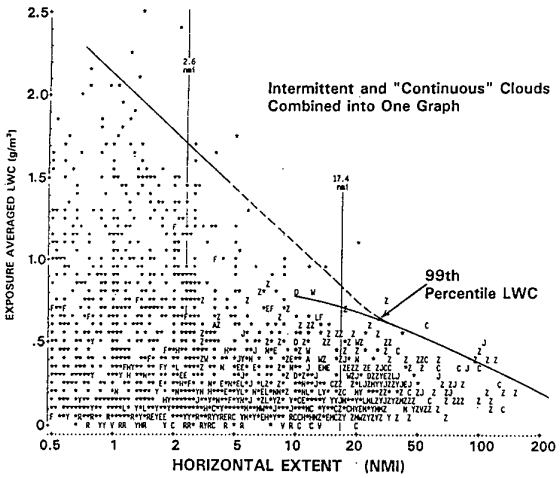

Fig. 2.2-1: The Supercooled Cloud Database Plotted in LWC vs. HE Format.

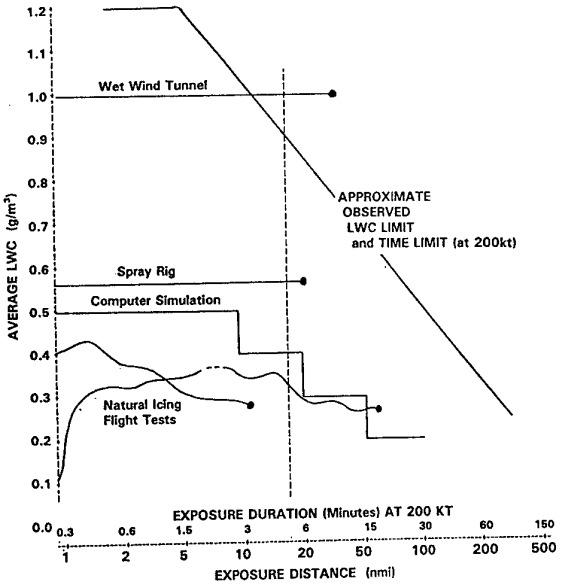

Fig. 2.2-2: Plotting LWC Histories in Addition to Conventional Test "Points".

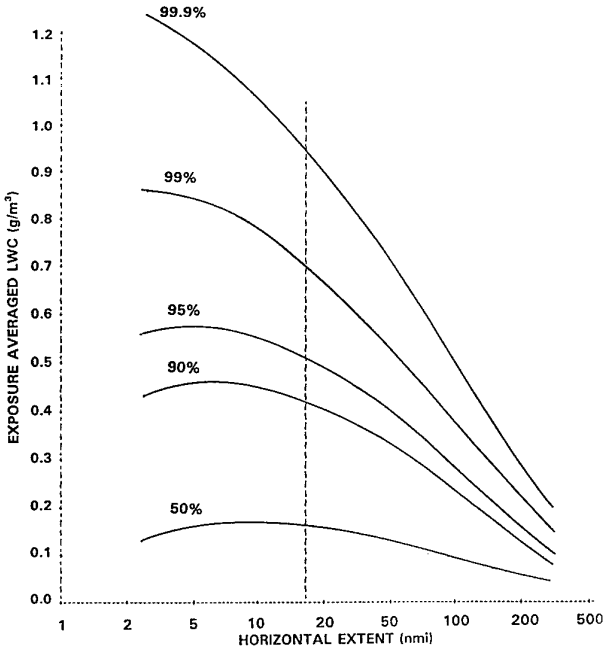

Fig. 2.2-3: Computed LWC Percentiles for Stratiform Clouds with Average MVD's (15 μm) and Temperatures from 0 C to -10 C.

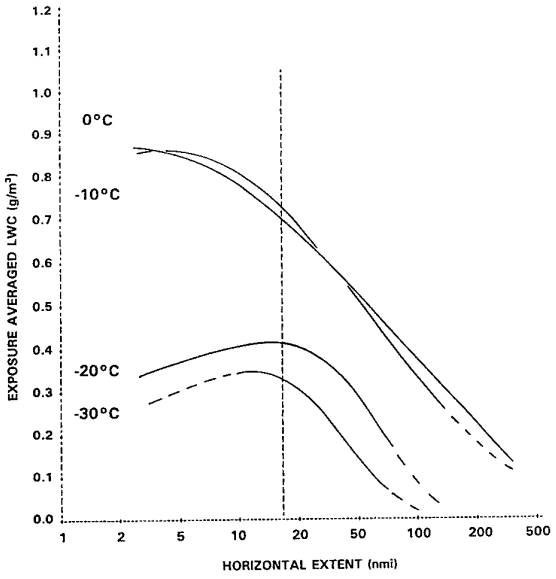

Fig. 2.2-4: Computed 99th Percentile Limits to LWC for 10 C Temperature Intervals in Stratiform Clouds with Average MVD's (15 μm).

minute mark (above the 50 nm position on the HE axis). Notice that nothing else changes---the graph keeps the same proportions and shape as before. This means that a chart with a single distance scale serves as universal graph paper. It can be converted to any desired time scale without redrawing anything. Different pages would be required for much different airspeeds, however.

2.2.2.2 ***"Tracking" LWC Variations During Exposures.*** Figure 2.2-2 also illustrates the natural way test data can be plotted in the distance- or time-based format. According to the usual practice, a test point (the large black dots) plotted on the envelopes simply represents the overall average of the LWC at the end of the measurement. The distance (or time-based) plotting format opens up a new dimension in that the entire history of the LWC can be plotted in addition to the final average, if desired. That is, all points begin somewhere along the left side of the figure (at HE=0 or t=0) and migrate to the right until the measurement is terminated. The true data track is actually a more or less wiggly line extending from HE=0 to the final location of the conventional "point", as illustrated by several arbitrary tracks in figure 2.2-2. In natural icing flights the LWC tracks may vacillate, remain steady, or trend downwards with increasing distance. The lines can trace the instantaneous LWC, the cumulative average LWC, or any other quantity as the exposure proceeds.

It is not necessary to plot the track of the data point if only the final LWC average is of interest. But the distance-based envelopes provide this new capability for cases where it may be desirable or useful.

2.2.2.3 ***Plotting In-Flight, Wind Tunnel, or Spray Rig Test Points.*** Keeping Within the Natural Limits. One subtle problem that has shown up with icing wind tunnel runs is the following. Tunnel icing exposures often last considerably longer than natural icing exposures under the same conditions. One result is that computer modeled ice shapes frequently cannot reproduce the large and irregular ice shapes occurring in the tunnel. This is often regarded as a failure of the computer model. But if the exposures were kept within the maximum time limits that are indicated in figures 2.2-1 to 2.2-7 for the selected LWC, MVD, temperature, and airspeed, the ice shapes would be smaller and perhaps less irregular. This would make it easier for the computer model to reproduce the ice shapes, and the number of "failures" may therefore be fewer. That is, if the computer can satisfactorily predict ice shapes that are realistically expected, who cares if it cannot do as well on ice shapes that may never be seen in nature?

One reason that this problem has gone unrecognized is that tunnel operators often show their tunnel operating points (LWC and MVD combinations) on figure 2.1-1 or 2.1-3 without considering any exposure time limitations. It is understood that these tunnel operating points can be maintained indefinitely, so for the purposes of showing which parts of the envelopes can be simulated in the icing tunnel there is no need to mention any exposure times. But this inattention to exposure times has apparently led to a disregard for natural time limits to exposures as well.

The time based plotting format helps to keep spray exposure times within natural limits. Because of the practical upper limit to the avearage LWC in unidirectional flight through natural icing conditions, the data tracks are not expected to penetrate this limit (represented by the slanted line in Fig. 2.2-2. In wind tunnels and spray rigs the LWC tracks would remain horizontal with time or distance, as long as the LWC is held constant. In these exposures the LWC tracks can penetrate right through the limiting curve if the exposure is too long, and the tracks will continue indefinitely until the exposure is terminated. Once they have penetrated the limiting curve then obviously they have exceeded the maximum to be expected in nature.

The exception to this rule is when simulations are intentionally extended, such as to represent a 45 minute holding pattern. It may be assumed that an aircraft in a holding pattern may be exposed to a longer, continuous exposure because it is circling within the specified icing condition rather than just passing through it once. The natural time limits then no longer apply, and unusually large ice accretions may occur.

The LWC vs HE envelopes prompt users to consider the implications of exposure duration and thereby to avoid exceeding natural exposures unintentionally.

2.2.3 Overlays of Useful Information.

Figures 2.2-3 to 2.2-6 illustrate some of the ways that useful auxiliary information can be added to the basic displays.

Note: At this writing these overlays have no official status as design envelopes for civil icing certification purposes. Nevertheless, they are research-quality results which may be used to obtain realistic values for icing variables aloft. And the distance-based graphing format can be used to compare test points and design points no matter where either were obtained.

2.2.3.1 ***LWC Percentile Limits.*** Figure 2.2-3 shows computed percentile curves for LWC. These give the LWC that will not be exceeded for selected percentages of exposures over any HE.

Although civil requirements specify at least the 99th percentile value of LWC for design purposes, military users have expressed a need for alternate percentile curves such as these. These overlays allow lower design limits to be selected for applications where higher icing risks are tolerable. For example, if a 10% risk level for

icing is considered acceptable, then the 90th percentile LWC curve can be used to obtain the maximum design value for LWC. Figure 2.2-3 shows that for in-cloud distances of 15 nm or less, the LWC will be less than 0.45g/m^3 in 90% of the cases. As the averaging distance increases beyond 15 nm, the 90th percentile value of LWC continually decreases.

Note that this decrease with distance is similar to the dependence conveyed by figure 2.1-2, but here the dependence is built-in instead of requiring a separate graph like figure 2.1-2.

The curves in figure 2.2-3 are computed for *all* available measurements in stratiform clouds and therefore they do not reveal the dependences on temperature, MVD, season, altitude, or other limiting factors. Figure 2.2-3 represents conditions which allow the largest values of supercooled LWC to occur---namely, OAT = 0 C and MVD = 15 μm in winter at altitudes between about 1 and 4 km (about 3000 Ft to 12,000 Ft). The curves will shrink along both axes as either the OAT or MVD changes from the above values, or for altitudes outside the stated range. That is, the curves in Fig. 2.2-3 will overestimate the LWC for each percentile for other values of temperature, MVD and altitude. To show the correct dependence, an overlay for each governing factor is required. Some of these are shown in the following Figures.

2.2.3.2 ***Temperature Limits.*** Figure 2.2-4 shows curves representing the computed 99th percentile LWC's as a function of flight-level temperature in clouds. The curves can be used to estimate the maximum LWC to be expected as an average over a given HE, at a given temperature. For example, over a 100 nm unidirectional path in cloud, the largest LWC to be expected as an average is about 0.4 g/m^3 at 0 C. Alternately, the curves indicate the longest distance over which a given LWC may be expected to last. For example, a LWC of 0.7 g/m^3 can be expected to persist, as an average, no longer than about 20 nm, and that would only be at temperatures of about -10 C or warmer. Similarly, at temperatures of -30 C or colder, no supercooled cloud is expected to last as long as 100 nm.

2.2.3.3 ***MVD Limits.*** Figure 2.2-5 shows the reduction in maximum available LWC as the MVD deviates from about 15μm, which is about the mean value for MVD's in stratiform clouds overall. The curves show, for example, that MVD's of 25 μm or larger are found in only 4% of icing encounters. For 25 μm MVD's, the observed LWC limit is about 0.4 g/m^3 over distances up to about 15 nm. The available LWC then drops off with increasing averaging distance beyond 15 nm. In fact, no clouds have been found to sustain an MVD of 25 μm over more than about 40 nm. In other words, the curves in figure 2.2-5 are limits to observed horizontal extent as well as to LWC.

This has implications for flight tests too. It means that if one is searching for MVD's of 25 μm or larger, they can be expected in only 4% of the icing encounters, assuming a mixture of cloud conditions like those represented by the data in figure 2.2-1. It also means that once found, the larger the MVD the shorter it may be expected to last.

2.2.3.4 ***Altitude Limits.*** Figure 2.2-6 shows the observed limits to LWC in stratiform clouds as a function of altitude above ground level (AGL). The largest LWC's occur in the altitude range between about 1.5 km (5000 Ft) and 4.5 km (15,000 Ft) AGL. Above 3 km the maximum available LWC decreases with increasing altitude. This is due to the generally thinner, colder, drier clouds at these altitudes.

2.2.4 Plotting Other Icing-Related Variables.

This continues the idea of converting the original axes to other useful variables. Basically, anything that is directly related to LWC can easily replace LWC on the ordinate.

2.2.4.1 ***The Water Catch Rate (WCR).*** This is an important variable because it governs how fast ice can build up on an object. The WCR is given by

$$WCR = E(d,v,g) \times LWC \times TAS$$

where E is the collection efficiency of the test article, LWC is the liquid water concentration in the icing cloud or water spray, and TAS is the true airspeed relative to the test article. The symbols in parentheses after E are put there to indicate that E is an involved function of the droplet sizes, the velocity of the impinging droplets, and the geometrical shape of the test article itself.

Depending on the details of the application, E can be either a macroscopic or microscopic collection efficiency. That is, it can be an overall (gross or net) collection efficiency for the entire test article or representative cross-section thereof, or it can be a point collection efficiency for finer work. An example of the latter would be studying the variation or the details of ice accretion at specific locations on the object. In either case, E ranges from 0 to 1. Typical gross collection efficiencies are of the order of 0.1 or 0.2. The numerical value of E can change with time as ice accretes on the object and changes the shape of the leading surface. These changes cause the flowfield to change near the object, and hence the droplet trajectories and resultant ice deposition can be affected.

The presence of E makes WCR dependent on the individual object, but the product LWC x TAS is independent of the object. This product of LWC x TAS can be termed the rate of water interception (RWI). It gives the rate at which water mass would be swept out of the airstream by unit area of the object if the collection efficiency were unity. The RWI is useful when

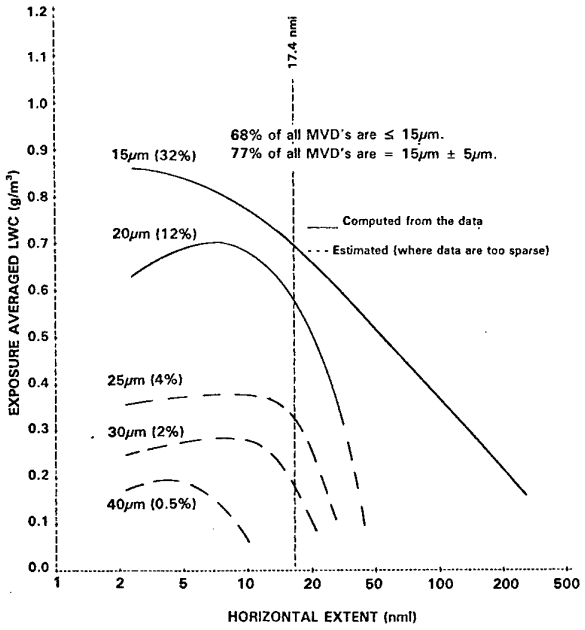

Fig. 2.2-5: The 99% Cumulative Maximum LWC for Different MVD's in Stratiform Clouds at Temperatures from 0 C to -10 C. (Percentages give the number of MVD's larger than the indicated value).

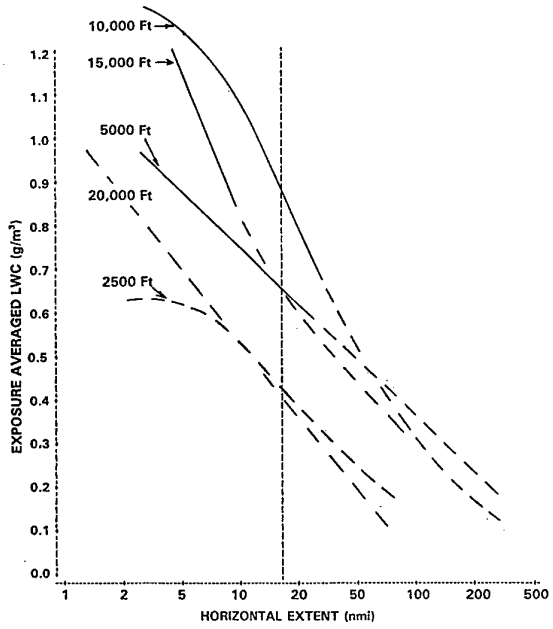

Fig. 2.2-6: The 99% Cumulative Maximum LWC at Different Altitudes (AGL) for Supercooled Clouds with Average MVD's (15 μm) and Highest Temperatures Available at the Altitude. (Summertime convective clouds excluded).

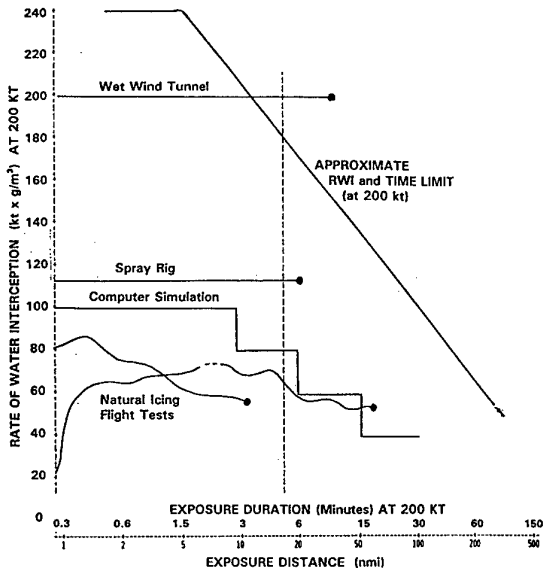

Fig. 2.2-7: Example of Converting the LWC Scale to Rate of Water Interception (RWI).

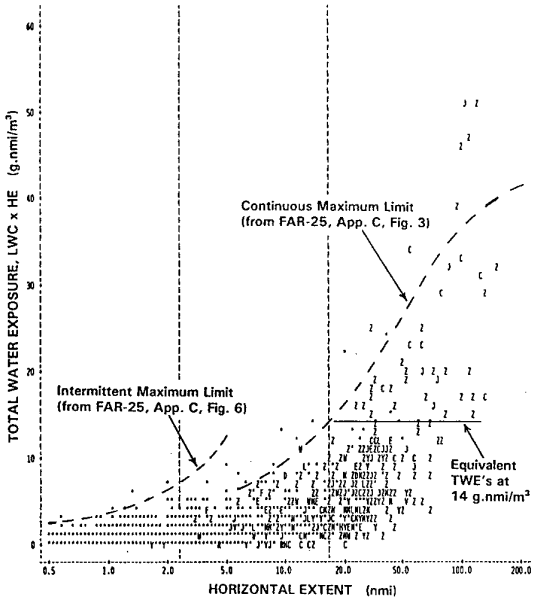

Fig. 2.2-8: The Supercooled Cloud Database Plotted in TWE vs. HE Format.

variable or unknown values of E makes it impractical to use WCR itself. One advantage of RWI is that it is more controllable and easier to measure than E.

Plotting RWI or WCR. The new plotting format nicely accomodates WCR or RWI as a variable replacing LWC on the vertical scale. One simply multiplies the LWC scale by the TAS of interest and it becomes an RWI scale. Figure 2.2-7 shows an example for TAS = 200 kt. Similarly, if E is known then E x RWI can be used to convert the ordinate to a WCR scale.

As with converting the horizontal axis to a time scale, neither the shape of the graphs nor the position of points and curves on them changes. The axes are relabeled, the original (LWC) data points are all automatically converted to RWI data points, and the LWC limiting curves automatically become RWI limiting curves. That is, for a given airspeed, the data points show what RWI's have been found in nature, and the limiting curves now show the maximum RWI's to be expected! This information can be used as guidance in selecting LWC and TAS combinations for icing wind tunnels or for computer simulations. The limiting curves can help ensure that RWI's are not selected that exceed natural limits.

Notice that the curves limit not only RWI but also the time that a given RWI can last in nature. That is, whatever the TAS may be, the limiting curves in Figs. 2.2-3 through 2.2-6 will automatically indicate the maximum RWI and exposure time to be expected at the chosen airspeed in natural icing conditions.

Principle of Equivalency for RWI. Because RWI is the product of LWC and TAS, different combinations of the two can produce the same RWI. This is an advantage for icing wind tunnels because practical limitations on available LWC can possibly be overcome by adjusting TAS accordingly. That is, LWC and TAS can be traded off reciprocally, as necessary, to achieve or maintain a desired value of RWI.

This tradeoff can also be applied to flights in natural icing conditions. There, an increase in TAS can compensate somewhat for a lower-than-desired LWC. Because E is a function of TAS but not of LWC, the collection efficiency, and hence the WCR, does not strictly obey this same equivalency rule. Greater airspeeds could also affect the actual ice formations through increased dynamic heating. But in practice, when the differences in TAS are not too large, WCR can be regarded as following the equivalency principle too, at least to a first approximation.

2.2.4.2 ***The Total Water Catch (TWC).*** The TWC is simply the mass of water (or ice) that has impacted (or accreted) per unit area on the surface of the object by the end of the exposure. The TWC is given by

$$TWC = E(d,v,g) \times LWC \times ED$$

where ED is the exposure distance (TAS x t) and t is the exposure time. As before, E is the collection efficiency.

Again, the presence of E makes TWC dependent on the individual object, but the product of LWC x ED is independent of the object. This product of LWC x ED can be termed the total water exposure (TWE). It is the total amount of water mass that would be swept out of the airstream by unit area of the object by the end of the exposure if the collection efficiency were unity.

Plotting TWC or TWE. The new plotting format also accomodates TWC or TWE as a variable replacing LWC on the vertical scale. One simply multiplies the LWC scale by distance and it becomes the TWC and TWE scale. Figure 2.2-8 shows the database plotted this way. Each former LWC datapoint is first multiplied by its HE to convert it to a TWE value. It is then plotted at its TWE value above the distance scale. Similarly, if E is known then E x TWE can be used to convert the points to TWC values. The ordinate scale remains the same.

In this case, however, the shape of the graph and the limiting curves are different than before. The data points now show which TWE's have been found in nature, and the limiting curves now show the maximum TWE allowable for any ED of interest. This information can be used as guidance in selecting LWC and exposure time combinations for icing wind tunnels or for computer simulations. The limiting curves can help ensure that TWE's are not selected that exceed those to be expected in nature.

Principle of Equivalency for TWE. Because TWE is the product of LWC and ED, different combinations of the two can produce the same TWE. This tradeoff can be used for gross ice accretion tests in natural icing flights. There, an extended ED (by successively re-penetrating the icing conditions, as necessary) can compensate for a lower-than-desired LWC. Because E may change with time as the ice builds up, TWC does not strictly obey this same equivalency rule. But in practice, when the changes in the size and shape of the ice are not too great, TWC can be regarded as following the equivalency principle too, at least to a first approximation.

Users must be cautious in substituting one LWC for another if ice shapes are important. A change in LWC will change the RWI too, and this could result in significantly different ice shapes even though the TWE is the same. The intricacies underlying these tradeoffs are more thoroughly reviewed in Chapter 4.

On the TWE graphs like figure 2.2-8, all the points along a given horizontal (TWE) line are equivalent. Points at different ED's along the line have different LWC's, but the product of LWC x ED is the same.

These graphs allow test results to be compared with each other and with design points in terms of their TWE's.

2.2.5 An Example Application.

Estimating Icing Exposures for Specific Situations. There is often the need to estimate how much ice and what ice shapes could accumulate on various components of an aircraft during various phases of flight in icing conditions. One example in particular is the turboprop commuter aircraft during takeoff and climb in icing conditions. During this critical time, it is possible for ice to accumulate on the wing leading edges. The deicing boots usually cannot be used effectively until a quarter- to half-an-inch of ice has accreted on them. In the meantime, the ice accretions could reduce performance and handling qualities of the aircraft during this critical phase of flight. Another example is the case where hot bleed air is temporarily unavailable for anti-ice protection of the wings on jet transport aircraft. This situation can also occur during the takeoff and climb phases when bleed air is purposely not extracted from the engines in order that full engine power is available for propulsion during takeoff and ascent. During this time it is possible for ice to accumulate on the wing leading edges if icing conditions are present along the flight path.

A procedure for estimating the maximum probable icing exposure is needed for this type of application. Presently, there are no such procedures described in the available advisory material on ice protection.

Using the overlay graphs in Figs. 2.2-3 through 2.2-6, one can easily estimate icing exposures as a function of altitude, outside air temperature (OAT), or other controlling factors. Flight scenarios can be defined in terms of airspeeds and durations at various altitudes, for example, and the worst case water catches (WC) and water catch rates (WCR) at different altitudes can be easily obtained from the overlays. These WC's and WCR's may then be used with available equations or computer models to estimate the total amount (mass) of ice accreted and its shape on components of the aircraft. A detailed example of estimating the icing exposures is worked out in the following section.

2.2.5.1 ***Basic Procedure.*** The present example uses a three-part process where one:

1) specifies a flight scenario (i.e., a flight path, airspeed, and time spent at various altitudes),

2) specifies the cloud conditions (i.e., cloud type (stratiform or cumuliform, or some mixture of both) and their vertical and horizontal extent), and

3) uses one or more of the overlays, as appropriate, to determine the maximum probable LWC exposure along the flight path through these clouds. A specific example follows. Any number of variations are possible, depending on the requirements.

Flight Scenario. Consider the flight phases of takeoff and ascent to cruise altitude. Assume a constant rate of climb such that the aircraft follows a slant path ascent of constant slope. Assume an airspeed of 200 kt during climb and assume a slope such that the aircraft travels about 20 nm in each 5000 Ft-deep layer centered at 5, 10, 15, and 20 thousand feet AGL.

Cloud Conditions. Assume that the aircraft is in continuous stratiform icing conditions from 2500 Ft AGL to 22,500 Ft AGL, and that cloud base is at 0 C (+32 F). Assuming a temperature decrease of about 1 C for every thousand feet in height, the cloud tops would be at about -20 C (-9 F). Also assume that the cloud droplets throughout the entire cloud have a median volume diameter (MVD) of about 15 μm (the average value for stratiform clouds in general).

Applicable Overlays. For this case both the temperature-limited and altitude-limited overlays (Figs. 2.2-4 and 2.2-6) are applicable. This is because the maximum available supercooled water concentration (SLWC) statistically varies with both altitude and in-cloud temperature. The amount of ice accumulated during the ascent can be estimated by summing the amounts of water accreted at various temperatures or altitudes along the flight path. Generally, the different sets of overlays will yield different estimates of total water interception for a given case. But one of the variables (either altitude or temperature in this case) will be dominant and will limit the LWC more severely than the other. After both sets of overlays have been tried, the one that limits the LWC to the smallest values is the one to be used.

2.2.5.2 ***Using the Altitude-Limited Overlays.*** These overlays (Fig. 2.2-6) may be used to estimate the maximum LWC exposure that could occur during the time spent at each altitude during the flight in icing conditions. Strictly speaking, this would involve an integration (sum) over many different altitude increments if the aircraft is continually changing altitude as in an ascent or descent. For simplicity, it is easier to divide the ascent into several coarse altitude intervals and assume that the LWC exposure within each interval is, on the average, the same as the central value. In the flight scenario specified above, this has been anticipated by postulating that the aircraft travels a distance of 20 nm within each 5000 foot altitude interval during ascent. Thus, the maximum LWC exposure for the interval between 2500 Ft and 7500 Ft AGL is represented by the maximum average LWC that would be expected for a 20 nm exposure at the mid-level altitude of 5000 Ft. From Fig. 2.2-6, this LWC is about 0.6 g/m^3.

The Total Water Exposure (TWE). The variable of importance in this particular application is really the total

water catch (TWC) and not just the LWC. The TWE is an atmospheric property that is readily available from the overlays and is independent of the aircraft. But TWC depends on the collection efficiency, E, and therefore varies with the aircraft component, airspeed, angle of attack, droplet size, etc. For this reason, we only show how to estimate the TWE in this exercise. The rest of the problem (computing ice accretion amounts and shapes) is beyond the scope of this chapter.

The maximum TWE's expected for each 5000 foot altitude interval are obtained simply by reading off the 20 nm-average LWC from the altitude-limited overlays in Fig. 2.2-6, and multiplying each LWC by the exposure distance (20 nm in this example). This gives the following table.

TWE ($nm.g/m^3$)	ED (nm)	LWC (g/m^3)	Altitude (Ft)
12	20	0.6	5000
16	20	0.8	10,000
12	20	0.6	15,000
8	20	0.4	20,000
48			

These values of TWE can be converted to more familiar units of grams per square centimeter, or pounds per square foot, etc. by use of the appropriate conversion factors.

The Rate of Water Interception (RWI). Like the total water catch, the water catch rate (WCR) is another important variable. The RWI is an atmospheric property that is readily available from the overlays and is independent of the aircraft. But WCR depends on the collection efficiency, E, and as before, this varies with the aircraft component, airspeed, angle of attack, droplet size, etc. As before, we show how to estimate the RWI in this exercise, and leave the rest of the problem (computing ice accretion amounts and shapes) to other chapters.

The maximum RWI's expected for each 5000 foot altitude interval are obtained simply by reading off the 20 nm-average LWC from the altitude-limited overlays in Fig. 2.2-6, as before, and multiplying each LWC by the TAS (200 kt in this example).

This gives the following table.

RWI ($kt.g/m^3$)	TAS (kt)	LWC (g/m^3)	Altitude (Ft)
120	200	0.6	5000
160	200	0.8	10,000
120	200	0.6	15,000
80	200	0.4	20,000

These values of RWI can also be converted to more familiar units of grams per second per square centimeter, or pounds per minute per square foot, etc. by the appropriate conversion factors.

In contrast to the water catch, the RWI's cannot be added for an overall total value. Each individual RWI (or WCR) must be used separately and sequentially in computations of ice shapes.

This illustrates a simple, realistic procedure for using one of the distance-based overlays for a hypothetical icing exposure. With these estimates of the rate and total amount of water interception, one can now compute ice accretion masses and shapes using other available formulas or computer codes, such as those described in Chapter 5.

Note: The *altitude*-limited overlays, as presented in the graph used here, give the limits to LWC for the warmest (but still sub-freezing) icing temperatures available at each altitude. These temperatures naturally decrease with increasing altitude, but in these altitude-limited overlays, the user has no control over the temperature selection for any given altitude. If particular temperatures are postulated, as in this example, the temperature may limit the available LWC more than the altitude does in certain cases. Therefore, the temperature-dependent overlays must be explored too, in order to arrive at the most realistic water exposures for a given flight scenario.

2.3 SPECIAL CASES OF ICING CONDITIONS--- FREEZING RAIN AND FREEZING DRIZZLE.

Freezing Rain and freezing drizzle (meteorological abbreviations are ZR and ZL, respectively) have been implicated in a number of recent commuter aircraft accidents and incidents. One notable example was the fatal crash of a commercial airliner on October 31, 1994 near Roselawn, Indiana in the U.S.A. Others include cases of uncommanded pitchovers of certain commuter aircraft during approach with ice on the tail section of the aircraft---a situation that has been given the name Ice Contaminated Tailplane Stall (ICTS). Nevertheless, no ice protection requirements currently exist for freezing rain or freezing drizzle. Theses conditions are presently considered to be "outside the envelopes" of normal icing conditions described by figures 2.1-1 and 2.1-3.

It is known from surface weather observations that freezing rain occurs mainly in central and eastern North America and in northern Europe. Freezing drizzle has a wider distribution over northern latitudes and has even been observed in the Arctic. Nevertheless, ZR and ZL are infrequent, occuring 4% of the time or less in North America during the colder seasons, and 1% of the time or less in Europe. Because of the possibly drastic effects, however, flight in ZR and ZL is normally avoided even by aircraft equipped with anti-icing or de-

icing devices. A distinction is made between ZR and ZL because of the differences in the formation mechanisms and the resulting differences in dropsizes and rain rates.

2.3.1 Freezing Rain.

Freezing rain results when snowflakes fall into warm (T > 0 C) air aloft, melt into raindrops, and then fall through a subfreezing layer of air again before reaching the ground. This is illustrated schematically in figure 2.3-1. The only difference between freezing rain and ordinary stratiform (widespread, steady, non-freezing) rain is the presence of a subfreezing layer from ground level up to perhaps a few thousand feet in the case of freezing rain. Ordinarily, air temperatures rise steadily with decreasing altitude, and therefore temperatures below the 0 C level aloft will ordinarily be warmer than freezing. Freezing rain requires a reversal in the temperature profile somewhere below the melting layer such that subfreezing temperatures are again present at or above ground level. This can occur in connection with a warm front when warm air overruns a subfreezing layer of air already in place.

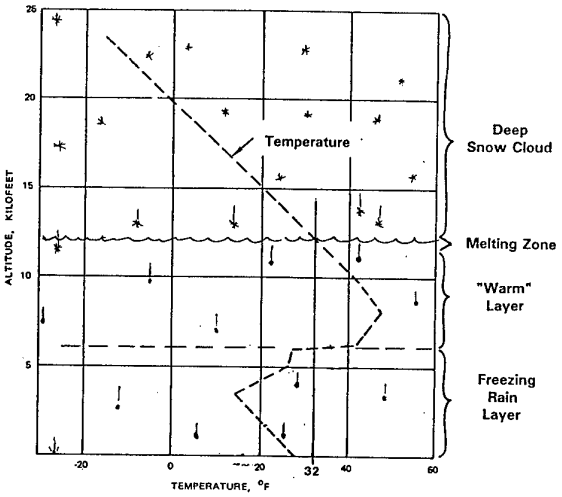

Fig. 2.3-1: Schematic Representation of Freezing Rain Conditions.

The warm interval aloft is a well-known feature which pilots are taught to use in order to escape inadvertent encounters with freezing rain in flight. The seemingly counter-intuitive rule-of-thumb is to *climb* to warmer temperatures. This is contary to the normal situation where you descend to find warmer air. In the freezing rain situation, there is no escape at lower altitudes because the temperatures may get even colder there, and the freezing rain continues all the way to the ground. The ground level temperatures may be only -1 C or -2 C, but in the middle of the freezing rain layer above, temperatures can reach -9 C or below. Freezing rain layers may be up to 7000 Ft deep (Jeck, 1996).

Although temperatures in the warm layer above can sometimes reach a comfortable, icing-free, +10 C, they may sometimes be barely warmer than 0 C. In this case, a cold-soaked airplane may still accumulate slushy ice from partially melted snowflakes impacting the cold airframe. The warm layer may or may not be cloud free.

Freezing rain usually causes conformal, widespread, glaze-like ice on the airframe and components. In thin amounts it may be clear, smooth, and difficult to see on the airframe. In larger amounts it may become somewhat knobby and easier to recognize. Although the effects are not well documented, they may range from an iced-over windshield to increasing power and angle of attack requirements in order to overcome the accumulating weight and drag of the ice.

2.3.2 Elevated Freezing Rain.

Freezing rain (ZR) and freezing drizzle (ZL) have been conventionally regarded as a ground-level phenomenon, or at least confined to a low-lying layer of frigid air less than 5000 Ft deep during the winter season in some geographic regions. But similar icing conditions can occur at higher altitudes in deep, vigorously growing convective clouds or thunderstorms in summer-like conditions. Changnon et al (1991) report that for large, growing convective clouds in Illinois, "Typical in-cloud results at -10 C reveal multiple updrafts that tend to be filled with large amounts of supercooled drizzle and raindrops". This means that aircraft penetrating the cores of these clouds in the 0 C to -20 C range can expect to encounter intense bursts of ZR or ZL too. It is not known how long these encounters can last, but because these clouds are usually of limited horizontal extent, the ZR or ZL is not expected to last as long as may be possible in stratiform clouds. Nevertheless, the windshield may ice over more than usual and prompt the flight crew to report severe icing conditions.

In these summertime, high-altitude exposures, there may be ample warm air below in which an aircraft can melt off any ice that it may have accumulated aloft. But it may not be realized that an aircraft may irrecoverably lose control due to ice accumulations aloft, even though warm air exists at lower altitudes. That was what happened in the "Roselawn" accident near Chicago on October 31, 1994. There, the freezing level in the area ranged from about 3000 Ft (1 km) to about 7000 Ft (2 km). So warm air was available for melting off the ice had the aircraft not lost complete control during the icing encounter at a higher level.

2.3.3 Freezing Drizzle.

Contrary to the rain process, drizzle develops totally within a liquid droplet cloud layer when the conditions are right. The melting snow process is not necessarily

involved and a "warm" layer is often absent. Drizzle is most familiar as experienced at ground level, where a "mist" of lightly falling droplets is descending from low clouds above. But drizzle is not confined to the region below cloud---it continues on up into and throughout the vertical extent of the cloud layer where it is being formed. Drizzle droplets may even be somewhat larger and more numerous *in* the cloud than below where partial or near total evaporation can reduce the sizes and numbers of the droplets on their way down.

Given enough time, some drizzle-sized droplets can eventually develop in any cloud that lasts long enough, is deep enough, and which contains enough condensed water. This process involves the gradual growth of some of the ordinary cloud droplets to a diameter of 30 μm or so until they begin to settle. Then they begin to collide and coalesce with other droplets on their way down through the cloud as they grow to drizzle droplet size (about 50 - 500 μm or so).

Most stratiform clouds do not seem to produce a significant amount of drizzle. But in certain conditions, including upslope clouds, warm front conditions, windy and turbulent cloud layers, and coastal maritime clouds, drizzle production can sometimes be unusually efficient.

Contrary to usual freezing rain conditions where a "warm" ($T > 0$ C) layer can be reached by climbing a few thousand feet, freezing *drizzle* often forms with no warm layer above it. In this case, the escape options are to turn back, climb above the cloud layer, or descend below the freezing level if it is high enough for ground obstacle clearance. Climbing above the drizzle-producing cloud layer may be preferable to descending below the freezing level. In flight below the freezing level a cold-soaked airplane may still accumulate ice from drizzle falling on the cold skin of the aircraft. This is especially true when the accessible "warm" temperatures are only one or two degrees celsius above zero. On the other hand, climbing increases the angle of attack which increases the rate at which freezing drizzle can accumulate as a thin but rough layer extending far back on the underside of the wing. Five minutes of exposure is known to produce considerable drag penalties and reduced rate of climb capability on some airplanes.

There is evidence that freezing drizzle can accumulate as an ice ridge behind the deicing boots of some aircraft, especially when the total air temperature (TAT) is slightly greater than 0 C. This ridge has the potential for modifying the airflow over the ailerons and causing roll anomalies.

Geographically, elevated ZL has been documented under certain conditions in stratiform clouds by research aircraft in California, northern Arizona, Colorado, Texas, and Newfoundland.

Low lying drizzle clouds can extend from near ground level up to 13,000 Ft (4 km) AGL (Jeck, 1996). This means that after takeoff the aircraft may not break out of the drizzle until it passes 13,000 Ft.

If there is cloud and drizzle below 5000 Ft AGL, then most likely there will be low ceiling conditions there too. This means that on descent you may be in freezing drizzle some or all the way to touchdown.

There may or may not be a warm ($T > 0$ C) layer at some level in the cloud. The upper part of the drizzle cloud may be warm and the lower part cold ($T < 0$ C), or vice versa. Or the cloud may be warm in the middle but cold in both the upper *and* lower parts.

2.3.4 Elevated Freezing Drizzle.

It has long been known that drizzle can readily form in low, warm, stratiform clouds at least 300 meters (1000 Ft.) thick in oceanic air masses. Dropsize measurements from instrumented aircraft flights in these clouds have been reported at least as far back as 1952. But until recently, "large droplets" indicative of elevated ZL in winter stratiform clouds were reported only occasionally (Lewis, 1947; Jeck, 1980; Cooper et al, 1984). All of these authors pointed out the potential significance for aircraft icing. Lewis noted the high collection efficiencies of large drops and that drops larger than 35 μm or so would probably be reported by pilots as "freezing rain" because of a similar appearance on the windshield. Jeck observed small concentrations of large droplets below some winter stratiform clouds and pointed out that helicopters flying below winter clouds to maintain visibility and to avoid icing may still experience some icing from these unexpected, large droplets. The first researchers to document performance degradations on an aircraft due to flight in ZL were Cooper et al. (1984). These were flights during cloud seeding experiments along the upslopes of the Sierra Nevada mountain range in California. They found that flight through these elevated ZL conditions could cause dramatic increases in drag due to the ZL droplets forming a thin but rough accumulation of ice under the wings.

With interest in ZR and ZL heightened among aviation-interested meteorologists and cloud physics research groups, the Canadians renewed their attention to ZR and ZL during recent field studies of storms and icing conditions in the Newfoundland coastal region. Indeed, at least two ZL episodes near 10,000 Ft (3 km) AGL were found and investigated by Cober et al (1995). They reported that these elevated ZL cases were the "most severe icing environment encountered" during the field study. In two of the four ZL cases, the ZL caused "a rapid accumulation of ice on the pilot's window". This prompted the pilot to quickly get out of the icing conditions, usually by climbing in altitude.

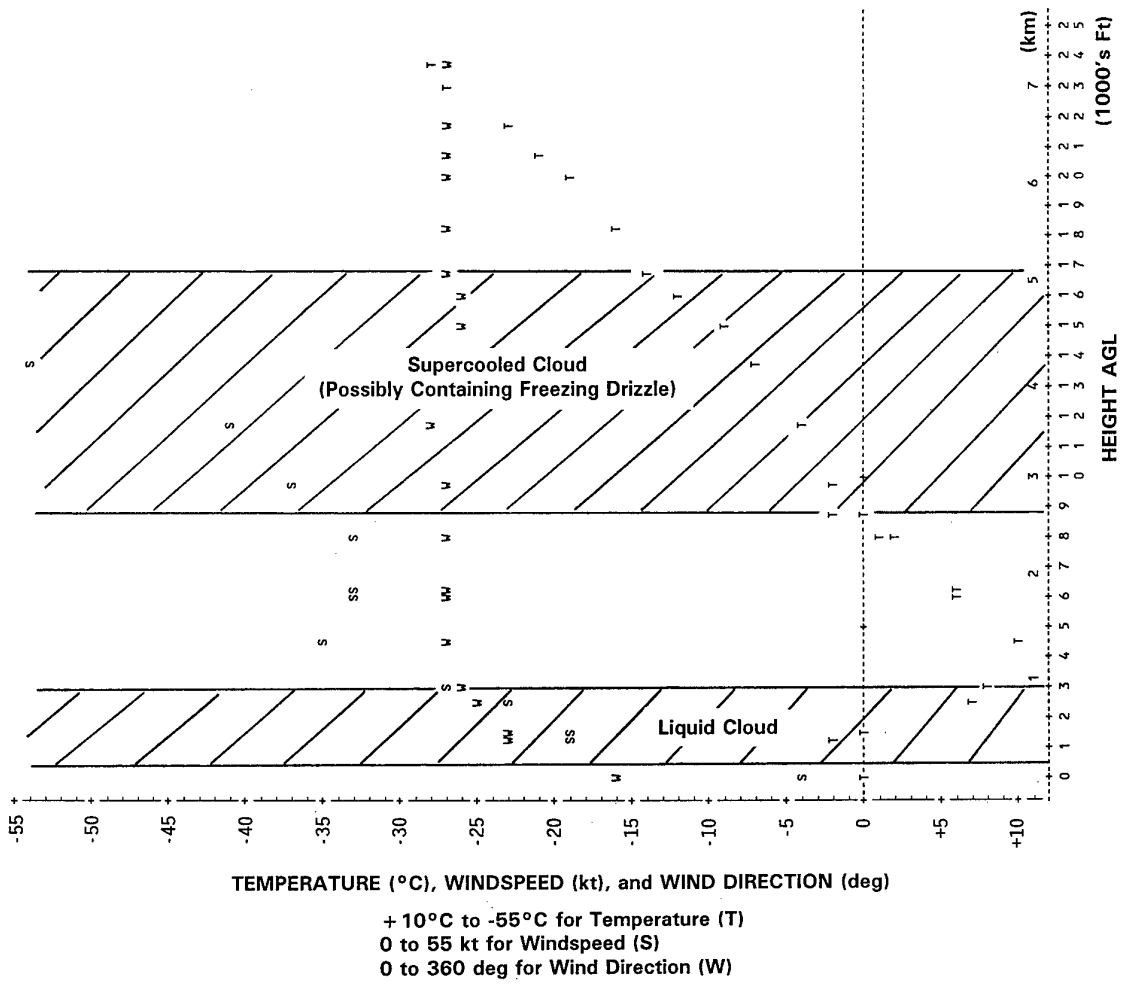

Fig. 2.3-2: Example of a Mid-Level Cloud Layer that May Contain Freezing Drizzle. Freezing drizzle and freezing rain were reported at the surface. Windshear and turbulence may be creating "large drops" (i.e., freezing drizzle) in the upper cloud layer at temperatures down to -15 C! Cloud layers were inferred from radiosonde humidity data (not shown). Case is for Washington, DC (IAD), Jan. 14, 1971.

Elevated freezing drizzle may occur in separate, non-glaciated (i.e., supercooled liquid droplet) clouds between 5000 Ft (1.5 km) and 20,000 Ft (6 km) AGL. These cloud layers are usually less than 8000 Ft (2.5 km) deep, with a drier, cloudfree interval above and below. The temperature is below 0 C throughout the elevated drizzle cloud. The temperature decreases steadily with height, sometimes reaching as low as -20 C at cloud top. Freezing drizzle may extend some distance below the cloud layer until the slowly falling droplets evaporate in the drier air below.

Figure 2.3-2 shows a case where the freezing drizzle that was observed at the ground may be forming in a turbulent cloud layer aloft.

2.3.5 Simulating Freezing Rain or Freezing Drizzle.

Simulation of these icing conditions in flight has not been a concern until recently. The relatively large droplet sizes may pose unanticipated problems for computer codes designed to represent normal sized cloud droplets. For one thing, the larger droplets mean a greater possibility of runback before freezing. This is a difficult aspect to model. Other problems exist for wet wind tunnels and airborne spray tankers. Until now, spray nozzles for these facilities have been selected and tuned to produce only small droplets that are typical of normal icing clouds. The large droplets that tend to occur in the sprays have been previously considered to be a troublesome nuisance. Now the nozzles are being re-examined in the hope of producing a drizzle-like spray of droplets when required. Tentative values of icing-related variables in ZR and ZL are given in a recent review (Jeck, 1996).

References

Changnon, S.A., Czys, R.R., Scott, R.W., and Westcott, N.E. (1991), "Illinois Precipitation Research: A Focus on Cloud and Precipitation Modification", *Bull. Amer. Meteor. Soc.*, Vol. 72, pp. 587 ff.

Cober, S.G, Isaac, G.A., and Strapp, J.W. (1995), "Aircraft Icing Measurements in East Coast Winter Storms". *J. Appl. Meteor.*,Vol 34, pp. 88-100.

Cooper, W.A., Sand, W.R., Politovich, M.K., and Veal, D.L. (1984), "Effects of Icing on Performance of a Research Airplane", *J. Aircraft*, Vol. 21, pp. 708-715.

FAA (1994a), Federal Aviation Regulation Part 25 (FAR 25), "Airworthiness Standards: Transport Category Airplanes", Appendix C, (Code of Federal Regulations, Title 14, Chapter 1, Part 25, Appendix C), Superintendent of Documents, Government Printing Office, Washington, DC 20402.

FAA (1994b), Federal Aviation Regulation Part 29 (FAR 29), "Airworthiness Standards: Transport Category Rotorcraft", Appendix C, (Code of Federal Regulations, Title 14, Chapter 1, Part 29, Appendix C), Superintendent of Documents, Government Printing Office, Washington, DC 20402.

FAA (1973), Advisory Circular AC 20-73 (1071), "Aircraft Ice Protection", Federal Aviation Administration, 800 Independence Ave. S.W., Washington, DC 20591.

Hacker, P.T., and Dorsch, R.G. (1951), "A Summary of Meteorological Conditions Associated with Aircraft Icing and a Proposed Method of Selecting Design Criterions for Ice-Protection Equipment", NACA TN 2569.

Jeck, R.K. (1996), "Representative Values of Icing-Related Variables Aloft in Freezing Rain and Freezing Drizzle", Technical Note DOT/FAA/AR-TN95/119, FAA Technical Center, Atlantic City New Jersey 08405.

Jeck, R.K. (1994), "Other Ways to Characterize the Icing Atmosphere", paper AIAA-94-0482, 32nd Aerospace Sciences Meeting, (Reno, Nevada, Jan 10-13, 1994), American Institute of Aeronautics and Astronautics, 370 L'Enfant Promenade, S.W., Washington, DC 20024.

Jeck, R.K. (1983), "A New Data Base of Supercooled Cloud Variables for Altitudes up to 10,000 Feet AGL and the Implications for Low Altitude Aircraft Icing", Report DOT/FAA/CT-83/21, FAA Technical Center, Atlantic City, New Jersey 08405.

Jeck, R.K. (1980), "Icing Characteristics of Low Altitude, Supercooled Layer Clouds", Report FAA-RD-80-24, FAA Technical Center, Atlantic City, NJ 08405.

Kline, D.B. (1949), "Investigation of Meteorological Conditions Associated with Aircraft Icing in Layer-Type Clouds for 1947-48 Winter", NACA TN 1793.

Lewis, W. (1969), "Review of Icing Criteria": page 3 in *Aircraft Ice Protection---Report of Symposium, April 28-30, 1969*; Engineering & Manufacturing Division, Flight Standards Service, Federal Aviation Administration, 800 Independence Ave., S.W., Washington, DC 20591.

Lewis, W., and Hoecker, W.H. (1949), "Observations of Icing Conditions Encountered in Flight in 1948", NACA TN-1904.

Lewis, W., and Jones, A.R. (1949), "Recommended Values of Meteorological Factors to be Considered in the Design of Aircraft Ice-Prevention Equipment", NACA TN 1855.

Lewis, W. (1947), "A Flight Investigation of the Meteorological Conditions Conducive to the Formation of Ice on Airplanes", NACA TN 1393.

Lewis, W., Kline, D.B., and Steinmetz, C.P. (1947), "A Further Investigation of the Meteorological Conditions Conducive to Aircraft Icing", NACA TN 1424.

Sand, W.R., W.A. Cooper, M.K. Politovich, and D.L. Veal (1984), "Icing Conditions Encountered by a Research Aircraft". *J. Climate Appl. Meteor.*, Vol. 23, pp. 1427-1440.

3. ICE ACCRETION AND ITS EFFECT ON AIRCRAFT

The operation of aircraft in a wide variety of weather conditions presents aircraft designers and operators with a wide range of issues. Furthermore the differences between aircraft, from small commuters, large jet liners, military aircraft and rotorcraft compound the complexity of assuring safety.

In the following chapter some of the most prevalent observations are described and discussed with particular reference to the aerodynamic effects of icing.

It is convenient to divide icing issues into two categories, according to whether they prevent an aircraft taking off, or impede it's subsequent flight. Take off is a particularly demanding phase of flight. Good performance is required both from the aerodynamics of the airframe, including flight controls, and the propulsion system. The subdivision of this section into ground icing and in-flight icing must not be taken to mean that the issues involved in one area can be ignored when dealing with the other. Consideration is needed for operational as well as technical issues.

3.1 TYPES OF ICE ACCRETION ON AIRCRAFT

3.1.1 Ground Icing

Way back in 1939, Jerome Lederer, President Emeritus of the Flight Safety Foundation stated:

"Strange as it may seem, a very light coating of snow or ice, light enough to be hardly visible, will have a tremendous effect on reducing the performance of a modern airplane. Although this is known in Canada for many years, only in the last three years has this danger been recognized here. It occurs only when the ship is on the ground, and makes take-off dangerous. To avoid this danger the airlines cover the wings with tarpaulins, or they make certain that all ice is off before the airplane is allowed to depart."

This warning has been embedded in three related Federal Aviation Regulations sections FAR § 121.629, FAR § 135.227 and FAR § 91. 527. For example: FAR § 121.629, operation in icing conditions, reads that: (a) no person may dispatch or release an aircraft, continue to operate an aircraft en route, or land an aircraft when in the opinion of the pilot in command or aircraft dispatcher, icing conditions are expected or met that might adversely affect the safety of the flight, and (b) no person may take off an airplane when frost, ice, or snow is adhering to the wings, control surfaces, propellers, engine inlets, or other critical surfaces of the aircraft etc., etc..

In a study of airframe ice related accidents from 1975 to 1981 (Cole and Sand 1991) an average of 13 accidents per year occurred on takeoff.

Ice presents a number of hazards to aircraft whilst on the ground. Deterioration of tire grip on the runway, pieces of ice falling into probes and engines, reduction of visibility through windows, obscuring of probes and antennae, and performance losses due to a contaminated airframe and disturbed engines can all become critical to safety.

Rain and Humidity

An aircraft can get quite cold whilst flying. Once it lands ice may well form on it even though the ground air temperature is above freezing point. Fuel in wing tanks has shown itself to have sufficient heat capacity to allow substantial sheets of ice to form.

Fig. 3.1-1a A piece of clear ice formed at the wing root of a cold soaked wing

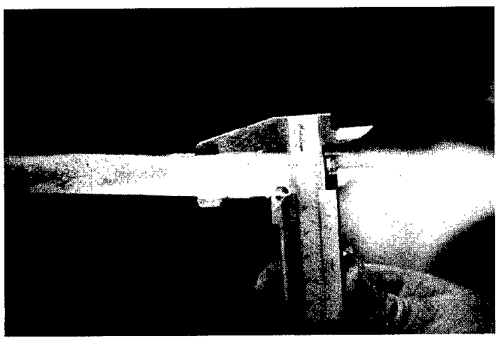

Fig. 3.1-1b The thickness of the layer, measured one hour after the incident, was 17 mm

Figure 3.1-1a and 3.1-1b (by courtesy of Mr. Paavo Turtiainen, Finnair) shows an ice shape removed from the upper wing of a grounded jet airliner. The aircraft was taking off at Helsinki airport on May 2, 1985 at 06.55 local time. During the take-off run at a speed of 80 kts the captain felt reduced acceleration. He noticed also

that the EPR-value of the right engine decreased momentarily. The take-off was aborted immediately. In the inspection on the apron a clear ice layer was detected on top of both wing tanks at the wing root area. The ice was about 20 mm at its thickness (Figure 3.1-1b). Some of the ice on both wings had separated and was ingested by the engines damaging fan blades. The aircraft had arrived after a flight of 3 hr 38 min to Helsinki the previous night. The aircraft stood on the apron six hours with 2400 kg fuel in both wing tanks. It was raining and snowing during that time. The temperature was near 0 C. The aircraft was de-iced before departure. It is noted that the photographs were made in the hangar one hour after the incident. Notice the very high translucency of the ice which makes identification very difficult for the crew. Ice was formed as a result of rain freezing on the cold-soaked wing in the vicinity of the fuel tanks. These ice formations can cause a severe hazard if they are able to slide into engines or strike the airframe. Following a number of incidents and accidents, ice detecting systems are becoming available to help recognize this hazard.

Snow, Sleet and Hail

Any icing precipitation, ice, water or mixed, falling on to an aircraft, or being ingested into probes and engines, may have the opportunity to warm and cool and adhere to whatever it comes into contact with. The effect of ice and snow on taxi-ways and the runway also needs consideration. It is worth noting that air movements generated by engines can concentrate ice particles into certain regions. Operational issues such as the use of reverse thrust for un-assisted taxiing can lead to unusual situations which may be unacceptable.

The possibility also exists that a loose layer of icing precipitation can conceal more significant ice which does adhere to the aircraft.

Hoar Frost

A hoar frost forms from atmospheric water vapour. It can form in apparently clear air and can occur at air temperatures above freezing point if the aircraft skin temperature is below freezing point. The pointed crystals can contribute to the roughness of the airframe. Often it's presence is obvious from the reduced visibility of any windows but it is not at all visible on light paint finishes when the light is diffuse.

Figure 3.1-2 shows different kinds of hoar frost samples. These were grown naturally by exposing flat aluminium plates to the night sky and preserved using a dissolved plastic solution (Kind and Lawrysyn 1991). It will be clear that this is not a real ice shape but the surface roughness is increased rapidly. Expressing the roughness in terms of an average height, k_f, of the highest 20 percent of the frost formations, the values of k_f for each frost sample shown equals: $k_f = 0.5$ mm for frost plate 2, $k_f = 0.4$ mm for frost plate 3 and $k_f = 0.27$ mm for frost plate 6.

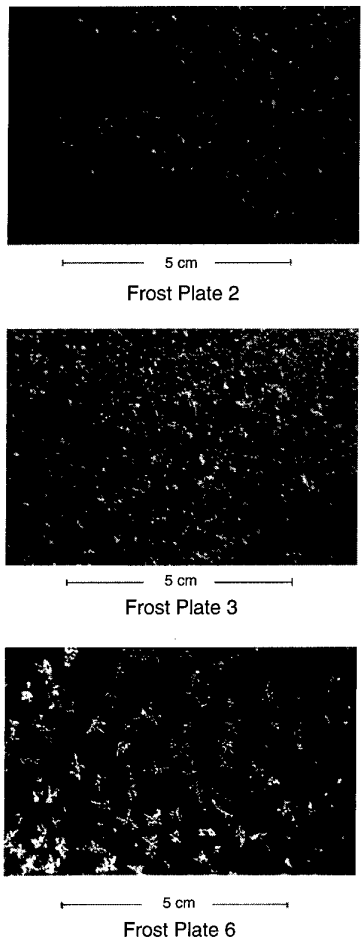

Fig. 3.1-2 Hoar frost samples

Freezing Fog

The influence of freezing fog is not limited to the leading edges of the wing or empennage, it will totally cover an aircraft when it is on the ground.

Low levels of distributed roughness can result in significant losses in lift and increases in drag. Since ice is highly variable and subject to melting and sublimation, it is more convenient to study the effects of distributed roughness by analogy with sand paper. In a study undertaken for the Fokker 50 (Van Hengst and Boer 1991) it was concluded that the deterioration could become very serious. Both the response of the elevator and the take off distance were strongly influenced by the simulated ice.

Rest Ice

Take off is a particularly demanding on the aerodynamic performance of the aircraft. Ice remaining on the airframe from the previous flight can contribute to control problems on take off even though it's effect was not noticeable during the previous cruise or decent. Tail planes can be particularly sensitive to this problem as well as being difficult to inspect.

In some circumstances, it is necessary to de-activate the anti-icing heating to probes when they are on the ground in-order to prevent them from overheating. This can make them vulnerable to ice build up during landing and ground movements (depending on the way they are controlled). They may well not work correctly on takeoff. Critical probes include those used for air-speed indication and those which provide data to engine and flight management systems.

Ground Ice Protection

The provision of ground de-icing facilities has provided considerable operational benefits to the aviation business. Currently fluids containing freezing point suppressants provide the means of both clearing and protecting aircraft.

The application of un-thickened solutions of freezing point suppressants or warm water is adequate to clear ice from an aircraft. Once cleaned however this method provides no protection against subsequent precipitation. This process is referred to as aircraft ground de-icing and the fluids are commonly referred to as "Type 1" fluids.

Further protection can be achieved by the use of the so called "Type 2" anti-icing fluids. These have non-Newtonian properties which help them form a more permanent film on the upper surfaces of the airframe. As the aircraft accelerates prior to take off the aerodynamically induced shear forces cause the viscosity of the fluid to fall and it slides off the airframe diluted by the icing precipitation which has fallen since it was applied. In practice some residues of the fluid may still be present as the aircraft rotates and lifts off, depending on the wing configuration, aircraft rotation speed and time to reach the rotation speed from brake release, amongst other factors, these residues can become significant (Hendrickson and Hill 1987 and Hill and Zierten 1991).

The length of time over which Type 2 fluids remain effective, the so called hold-over time, depends on a number of factors. There is current interest in developing sensors which can monitor the condition of the applied fluid.

The aerodynamic effects of type 2 anti-icing fluids has been studied further (Carbonaro 1991 and Laforte et al. 1991) and an aerodynamic acceptance test is available (Proceedings of the FAA Reston Conference 1992).

The environmental and operational cost of fluid based ground de-icing is prompting serious consideration of the re-cycling of fluids and the development of alternative methods. An experimental gas driven infra-red ground de-icing installation supported by NASA is in operation at Greater Buffalo International Airport.

Icing contamination can be detected by a number of methods and a number of sensors suitable for ground use are becoming available. It is relatively easy to conceive systems for guidance, but the current terms of reference for pilots reduce the value of such indicators. The development of acceptance criteria and instrumentation for individual aircraft types could yield significant operational benefit, a reduction in the number of aircraft treated, and valuable support for the flight crew.

3.1.2 In-Flight Icing

Flight through clouds is now accepted as normal for many types of aircraft. The water droplets in clouds frequently remain liquid even though the ambient temperature is well below freezing point. (in clear air the temperature drops approximately 7 C for every 1 Km of altitude gained). It is the encounter of these droplets by the aircraft which causes the build-up of airframe ice. The effect of ice formation on an airplane in flight is threefold: (1) changes of stability characteristics, (2) changes in lift and drag, (3) added weight to the airplane.

Statistical analysis of meteorological and cloud physics data, collected both on ground as well as in flight, has given us the JAR/FAR 25 appendix C guidelines for icing clearance. It was decided to use this statistical approach (1946) because of the lack of knowledge of the fundamental physical processes that determine the structure of clouds and cloud systems. The collected data, recently reviewed by R. Jeck (AIAA-94-0482), provide a convenient series of cases which give a good impression of the most severe cloud conditions an aircraft is likely to encounter. In practice the complex interaction between different aircraft and different meteorological conditions means that additional moderation is required from the aviation authorities from time to time.

Only limited flight testing is done in storms, and, thanks to the wide spread use of weather radar, very little flying is done in such conditions. There are however issues relating to the avoidance of storms as it is not always easy to gauge their severity from radar data. In addition to the threat from supercooled water, the strong winds in and around the storms can contain large concentrations of ice particles which can interfere with engines and probes.

Ice accretions on aircraft form either directly by the freezing of the water droplets with which they collide, or indirectly, by the freezing of water liberated by melting ice, or other water sources, as it runs over the aircraft and freezes. Ice formed from collision with water droplets is called "Impact ice". Ice formed from running water on the surface downstream of leading edge is called "run-back ice".

Ice partially remaining on the de-icing devices due to incomplete shedding is called residual ice. This type of ice will also occur in the case of large droplets impinging behind the active boots. Only the ice on the boots will shed and the ice behind the boots may form a ridge.

Ice can also form in gas lines when condensation freezes.

Rime and Glaze Ice

As super cooled water droplets strike a body, they begin to freeze. If the conditions are sufficiently cold and dry, the freezing rate will be limited only by the rate of water uptake. In this case the freezing process is very rapid and the water only permeates the existing ice to a small degree. This gives a highly porous, optically opaque ice, often having a rounded profile. This is widely referred to as rime ice.

If the freezing rate is being determined by the rate of heat removal the water has more time to flow over the existing ice before it freezes and the accretion will be more dense. It will have a gray or even transparent appearance and a smooth, though often irregular surface. This is referred to as glaze ice. There may be what amounts to run-back ice around the periphery of the accretion.

As described above, rime and glaze ice represent extremes. In fact all impact ice accretions may be referred to as rime or glaze, depending on their subjective appearance. It is not easy to delineate between rime and glaze on the grounds of any one parameter as many factors combine to influence the final ice density. The terms however are widely used to give an impression of the ice. See Figure 3.1-3.

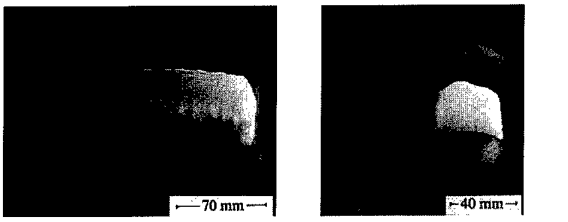

Rime Ice a) general view b) cross section view

Glaze Ice a) general view b) cross section view

Fig. 3.1-3 Two small ice accretions, one having a rime like appearance, the other, glaze

Ice accretions frequently develop as very irregular shapes and whilst water droplet temperatures may be reasonably uniform, the surface temperature of the accretion will not be. This does influence the degree of coalescence of water droplets with the ice prior to freezing. Ice accretions can then appear to be glaze like in some regions, and rime like in others. The term "mixed ice" is sometimes used in this case.

In natural icing encounters, clouds may be patchy and the ice accretions will reflect this in their micro structure. Figure 3.1-4 shows a fragment from a small ice formation made in an icing tunnel, but with periodic fluctuations in water droplet size and concentration. The ice has been sectioned and is viewed in transmission with light of mixed polarization. Darker regions are associated with greater porosity (more rime like).

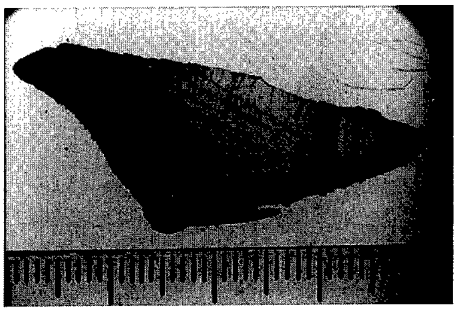

Fig. 3.1-4 Section of an ice accretion showing banded "tree ring" structure associated with variations in growth conditions

Glaze Ice

As we have already shown, glaze ice is not an easily definable type of ice but more an impression of general character. The internal structure of an ice accretion can however be characterized by using such criteria as density and grain size.

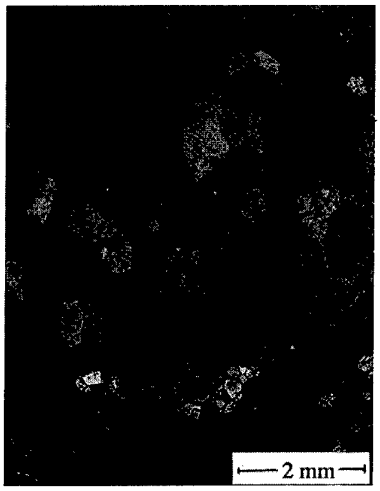

Fig. 3.1-5 300 µm thick slice of glaze ice

Figure 3.1-5 shows a 300 µm thick slice taken from the glaze like ice accretion shown in Figure 3.1-3. The piece of ice formed at -5 C, 0.8 g/m^3 LWC. It is illuminated in transmission using coloured light of circular polarization. It is then viewed in transmission (the use of white light gives a fine coloured image). Regions on the image

of uniform density are individual crystallites or grains within the accretion. It is clear that these grains have a length which is comparable with the thickness of the accretion, showing that the water has flowed freely and frozen coherently on to the underlying ice.
The width of the grains also tells us something about the initial speed of the freezing process. The lower the temperature, the narrower the grains.

Fig. 3.1-6 A thin section through a small glaze like ice accretion

The porosity of this ice accretion is low and mostly confined to irregularly shaped regions on the edges, where discrete ice protuberances have become bridged together.

The irregular shapes of glaze like ice accretions can make their effect on aerodynamics very severe.

Rime Ice
Rime ice has a finer structure than glaze ice as the water has less time to flow over and into the underlying ice. Figure 3.1-7 shows a thin section through the rime like ice accretion shown in Figure 3.1-4. The piece of ice formed at -20 C, 0.6 g/m^3 LWC.. The distributed porosity and fine grain size make it difficult to resolve the grain structure using the same procedure and equipment used to prepare Figure 3.1-7.

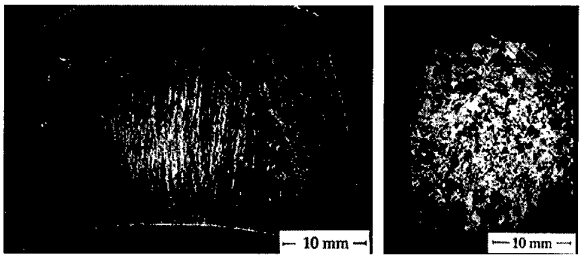

Fig. 3.1-7 Thin sections through a small rime like ice accretion. (parallel and perpendicular to growth direction respectively)

Run-back Ice
Run back ice is often associated with the re-freezing of water aft of a thermal anti-icing system. The ice forms slowly and is therefore dense and relatively clear (glaze like). It can form as a ridge aft of a heated area, often where some structural discontinuity might cause localized cooling. Figure 3.1-8 shows runback ice on the engine inlet of the Fokker 50 during a certification flight. Such a ridge can have a de-stabilizing effect on the boundary layer.

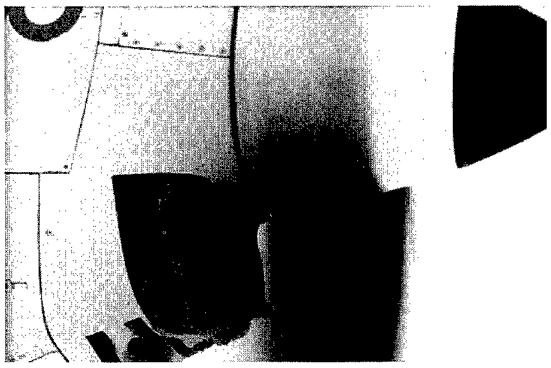

Fig. 3.1-8 Runback ice on nacelle intake

Specific to rotor blades, at combinations of high speed (rotor tip) and warm ambient temperatures, the only place where ice can form is the region of low pressure on the upper surface of the rotor blade close to the leading edge. Under these circumstances, a 'slushy' ridge of ice forms, termed **beak ice**. These accretions have been observed in rig tests and on rotors in flight. The accretion extends typically 2% chord in both, chordwise extent and height. The potential for performance degradation from this form of accretion is significant and should not be over-looked.

Ice from the Vapour Phase
In some circumstances ice will form direct from the vapour phase in sufficient quantity to threaten aircraft. One prevalent example of this is the congestion of carburettors on light aircraft. The significant expansion of air entering these components causes local cooling which can promote a rapid ice build-up even in clear mild air . In an analysis of icing related accidents from 1975 to 1988 (Cole and Sand 1991) 55% of the accidents were attributed to carburettor icing.

3.1.3 Examples of In-flight Ice Accretions

The extreme variety of icing which occurs in flight in natural conditions makes it impossible to deal with observations systematically. Incidents and accidents can involve patterns of icing which are completely unfamiliar before the observation is made. The following sections however provide examples of real icing situations to give an impression of how ice can look on an aircraft.

3.1.3.1 Wing and Empennage Leading Edges

Lifting surfaces such as wings, horizontal and vertical stabilizers will be significantly affected by icing, so these parts of an aircraft will be addressed first. Figure 3.1-9 and 3.1-10 (from AGARD 1978, paper 5) show typical rime and glaze ice accretion on a swept airfoil.

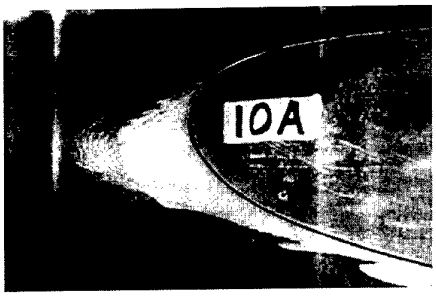

Fig. 3.1-9 Typical rime ice formation a on swept airfoil

Rime ice forms in conditions of low temperatures and low water liquid contents. The water droplets freeze on impact. Glaze ice forms in conditions of surface temperatures near freezing and high water contents. The water droplets freeze partially on impact and some run a short distance before freezing resulting in a double horn ice shape, Figure 3.1-10.

Fig. 3.1-10 Typical glaze ice formation on a swept airfoil

An other typical glaze ice shape is shown in Figure 3.1-11. This so called lobster tail ice accreted on a half model of a 75 degrs. swept delta wing at 15 degrs. angle of attack in an ONERA wind tunnel (AGARD 1978, paper 6). The ice shapes shown in the previous figures were obtained in windtunnel tests. The following pictures were taken during flights in icing conditions on various airplanes.

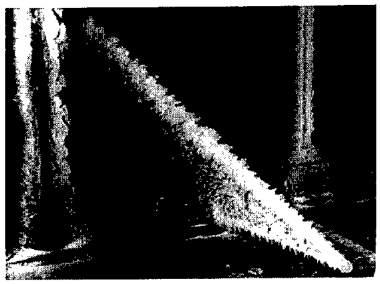

Fig. 3.1-11 Glaze ice formation on a delta wing

A very rough type of glaze ice, as shown in Figure 3.1-12a and -12b, accreted on the Fokker 50 during certification flight tests in icing conditions (Boer and van Hengst 1991). As part of the tests the boot activation was intentionally delayed until the ice thickness was 1 to 2 inch. Note that on the right hand inner wing ice was accreted on the whole boot area and possibly on the adjacent wing box also.

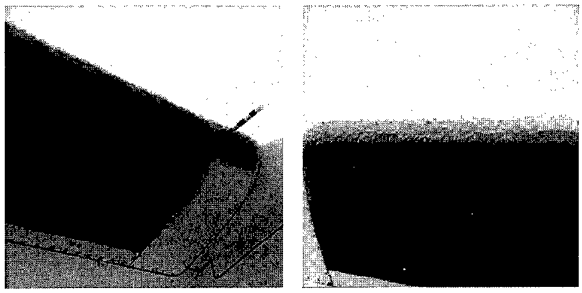

a) L/H inner wing b) R/H inner wing

Fig. 3.1-12 Rough glaze ice on a Fokker 50

Figure 3.1-13a and -13b show the ice accretions on the unprotected parts of the Fokker 50 wing. Ice also accreted on the outer wing flap fairing body, see Figure 3.1-13b.

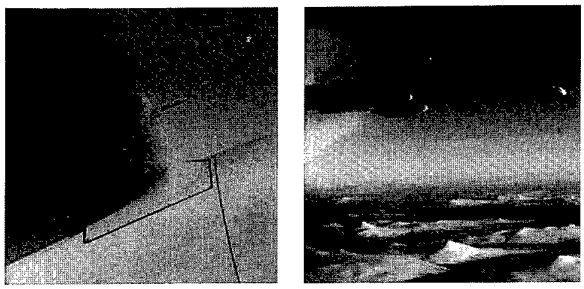

a) inner wing b) outer wing

Fig. 3.1-13 Typical ice formation on unprotected wing

Figure 3.1-14 shows the ice accretion on the leading edge of an Airbus aircraft. Note that the wing leading edge adjacent to the pylon remains free of ice.

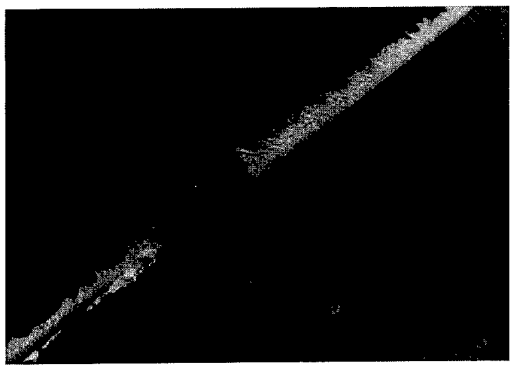

Fig. 3.1-14 Ice formation on an Airbus aircraft wing

Figure 3.1-15 shows the iced empennage of the Dornier 328 taken from a video camera installed in the rear fairing of the fuselage. Unfortunately there is no picture showing the shapes, but there is more ice at the unprotected tips of the horizontal tail and on the swept leading edge of the vertical fin there is typical lobster tail ice.

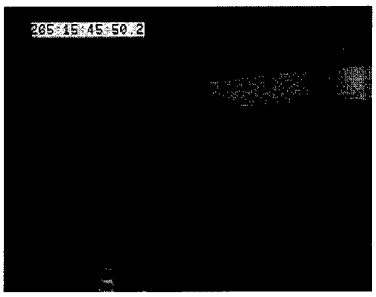

Fig. 3.1-15 Ice formation on the empennage of the Dornier 328

Residual Ice can be seen on Figure 3.1-16. This type of ice indicates the rest ice which will remain on or behind the de-icing boots following incomplete removal. One piece can be seen on the leading edge of the wing. The translucency of the ice indicates that it has already broken, but the adhesion forces still resist the aerodynamic forces. On the other hand there are a lot of ice feathers still remaining behind the mean ice shape on the boots. These feathers are thought to be the result of impinging single large drops, building a start-up for isolated ice accretion and will finally grow and look like fingers perpendicular to the surface.

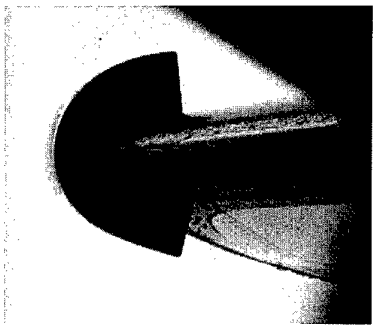

Fig. 3.1-16 Residual ice on the outer wing part

Finally, the ice accretion on the wing of the Fokker 100 is shown in Figure 3.1-17. Notice the ice accretion on the boundary layer fence.

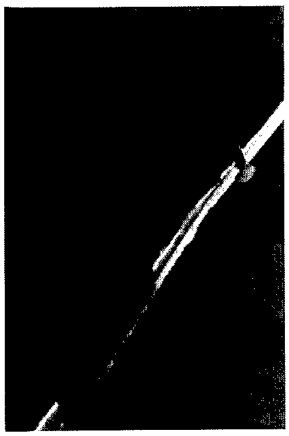

Fig. 3.1-17 Glaze ice on the Fokker 100 wing

3.1.3.2 Flaps, Slats, Balance Horns

This subchapter will describe what ice accretion on high lift devices and aerodynamic balances can look like. It is common for ice accretions on a deflected slat to look similar to ice accretions on a clean wing. A shape will accrete at the leading edge, forming rime, glaze or intermediate ice. At higher angles of attack ice will occur on the lower leading edge of the main profile just behind the slat and also at the leading edges of the deflected flaps. Additionally sometimes frost will cover the whole lower side of the flaps. Ice profile tracings on multi-element airfoil and corresponding performance losses (Potapczuk 1989) will be discussed in chapter 3.2.2. Figure 3.1-18 shows the shape of ice that can accrete on a protruding flap hinge bracket.

Fig. 3.1-18 Ice accretion on a protruding flap hinge bracket

Another problem which needs attention from the aircraft manufacturers is the icing of balance horns when control surfaces are aerodynamically balanced. If the aircraft is trimmed or the control surfaces are moved, the horn balances are exposed to free stream and to incoming water droplets so that they can collect ice. Dornier has investigated that problem with the Dornier 328. As a result the horn balances of that airplane are anti-iced by electric heating!

3.1.3.3 Propellers and Spinners

As propellers and spinners are exposed to incoming supercooled water droplets, they will accumulate ice. Propeller icing at the leading edges of the blades is normally limited to the inner 30% of the radius because increasing centrifugal loads on the outer blade radial stations together with the beneficial effects of kinetic heating force the ice to shed. Figure 3.1-19a and -19b shows a high speed photograph of rotating propeller taken during flight in icing conditions (Neel and Bright 1950). In some of the pictures of the thrust face of the blades (Figure 3.1-19b) the leading edge abrasion strips unfortunately give the appearance of ice formations and, therefore, should not be confused with the actual formations. The propeller rotational speed was 1025 rpm, the flight speed was 132 kts, the altitude was 8200 ft and the outside air temperature (OAT) was -13 C.

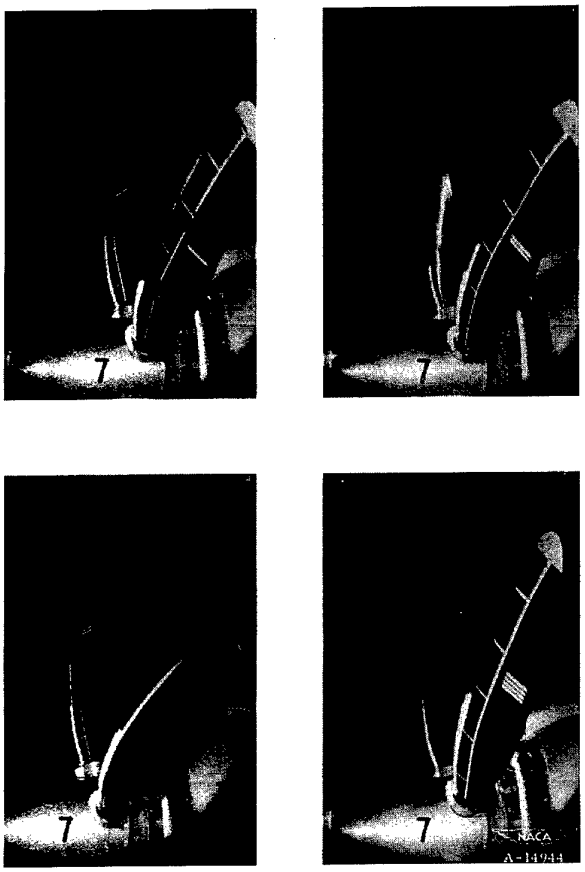

Fig. 3.1-19a Ice formation on a rotating propeller (camber face)

The icing condition during build-up was as follows: average LWC of .27 g/m^3, max. LWC of 1.08 g/m^3, MVD of 17 μm and average icing rate of 97 mm/hr. The ice build-up time was 20 minutes and the formation extended to 42 to 54 percent of the blade radius. The ice thickness was over 25 mm. On one blade the ice formation extended to 85 to 95 percent of the blade radius for which the thickness was less than 6 mm.

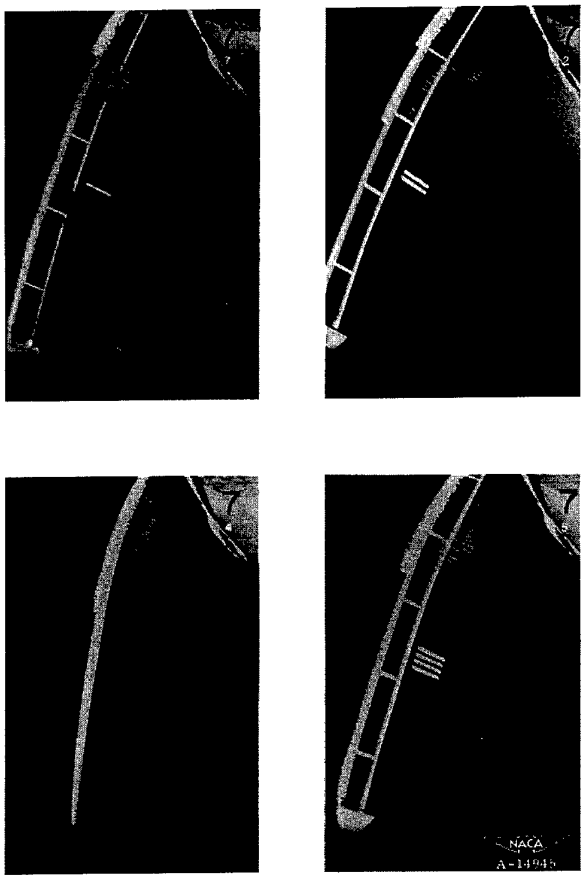

Fig. 3.1-19b Ice formation on a rotating propeller (thrust face)

Figure 3.1-20 shows the ice formation on the propeller and spinner of the Saab 340 (Rodling 1989). The flight conditions were altitude 8000 ft, 140 kts indicated airspeed, OAT= -12 C and the propeller speed was 1260 rpm. The propeller de-icing cycle time was 10 s on and 80 s off.

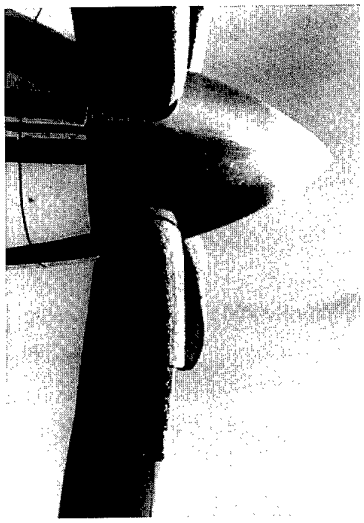

Fig. 3.1-20 Ice formation on propeller and spinner of a SAAB 340

3.1.3.4 Engine and Auxiliary Intakes

Any probe or inlet exposed to the free stream is vulnerable to icing in icing conditions. Figure 3.1-21 shows the inlet of the Dornier 328 when the boots have been inflated for the first time. Note the residual ice at the boots, the ice behind the spinner and at the upper lip cutback.

Fig. 3.1-21 Residual ice on intake lip after one de-icing cycle

The Fokker 50 engine intake lip is provided with an ice protection system consisting of integral electric heater elements. During certification flights the effect of reduced heating was investigated and the resulting run-back ice formation collected aft of the heated lip area was already shown in Figure 3.1-8.

Auxiliary inlets of the same pitot type may collect ice in a similar way (Figure 3.1-22), but it was also found that submerged inlets, such as a NACA type will accrete ice, even when placed in an area, where super-cooled water droplets do not normally impinge.

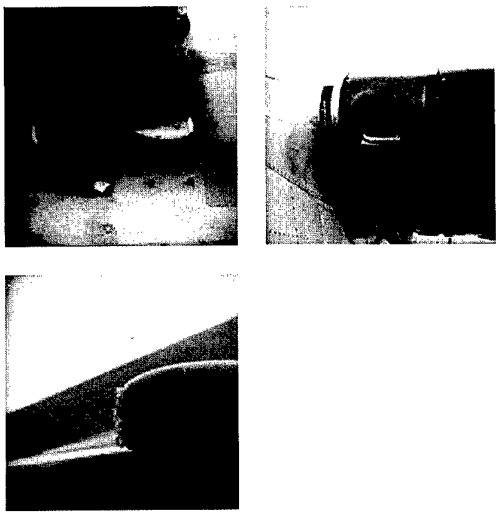

Fig. 3.1-22 Ice formation on unprotected auxiliary inlets

Figure 3.1-23 shows ice on the lip of a NACA inlet located in the Dornier 328 nacelle where the surrounding area is free of ice.

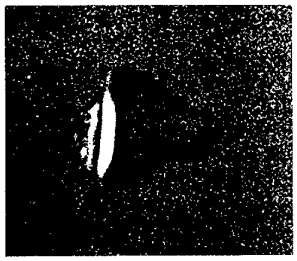

Fig. 3.1-23 Ice formation on a NACA type submerged inlet

Figure 3.1-24 shows the submerged vent inlet at the lower side of the Dornier 328 wing. Note the ice horn at the intake while the surrounding boot is clean.

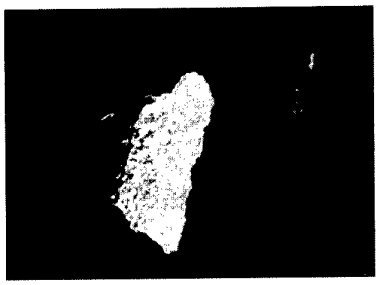

Fig. 3.1-24 Ice formation on a submerged vent inlet

3.1.3.5 Landing Gears, Wing Struts and Hinge Brackets

Fixed landing gears are vulnerable to icing like other unprotected parts of an aircraft and so they have to be addressed for definition and ice certification (see JAR/FAR 25-1419). NASA Lewis Research Center conducted an icing research program on their research aircraft, a twin engine commuter type aircraft. Examples of ice accretion shapes on wheel, landing gear strut, and wing strut were documented (Mikkelsen, et al. 1985) and are shown in Figure 3.1-25a and -25b.

(a) (b)

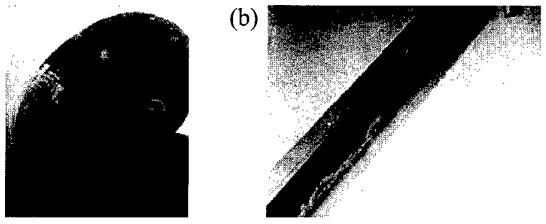

Fig. 3.1-25 Glaze ice formation on wheel and landing gear strut (a) and on wing strut (b)

Retractable landing gears may be critically affected if the wheel doors, especially the ones for the nose wheel, get blocked by ice accretion. It is worth noting that moisture in braking systems can freeze and create a wheel seizure to light aircraft on landing.

Two different types of ice formation on the aileron hinge brackets of a research aircraft, encountered in two different flights are shown in Figure 3.1-26a and -26b (Ranaudo, Mikkelsen, McKnight and Perkins 1984). Figure 3.1-26a shows glaze ice and Figure 3.1-26b shows rime ice on the bracket, both photographed after the landing. The icing conditions between the two flights were nearly the same, for Figure 3.1-26a: OAT of -4.6 C, the average LWC of 0.31 g/m^3 and MVD of 13 μm and for Figure 3.1-26b: OAT of -10.6 C, the average LWC of 0.29 g/m^3 and MVD of 13 μm. The only difference between the two flights was the duration of the ice encounter 26 minutes for Figure 3.1-26a and 46 minutes for Figure 3.1-26b.

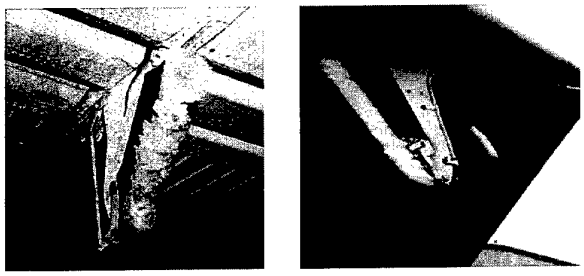

a) Glaze ice formation b) Rime ice formation

Fig. 3.1-26 Ice formation on aileron hinge bracket taken after landing

3.1.3.6 Radome, Antennas, Lights, Probes and Other Miscellaneous

Radomes and nose caps of an aircraft are very vulnerable to icing. Because of the fuselage size, the ice accretion at the nose is not so extensive as at a wing or tail. Figure 3.1-27 shows glaze ice formation on the radome of the aforementioned NASA icing research aircraft (Ranaudo, Mikkelsen, McKnight and Perkins 1984).

Fig. 3.1-27 Glaze ice formation on radome taken after landing

Figure 3.1-28 shows the ice shape after a flight through freezing rain on the same NASA icing research aircraft. Any type of antennae, lights or probes can also ice if they encounter water droplets. As these parts are very small, compared to a wing or a fuselage, the combined effects of the enhanced catchment of water drops and the small scale makes icing very significant.

Fig. 3.1-28 Ice formation from freezing rain on radome

The appearance of ice on such small parts is shown in Figure 3.1-29a and -29b. The photographs were taken of the cockpit entry step on the same aircraft and under the circumstances mentioned in Figure 3.1-26a and -26b (Ranaudo, Mikkelsen, McKnight and Perkins 1984).

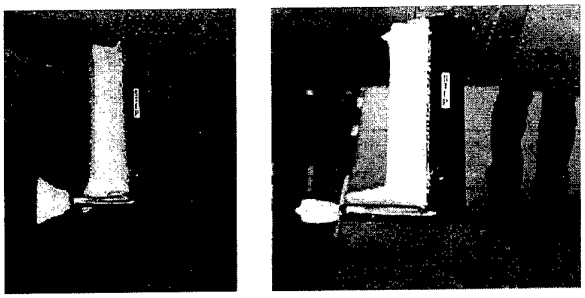

a) Glaze ice formation b) Rime ice formation

Fig. 3.1-29 Gaze ice formation on cockpit entry step taken after landing (a), rime ice formation on cockpit entry step (b)

The ice formation on the antenna of the icing research aircraft is shown in Figure 3.1-30. Ice on antennas and radomes, in addition to affecting the aerodynamics of the aircraft can have a major impact on the functionality of the radar and communication equipment. The icing of probes such as angle of attack or pitot static probes has to be prevented at all times. Electrical heat is presently the appropriate way to establish that.

It is also noted that vortex generators can collect ice, especially if installed at the leading edge of an aircraft part.

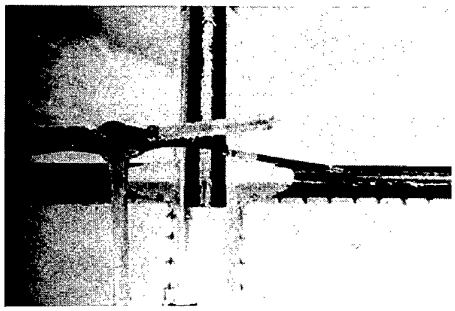

Fig. 3.1-30 Mixed ice (i.e., rime/glaze) formation on antenna mast

3.1.3.7 Windshield

If the anti-icing system is correctly designed, built, maintained and operated a windshield will never ice. In a case of a failure, ice will accrete because water droplets will always hit the screen. Figure 3.1-31 shows a picture of a windshield taken from the cockpit showing ice particles on the unheated part of windshield center frame.

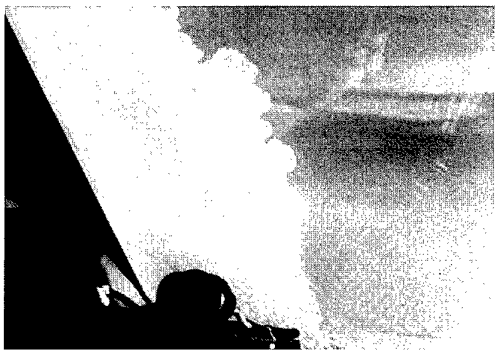

Fig. 3.1-31 Ice formation on unprotected windshield center frame of Fokker 50

Windshield wipers are not protected against icing, see Figure 3.1-32. These parts of the windshield can be used as a visual cue of icing to the pilot.

Fig. 3.1-32 Ice formation on windshield wiper and frame of Fokker 50

3.1.3.8 Rotors

Unlike ice accretion on wings and other non-rotating components, the type and extent of ice accretion found on rotors will normally change with distance from the root of the blade due to radial increase in freestream velocity and changes in centrifugal loading. It is therefore possible to have rime ice accretion form at inboard stations and for glaze ice accretion to form further outboard. In addition, and believed to be specific to rotors, under combinations of relatively warm ambient temperature and high speed, the only place ice can accrete is in the low pressure region close to the leading edge on the upper surface of the rotor. The slushy ridge of ice that forms has been termed 'beak' ice. This type of accretion has been readily observed during tests in icing wind tunnels on airfoils in non-rotating tests. The accretion tends to form and shed at regular intervals and typically extends to a maximum 2% chord in width and height. Examples of beak ice on a rotor are rare since the accretion tends to shed once the icing conditions have been vacated. However, during an icing trial on the EH101 helicopter being developed by EHI for the British Royal Navy, a special camera mounted on the main rotor head photographed the ice accretion shown in Figure 3.1-33. The photograph shows a ridge of beak ice on the upper surface which formed before the rotor ice protection system was energised. The approximate ambient conditions were: OAT of -4.9 C, LWC of 0.25 g/m^3 and MVD of 11 µm.

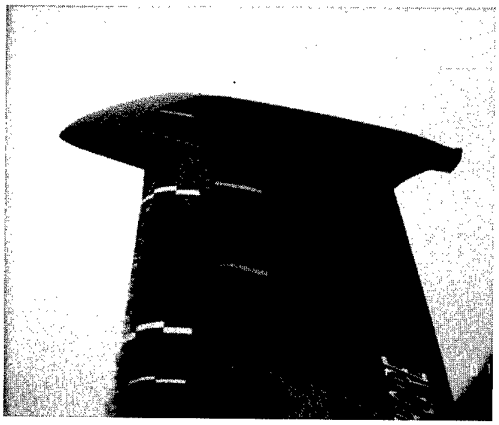

Fig. 3.1-33 Beak ice formation on a rotating main rotor of the EH101 helicopter

3.2 AIRCRAFT BEHAVIOR DEGRADATION

This subchapter will address adverse affects of icing on aircraft behavior and flight envelope with special reference to general aviation, commuter aircraft, and small transport aircraft. These categories of aircraft, because of their absolute size, are much more sensitive to icing than the large commercial transport aircraft. For example, J. Reinman explains (Reinman 1994), that the wings of a C-5A cargo aircraft are so large, that only a very small strip of ice will accrete on it, and as a result, the C-5A does not require any ice airframe protection!

3.2.1 Degradation of Aircraft Performance and Handling

From the aerodynamic point of view it must be said that especially for small aircraft there is no such thing as a little ice. Ice contamination on wings and tails reduces maximum lift and stall angle of attack and increases drag. Ice accretion on propulsion system components like air intakes, engine nacelles, inlet ducts, propellers, fan blades, spinners or inlet guide vanes reduces the propulsion efficiency and adds to aircraft drag.

During take off, iced aircraft will have increased ground roll, decreased stall safety margins and decreased climb rate. Ice on wing and/or tail surfaces during take off may cause serious stability and control problems with nearly every kind of aircraft, resulting in pitch up or down, roll off and possibly even crash.

In cruise iced aircraft have to be considered to suffer decreased speed and efficiency, reduced ceiling height, higher fuel consumption and a significant change in trim characteristics. For smaller fixed wing aircraft or multi-engined aeroplanes with one engine failed, the combination of reduced lift, increased drag and insufficient power can result in the loss of the capability for level flight.

During approach or landing, the combination of extended flaps and ice on the horizontal tail may cause tail plane stall, resulting in uncommanded pitch-overs for some aircraft. Ice on aircraft probes can give wrong airspeed indication or wrong engine pressure ratios that lead to wrong inputs to the FMS (Flight Management System) resulting in incorrect engine power settings and finally loss of aircraft.

3.2.2 Influence on Lift, Drag and Pitching Moment

This chapter will, in turn, address the aerodynamic penalties of ice contamination to two dimensional single airfoil sections, multi-element airfoils and the whole aircraft. Roughness will be addressed separately. The following pictures are taken from an investigation of ice accretion patterns and aerodynamic characteristics of a multi-element two dimensional airfoil conducted in the NASA Lewis Icing Research Tunnel (Potapczuk and Berkowitz 1989). Several configurations of main airfoil, slats, and flaps were employed. These tests have been run to provide information on performance change for a modern multi-element airfoil with ice accretion at many locations on the airfoil other then on the leading edge.

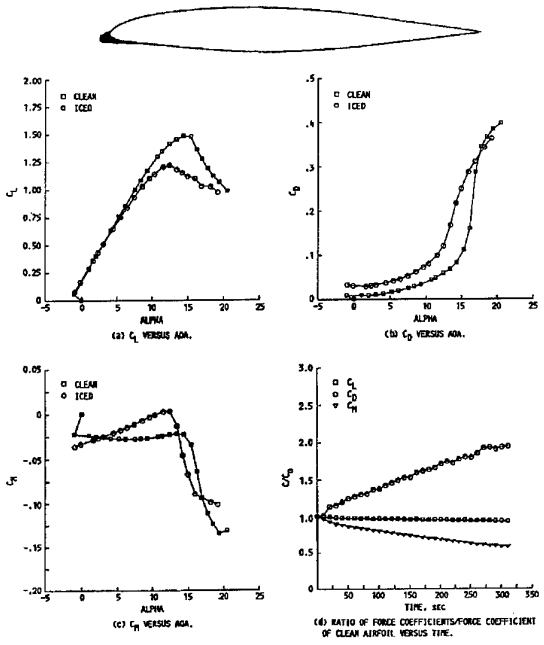

Fig. 3.2-1 Rime ice shape tracings and force balance measurements (cruise config., 5° AoA)

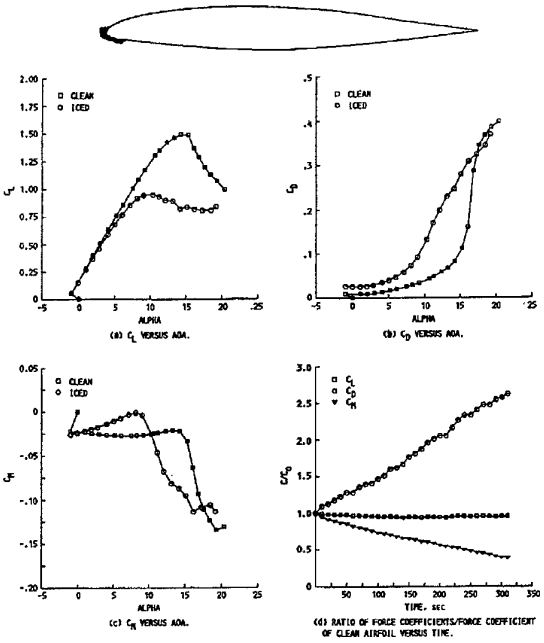

Fig. 3.2-2 Glaze ice shape tracings and force balance measurements (cruise config., 5° AoA)

The figures show lift, drag and pitching moment coefficients and a time history for the change of force coefficient over the icing time. Figure 3.2-1 shows data for typical rime ice, and Figure 3.2-2 data for typical glaze ice on the same single airfoil simulating cruise conditions. Ice was accreted at an angle of attack of 5° (5° AoA). Note that there is a maximum lift loss of about 40% for the glaze ice, which is about twice as high as in the case of rime ice. For both ice shapes, the drag coefficient is four to five times greater than for the clean airfoil (which means free of ice). The angle of maximum lift is reduced by 5°, also twice as high as for rime ice. The gradient in the pitching moment significantly increases in both cases. All these results indicate significant changes in aircraft performance and handling characteristics.

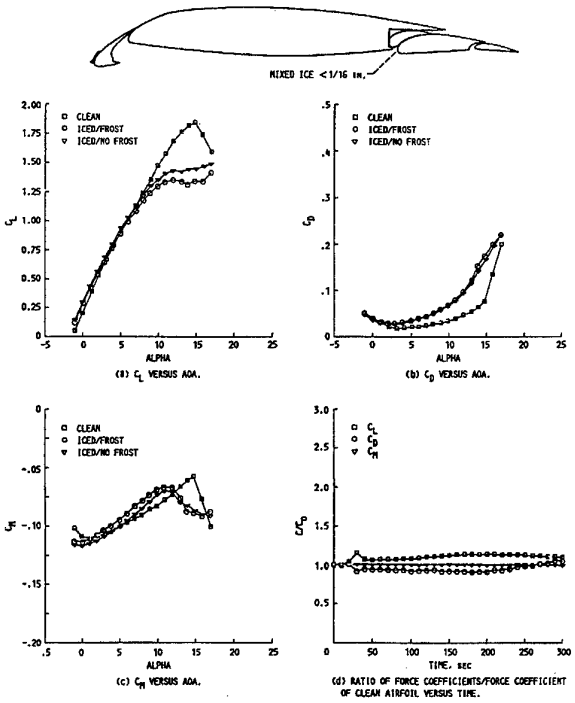

Fig. 3.2-3 Glaze ice shape tracings and force balance measurements (flaps 1° config., 0° AoA)

Figures 3.2-3 and 3.2-4 show data for a multi-element airfoil with the slat extended and the flaps at 1°, with glaze ice and frost accreted at 0° and 5° angle of attack respectively. Figure 3.2-5 shows data for the airfoil section with extended slat and flaps set to 5°; mixed type ice was accreted at 5° angle of attack.

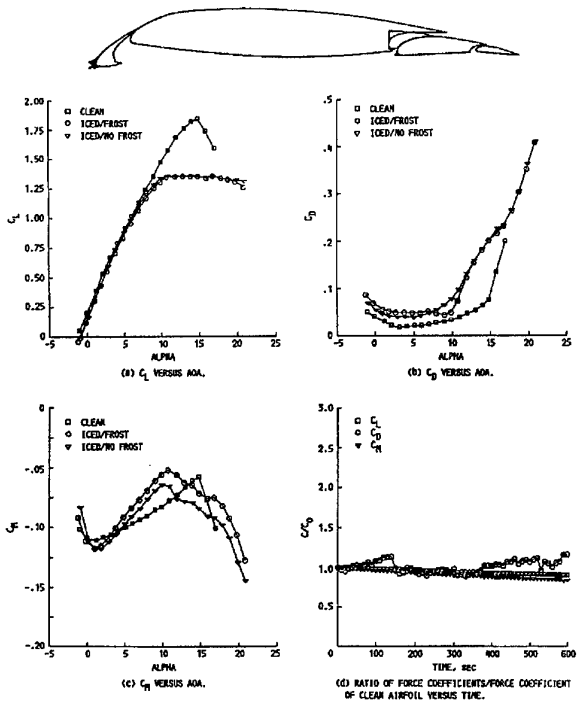

Fig. 3.2-4 Glaze ice shape tracings and force balance measurements (flaps 1° config., 5° AoA)

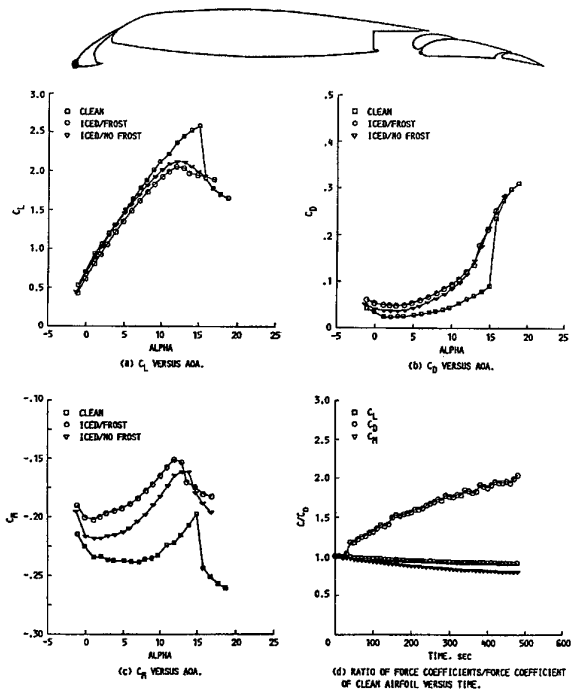

Fig. 3.2-5 Mixed ice shape tracings and force balance measurements (flaps 5° config., 5° AoA)

Finally Figures 3.2-6 and 3.2-7 show data for the airfoil with flaps at 15°; rime and glaze ice was accreted on the main profile, the slat and the various flap components. The results shown in Figure 3.2-6 have to be considered questionable, because it was found later that the force balance operated intermittently during this run.

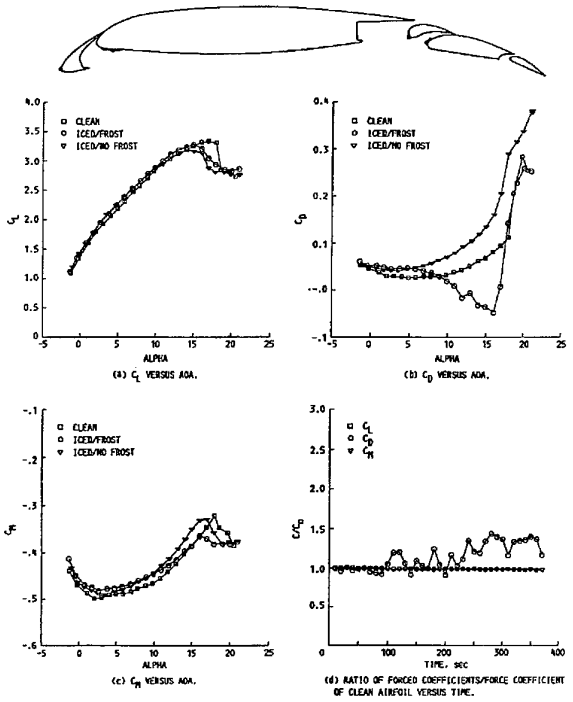

Fig. 3.2-6 Rime ice shape tracings and force balance measurements (flaps 15° config., 5° AoA)

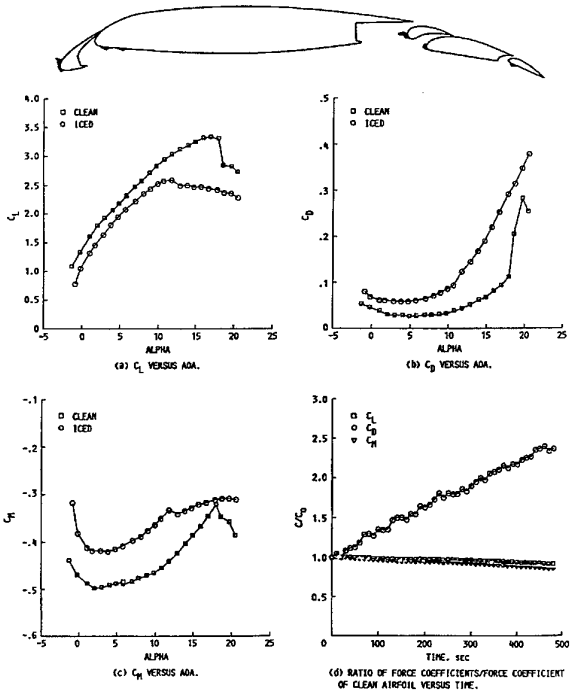

Fig. 3.2-7 Glaze ice shape tracings and force balance measurements (flaps 15° config., 5° AoA)

The salient changes in lift, drag and pitching moment for the configurations with flaps deflected are comparable to that of the clean airfoil, in particular when they are related to the type of ice and the extension of the shape.

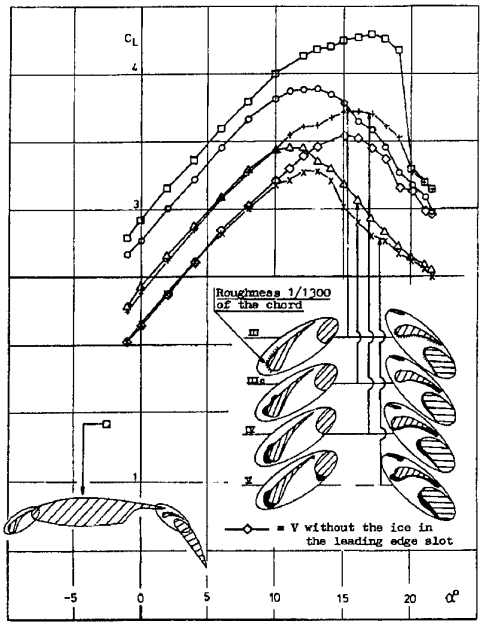

Fig. 3.2-8 Lift changes due to ice shapes on flaps and slats in approach configurations (slats 25°/flaps 45°)

Figure 3.2-8, taken from a Swedish-Soviet investigation on aircraft icing (Ingelman-Sundberg and Trunov 1977) also shows the influence of different leading edge ice shapes on the lift characteristics of a multi-element airfoil. This figure shows that all kinds of ice formation lead to a significant loss in maximum lift and stall angle of attack.

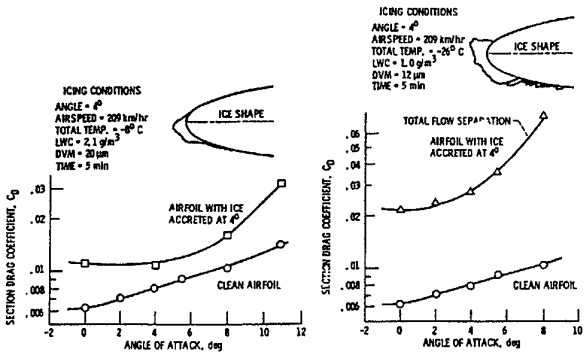

(a) Rime ice (b) Glaze ice

Fig. 3.2-9 Effect of ice shapes accreted at 4° on section drag coefficient

The effects of various atmospheric conditions on the drag characteristics of a 0.53m chord NACA 0012 airfoil was measured in the NASA Lewis Icing Research Tunnel (Olsen, Shaw and Newton 1983). Figure 3.2-9a shows how the section drag coefficient varies with angle of attack for a typical rime ice shape (accreted at a 4° angle

of attack). The drag measured for the clean airfoil is also plotted. The drag is at least 50 percent higher than the drag for the clean airfoil.

Figure 3.2-9b contains a similar drag-AoA sweep, except that the ice is a severe glaze ice shape. This glaze ice shape increased the drag coefficient considerably (about four times larger than the clean airfoil drag coefficient).

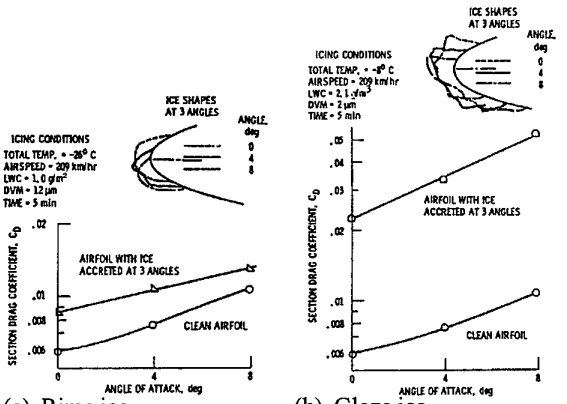

(a) Rime ice (b) Glaze ice

Fig. 3.2-10 Effect on section drag coefficient of ice shapes accreted at 3°

In Figures 3.2-10a and 3.2-10b the ice accretion at different angles of attack is shown. The effect of angle of attack upon the ice shape and the resulting drag are shown in Figure 3.2-10a for rime ice conditions, and in Figure 3.2-10b for glaze ice conditions.

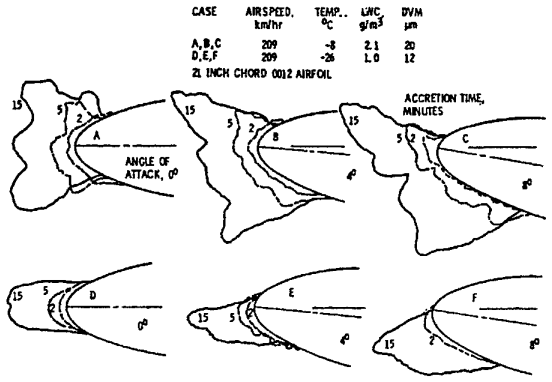

Fig. 3.2-11 Effect of accretion time and angle of attack on ice shape

The effect of the accretion time on the ice shape is shown in Figure 3.2-11. The ice was accreted at several angles of attack, each for two icing conditions. Cases A, B and C share the same icing conditions, which produced glaze ice. Each case is at a different angle of attack and involves typically three periods of spraying giving accretion times of 2, 5 and 15 minutes. Cases D, E and F are similar, except that the icing conditions for these three cases produced a rime type of ice. The ice shapes clearly show the ice history, starting from the clean airfoil out to a 15 minute growth.

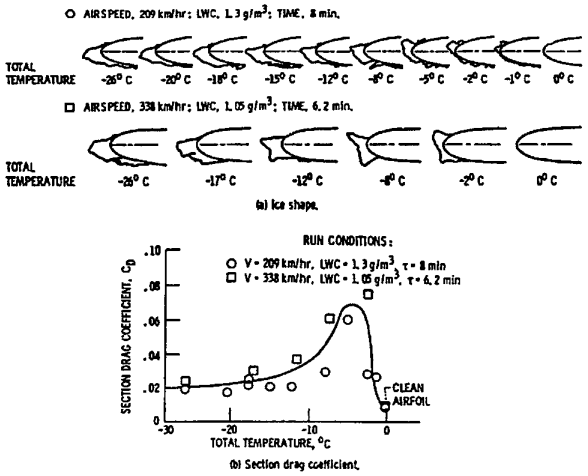

Fig. 3.2-12 Effect of total temperature on (a) ice shape and (b) section drag

As temperature has the greatest effect upon the ice shape and the ice structure, Figure 3.2-12a shows how the ice shape changes with increased temperature for two icing conditions. The ice at the coldest temperature is typically rime, gradually changing to a horn shaped glaze ice with increasing temperature. When the total temperature is very close to 0°C the impinging water droplets run off and do not freeze. Runs have been performed with the ice accumulation parameter (LWC x Velocity x Time) held constant with the airfoil at 4° angle of attack. The variation of the section drag coefficient with temperature for each icing condition is plotted in Figure 3.2-12b. The peak drag coefficient occurs at about -5 C, which corresponds to where the horns are the largest.

Airspeed can also have a large effect on the ice shape and the resulting drag coefficient, as is evident from the results shown on Figure 3.2-13.

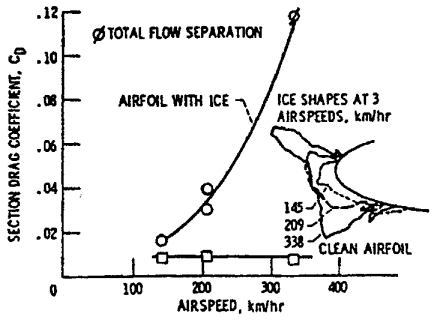

Fig. 3.2-13 Effect of forward speed on ice shape and section drag

The effect of drop size (MVD) is shown on Figures 3.2-14a and 3.2-14b for a number of cases (A to F). Each case involves a large variation in the drop size with the other parameters held constant. Figure 3.2-14a shows the drag increase, while Figure 3.2-14b shows the effect on ice shape. Using the results from Figure 3.2-12 additionally, it can be said that the drop size effect is greatest, wherever the temperature effect is greatest.

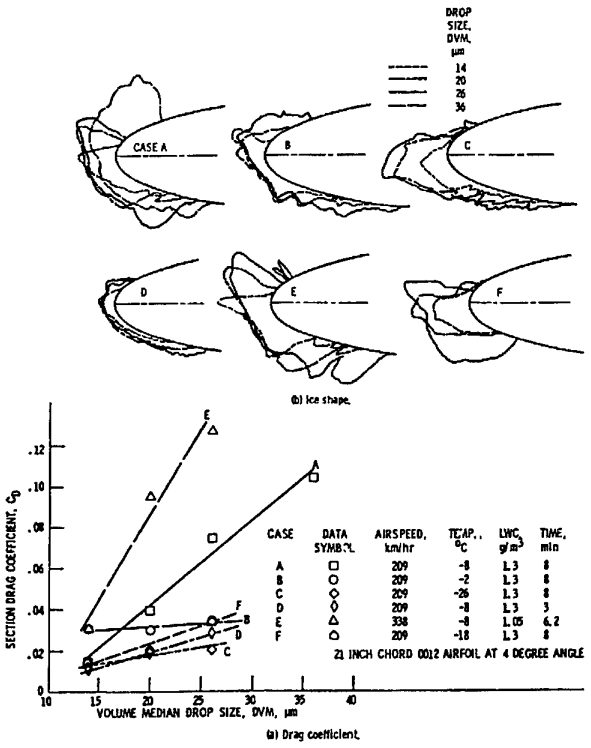

Fig. 3.2-14 Effect of drop size on (a) section drag and (b) ice shape

Figure 3.2-15 shows the effect of liquid water content (LWC) on the ice shape and the resulting drag. In combination with the results presented in Figure 3.2-12 again, the effect of varying the LWC is greatest, wherever the temperature effect is greatest.

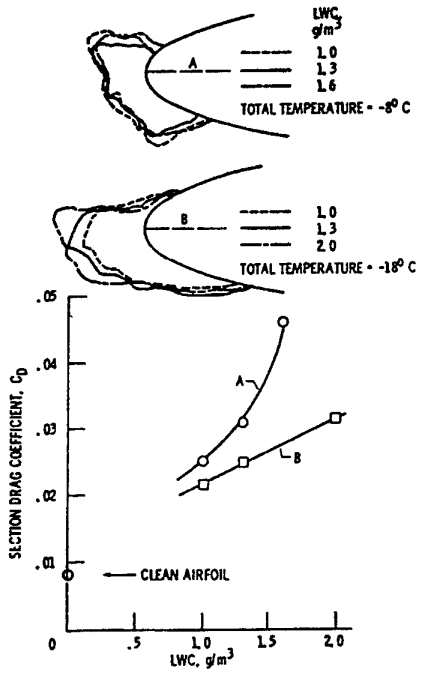

Fig. 3.2-15 Effect of LWC on ice shape and section drag

Finally Figure 3.2-16 presents the effect of partial ice removal shown for three drag-AoA sweeps. It clearly shows that the horn on the lower (pressure) side is less important than the horn on the upper (suction) side, but it cannot be neglected!

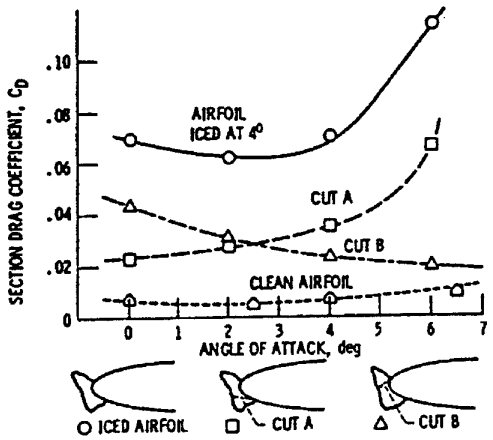

Fig. 3.2-16 Effect of partial ice removal on section drag

Continuing with the aerodynamic degradation of the aircraft due to icing, Figure 3.2-17 shows the overall effect of ice contamination on the lift characteristics of the Fokker 27 (Cattaneo 1991). This provides a further example showing essentially the same features. It will be discussed later how much loss in maximum lift and reduction in angle of attack for maximum lift can occur on contaminated aircraft at different flap angles and various ice and sand grain roughness.

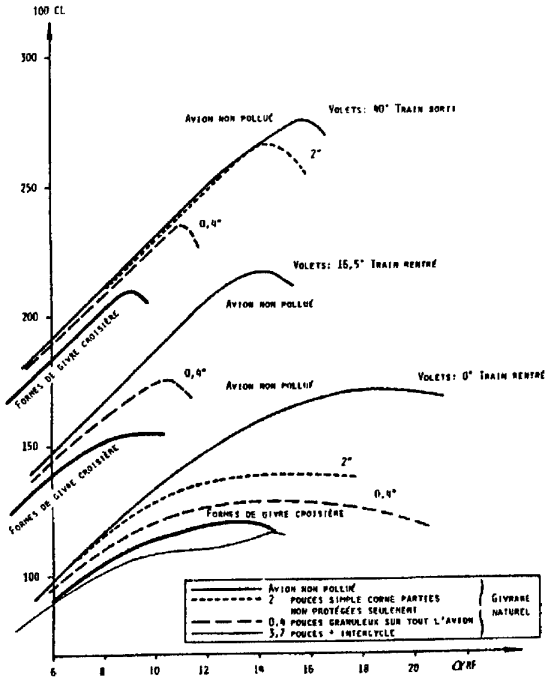

Fig. 3.2-17 Effect of ice accretion on F27 lift curve

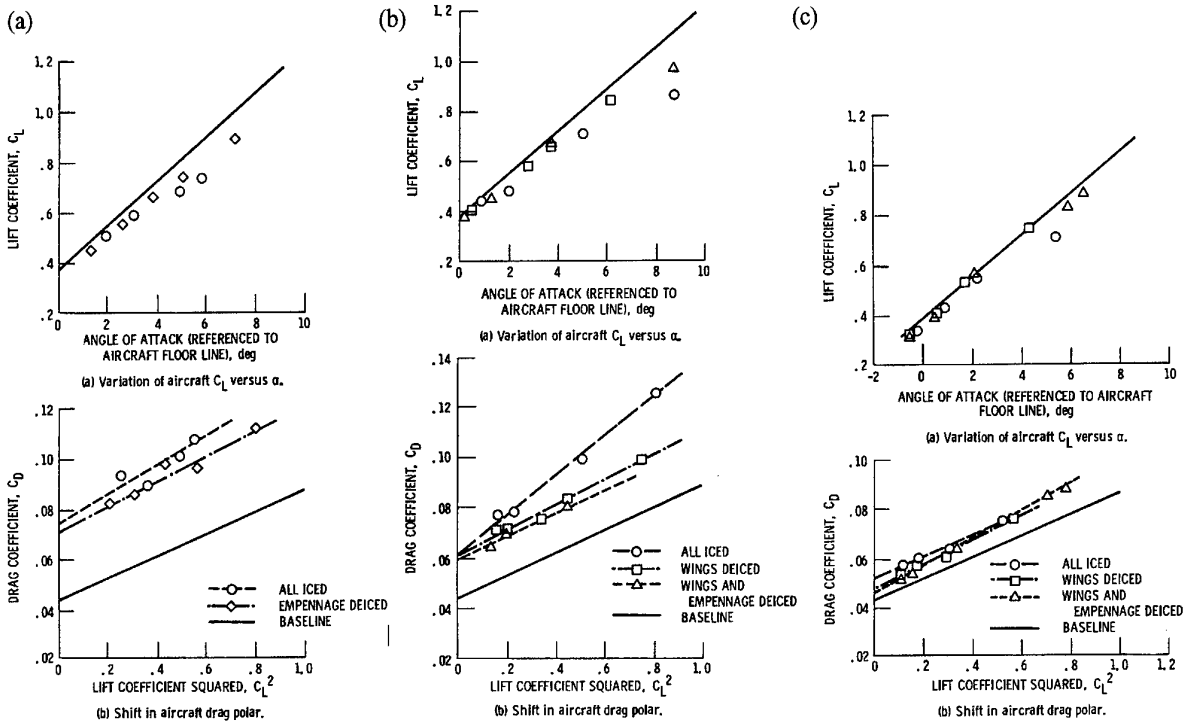

Fig. 3.2-18 Effect of heavy glaze icing (a), effect of glaze icing (b), effect of rime icing (c) on aircraft lift curve and drag polar

In Figures 3.2-18a, 3.2-18b and 3.2-18c, the lift curves and the drag polars (drag over squared lift) are plotted for flights of the NASA Lewis research aircraft (mentioned in subchapter 3.1.3.5) in three different icing conditions indicated as Flight 83-9, Flight 83-10 and Flight 83-11 respectively (Ranaudo, et al. 1984). In Flight 83-9 heavy glaze icing, in Flight 83-10 glaze icing and in Flight 83-11 rime icing was encountered. Data from the ice free baseline are also plotted for comparison.

Figures 3.2-19a, 3.2-19b, and 3.2-19c show the more common lift over drag polar for the same three flights in icing. Heavy ice accretion affected the aircraft lift curve considerably as depicted in Figure 3.2-18a (Flight 83-9). At 6°, for example, the iced aircraft lift coefficient is 17% lower than the ice free baseline. However, when the tail is de-iced the lift coefficient only reduces by 10%. This upward shift in the lift curve toward the baseline may be attributed to the recovery of elevator effectiveness after ice is removed from the leading edge of the horizontal tail.

The CL^2 vs. CD drag polar shows increased drag for both the all iced and the tail de-iced condition. At a CL of 0.5 the aircraft drag increases by approximately 62% over the baseline, the drag was reduced by 16% when the tail was de-iced.

For Flight 83-10 (glaze ice accretion) the penalties are shown in Figures 3.2-18b and 3.2-19b. Also here a lift loss of 16% at an angle of attack of 6° was measured.

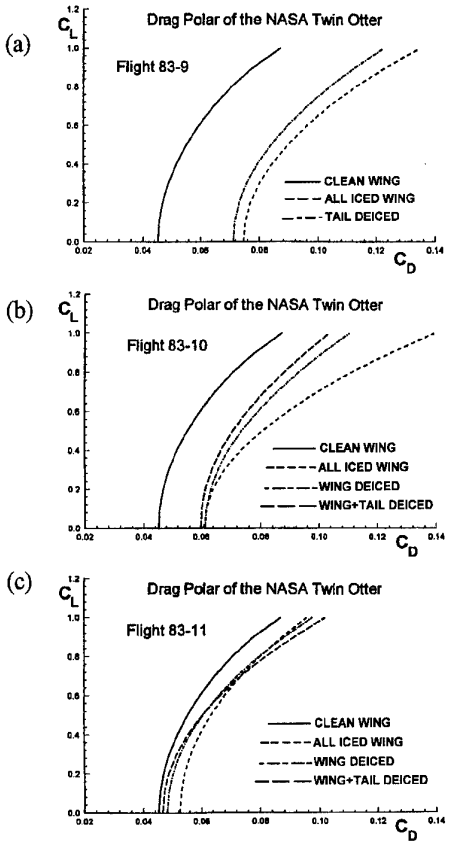

Fig. 3.2-19 Effect of heavy glaze icing (a), effect of glaze icing (b), effect of rime icing (c) on aircraft linearized drag polar

After de-icing the wings (only the wings outside the nacelle) the lift loss was reduced to 4%. Subsequent de-icing of the tail plane does not appear to provide any appreciable improvement. Note that even with wings and tail de-iced, the lift curve always remains below the baseline because of residual ice on the boots and/or ice on unprotected parts like inner wing, nacelle, wing struts, antennas and hinge brackets, etc. The drag at CL=0.5 is about 45% higher than for the clean aircraft at that point. When the outer wing was de-iced the drag coefficient reduced to 33% above baseline, and which reduced further to 26% when the tail was de-iced. Note that about 60% of the drag remains for the de-iced aircraft due to ice accretion on unprotected parts.

In Flight 83-11 with Rime ice conditions as encountered and described in Figures 3.2-18c and 3.2.19c the same penalties for the iced aircraft are shown as the flights described before. The main conclusion that can be drawn from these figures, is that much lower lift and drag penalties are incurred with rime ice accretion than with glaze ice accretion.

Figure 3.2-20, 3.2-21 and 3.2-22, present a comprehensive and valuable collection of wind tunnel and flight test data in which the percentage loss in maximum lift is correlated with a non-dimensional roughness height, k/c (Brumby 1991, van Hengst 1993, and Lynch et al. 1991). It is shown that small perturbances cause a significant loss in aerodynamic performance for both slatted and unslatted wings. Brumby's correlation for the entire upper surface covered with roughness (Figure 3.2-20) can be considered an upper limit on percentage loss in maximum lift for unslatted wings or tails. It should be noted that there is no data allowing Brumby to extrapolate the curves to the x-axis. It suggests the existence of distributed roughness without maximum lift losses. Figures 3.2-21 and 3.2-22 indicate a lower loss in maximum lift coefficient for slatted wings at higher k/c values than the Brumby correlation suggests, based on data derived from Boeing, Fokker and McDonnell-Douglas. Figure 3.2-23 and Figure 3.2-24 show the loss of angle of attack, which varies approximately in proportion with percentage reduction in maximum lift and the non dimensional roughness height.

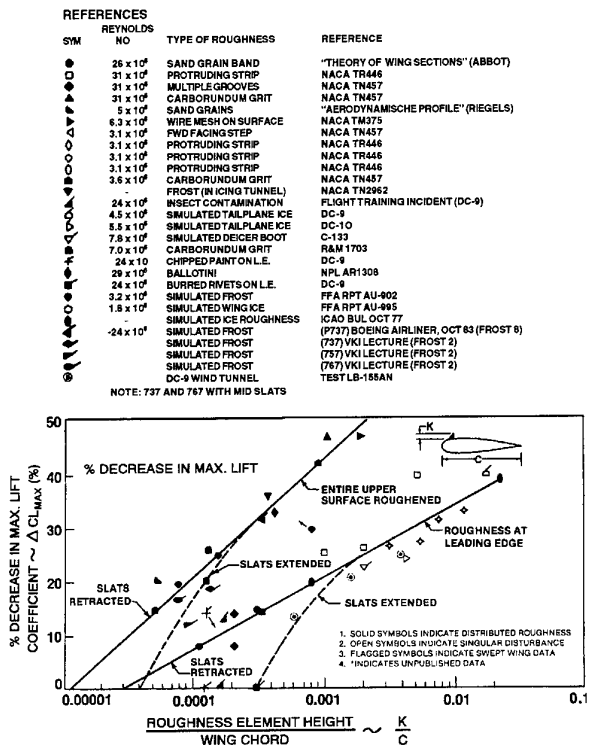

Fig. 3.2-20 Correlation of the effect of wing surface roughness on maximum coefficient

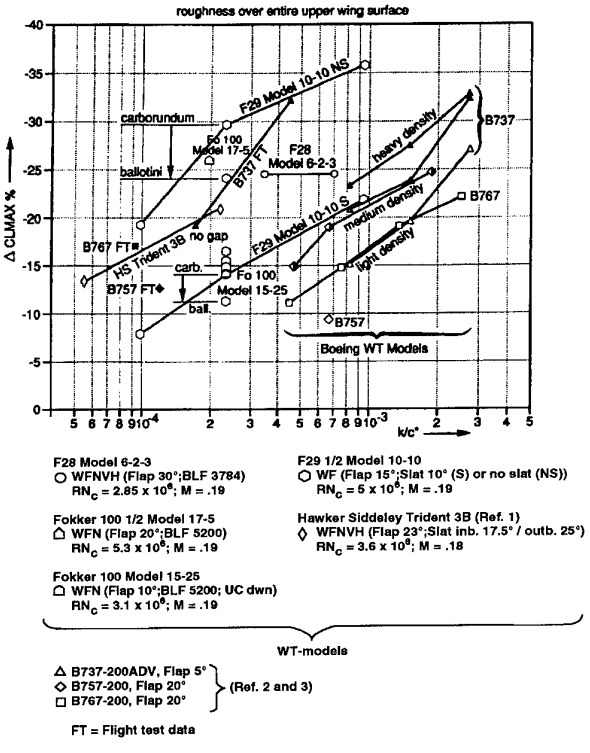

Fig. 3.2-21 Effect of wing surface roughness on maximum lift coefficient

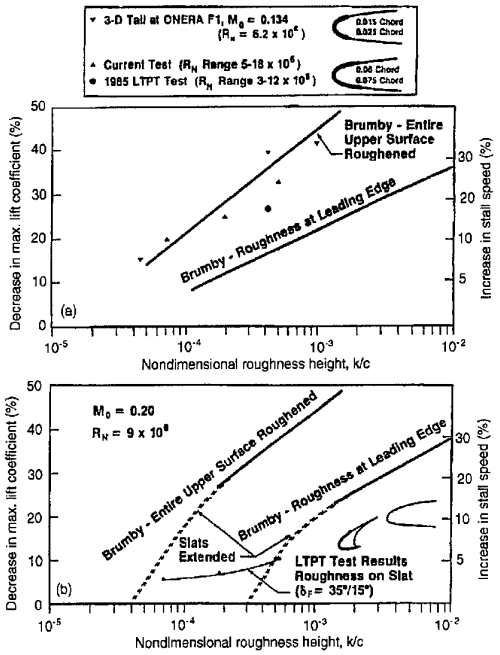

-Effect of roughness on maximum lift (a) Single element airfoil and tail. (b) Four element airfoil

Fig. 3.2-22 Effect of leading edge wing surface roughness on maximum lift coefficient

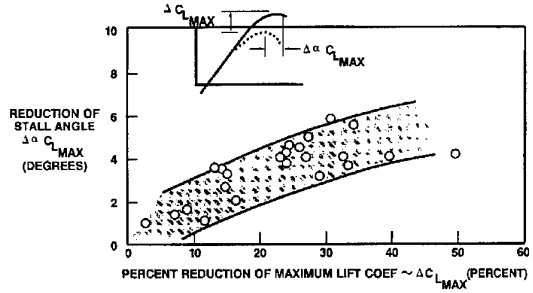

Fig. 3.2-23 Loss of the angle of attack at stall due to wing surface roughness

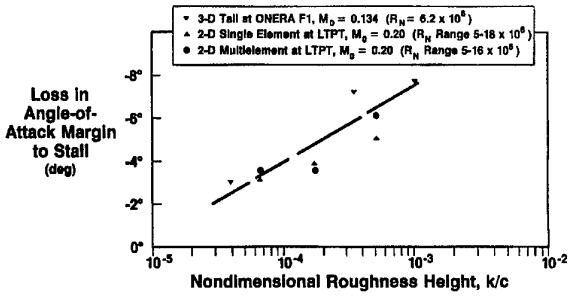

Fig. 3.2-24 Effect of roughness on loss of angle of attack margin to stall

Finally Figure 3.2-25 (Boer and van Hengst 1991) depicts the aerodynamic penalties of residual ice behind an active de- or anti-icing device, simulated by single roughness elements on the upper wing surface.

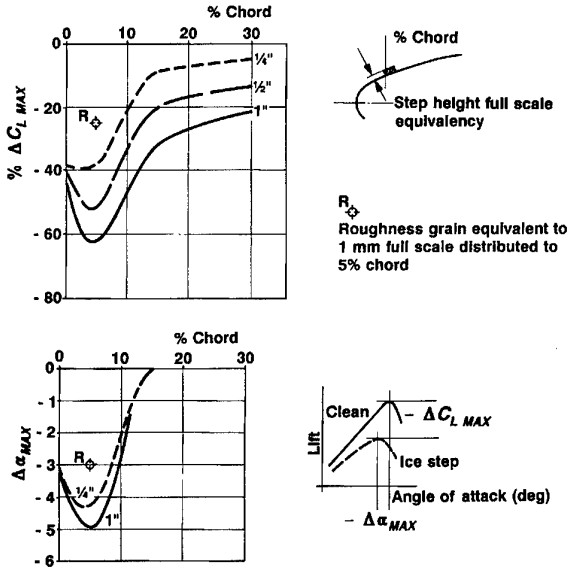

Fig. 3.2-25 Effect of an ice step at various positions along an 80 inch airfoil section

Figures 3.2-20 through 23.2-25 contain enough information to get a representative estimate of the effects of roughness on wing or tail aerodynamics.

3.2.3 Stall Speed, Power Setting

As the lift and drag of an aircraft are adversely affected by ice contamination, it should then be obvious, that the stall speed will increase when the aircraft is iced. Continuing the discussion with perturbances produced by roughness, Figure 3.2-22 shows that even a non dimensional roughness height of $5x10^{-4}$, (which is comparable to about a 0.2 mm roughness height on a small jet transport wing), can reduce the maximum lift of the clean wing by 35% and the stall angle by about 6°. The percentage increase in stall speed, operationally a more significant parameter, is given in equation (3.1)

$$\frac{\Delta V_S}{V_S} = \left(\frac{1}{\sqrt{1 + \left(\frac{\Delta C_{L_{MAX}}}{C_{L_{MAX}}} \Big/ 100 \right)}} - 1 \right) \times 100\% \qquad (3.1)$$

So for the present example, a 35% loss (-) in maximum lift translates to a 24% increase (+) in stall speed. As a modern transport aircraft is required, for certification, to have a 13% stall speed margin for take off, that amount of maximum lift loss causes the take off safety speed to be lower than the stall speed for the contaminated wing. This means that the wing cannot generate enough lift to take off.

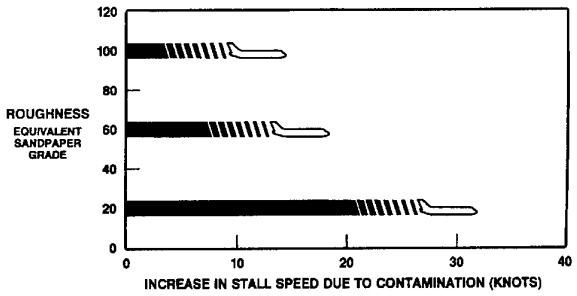

Fig. 3.2-26 Approximate effect of wing upper surface ice contamination on the stall speed of a typical small turbojet transport

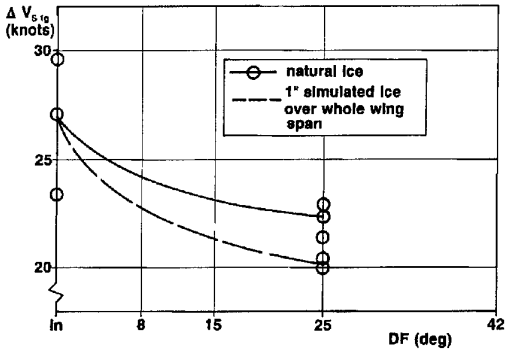

Fig. 3.2-27 Increase in 1g stall speed due to ice accretion on a Fokker 100

Figure 3.2-26 (Brumby 1991) shows the increase of stall speed for a typical small turbojet aircraft in relation to roughness, which is expressed as an equivalent sand-grain roughness grade. For the Fokker 100 (Boer and van Hengst 1991) the increase in stall speed is related to the flap setting, as shown in Figure 3.2-27 for an 1" (25.4mm) artificial ice shape.

It is shown that the clean wing (no flaps or slat) is mostly affected by ice accretion at the wing leading edge. As drag is rapidly increased by ice contamination on an aircraft, the required engine power to compensate must be increased too. The most critical case which has to be considered, is the single engine take off and climb. Figures 3.2-28a, 3.2.-28b and 3.2-28c (Ranaudo et al. 1984) show the one engine-out capability for the NASA Twin Otter, based on test data of flights in the three icing conditions as discussed in the previous subchapter. In the upper half of these figures, the test data had been corrected to standard day, sea level, and standard weight conditions and in the lower half, the test data was corrected to standard weight conditions only. In Flight 83-9, with heavy glaze ice accretion, Figure 3.2-28a shows that with no de-icing capability, the aircraft will descend if an engine fails. However by de-icing the tail, a rather limited single engine capability exists only at sea level. At a

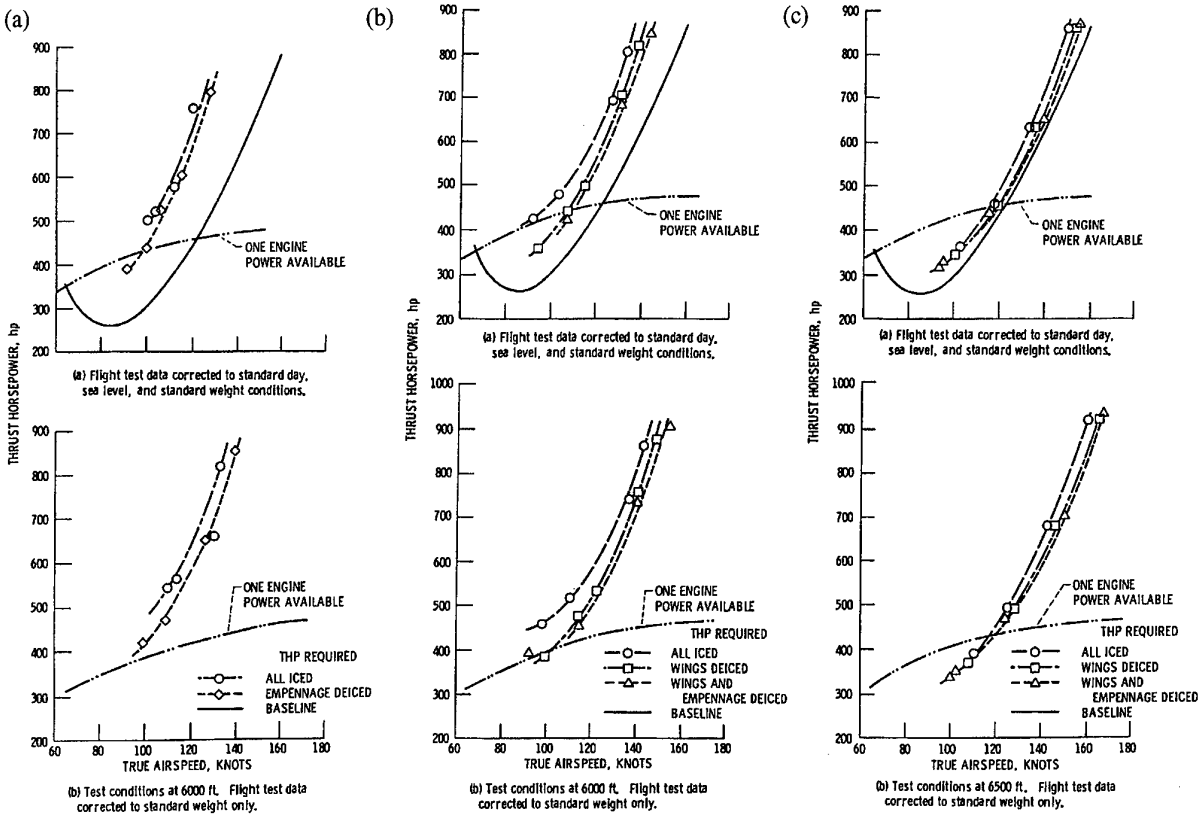

Fig. 3.2-28 Effect of heavy glaze icing (a), effect of glaze icing (b), effect of rime icing (c) on thrust horsepower required relative to calculated one-engine thrust horsepower available

pressure attitude of 6000ft, de-icing of the tail assembly is not sufficient to reduce drag to the point, where level flight could be maintained. A comparison between the performance penalties due to glaze and rime ice accretion on the aircraft can be obtained from Figure 3.2-28b and Figure 3.2-28c. It can be seen that a large amount of rime ice can accumulate on an aircraft before engine out capability suffers. Conversely, it appears that only a small amount of glaze ice will rapidly erode that capability.

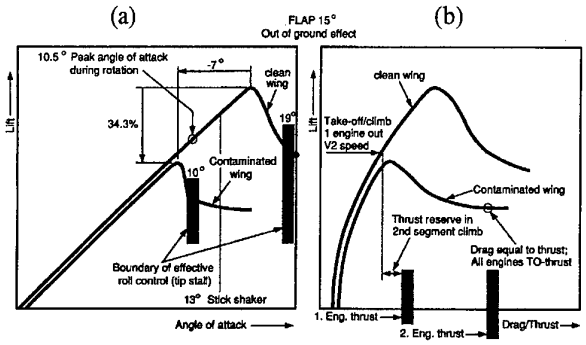

Fig. 3.2-29 Effect of wing contamination on aircraft lift and drag

Figure 3.2-29a and Figure 3.2-29b (van Hengst 1993) illustrate the typical effects of hoar frost contamination over the entire wing upper surface on the aerodynamics of a twin jet aircraft during take-off. It can be seen that there is only a limited available thrust left for the single engine climb.

3.2.4 Longitudinal, Lateral and Directional Stability

During a normal take off, the aircraft speed schedules are established for angles of attack below that for the onset of stall or the activation of stall warning devices. However, for an airplane with ice contamination, not only does the onset of stall occur at a lower than normal angle of attack, the airplane angle of attack must be increased in order to produce the required lift at normally scheduled speeds. This compounding effect rapidly results in the aircraft's operating into the onset of stall. In order to ascertain proper stalling of an iced aircraft, the margins for the stick shaker/pusher firing have to be adjusted. Figure 3.2-30 (Cataneo 1991) shows how this shaker/pusher adjustment was done for the ATR 72.

Figure 3.2-31, addresses the influence of wing ice contamination on the pitching moment of an airplane (Brumby 1991). For aeroplanes trimmed for takeoff, the stabilizer is set to balance the moments due to both aerodynamic forces and center of gravity position so that the stick force at climb-out ranges from nothing to a slight pull up. This balance is upset by contamination, particularly on contemporary aircraft with tapered, swept wings. With contamination on the wings, the aircraft will

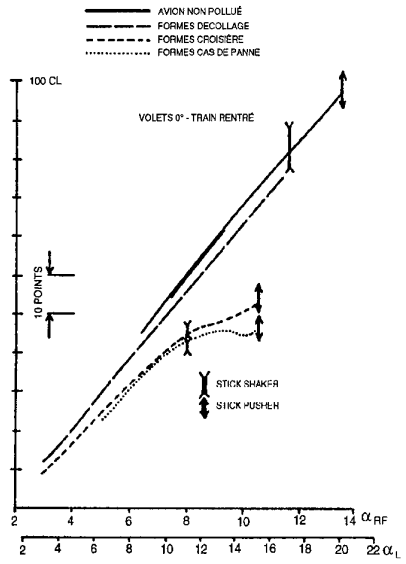

Fig. 3.2-30 Adjustment of stick shaker/pusher setting

increasingly behave as if it was mis-trimmed in nose-up direction as the angle of attack is increased. This will result in the aircraft's pitching up more rapidly than normal during the takeoff rotation, and will require an abnormal push force to maintain the desired airspeed during take off climb.

As with other effects, this pitch up tendency becomes more pronounced as the amount of ice accretion increases. But it is not only the longitudinal stability which is adversely affected by ice accretion. The lateral and directional stability will also be affected. The adverse effects on lateral or directional stability will be greatest, wherever the penalties in longitudinal stability are greatest. Figure 3.2-29a (van Hengst 1993) illustrates the reduction of the effective roll control boundary during the take-off run as caused by wing contamination on a twin jet aircraft. Due to wing flow separation aileron capacity and aircraft roll damping are reduced. During the rotation any roll tendency of the aircraft will become uncontrollable. Roll tendencies may most likely occur due to an unequally distributed contamination over both wings.

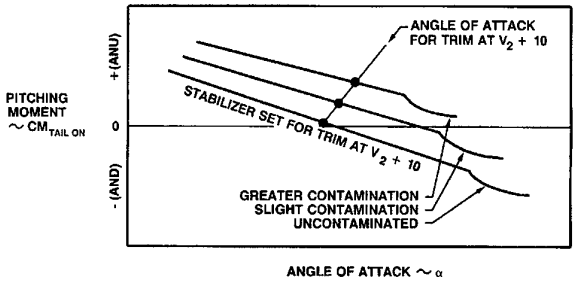

Fig. 3.2-31 Effect of wing ice contamination on pitching moment

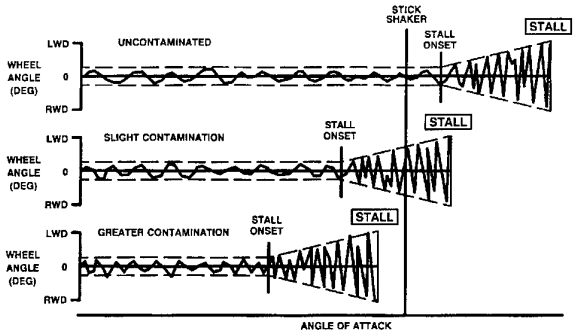

Fig. 3.2-32 Effect of wing ice contamination on lateral control characteristics

In Figure 3.2-32 (Brumby 1991), the stall onset is defined, at which point the wheel angle to keep the wings level will increase rapidly. The angle of attack at which this will occur is continually lowered with increasing ice accretion.

Adverse effects on the directional stability of an aircraft can result in an abnormal pitch up or down when the rudder is fully deflected and high yaw angles are reached under icing conditions. This means, that in case of an iced aircraft rudder deflections have to be limited, a limitation which always remains, even when the aircraft is free of ice. The minimum control speed is therefore increased and the save single engine take-off distance increases.

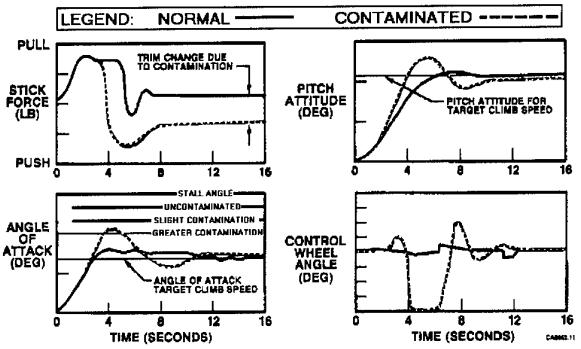

Fig. 3.2-33 Effect of wing ice contamination on longitudinal control characteristics

The overall effects of wing ice contamination on various flight characteristics of an airplane during take off are summarized in Figure 3.2-33 (Brumby 1991). It is shown that the iced aircraft begins pitching up faster than normal. If the flight crew is familiar with the plane, they may recognize the abnormal rate of rotation and counter it with an immediate forward push of the control column. Failure to recognize any abnormal increases in the rotation rate or the subsequent lift-off can result in significant angle of attack overshoot, accompanied by an abrupt roll excursion and aerodynamic stall.

The same information can be read in Figure 3.2-34a and 3.2-34b, where the take off sequence for the Fokker 50 and Fokker 100 with clean and contaminated wings are recorded (van Hengst 1989). The contamination represents roughness of freezing drizzle distributed over the entire upper wingsurface. On the other hand, during approach or landing, ice contamination on tail planes inducing a stall is considered to cause most of the accidents in icing conditions.

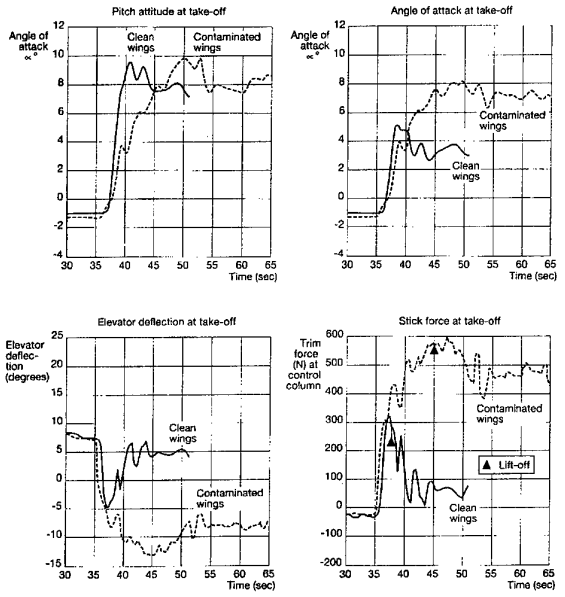

Fig. 3.2-34a Comparison of Fokker 50 take-off performance with clean and contaminated wings

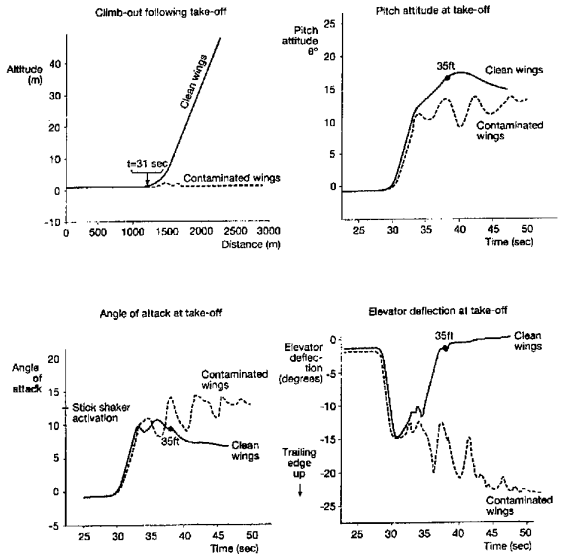

Fig. 3.2-34b Comparison of Fokker 100 take-off perfor-mance with clean and contaminated wings

Reinman (Reinman 1994) describes the effects of a tail plane stall, interpreting a report written by Hellsten (Hellsten 1993) who considers a generic airplane, which was summarized from typical recent aeroplanes, to demonstrate the characteristics of iced wings and tail planes during approach and landing.
Figure 3.2-35 shows plots of wing lift coefficient versus wing angle of attack for the cruise, approach and landing configurations. Superimposed are the operating points for that sequence. Starting with a cruise speed of 200kt (point 1) the pilot decreases speed to 126kt (point 2) while increasing the angle of attack, AoA, from 2.5° to 9.5°. Next, the pilot deploys half flaps and lowers the wing AoA to 7° (point 3) and then further decrease speed to 114 kts while increasing wing AoA to 9.5° (point 4). Finally, the pilot extends full flaps and lowers wing AoA to 4.5° (point 5). Eventually the pilot reduces speed and increases wing AoA while slowing to touch down.

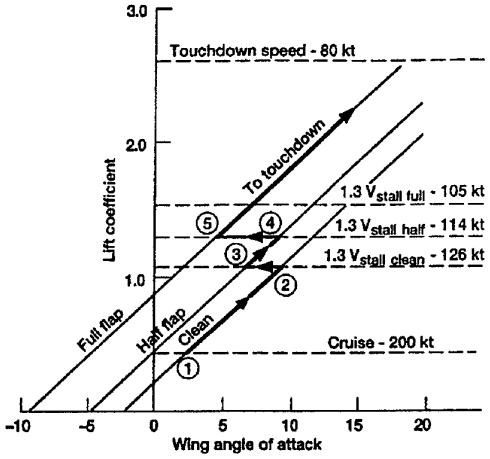

Fig. 3.2-35 Angle of attack changes during transition from cruise flight to touch down

Several aircraft responses can accompany the deployment of flaps. First, when the flaps are initially deployed, say at point 2, the wing AoA has not yet changed and the airplane is lifted because it is temporarily operating on the half-flap lift curve at an AoA of 9.5°. Secondly, the deployed flaps move the center of pressure further aft of the wing, causing a nose-down pitching moment. Thirdly, the extended flaps increase the wing down wash angle, which in turn increases the AoA on the tail and produces a greater downward force on the tail. The pilot compensates for these effects by trimming the aircraft. So, the nose pitches down to a lower wing AoA and the tail pitches up to a higher AoA. During the upward motion of the tail there is an increased downward relative velocity on the tail which further increases the tail AoA. The critical moment occurs when deploying full flaps because this results in the largest trim adjustment to get the smallest wing AoA, (point 5) and conversely, to the largest tail AoA. This is the critical point where tail stall margin is least and tail stall might occur. Also, if the pilot suspects that wing ice contamination has increased the wing stall speed and he increases speed to compensate, the wing AoA will decrease, but the tail AoA will increase. The increased tail AoA might possibly reduce tail stall margin to the point where a sudden down-burst or nose-down pitch can stall the tail.

3.2.5 Propeller Performance

Saab from Sweden (Rodling 1989) has conducted an interesting study into propeller icing because of a tremendous loss in propeller efficiency on the Saab 340 flying in icing conditions. This performance degradation made the plane unable to climb over 12000 ft in light or moderate icing. Theoretical investigations (icing tunnel test and flights in natural icing conditions) were performed and showed a loss in propeller efficiency up to 20% with an iced propeller. Additionally, 20% of the efficiency was lost when run back ice at the blades occurred due to an inadequate operation of the electrical de-icing system for the propeller. According to the tests Saab evaluated that the variety of icing conditions required a well tuned de-icing system. The main task for the de-icing system is to lower the adhesion forces so that the ice will shed. Run back ice on the blades is disastrous and must be prevented.

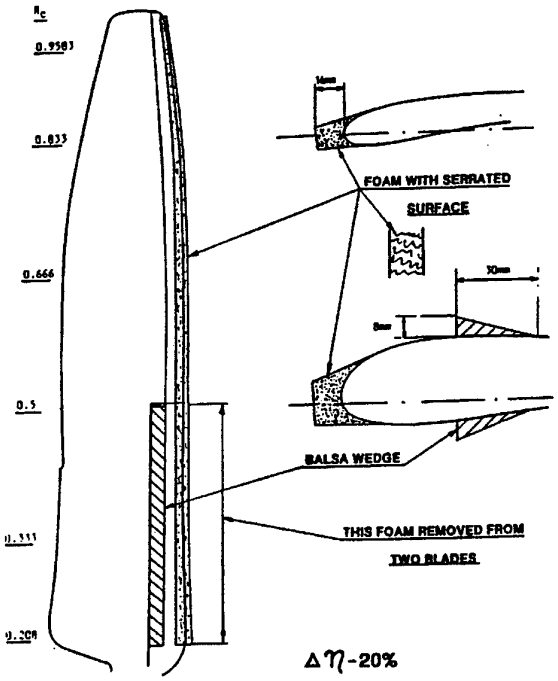

Fig. 3.2-36 Artificial ice shapes on propeller blades resulting in a 20% loss of efficiency

Figure 3.2-36 shows one of the configurations with artificial ice shapes used by Saab for the propeller tests with the Saab 340. This ice shape is shown to be associated with an 20% loss in propeller efficiency.

Figure 3.2-37 principally shows the relation of lift to drag for an iced propeller compared to the clean one. It is noted that in the past NASA has conducted measurements of propeller performance loss due to ice formation during flights in natural icing condition. The measurements were supplemented by analysis of factors contributing to the performance loss (Neel and Bright 1950).

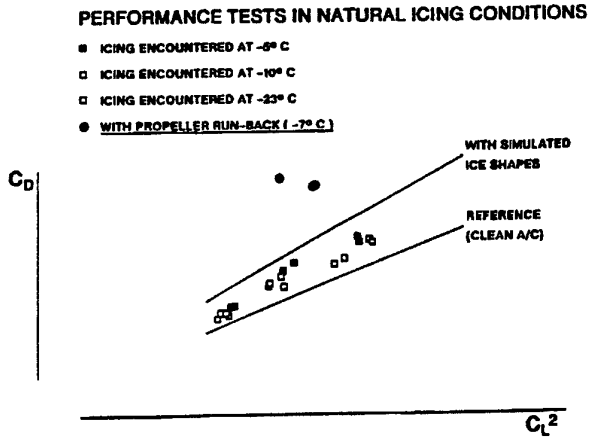

Fig. 3.2-37 Effect on aircraft drag polar of runback ice on propeller

3.2.6 Ice Shedding, Vibration, and Weight

In addition to the aerodynamic penalties of icing, there are structural and systems penalties. Pieces of ice shed from the wing or propeller can cause structural damage to the airframe. Although it is less severe for wing mounted engines with tractor propellers, it can lead to specific problems with rear mounted engines or pusher props. Ice fragments shed from the wings and intakes can hit the propeller or may be sucked into the engine inlet causing an engine flame out or damaging the fan blades. In particular, ice shedding from single propeller blades causes vibrations on the propeller, the engine, nacelle and can be transmitted to the whole aircraft. Ice on control surfaces such as elevators, rudders, ailerons, flaps or slats or also balance horns or hinge brackets may cause an intolerable blockage, which has to be avoided. Attention must be paid to water running into the stream wise gap when an all movable tip is used as a kind of aerodynamic balance. Ice accretion on antennas, struts or external stores may also cause vibration up to destruction as well as impeding their correct operation. Finally all ice which is accreted on the surface of an airplane will add additional weight. Ice on the tail moves the center of gravity back, which can lead to unacceptable trim characteristics up to instability.

3.2.7 Other Icing Threats

Ice particles in the atmosphere pose a range of threats to aircraft. The structural implications of an encounter with large hail stones is easy to understand. In the period 1976 to 1994 six accidents have been attributed to hail damage (CAA, 1976). The engines are particularly vulnerable to structural damage. The systems implications are less evident to the lay man but well known to the industry. Engines can experience difficulties coping with the thermodynamic load of evaporating the ice particles and ice can become concentrated in particular regions of engines resulting in blockage and other problems. Heated probes represent a particular problem and can be susceptible to blockage or malfunction when they ingest ice particles. The output of such probes often influences engine and flight control systems. Ground based tests on the reaction of components to ice cannot produce the full range of conditions which prevail in natural flight. The effect of ice particle size, density, shape, break up and melting properties need to be borne in mind in order to choose the most demanding and appropriate conditions. It is likely that current test facilities are not able to reproduce both the desired ice and the required flow conditions so exhaustive testing may require different kinds of experiment related by physical understanding and direct observation of the phenomena most pertinent to the test. This is not an activity which most design and product development functions can sustain. A working group of the AGARD Propulsion and Energetic Panel was recently active in this area (AGARD 1991).

3.3 CERTIFICATION/QUALIFICATION ASPECTS INCLUDING THE USE OF ARTIFICIAL ICE SHAPES

It has been shown that a great variety of ice shapes can occur during aircraft operation. Safe flight and a minimum performance shall be guaranteed under all known (or forecast) icing conditions within the meteorological certification envelope defined by the certification authorities - even in special situations, as e.g. one engine inoperative. In case of failure of de- or anti-icing systems sufficient time must be available to safely escape from the icing environment before excessive ice accretion occurs. However, this escape procedure and any other change of the usual flight procedures due to icing must be thoroughly stated in the Airplane Flight Manual AFM.

Flight tests in natural icing conditions are quite expensive and time consuming, especially since well defined icing conditions corresponding to the expected critical meteorological conditions cannot easily be found. The extreme cloud developments needed for certification conditions occur rather seldom. Insufficient LWC may frequently be compensated by extended exposure time in the sense discussed in chapter 2. However, switching from glaze to rime ice can happen by this change due to changes of 'convective/latent heat ratio' in the heat balance (see chapter 4.1.1 for details) but this modification of ice type should be avoided.

It is of great importance for all companies developing and manufacturing aircraft to reduce time and to lower costs for achieving ice certification and qualification of new aircraft. Although some representative flight tests under natural icing conditions are always indispensable, a great improvement can be realised by the use of possible artificial ice shapes for the flight tests and also for the corresponding wind tunnel experiments in dry air. The essential question to be answered for this methodology is: How can we predict reasonable ice shapes and to what extent can we make sure that the shapes chosen are realistic for the flight conditions to be simulated? And if a positive answer has been found on this question, also the certification and qualification authorities must have confidence in what has been done.

Fortunately, during recent years the theoretical prediction methods have been improved in capability and reliability and, in addition, some of the national authorities do more or less accept this progress for defining artificial ice shapes. Alternately, it is a frequent practice to use ice tunnel experiments for finding realistic ice shapes but this procedure also needs acceptance from the authorities since applying the similarity laws cannot fully guarantee correspondence to real in-flight ice accretion. Flight tests behind icing spray tankers are also attractive for this purpose but there exist even more problems concerning acceptance due to possible deficiencies in the artificial spray clouds and their calibration. Therefore, theoretical calculations as well as icing tunnel experiments where sub-scale tests have been performed and eventually also spray tanker tests may be used besides flight tests in natural icing environment for defining artificial ice shapes that will then be applied to aircraft components for investigating performance and handling qualities degradation in wind tunnel and flight tests. The use of artificial ice shapes essentially reduces time and costs for flight tests and is therefore extremely important for industrial certification and qualification procedures.

The present chapter will discuss the certification/qualification process and the state of the art for using artificial ice shapes in flight tests and for gaining certification and qualification. The corresponding experiences in aircraft industry and in certification authorities will be shown.

Certification rules are subject to periodic review. Further changes - either for a specific aircraft type or a class of aircraft - may also be decided by the certification authorities due to actual events or serious safety concerns. An actual example is the freezing drizzle encounter of turboprop aircraft which always up to now has been outside of the certification conditions.

However, as part of the Special Certification Review conducted by the FAA (Federal Aviation Administration in the United States) and the DGAC (French authority) and the continuing investigations into the loss of American Eagle Flight 4184 (end of October 1994 close to Roselawn), an extensive icing tanker test program on the ATR 72 was carried out. From this test program, ten changes were implemented for all ATR aircraft during operations in icing conditions and were incorporated in the airplane flight manual, AFM. Three arbitrarily selected changes will be cited: "Dispatch into known or forecast freezing drizzle/rain is prohibited.", and "If visual cues associated with freezing rain or drizzle occur on one or both cockpit forward side windows, with any flaps extended, the flaps must not be retracted until the airframe is clear of ice. This includes missed approach, and go around.", and "As soon as visual cues associated with freezing rain or drizzle occur on one or both forward side windows, immediately disconnect the autopilot while holding the control wheel firmly and exit these conditions. Fly manually until the airframe is clear of ice.".

Extensive discussions and research on the freezing drizzle and freezing rain topics are being conducted, which may result in similar restrictions for all turboprop aircraft in the future. The policy with respect to these exceedance encounters is to reduce the probability of such events (1:1000 icing encounters) by improving weather information and forecast for the pilots and developing means of exceedance detection (e.g. 'visual cues' as indicated above in the rules for ATR). Of course, also systematic pilot training may be very helpful with respect to recognition of these situations and safe escape procedures.

3.3.1 General Aspects of Certification and Qualification

The ice certification of a large (20 and more passenger) civil transport aircraft has to be performed as prescribed in JAR/FAR (Joint Airworthiness Requirements/Federal Aviation Regulations) § 25.1419. The critical icing conditions are given in appendix C of that document (see chapter 2 of this report for details). Additional advisory material is provided by FAA (Federal Aviation Administration) in the so-called 'Advisory Circulars', AC, and in 'Orders'. Similarly the JAA (Joint Airworthiness Authority in Europe) issued the 'Interpretative Material and Acceptable Means of Compliance' ACJ (Advisory Circular Joint) 25.1419 which includes differences between some European national authorities and to the United States. Also the JAA presented a 'Notice of Proposed Amendment' NPA 25F-219 which is a draft for an 'Advisory Material Joint' AMJ 25-1419 concerning handling characteristics and performance under icing conditions. The latter provides detailed guidance for demonstration of safe flight with realistic ice contamination on various aircraft parts. However, this material - although it is generally felt to be very useful for certification - is (yet) not fully accepted by the national authorities.

Usually, the qualification of military transport aircraft adapts the civil rules just mentioned. For fighter type aircraft the requirements are normally reduced but even for this type of aircraft some concern on icing exists and is considered during qualification.

For smaller transport aircraft and general aviation JAR/FAR § 23.1419 must be fulfilled if an ice protection system is installed and ice certification is desired. For large helicopters ('Transport Category Rotorcraft') special guidelines can be found in FAR/JAR part 29. FAR/JAR 27 deals with smaller helicopters ('Normal Category Rotorcraft'). Appendix C of FAR/JAR part 25 on the meteorological conditions is in principle valid for all cases. However, part 29 contains it's own appendix C which allows for a 'pressure altitude limit' in icing conditions due to the limited flight altitude of helicopters. JAR/FAR part 33 and part 35 concern icing effects on engines and propellers, respectively.

The ice certification programme for a fixed wing transport aircraft shall determine the impact of ice accretion on unprotected parts of the aircraft as well as on parts protected by de-icing (e.g. boots) or anti-icing systems. Power or thrust losses due to the proper function of the systems and eventual losses in propeller efficiency have to be taken into account. For unprotected surfaces a maximum thickness of 3 inches (75 mm) can be assumed for the ice shape under most critical icing conditions, while on surfaces protected by a cyclically operating de-icing system ice shapes of appropriately reduced height may be applied. For anti-icing systems the application of any residual ice is not needed if proper function of the ice protection system can be demonstrated under all relevant icing conditions. Also the possibility of building up runback ice has to be considered. This is formed when water runs downstream and freezes after some distance or by partially melted ice pieces which travel streamwise and freeze again on the surface. Recently interest has focused on ice ridges that may occur aft of the area protected by cyclically operating de-icing systems. These ridges may sometimes grow under very extreme meteorological conditions (e.g. large supercooled droplets of freezing drizzle up to 400 μm diameter - outside of the meteorological certification envelope -) starting from ice remaining behind the inflating rubber boots after removal of the ice. Special attention has also to be paid to the ice shape roughness that may be present in real icing flights. The roughness is prescribed for the artificial ice shapes with respect to height and distribution of roughness elements in the AMJ 25.1419 (3 mm height normally, reduced to 1 mm for take-off ice, and 8-10 particles/cm^2). Especially, the so-called 'sand paper ice' for simulation of critical ice accretion produced by large droplets hitting the aircraft surface or by hoar frost effects has to be simulated by pasting carborundum paper with grains of prescribed size (Carborundum paper No. 40) on the aircraft surface. In any case when using artificial ice shapes it must be guaranteed that the performance degradation by natural ice accumulation does not exceed that one occurring with artificial ice.

Lift, drag and pitching moment changes due to the most critical ice shapes have to be investigated with respect to performance degradation. Special attention must be paid to any increase of stall speed. Ultimately, the stall warning has to be set to lower angles of attack than without ice thus establishing a sufficient margin before stall under ice accretion. During flight tests with both artificial ice and in natural icing conditions the handling qualities will be investigated up to and including stall. Increase of stall speed due to ice accretion and corresponding decrease of stall angle of attack must be investigated. Sufficient longitudinal and lateral control capability, static longitudinal, lateral directional and dynamic stability have also to be shown. Starting from trimmed flight a 0g (push-over) manoeuvre is proposed by the authorities to be flown by applying sufficient push force on the stick until 0g - or, if this exceeds the tail-plane capability, the minimum possible load factor - is reached. That manoeuvre can dramatically reveal any critical susceptibility of the horizontal tail to ice accretion effects. Furthermore it is said that vibrations and buffeting must be avoided.

The flight in icing conditions includes take-off, climb, cruise, holding, descent and landing. Ice accretion before take-off must principally be avoided (clean wing concept). But some ice build up during take-off shall be presumed irrespective of the existence of an ice protec-

tion system if icing conditions are present at and close to the ground. It is assumed that de-icing systems are generally not switched on prior to and during take-off except that an early switch-on is required in the AFM. In the first take-off segment the ice accretion accumulated at the time the landing gear is fully retracted has to be taken for performance analysis. For the second segment flight phase the ice accretion at the point where the aircraft reaches 400 ft height above the take-off surface is applicable. It may be presumed that an eventually installed de-icing system is switched on at this height. Of course, both take-off segments can be treated at once if the worst case artificial ice shape is used for demonstration. Corresponding safety demonstrations have to be flown under the additional assumptions of most critical thrust/power-to-weight conditions and critical engine failure. Since cumuliform clouds do not occur in ground proximity, only maximum continuous icing conditions - as given by JAR/FAR § 25.1419 appendix C - have to be considered.

For the other flight phases, protected and unprotected surfaces may be distinguished and considered similarly. The artificial ice shapes to be applied have to be defined for the most critical icing conditions during the corresponding flight segment and appropriate power setting is demanded. In addition, for protected surfaces a failure or malfunction of the ice protection system has to be considered, i.e. failure ice shapes also have to be applied. It is stated in the JAA proposal AMJ 25.1419 that one half of the ice shape size for unprotected surfaces must be applied, i.e. 1.5 inch unless another value is substantiated. However, it must also be shown for this situation that the aircraft can safely escape from the icing conditions before the ice horns grow to larger height. Also the possible delay time in crew's recognition of aircraft icing and switch-on of ice protection systems must be regarded.

3.3.2 Certification/Qualification Rules

Besides the basic demands for certification in JAR/FAR § 25.1419, the meteorological conditions for the worst cases in appendix C of that document and the material of ACJ 25.1419 and various Advisory Circulars of FAA, the JAA proposal AMJ 25.1419 (1992) contains quite detailed and concrete guidance on how safe flight under performance degradation by icing shall be proved during certification. The most important aspects of all guiding material may be summarised as follows (due to different sources and national particulars it has to be viewed as a collection which is not obliging in all details):

Meteorological Conditions for worst case simulations:

a) *Maximum Continuous Icing* → flight through one cloud of suitable extent (standard 17.4 nm) and conditions as defined in appendix C or continuous flight of 30 minutes duration through one cloud at given temperature and LWC combinations, corresponding to a standard droplet diameter of 20 μm
b) *Maximum Intermittent Icing* → flight through clouds of suitable horizontal extent (standard 2.6 nm) and conditions as defined in appendix C, or flight through 3 standard clouds of 5 km extent with intermediate 5 km clear air distances of 5 km at same temperature and droplet size (20 μm) combinations as a) but higher LWC values
c) However, for the *rate of catch* the full spectrum of droplet sizes has to be used (Langmuir D spectrum is agreed to be sufficient), for the *impingement limits* a maximum droplet diameter of 50 μm has to be considered.

Flight Conditions → The most unfavourable flight conditions must be selected with respect to speed, altitude, angle of incidence, center of gravity location, flap and trim setting and power supply.

Natural Icing Tests must be carried out to validate other work for certification, e.g. to validate predicted ice shapes for artificial ice.

Artificial Ice Shapes are commonly used for tests in dry air. If these shapes are added to the aircraft components step by step handling and performance degradation of the aircraft can be tested safely. Artificial ice shapes can be used for unprotected and protected surfaces as follows:

<u>*Unprotected Surfaces:*</u>

a) The *most critical main airfoil surface parts* have to be equipped with ice shapes of 3 inches height.
b) *Other main airfoil surface parts* have to be equipped with same height, unless analysis demonstrates that a smaller value is appropriate.
c) The *ice shape and its surface texture (roughness)* must be realistically modelled, i.e. taken from experiments in natural icing if no other accepted approach can be taken (by analysis or experience).

<u>*Protected Surfaces:*</u>

a) *Ice Protection System Operating.*
The most critical ice shape accreted during the rest time of the de-icing system has to be applied. Typically for a commuter turboprop aircraft, the more critical intermittent maximum icing conditions produce ice shapes of about 1/2 inch.
b) *Delay in System Activation*:
Maximum icing exposure time prior to crew recognition and system activation must be established. A delay time of some minutes (normally 3 minutes) has to be considered
c) *After System Failure*:
One half of the ice accumulation specified for unprotected surfaces has to be assumed if not another value - not exceeded during a flight time of 30 minutes - is substantiated by analysis or experiment. This time is considered to be sufficient to leave icing conditions in a case of a system failure.

Tests Using a Simulated Icing Environment can be done in ground facilities (icing wind tunnels or outdoor spray rigs) or in-flight, i.e. flying behind a spray tanker. Both methods are not yet accepted as the only means of compliance for flight in icing conditions by the authorities due to shortcomings in similarity laws or deficiencies in cloud simulation:

Icing Facility Tests for components, e.g. airfoils, wings, engine inlets can be performed to document the ice build up, the typical shape and the resulting performance degradation. These results can be used to define the most critical ice shape which will be used for artificial ice shapes.

Icing Spray Tanker Tests can be used for component testing in dry air. Components sensitive to icing, e.g. propellers, engine inlets, control surfaces can be tested safely because the aircraft can leave the spray cloud immediately if any problems occur. The measured ice build-up can be used for defining artificial ice shapes. For helicopters full scale tests behind icing spray tankers are possible.

Flight Testing should address all phases of flight (take-off, climb, cruise, hold, descent, landing and go-around), while extraction of bleed air for ice protection and loss of propeller efficiency must be taken into account:

a) Handling Flight Tests

- *With Natural Ice*:
  - Qualitative assessment for comparison with artificial ice shape tests
  - Verification of sufficiently early stall warning for various sizes and shapes of ice contamination
  - Investigation that flight controls remain free from jamming due to ice
- *With Artificial Ice Shapes* demonstration of adequate stability and control with the most critical ice accretion pertinent to each flight phase:
  - Longitudinal 0g manoeuvre to check the danger of tail stall for various speeds, configurations, power settings at most critical icing conditions and loads
  - Demonstration that manoeuvring capability can be maintained up to stall warning
  - Ability to trim has to be maintained to limit control forces for safe flight under icing conditions.
  - Increase of stall speed and reduction of stall angle must be compensated by sufficiently early natural or artificial stall warning.
  - Vibrations and buffeting must not excessively occur.

b) Performance Flight Tests

These have to be carried out if the ice contamination increases stall speed by more than 5kt or 5% (greater value) or increases drag by more than 5%:

- *With Natural Ice*:
  - To prove that actual performance degradation does not exceed that with artificial ice shapes.
- *With Artificial Ice Shapes*:
  - 1g stall speeds should be demonstrated in each configuration for take-off, en-route, approach and landing phases.
  - Drag characteristics should be determined in each configuration for the flight phases mentioned.
  - Additional performance tests for take-off conditions if the above limits (5kt or 5%, the greater value) are exceeded and the aircraft is operated in accordance with the AFM (see below).

c) System Tests in Natural Ice:

- Demonstration of proper function of all parts of ice protection systems, e.g. for the wing, empennage, engine inlets, propellers, windshield, probes.
- Demonstration of proper modes for de-icing systems.

Ice Shedding must not affect the continuous safe operation of the engines or essential surfaces. It must be demonstrated that any pieces of ice shed are too small to cause unacceptable damage or that their trajectories are safe.

Ice Crystal Conditions must not affect the turbine inlets and bends, pitot heads, ducts supplying essential air, APU inlets etc.. Corresponding atmospheric ice crystal conditions are also prescribed in ACJ 25.1419.

Demonstration of Compliance can be done by a suitable combination of the following methods:

a) *Flight testing* using ice shapes - either accreted naturally or applied artificially
b) *Icing tunnel test* data
c) *Spray tanker test* data (rather limited up to now)
d) *Read cross* from earlier version or ancestor of a/c

Flight Manual → all appropriate limitations, performance information and procedures for flight in icing conditions must be provided in the Airplane Flight Manual (AFM):

- Limitations under icing conditions must be stated.
- Procedures for normal operation of the ice protection system and in case of failure must be stated.
- Performance effects for all flight phases should appear in the AFM.

It has to be emphasised that not all of the rules in the JAR proposal AMJ 25.1419 are accepted by the national authorities but most of them have become the basis of an actual rule-making process.

3.3.3 Reproducibility of Ice Shapes

Application of artificial ice shapes to an aircraft during flight testing is a way to keep the certification process within an acceptable time frame and at a moderate cost level. The use of artificial ice shapes provides the additional advantage that the ice shape and its height are well defined and that the tests may be reproducible and repeatable. The question which arises is, which shapes are realistic and particularly which represent the most critical ice accretion effects. The reference points for this problem are the ice accretions observed in real flight under natural icing conditions. However, the natural icing conditions always vary somewhat and can never exactly be reproduced. This difficulty also exists in comparison to ice tunnel experiments where the actual icing conditions are well defined and can be reproduced reasonably. For calculated ice shapes clearly the reproducibility should be excellent but the overall agreement with natural ice has to be validated. Even if the overall predicted shapes are reasonably similar, current predictive methods cannot reliably predict every detail as for example the surface texture of the ice accumulated.

The main aim of applying artificial ice shapes to a model in dry air wind tunnel experiments is to explore the effects of ice accretion on the characteristics of a design in it's early stages. These tests can also provide the designer with information where to apply and how to design the ice protection system. For example Boer and van Hengst, 1989, showed by suitable experiments with small ridges how the extent of the de-icer boots in chordwise direction could be optimised.

An interesting discussion of the artificial ice shape problem can be found in a recent AGARD Paper (Potapczuk and Reinmann, 1991), where further work is referenced, especially the NASA investigations using a research aircraft (Ranaudo et al., 1989) and comparing thoroughly flights with artificial ice shapes to those with natural ice accretion with respect to performance and handling. Also the experience concerning replication of ice shapes observed in flight and in ice tunnel experiments is outlined there and the research for validation of computational codes.

In flight, the natural ice shapes are usually characterised using photographs while a reference screen is mounted as background. This method suffers from a number of problems. During ice tunnel experiments the better access to the accreted ice makes it possible to form an accurate female model. A male molding can then be made and used as the artificial ice shape. Furthermore, the ice shapes for experimental simulations may be determined by sufficiently reliable prediction codes that usually contain some semi-empirical presumptions besides pure theoretical modelling. Especially, three computational codes are accepted by some of the European national airworthiness authorities with respect to sufficiently validated prediction capability for defining artificial ice shapes, namely the Lewice program of NASA Lewis Research Center, and the prediction codes of RAE and ONERA, which will be discussed to some extent in chapter 5 of this report. Of course, some details cannot be modelled in those prediction methods even in the far future, e.g. the development of the real surface texture characterised by it's specific roughness. Finally, also flight tests behind a spray tanker aircraft would be a valuable means of artificial ice shape determination on aircraft components if accepted by the authorities.

The ways just outlined for defining artificial ice shapes have been reasonably validated in the past but some difficulties with glaze ice still exist due to the complicated heat transfer processes involved which cause some remaining uncertainties. Nevertheless, no certification of a new aircraft will be admitted without cross-checking the results in some selected flight cases by flying in real icing conditions and measuring performance and investigating handling qualities after corresponding ice accretion.

The usual objective of using artificial ice forms is to approximate, as exact as possible, the size and shape of natural ice for two cases; the failure ice (unprotected surface or failure of ice protection system, size prescribed in JAA ACJ 25.2419) and the residual ice during proper function of the de-/anti-icing system (e.g. the so-called 'inter-cycle ice', accreted between two cycles of a periodically acting de-icing system). The shapes must represent those produced under meteorological conditions corresponding to the worst cases of maximum continuous and maximum intermittent icing conditions as described in JAR/FAR § 25.1419 appendix C. Some slight flexibility may be achieved for testing in natural icing environment in the sense that the times of ice accretion need not necessarily agree with the worst case assumptions. In particular the cycle ice accretion time does not need to agree with the normal cycling time of the system. As explained in chapter 2 of this report the times of exposure to natural icing conditions can be extended if the necessary size of ice accretion can only be achieved in a longer time due to smaller liquid water content of the clouds; but this simplification should not essentially affect the similarity relations. If protected and unprotected surface parts of the aircraft surface coexist, both types of regions should have their corresponding minimum size of ice shapes as defined in JAA ACJ 25.1419. The final aim to be reached with the natural ice shapes is the proof that the natural ice case envelope for degradation in performance and handling characteristics does not exceed the results found in flight tests with artificial ice shapes. Or in other words: The artificial ice shapes must represent the worst cases for degradation of performance and handling qualities.

3.3.4 Strategy for Application of Artificial Ice Shapes

Some recent papers have reasonably summarised the predominant effects of ice accretion on aircraft performance and on stability and control. Chapter 3.2 of this report is a summary of present knowledge that may be useful when artificial ice shapes are to be defined and subsequently applied. From experience it can be said that the following basic cases have to be considered during certification:

- ***Unprotected surface ice*** being applicable to unprotected aircraft components.
- ***Failure ice*** representing the exceptional case, that the ice protection system does not correctly work.
- ***Residual ice*** which occurs during normal function of the ice protection system (reduced or vanishing ice shapes in protected regions, e.g. the so-called 'intercycle ice' on cyclically operated rubber de-icing boots).
- ***Take-off ice*** which represents the ice shapes which can be accreted during both take-off segments until 400 ft altitude is reached while the ice protection system usually remains switched off.
- ***Surface roughness due to icing*** by ice accumulation due to large droplets hitting the surface or due to hoar frost effects ('sandpaper ice').
- ***Adequate surface roughness*** has to be applied to all kinds of artificial ice.

Except for the pure surface roughness no simple way exists to find the relevant, most critical ice shape. An individual, elaborate procedure has to be set up for each aircraft and adjusted to the certification authorities' requirements. The only guidance comes from JAA ACJ 25.1419 which prescribes for unprotected parts a maximum ice thickness of 3 inches (75 mm) unless by analysis, or experimentation a lower figure can be established independent of aircraft size. Concerning the ice thickness on normally protected parts following a failure of the ice protection system, AMJ 25.1419 proposes one half the thickness for unprotected parts, i.e. 1.5 inches (35 mm), unless another value is substantiated.

For residual and take-off ice the most critical ice shape has to be individually found for each relevant aircraft component and has to be agreed by the certification authorities. For the pure surface roughness case concrete guidance is given by the prescribed roughness heights in FAA ACJ 25.1419. It may be emphasised, that the flight test results on this case cannot be used to obtain relief for the operator to comply with FAR § 121.629. In this FAR paragraph, it is prohibited to dispatch or release an airplane when icing conditions are expected or met that might adversely affect flight safety. However, the sandpaper roughness acts as an estimate for any icing start-up, especially also during the take-off process.

Also outside of the meteorological certification envelope given in JAR/FAR § 25.1419 appendix C artificial ice shapes have been used to investigate special threat situations. Especially, the effects of ice ridges behind the de-icing devices which can eventually occur in freezing drizzle conditions - often also called 'residual ice' - have been simulated using artificial ice shapes. The corresponding shapes found in flights behind icing spray tanker aircraft have been accepted by the authorities for simulation.

Summarising, it may be stated that the application of artificial ice shapes is of great help to shorten the certification time, to reduce flight test hazards and to save costs. It remains necessary to perform some tests in natural icing conditions to validate the artificial ice results since the artificial ice shapes selected must be shown to represent the worst cases with respect to performance and handling. Finally, it may be mentioned that artificial ice shapes are definitely less popular for helicopter rotors than for fixed wings.

3.4 DESIGN CONSIDERATIONS

FAA Technical Center has issued a three volume Aircraft Icing Handbook (FAA 1991), to serve the needs of airframe and powerplant ice protection system design engineers. Through an update on 9/93, contemporary and updated information from recent research investigations and experience are included in this Handbook.

3.4.1 Wing Icing

It is valuable to explore the effect of ice accretion on aerodynamic characteristics of the wing at an early stage of the design process. The size of the wing and the projected flight altitude/speed envelope, play a role in determining where and how much ice protection is required.
The following points are considered.

- Statistics show that approximately 60% of the cases of icing occur at altitudes less than 3000m (10 000ft) The probability of icing decreases with increase in altitude, and is no more than 7% at an altitude of 8000m (26 000ft). Icing occurs most frequently at an outside air temperature from 0 to -15 C (Shpilev and Kruglov 1974). Terrain also affects the frequency of occurrence of icing.

- The droplet impingement efficiency of an airfoil E is a function of droplet diameter d, droplet density ρ_{dr}, free stream velocity V_∞, air viscosity μ, and wing chord c:

  $$E = f(d^2, \rho_{dr}, V_\infty, 1/c, 1/\mu) \qquad (3.2)$$

  The impingement efficiency increases when the droplet diameter and/or the free stream velocity and/or droplet density increase and when the chord and/or air viscosity decrease. As the efficiency increases so will the rate of ice accretion and hence the aerodynamic degradation. This is clearly illustrated for the drag coefficient in Figures 3.2-13 and 3.2-14 in chapter 3.2. The degree to which the size of the ice accretion reduces with chord length is shown in Figure 3.4-1 (Ritz 1938).

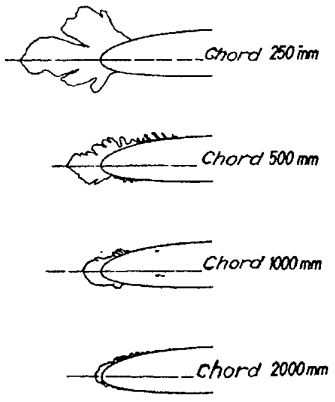

Fig. 3.4-1 Effect of airfoil section chord on ice shape

- Increasing free stream velocity has two opposing influences on ice shape: the increased convection heat and mass transfer encourages freezing while the increased kinetic heating discourages freezing. Ultimately, a Mach number will be reached, beyond which kinetic heating will dominate and ice will not form.

- The methods used to predict the ice shapes on wings, are currently, without exception, based on Messinger's heat and mass balance. See chapter 5.0 for more information on ice accretion prediction codes. It is good to make one self acquainted of the limitations of the methods before using the resulting answers.

- If de-icing boots are chosen to protect the wing from icing, allow some oversizing of the boot coverage. Johnson, chief designer at Lockheed about 1940, examined test data on the effect of simulated ice shapes on lift, drag and stability of a complete aircraft (Johnson 1940). The ice shapes were obtained from flight tests and included a very severe icing condition of a type not adequately removed by the type of wing de-icing boot in use in those days at Lockheed. Photographs are presented showing insufficient de-icing boot coverage. Under heavy icing conditions 4 inches of ice was accumulated on all forward facing components of the wing and extended aft of the de-icing boot. In those days the de-icing boots extended only to 5% chord on the leading edge. From these tests Lockheed introduced improved de-icing boots which extend on the upper surface of the wing to 15% chord and on the lower surface to 10% of the chord on their products.Such an extention of boots also reduces the effects of any residual ice "steps" behind the boots as shown in Figure 3.2-25 in chapter 3.2.

- If heating of the leading edge is selected and partial evaporation of the water is allowed, test should be conducted to investigate the effect of run-back ice, which may be represented by wires glued on either side of the wing at the estimated location of the ice ridges.

- For a wing provided with leading edge slats, the gap between slats and the main wing is mostly closed to obtain the best (L/D) in take-off. Incorporating an automatic slat-gapping mechanism in the slat system will restore the performance degradation due to icing (Zierten and Hill 1987).

As already mentioned the wings of C-5A are so large that no ice protection has been installed On McDonnell Douglas MD-11 and -12, Boeing B- 747, 767,and 757 series and Airbus A-300, 310, 320, 330, and 340 series only the leading edge of the slats located in the out board wing are equipped with an ice protection system. The sizes of the inboard wings of these aircraft are so large that their catch efficiencies are so small that no ice protection provision is required for the inboard wing.

3.4.2 Tail Icing

As discussed previously, ice protection is also an issue for horizontal and vertical tail planes. Due to their size both types of tail plane will collect more ice than the wing. The need for ice protection on tail planes may therefore be more pressing than on the wings. The problems associated with horizontal tail plane icing have been studied by Ingelman-Sundberg and Trunov (Ingelman-Sundberg and Trunov 1977, 1979 and 1985) and recently by Hellsten (Hellsten 1993). Tail planes however can sometimes be sized and designed to provide acceptable characteristics in icing conditions without ice protection.

- A critical flow condition at the horizontal stabilizer occurs when a push-over manoeuvre is made at low speed in the approach/landing configuration. In this flight condition the horizontal tail has to cope with extreme negative angles of attack (Obert 1974). The total angle of attack α_{Htot} of the horizontal stabiliser during a push-over manoeuvre is composed of (a) the tail angle of attack during the initial trimmed flight condition plus (b) the change in tail angle of attack due to the downward vertical acceleration of the aircraft plus (c) the change in tail angle of attack due to the pitching motion of the aircraft. So the relationship between α_{Htot} and tail area can be derived. If the maximum allowed negative angle of attack α_{Hmax} of the horizontal tail is given, i.e. $\alpha_{Hmax} = \alpha_{Htot}$, a particular push-over manoeuvre will require a certain minimum value of tail plane area.

- The stalling characteristics of a tail plane are determined by the selection of its planform, aspect ratio, taper ratio, leading edge sweep, and airfoil section thickness distribution (chord wise and span wise). A combination of a low aspect ratio, moderate to large leading edge sweep and small taper ratio results in a gradual stall behavior at a large angle of attack for the maximum lift and at a moderate maximum lift coefficient. Interesting test data for two different tail plane models, one with 44° and the other with 18° leading edge sweep, are reported by Ingelman-Sundberg and Trunov (Ingelman-Sundberg and Trunov 1979).

- The inclusion of a small degree of leading edge upward droop into the horizontal tail plane will increase the angle of attack for maximum lift and the maximum lift coefficient of the tail plane. Also the application of leading edge extension at the root sections of the tail planes will increase the angle of attack for maximum lift. Applied to a vertical tail plane this extension is called the dorsal fin and its purpose is to increase to side-slip capability of the vertical tail.

In case of a T-tail configuration the dorsal fin can be optimized under ice accretion with respect to sweep angle and extent of the dorsal fin in the sense that flow separation in the corners between horizontal end vertical tail is delayed by suitable vortex generation with increasing α and β. This procedure can noticeably reduce the necessary vertical tail area and has been exercised in developing the Dornier 328.

An example of a horizontal tail which was designed to obtain optimum long range cruise performance of the aircraft can be found on the McDonnell Douglas MD-11. Compared to its predecessor, the DC-10, the tail area is reduced by 30%, the airfoil sections were cambered and the elevator is improved. Consequently the horizontal tail of the MD-11 has been equipped with an anti-icing system. (Field 1987). In this respect it is interesting to note that all other large commercial transport aircraft are not equipped with an ice protection system for the tail planes.

To improve the horizontal tail stall characteristics of the Fokker F-27 in icing conditions two modifications were incorporated. Firstly the tail plane leading edge to 10% of the chord was drooped 14° upward and secondly the maximum deflection of the flap between fuselage and nacelle was reduced from 40° to 25°.

3.4.3 Control Surface Icing

Ice accretion on the tail planes will not only affect the tail plane aerodynamics but also the effectiveness and hinge moment characteristics of the corresponding control surfaces (elevator and rudder and for the wing ailerons). The control surfaces themselves may also become iced if they are deflected.

- The effects of icing, such as hinge moment reversal on the controls, are eliminated when the control system is irreversibly boosted.

- In manual control systems, the control surfaces need some form of aerodynamic balance to reduce the hinge moments in order to keep the control forces within acceptable levels. In stability and control considerations the rate of change of the hinge moment with angle of attack ($C_{H\alpha}$) and with control surface deflection ($C_{H\delta}$) is very important.
  For an unbalanced control surface $C_{H\alpha}$ and $C_{H\delta}$ are negative as sketched in Figure 3.4-2

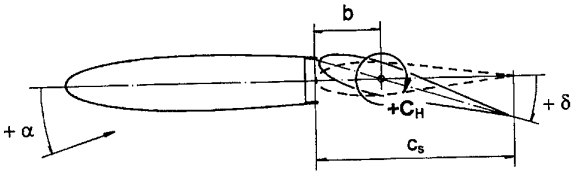

Fig. 3.4-2 Sign convention for control surfaces

By setting back the hinge point i.e. by increasing b over c_s, see Figure 3.4-2, $C_{H\alpha}$ and $C_{H\delta}$ can become less negative or even positive. A positive $C_{H\delta}$ is an undesirable characteristic and is called overbalanced. To achieve the same stick-fixed and stick-free stability $C_{H\alpha}$ ought to be zero.

Of the many other types of control surface balances, the two most familiar ones are the horn balance (a type of balance concentrated at the tip of the control surface) and the tab (a small movable trailing edge portion of the control surface geared to operate in the opposite sense to the main control).

- The ratio $C_{H\alpha}/C_{H\delta}$ also plays an important role in stability considerations. When these hinge moment coefficients are modified by the effect of ice on the air flow on the main lifting surface, so will the aircraft stability and control as studied by Morris for a horn balanced control surface (Morris 1952). Two simulated shapes of ice accretion were tested extensively as shown in Figure 3.4-3.

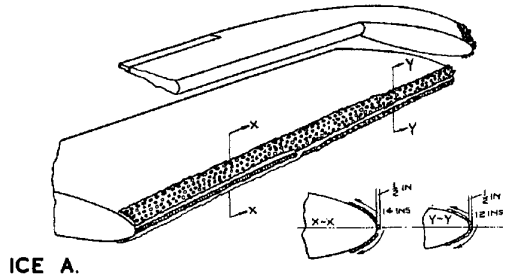

ICE A.

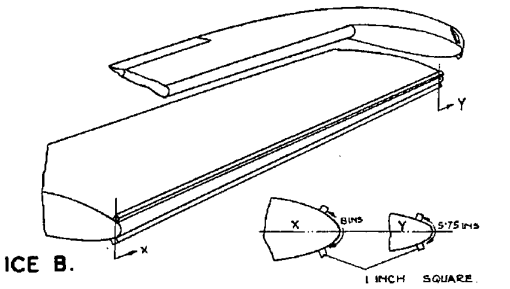

ICE B.

Fig. 3.4-3 Ice shapes tested

Type A represents a rough ice formation, caused by insufficient de-icing of the surface as observed in flight tests and Type B represents an extreme form of Type A. Type A has a thickness of 1/2" and covered the whole leading edge of the horizontal stabilizer on each side up to 14" at the root and to 12" at the tip respectively but with no ice on the porous metal strips. Type B consisted of two, 1x1 inch, ridges placed back from the leading edge 4" at the root and 3" at the tip respectively on each side of the stabilizer. It is interesting to note from the wind tunnel test, as shown in TABLE 3.4-1, that Type B (the extreme form of Type A), though it had a much larger effect on $C_{H\alpha}$, had a much smaller effect on $C_{H\delta e}$.

TABLE 3.4-1 Summary of wind tunnel test data

Condition	$C_{H\alpha}$	$C_{H\delta e}$	$\Delta C_{H\alpha}$	$\Delta C_{H\delta e}$
No ice	0.195	-0.055	-	-
With ice A on horn only	0.225	-0.035	0.030	0.020
,, B ,,	0.195	-0.035	0	0.020
,, A on tail plane only	0.250	**0.000**	0.055	**0.055**
,, B ,,	0.360	-0.030	0.165	**0.025**
,, A on both horn and tail plane	0.265	**+0.020**	0.060	0.075

The elevator even became overbalanced with ice A on both the horn and tail plane. Moreover the table also indicates how important it is to apply the proper shape of ice accretion in tests which are meant to explore the effect of fixed lifting surface leading edge contamination on control surface hinge moment characteristics. Simplification by strips or such alike can however give false conclusions.

Ice on the tail plane leading edge, which would make $C_{H\delta e}$ still smaller and possibly overbalanced and at the same time would make $C_{H\alpha}$ still more positive gives the conditions required for a dangerously undamped pitching oscillation. Although the results presented (Morris 1952), are for a horizontal tail plane, the conclusions of this investigation are also applicable to control surfaces for lateral (ailerons) and directional (rudder) control systems. Figure 3.4-4 shows theoretically derived boundaries of rudder hinge moment coefficients for damping of rudder free oscillations (Neumark 1945).

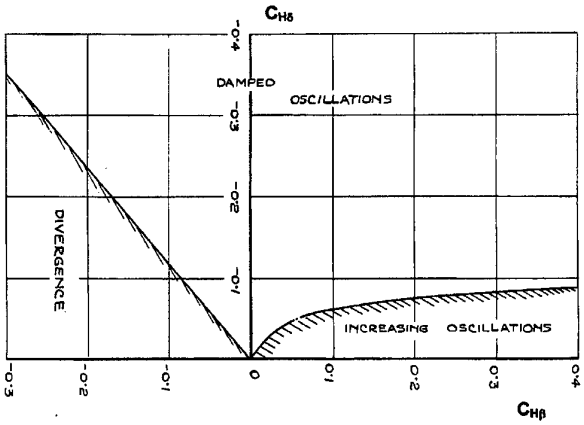

Fig. 3.4-4 Boundaries of rudder hinge moment coefficients for damping of rudder free oscillations

Similar studies for aileron control systems were carried out by NASA (Cohen 1944) and discussed in various text books (Perkins and Hage 1949 and Etkin 1967). For details of these studies the reader is referred to the original reports and text books. It is obvious that the above mentioned notes on control surface hinge moment characteristics and resulting control surface forces and aircraft response do not apply to irreversible powered control systems.

- A design criterion for deflected control surfaces to avoid ice accretion on the protruding balance noses (Root 1945) is illustrated below

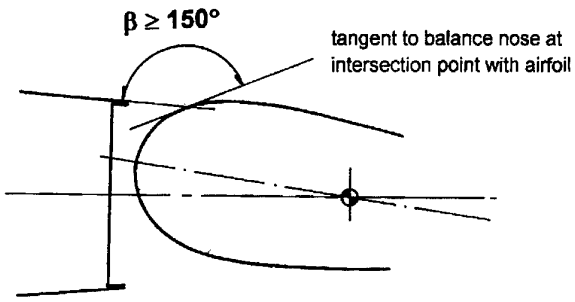

Fig. 3.4-5 Ice free criterion for deflected overhang balance noses

This criterion is of importance when after a failure of an engine, the asymmetric thrust must be trimmed out for a considerable length of time well within the limits for critical ice formation to occur.

- Application of moveable stabilizers will reduce the sensitivity of longitudinal control to ice-induced anomalies in elevator behavior.

- Prevent freezing of control surfaces by introducing of sufficient clearance between the moving control surface parts and adjacent fixed aircraft parts.

- Incorporate design provisions (drain holes and/or cover or plates at the pivot points) in order to prevent build up water inside the structure. Water collected from rain whilst the aircraft is on the ground can freeze in flight at altitude. The mass unbalance caused by the frozen water inside the control surfaces can create serious flutter problems.

3.4.4 Intake Icing

Engines are the heart of an aircraft and should always be equipped with an ice protection system. It is noted that icing of an engine intake duct may occur also at a positive outside air temperature of +3 to +5 C; the expansion of the air in the intake can result in a decrease of temperature by 8 to 10 C.

- Selecting a de-icing system for an intake implies that one must be assured that the engine can resist the expelled ice fragments from the system during operation. Otherwise a provision must be installed in order to prevent the expelled ice parts from entering into the engine, e.g. a by-pass duct in case of the curved intake contour of most turboprop intakes.

- Selecting an anti-icing system for an intake means that care must be taken that the system has sufficient power and coverage to evaporate all the impinged water particles in order to avoid runback icing in the intake.

For more information on pro's and con's of system selection, the reader is referred to the FAA Aircraft Icing Handbook (FAA 1991).

3.4.5 Icing of Propellers and Spinners

Ice protection on propeller and spinner is employed because: (1) leading edge ice accretion may reduce the propeller efficiency, (2) unsymmetrical shedding of ice may result in propeller unbalance, (3) large pieces of ice shed from the propeller or spinner may be ingested by the engine, and (4) ice accretion on the spinner may affect the flow conditions towards the root sections as well as the intake. On contemporary propeller designs, airfoil sections are employed at the blade roots instead of the circular sections in former propeller designs.

The chordwise coverage of the de-icer is mostly based on the experience of the propeller manufacturer and is about 26% at the root and 14% at the tip. The radial coverage of appreciable ice accretion depends on: (1) the rpm, (2) kinetic heating which increases with increasing radius, and, (3) the centrifugal force, expressed as "g" force. Here also the experience of the propeller manufacturer is of importance. For modern propeller designs the spanwise coverage varies from 50 to 70% blade radius.

For more information on pro's and con's of system selection, the reader is referred to the FAA Aircraft Icing Handbook (FAA 1991).

3.5 REFERENCES

AGARD (1978), "Aircraft Icing", AGARD-AR-127.

AGARD (1986), "Rotorcraft Icing - Status and Review", AGARD-AR-223.

AGARD (1991), "Low Temperature Environment Operations of Turbo-engines (Design and User's Problems). Propulsion and Energetic Panel (edit), AGARD-CP-480.

Aviation International News, 1.1.1993., "Ice: Insidious Cruel Entropping".

Andrews, E. H., and Lockington, A. (1983), "The Cohesive and Adhesive Strength of Ice", *J. Math. Sci.*, Vol 18, pp1455-1465.

Boer, J. N., and van Hengst, J. (1991), "Certification of Fokker 50 and Fokker 100 for Operation in Icing Conditions", AIAA-91-0561.

Bowden, T. D., Gensemer, A. E., and Skeen, C. A. (1964), "Engineering Summary of Airframe Icing Technical Data", FAA Technical Report ADS-4, AD 608865.

Brumby, R. E. (1991), "The Effect of Wing Ice Contamination on Essential Flight Characteristics", in: *Effects of Adverse Weather on Aerodynamics*, AGARD-CP-496.

C.A.A. (1976), Civil Aviation Authority, "World Airline Accident Summary, Volume 2 - 1976 and onward", C.A.A. Document No. 479 (updated twice a year).

Carbonaro, M. (1991), "Aerodynamic Effects of De/Anti-Icing Fluids, and Description of a Facility and Test Technique for Their Assessment", in: *Effects of Adverse Weather on Aerodynamics*, AGARD-CP-496.

Cattaneo, G. (1991), "Evolution Réglementaire en Matière de Certification des Avion Civils en Conditions Givrantes", in: *Effects of Adverse Weather on Aerodynamics*, AGARD-CP-496.

Cober, S. G., and List R. (1993), "Measurements of the Heat and Mass Transfer Parameters Characterising Conical Graupel Growth", *J. Atm. Sci.*, Vol 50, pp 1591-1609.

Cohen, D., (1943), "A Theoretical Investigation of the Lateral Oscillations of an Airplane with Ailerons Free", NACA Report 787.

Cole, J. A., and Sand, W. R., (1991), "Statistical Study of Aircraft Icing Accidents", AIAA-91-0558.

Etkin, B., (1967), "Dynamics of Flight", John Wiley & Sons, Inc., 6th. Edition, pp 226-240.

FAA Technical Center, (1991), "Aircraft Icing Handbook", DOT/FAA/CT-88/8-1, Vol. I, II and III, 1st. update, 9/93.

Field, G. G. (1987), "MD-11 Design-Evolution, Not Revolution", AIAA-87-2928.

Hawkes, I., and Mellor, M. (1972), "Deformation and Fracture of Ice under Uniaxial Tension", *J. Glaciology*, Vol 11, pp103-105.

Hellsten, P. (1993), "Aerodynamic Analysis of Susceptibility to Ice-Induced Tailplane Stall", *Conference Proceedings of International Tailplane Icing Workshop II*, San Hose, CA, USA, April 21-23.

Hendrickson, G. S., and Hill, E. G. (1987), "Effects of Aircraft De/Anti-Icing Fluids on Airfoil Characteristics", VKI Lecture Series: *Influence of Environmental Factors on Aircraft Performance*, Brussels, Belgium, Feb. 16-19.

Hill, E. G., and Zierten, T. A. (1991), "Flight and Wind Tunnel Tests of the Aerodynamic Effects of Aircraft Ground Deicing/Anti-Icing Fluids", AIAA 91-0762.

Hoffmann, H.-E., Roth, R., and Demmel, J. (1985), "Ergebnisse der Vereisungsflüge im Winter 1983/84: Eisansatzdicke in Abhängigkeit von wolkenphysikalischen Parametern, Objekt- und Wolkenparametern", DFVLR-FB-85-39, also available in English as ESA-TT-969 (1986).

Ingelman-Sundberg, M., and Trunov, O. K. (1977), "Methods for Prediction of the Influence of Ice on Aircraft Flying Characteristics", *JR-1, A joint report from the Swedish Soviet Working Group on ScientificTechnical Cooperation in the Field of Flight Safety.*

Ingelman-Sundberg, M., and Trunov, O. K. (1979), "Wind Tunnel Investigation of the Hazardous Tail Stall due to Icing", *JR-2, A joint report from the Swedish Soviet Working Group on Scientific-Technical Cooperation in the Field of Flight Safety.*

Ingelman-Sundberg, M., and Trunov, O. K. (1985), "On the Problem of Horizontal Tail Stall due to Ice", *JR-3, A joint report from the Swedish Soviet Working Group on Scientific-Technical Cooperation in the Field of Flight Safety.*

JAR/FAR 25.1419 (continuously amended), "Ice Protection", including Appendix C and ACJ 25.1419.

JAR AMJ 25-1419 (1992), "Flight in Icing Conditions - Acceptable Handling Characteristics and Performance Aspects", in: *NPA 25F-219 Issue 2* (22 Jan. 1992).

Jeck, R. K. (1994), "Other Ways to Characterise the Icing Atmosphere", AIAA-94-0482.

Johnson, C. L. (1940), "Wing Loading, Icing and Associated Aspect of Modern Transport Design", *J. Aero. Sci.*, Vol. 8, No. 2.

Kind, R.J., and Lawrysyn, M. A. (1991), "Aerodynamic Characteristics of Hoar-Frost Roughness", AIAA 91-0686.

Kind, R. J., and Lawrysyn, M. A. (1991), "Effects of Frost on Wing Aerodynamics and Take-off Performance", in: *Effects of Adverse Weather on Aerodynamics*, AGARD-CP-496.

Laforte, J. L., Bouchard, G., and Louchez, P. R. (1991), "Aerodynamic Acceptance Testing of Aircraft Ground Deicing/Anti-icing Fluids Flat Plate Test", University of Quebec, TP 11078E.

Lynch, F. T., Valarezo, W. O., and McGhee, R. J. (1991), "The Adverse Aerodynamic Impact of Very Small Leading-Edge Ice (Roughness) Buildups on Wings and Tails", in: *Effects of Adverse Weather on Aerodynamics*, AGARD-CP-496.

Mikkelsen, K. L., McKnight, R. C., Ranaudo, R. J., and Perkins Jr., P. J. (1985), "Icing Flight Research: Aerodynamic Effects of Ice and Ice ShapeDocumentation with Stereo Photography", NASA TM 86906 / AIAA-85-0468.

Morris, D. E. (1952), "Designing to Avoid Dangerous Behavior of an Aircraft due to the Effects on Control Hinge Moments of Ice on the Leading Edge of the Fixed Surface", A.R.C. C.P. No.66.

Neel, C. B., and Bright, L.G. (1950), "The Effect of Ice Formations on Propeller Performance", NACA TN 2212.

Neumark, S., (1945), "A simplified theory of the lateral oscillation of an aeroplane with rudder free, including the effect of friction in the control system", ARC R&M 2259.

Obert, E., (1974), "Low Speed Stability and Control Characteristics of Transport Aircraft with Particular Reference to Tailplane Design", AGARD CP 160, paper No. 10.

Olsen, W., Shaw, R., and Newton, J. (1983), "Ice Shapes and the Resulting Drag Increase for a NACA 0012 Airfoil", NASA TM 83556.

Perkins, C. D., and Hage, R. E., (1949), "Airplane Performance Stability and Control", John Wiley & Sons, Inc., pp 350-367, and pp 458-470.

Potapczuk, M. G., Berkowitz, B. M., (1989), "An Experimental Investigation of Multi-Element Airfoil Ice Accretion and Resulting Performance Degradation", AIAA-89-0752.

Potapczuk, M. G., and Reinman, J. J. (1991), "Icing Simulation: A Survey of Computer Models and Experimental Facilities", in: *Effects of Adverse Weather on Aerodynamics*, AGARD-CP-496.

Proceedings of FAA International Conference on Airplane Ground Deicing (1992), Reston, Va., FS-92-1.

Ranaudo, R. J., Batterson, J. G., Reehorst, A. L., Bond, T. H., and O'Mara, T. M. (1989), "Determination of Longitudinal Stability and Control Derivatives Using Flight Data from an Icing Research Aircraft", NASA TM 101427 / AIAA-89-0754.

Ranaudo, R. J., Mikkelsen, K. L., Mc Knight, R. C., and Perkins, P. J. (1984), "Performance Degradation of a Typical Twin Engine Commuter Type Aircraft in Measured Natural Icing Conditions", NASA TM 83564 / AIAA-84-0179.

Reinman, J.J. (1994), "Icing: Accretion, Detection, Protection", In: AGARD-LS-197 *Flight in an Adverse Environment.*

Ritz, L, (1938), "Vereisung", *Jahrbuch 1938 der deutschen Luftfahrtforschung - Ergänzungsband*, pp106-111.

Root, L. E. (1945), "The Effective Use of Aerodynamic Balance on Control Surfaces", *J. Aero. Sci.*

Rodling, S. (1989), "Experience from a Propeller Icing Certification", SAE SUBCOMMITTEE AC-9C *Aircraft Icing Technology,* Meeting No. 11.

Scavuzzo, R. J., Chu, M. L., and Olsen, W. A. (1987), "Structural Properties of Impact Ices Accreted on Aircraft Structures", NASA CR-179580.

Schulson, E. M., Hoxie, S. G., and Nixon, W. A. (1989), "The Tensile Strength of Cracked Ice", *Phil. Ma. A..*, Vol. 59, pp303-311.

Shpilev, K. M., and Kruglov, A. B. (1974), "The Aircraft and Natural Climate Conditions", NASA TT F-793.

van Hengst, J. (1989), "Snow, Ice and Frost", Wingtips (Fokker Aircraft) No. 14.

van Hengst, J. (1993), "Aircraft De-Icing and Future Technical Developments - An Aircraft Manufacturer's Point of View", Wingtips (Fokker Aircraft) No. 26.

van Hengst, J., and Boer, J. N. (1991), "The Effect of Hoar-Frosted Wings on the Fokker 50 Take-Off Characteristics", in: *Effects of Adverse Weather on Aerodynamics*, AGARD-CP-496.

Zierten, T A., and Hill, E. G. (1987),: "Effect of Simulated Ground Frost on Airplane Performance", VKI Lecture Series *Influence of Environmental Factors on Aircraft Performance*, Brussels,Belgium , Feb. 16-19.

4. EXPERIMENTAL TECHNIQUES AND FACILITIES

Experiments are obviously an important tool for a phenomenon as complex as ice accretion on aircraft. This chapter reviews the techniques that are available for ice accretion simulation work relating to qualification or certification of aircraft or for research studies. Similarity considerations are first discussed since they are fundamental to ice accretion experiments; ground facilities and techniques are oulined next, followed by in-flight techniques. The chapter concludes with a description of instrumentation used in ice accretion tests.

4.1 REVIEW OF SIMILARITY REQUIREMENTS FOR ICE ACCRETION TESTS

In icing tests one normally wishes to simulate natural in-flight icing situations as realistically as possible. That is, model test conditions should, ideally, be dynamically similar to full-scale conditions. Dynamic similarity is often, however, difficult to achieve, particularly if the model tests are to be at reduced scale. Test facility size limitations frequently necessitate reduced or sub-scale testing; this is especially true for rotorcraft. Compromises are usually necessary and an appreciation of similarity requirements is essential to choosing the best compromises and understanding their consequences.

Another application where similarity considerations are important is when flight or ground test exposures conducted in one set of environmental conditions are to be used to assess icing behaviour in a different set of conditions.

The similarity requirements are, of course, a direct reflection of the physical phenomena involved in ice accretion. A description of the ice accretion process, as currently understood, appears in Chapter 1.

4.1.1 Similarity Considerations, Fixed-Wing Aircraft

A routine dimensional analysis would begin with a list of the independent physical parameters which are judged to have an important influence on the phenomenon. In the case of ice accretion the list would be long and a large number of independent non-dimensional parameters would have to be matched to ensure similarity between model and full-scale conditions. Simultaneous matching of all these parameters is, however, impossible except by exact replication of full-scale conditions. The routine approach is therefore not very useful in the case of ice accretion. In making this point, Bilanin (1991) lists 18 non-dimensional parameters.

A substantial number of the 18 parameters listed by Bilanin are ratios of properties (specific heats, latent heats, etc.) which are easily matched by using the full-scale substances, water and air, for the model tests. Indeed water and air would appear to be the only practicable substances to use in model icing tests because of the need to match numerous property ratios. There are, however conflicts between several of the remaining non-dimensional parameters identified by a routine dimensional analysis. It is necessary to resort to more detailed physical understanding and to mathematical models in efforts to find more flexible similarity requirements and to identify reasonable compromises and approximations.

Ice accretion tests require proper scaling of three main phenomena: the air flow field, the particle trajectories and the impingement-freezing process. Each will be considered in turn.

The streamline pattern and the aerodynamic pressure, force and moment coefficients must be the same for model and full-scale flows. The scaling requirements to achieve this are familiar to aerodynamicists. The model and full-scale bodies must be geometrically similar and, ideally, the Reynolds number based on body size and free stream velocity should be matched. In addition, if compressibility effects are significant, Mach number must be matched. It is usually not possible to match the Reynolds number, but there are well-established techniques for recognizing and alleviating problems that may stem from this. As mentioned elsewhere, icing problems usually occur in flight at relatively low Mach numbers so that compressibility effects can usually be neglected in icing studies for fixed-wing aircraft.

Droplet trajectories are determined by aerodynamic drag and inertia forces acting on the droplets as they approach the aircraft. The drag forces are due to the relative velocity between the droplets and the air. Aerodynamic lift forces are negligible because shear velocity gradients are negligible in the bulk of the air flow and droplet angular velocity is negligible. Gravity forces are negligible relative to inertia forces because the ratio of inertia to gravity forces on the particles, that is, the Froude number V^2/Lg, is of order 100 or more in full-scale situations. V is the flight speed and L is a reference length of the aircraft (e.g. mean chord length of the wing). Application of Newton's law readily yields the equations of droplet motion for the three axis directions. The requirements for similarity of droplet trajectories can be found by putting these equations into suitable non-dimensional form. Langmuir and Blodgett (1946), Etkin (1971), Armand et al. (1977), Bongrand (1978) and Bragg (1982) have done this and obtained similar results.

Bragg's (1982) analysis is the most thorough and his result gives the most precise droplet-scaling law.

Using Bragg's result, droplet trajectories will be correctly scaled if the following relation is satisfied:

$$\bar{K}_m = \bar{K}_f \qquad (4.1a)$$

$$\text{where } \bar{K} = K/(R_{dr})^{\lambda} \qquad (4.1b)$$

$$\text{and } R_{dr} = \rho V d/\mu \qquad (4.1c)$$

$$K = (\rho_{dr}/\rho)(d/L)(R_{dr})/18 \qquad (4.1d)$$

The subscripts m and f denote model and full-scale, respectively. The symbols ρ, ρ_{dr} , d and μ denote air density, droplet density, droplet diameter and air viscosity, respectively. λ is the slope of a straight-line fit, in log-log coordinates over the range of R_{dr} covered by the model and full-scale droplets, to the droplet drag law:

$$C_D R_{dr}/24 = \text{function of } R_{dr} \qquad (4.2)$$

R_{dr} is the droplet Reynolds number based on droplet diameter and relative velocity and C_D is the droplet drag coefficient. Recall that the right hand side of eqn. (4.2) is unity for $R_{dr} < 1$ (Stokes, 1851). The value of λ can be optimized for each application but Bragg's work indicates that a value near 0.35 is quite satisfactory for most cases.

It can be shown that eqn. (4.1) is equivalent to requiring that the ratio (inertia force/drag force) be matched for the model and full scale droplets. It should be noted that eqn. (4.1) is a substantially less restrictive droplet-scaling requirement than that suggested by a routine dimensional analysis. The latter would suggest that d/L , ρ_d/ρ , and R_{dr} would each have to be matched. Equation (4.1), on the other hand only requires that a single combination of parameters be matched and this gives more flexibility.

Equation (4.1) does entail an approximation, namely the use of an approximate fit to the drag law, eqn. (4.2). Typically, however, droplet Reynolds numbers only vary from 0 to about 500 during their trajectories so the approximation is a good one. Bragg (1982) has shown that eqn.(4.1) gives excellent scaling of droplet trajectories. Figure 4.1-1 shows that eqn. (4.1) produces excellent collapse of experimental data for overall droplet collection efficiency for three different droplet sizes. Figure 4.1-2 shows excellent collapse of local collection efficiency both for the parameter of eqn. (4.1a) and for the earlier Langmuir and Blodgett(1946) parameter, K_0. K_0 is an average of $24K/C_D R_{dr}$ over the droplet Reynolds number range 0 to R_{dr} (Bragg,1982).

The impingement-freezing process will be considered next. For glaze icing cases, correct scaling of this process presents the most difficult challenges because of the complex dynamic, capillary and thermal phenomena that are involved. This problem can be sub-divided into two: obtaining the correct distribution over the body surface of (1) volume of impinging water and (2) freezing fraction and splashing.

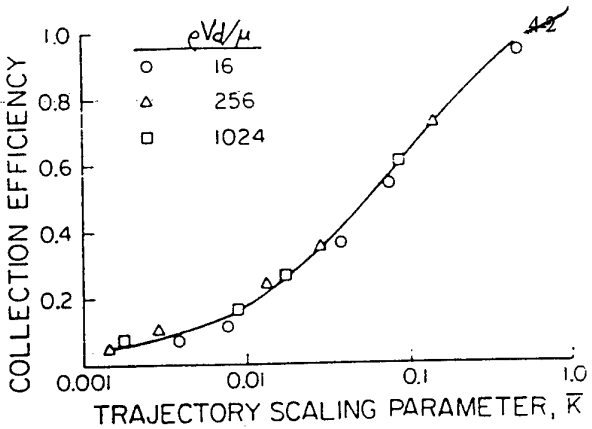

Fig. 4.1-1 Comparison of K_0 and $\bar{K}$ in scaling the local droplet impingement (Bragg, 1982)

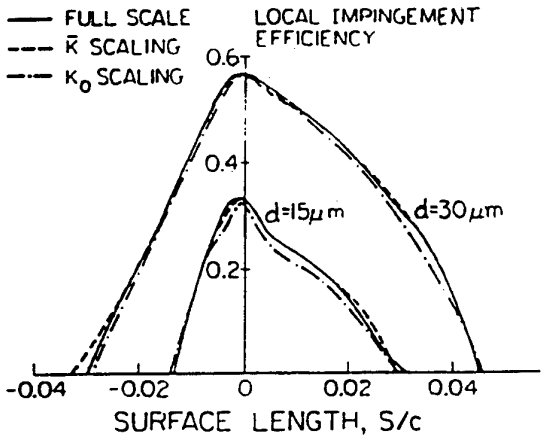

Fig. 4.1-2 Collection efficiency of a NACA 65A004 airfoil as a function of $\bar{K}$ (Bragg, 1982)

Impingement distribution will be correctly scaled if the following relation is satisfied everywhere on the bodies:

$$(\text{impingement volume}/L^3)_m = (\text{impingement volume}/L^3)_f$$

that is

$$(LWC\, L^2 V\beta\tau/\rho_i L^3)_m = (LWC\, L^2 V\beta\tau/\rho_i L^3)_f \qquad (4.3)$$

where LWC is the liquid water content (gm/m^3), ρ_i is the density of the ice (assumed equal for model and full scale), β is the local droplet-collection efficiency and τ is time. Assuming that the flow field and droplet trajectories are correctly simulated (i.e. kinematically similar) β will be equal at all corresponding points on the model and the full-scale body. Equation (4.3) can then be simplified to

$$(LWC\, V\tau/L)_m = (LWC\, V\tau/L)_f \qquad (4.4)$$

Equation (4.4) can be regarded as a time-scaling equation and it allows some flexibility of choice regarding LWC and V.

For rime icing the freezing fraction is unity throughout the impingement region and complete freezing occurs

immediately upon impact of the water droplets. Correct simulation thus requires only flow field similarity and satisfaction of eqns. (4.1) and (4.4). Of course one must also ensure that test conditions are such that the freezing fraction actually is unity everywhere. Satisfaction of the simulation requirements for rime icing is quite feasible. Armand et al. (1977) found good agreement between icing tunnel test runs with circular cylinders at different size-scaling ratios, 6:1 and 12:1 , for what appear to be rime ice deposits. Anderson (1994) also found good agreement in similar tests with both size scaling (2:1) and velocity scaling (1:1 and 2:1) for rime icing conditions; agreement was not as good for mixed and glaze icing conditions. Some of the Armand et al. and Anderson results are shown in Figs. 4.1-3 and 4.1-4 .

As outlined earlier, glaze icing occurs when LWC is relatively high and /or the ambient air temperature is only a little below 0 C. Latent heat release then tends to exceed convective heat loss to the air, causing the temperature to reach 0 C and the freezing fraction, n, to be less than unity in at least parts of the impingement region. The unfrozen water can either run downstream under the influence of aerodynamic shear stress ("runback water") or, perhaps, as suggested by Bilanin (1991), be splashed out into the airstream. At steady state, for any small patch or control volume on the surface, mass conservation requires that:

$$\begin{pmatrix}\text{rate of water}\\ \text{leaving patch}\end{pmatrix} =$$

$$\begin{pmatrix}\text{impingement}\\ \text{rate}\end{pmatrix} + \begin{pmatrix}\text{rate of entry of runback}\\ \text{water from upstream}\end{pmatrix} (1-n) \qquad (4.5)$$

Consequently, if all of the preceding scaling requirements are met, the ice-accretion distribution will be correctly simulated if the distribution of n is correct from the stagnation line onwards and splashing, if any, is correctly simulated. Simulation of splashing is considered later.

Let us consider the freezing fraction, n, assuming that splashing either does not occur or is correctly simulated. Following Messinger (1953), a heat balance equation can be written for the water in any small control volume in the ice accretion region. The most important terms in this equation are the rate of release of latent heat by the freezing water and the rate of heat loss to the ambient air due to convective heat transfer and evaporation. The evaporation is also due to convection and for water/air the convective mass-transfer coefficient is approximately proportional to the convective heat transfer coefficient (Kreith,1965). Calculations show that if the ambient air is saturated, as it would tend to be in icing situations, the evaporative heat loss rate, q_e , is roughly equal to the convective heat transfer rate, q_c. Other terms in the heat balance include the heat to warm the impinging water to 0 C and the heat equivalent to the kinetic energy of the impinging water; of these terms, the first can sometimes be of comparable magnitude to the convective heat loss term but the other is normally negligible in glaze icing situations. The approximate heat balance equation is:

$$n(m_i + m_r)h_{fs} = (1 + q_e/q_c)h_c(T_s - T_\infty) + m_i c_w(T_s - T_\infty) \qquad (4.6)$$

where m_i and m_r are the rate per unit surface area of impingement and runback, respectively, of liquid water into the control volume, h_{fs} is the latent heat of fusion, h_c is the convective heat transfer coefficient, c_w is the specific heat of water and T_s and T_∞ are the temperature of the surface and of the ambient air, respectively. The evaporative heat loss is included in the convective term of eqn. (4.6) by insertion of the factor $(1 + q_e/q_c)$; as already noted, $q_e/q_c \approx 1$. Note that T_s is 0 C for glaze icing and that m_i = LWC Vβ . Equation (4.6) can be solved for the freezing fraction, n :

$$n = \frac{(1+q_e/q_c)\, h_c\,(T_s - T_\infty)}{(LWC)(V)\beta(1+m_r/m_i)\, h_{fs}} + \frac{c_w(T_s - T_\infty)}{(1+m_r/m_i)\, h_{fs}} \qquad (4.7)$$

Since preceding requirements plus correct scaling of n imply that all liquid massflows will be correctly scaled, eqn.(4.7) shows that n will be correctly scaled if the two parameters

$$A = c_w(T_s - T_\infty)/h_{fs} \qquad (4.8)$$

and

$$B = \frac{(1+q_e/q_c)\, h_c\,(T_s - T_\infty)}{(LWC)\,(V)\, h_{fs}} \qquad (4.9)$$

are matched for model and full scale. Instead of A one could use b, where

$$b = 2\beta A/B \cong LWC\, V\beta c_w/h_c \qquad (4.10)$$

b is the 'relative heat factor' introduced by Messinger (1953) and used by Armand et al.(1977) in developing their scaling requirements. Note however that c_w/h_{fs} is only 0.012/C for water so that the last term of eqn. (4.7) will often be relatively small; it will only seldom be as much as half the other term on the right. Thus it would normally be substantially more important to match the parameter B of eqn. (4.9) than A or b of eqn. (4.8) or (4.10). The parameter B has a clear physical significance; it represents the ratio of convective heat loss to potential for latent heat release. B $\approx$ 1.0 would represent the approximate boundary between glaze and rime icing, glaze icing being expected for B < 1.0 . B will be referred to as the 'convective/latent heat ratio'.

Matching of the convective/latent heat ratio, B, of eqn. (4.9) entails adjusting the product $h_c(0\text{ C} - T_\infty)$;

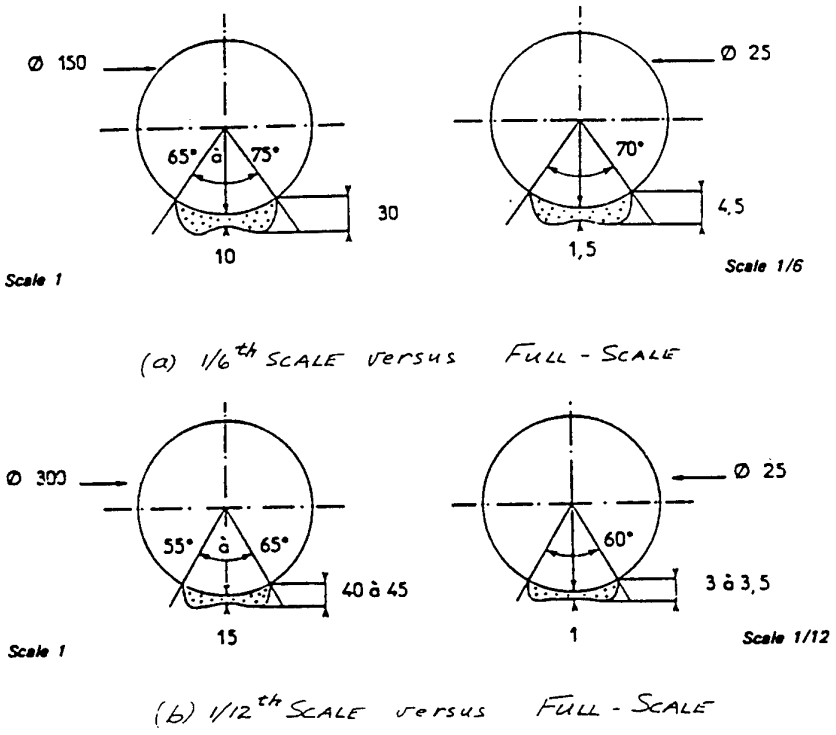

Fig. 4.1-3 Comparison of Reduced-Scale and Full-Scale Ice Deposits, Rime Icing Conditions (Armand et al. 1977) (dimensions in mm)

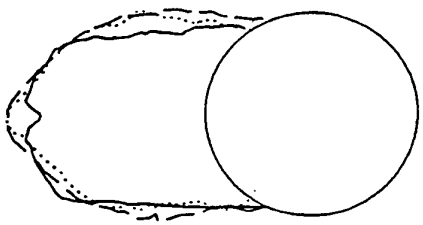

	D cm	T_{tot} °C	V m/s	d µm	LWC g/m³	t min
—— Reference	5.1	-26	94	30	1.3	7.8
— — Swedish-Russian	2.5	-29	47	30	1.3	7.8
····· French	2.5	-28	47	25	1.7	5.9

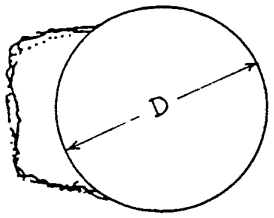

	D cm	T_{tot} °C	V m/s	d µm	LWC g/m³	t min
—— Reference	15.2	-13	76	28	.8	18.3
— — Swedish-Russian	7.6	-14	61	22	.8	11.4
····· French	7.6	-14	61	20	.95	9.5

Fig. 4.1-4 Comparison of Ice Deposits for Scaled and Reference Cases, Rime Icing Conditions (Anderson, 1994)

recall that (LWC•V) appears in the earlier scaling requirement eqn. (4.4). The air temperature T_∞ in the model tests could be made equal to the full-scale value, in which case the parameter A of eqn.(4.8) would also be matched. In the light of the preceding paragraph it would often appear preferable, however, to use a different value of T_∞ in order to compensate for the change in value of h_c associated with differing model and full-scale Reynolds numbers.

It is difficult to ensure that h_c , the local convective heat transfer coefficient, assumes the desired value at all points in the ice-accretion region. The correlation for h_c can be written as

$$h_c(L/k_A) = F(\text{Re, Pr, position, } k/L, \Lambda) \qquad (4.11)$$

where F denotes a functional dependence and k_a, Re, Pr, k and Λ are, respectively, the thermal conductivity of the air, the flow Reynolds number $\rho VL/\mu$, the Prandtl number for the air, the roughness height and a roughness-spacing parameter. The spacing parameter Λ is defined as the reciprocal of frontal area of roughness elements per unit surface area (Simpson, 1973; Kind and Lawrysyn, 1992).

k_a and Pr will always be virtually the same in the model and full-scale cases but in sub-scale testing Re will almost invariably be less than the full-scale value. As mentioned earlier this usually presents few problems for aerodynamic scaling but heat transfer is quite sensitive to Re. The dependence on Re in eqn. (4.11) is of the form

$$h_c(L/k_a) \propto Re^x \qquad (4.12)$$

The exponent, x, is 0.5 for laminar flow. Values for turbulent flow are substantially higher and depend on Re. For both smooth and rough circular cylinders the exponent for the total heat transfer rate varies from 0.63 for sub-critical flow ($Re < 2x10^5$) to about 1.0 for $Re > 10^6$ (Achenbach, 1975, 1977). This gives an indication of the range of variation of x . Data collected by Kind et al.(1983) indicate that values of x are not greatly affected by body shape. Icing researchers have used values of x ranging from 0.5 to 0.8 (see Anderson, 1995).

For rough circular cylinders Achenbach (1977) found values of h_c up to 7.5 times higher than the corresponding smooth value ($Re = 4x10^6$, k/L=0.003 and 0.006, Λ=4.2). This shows that h_c can be very sensitive to roughness. As mentioned earlier, it appears that ice accretion in glaze conditions is strongly influenced by roughness effects. The roughness can be either on the aircraft surface itself or it can be in the form of water beads and/or rivulets and/or irregularities on the accreting ice surface. Unfortunately there is little data available regarding the effects of roughness on heat transfer and no reliable overall correlation is available. The little data that is available is for distributed roughness of relatively small height (e.g. knurled surfaces) and there is no data at all for large roughness elements similar to those that can occur on ice accreted surfaces. Experimental work in this area would be very useful.

It would appear that the best approach for icing tests is to attempt to simulate the development of the full-scale roughness as closely as possible. This entails correct scaling of surface tension phenomena so that surface droplet and rivulet formation are correctly scaled. Moreover this would also ensure correct scaling of splashing which the recent experiments of Bilanin and Anderson (1995) suggest is very important. The requirement is to match surface wettability and the ratio of aerodynamic pressure and shear forces to surface tension forces. This would be ensured by satisfaction of the following condition (Bilanin,1991):

$$(\text{Re}, \gamma, \rho V^2 L/\sigma)_m = (\text{Re}, \gamma, \rho V^2 L/\sigma)_f \qquad (4.13)$$

γ is the contact angle for liquid water on the surface and σ is the surface tension of the water in air. $\rho V^2 L/\sigma$ is known as the Weber number and it represents the ratio of aerodynamic or inertia forces to surface tension forces.

Equation (4.13) can seldom be satisfied precisely in sub-scale tests because $Re = \rho VL/\mu$ cannot usually be matched. However the consequences of this should not be serious provided that the usual precautions are taken to ensure good flow similarity. At least in principle, γ and σ can be manipulated for model tests by use of different materials or coatings for the model surface and use of surfactants in the spray water. However this has not yet been tried in a systematic way and may well present practical difficulties. As mentioned earlier, Hansman and Turnock (1989) and Bilanin and Anderson (1995) found that addition of a surfactant had a substantial effect on the shape of an ice deposit. Indeed Bilanin and Anderson describe the effect as dramatic!

In summary, for model tests relating to fixed-wing aircraft flying at incompressible Mach number the following conditions should be satisfied for rime icing cases:

- flow-field similarity
- equation (4.1)
- equation (4.4)

In addition, for glaze icing cases the following conditions apply:

- match B of eqn. (4.9) throughout the ice accretion region
- if possible, also match b of eqn. (4.10); priority should be given to matching B
- match γ and Weber number, eqn. (4.13)

Satisfaction of all the requirements in full-scale tests is quite feasible. At reduced scale, on the other hand, satisfaction of the last three requirements would be rather difficult and has not yet been attempted in a systematic way. Good simulation of glaze ice accretion at reduced scale for a wide range of conditions has yet to be demonstrated.

4.1.2 Similarity Considerations, Rotors and Propellers

For rotorcraft and propellers all the similarity considerations of the preceding sub-section apply. In addition, compressibility and dynamic effects due to blade rotation must be considered.

As is well known, flow-field similarity requires matching of advance ratio and pitch settings etc. as well as geometric similarity of the rotors. The usual Reynolds number considerations also apply. In effect the aerodynamic performance coefficients must be the same in the model and full-scale cases. Mach numbers are likely to be in the transonic range near blade tips in the full-scale case and Mach number must then be matched in model tests.

Since advance ratio must be matched, the reference velocity, V, in the above scaling laws can be either the free-stream velocity or the tip speed and L can be any convenient reference length, for example the blade chord length or rotor diameter.

Other than Mach number, the main additional scaling requirement is matching of the ratio of centrifugal force to adhesion force for ice deposits on the model and full-scale rotors. Assuming correct scaling of the ice deposits this requires that

$$(\rho_i \Omega^2 L^2/\varsigma)_m = (\rho_i \Omega^2 L^2/\varsigma)_f \qquad (4.14)$$

where ρ_i and Ω are the density of the ice deposit and the angular speed of the rotor, respectively, and ς is the adhesion strength, that is the failure stress of the bond between the ice and the blade surface. Assuming equal ρ_i and equal ς, eqn. (4.14) would require the rotor tip speed in the model test to equal the prototype value. Since temperature T_∞ will not differ greatly between model and full scale, this would imply approximate equality of Mach numbers as well. Looking at this the other way around, equality of model and full-scale adhesion strength would require matching Mach numbers even if compressibility effects were unimportant. On the other hand, eqn. (4.14) would not require matching of tip speeds if the adhesion strength in the model test, ς_m , were made to differ from the full-scale value. This is possible, at least in principle, by suitable choice of surface material or coating for the model blades, although control of values is problematical (Reich,1994). The effects on contact angle, γ, would also have to be recognized.

If the value of the reference velocity, V, in the model tests is dictated by a need to match Mach number or tip speed (by virtue of eqn. (4.14)), the surface tension of the spray water must be adjusted to satisfy eqn. (4.13) if surface tension effects are to be properly scaled.

Note that blade flexing behaviour may also be important to ice shedding behaviour and should be simulated if possible.

4.1.3 Current Scaling Practices

The preceding sub-sections have presented the scaling requirements that are thought to apply if all effects important to ice accretion are recognized. For glaze icing it is difficult to even approximately satisfy all the pertinent requirements in sub-scale testing. Current scaling practices vary widely and sub-scale testing appears to be relatively uncommon. Anderson(1994) conducted comparative icing tests to assess three sets of scaling practices that are currently used in different laboratories. His paper gives a good picture of current practices.

The three practices assessed by Anderson will be referred to as practices 1, 2, and 3.

Practice 1 requires model size, airspeed, pressure, temperature and water droplet size to be the same as the full-scale values. This ensures proper scaling of the flow field and droplet trajectories and of compressibility effects. Surface tension effects will also be properly scaled if the model surface material and surface tension of the spray water are the same as in full-scale. Practice 1 also requires that eqn. (4.4) be satisfied. This is in fact its only element of flexibility; that is, it does not require matching of LWC. Unfortunately, however, if LWC is not matched the parameters B and b of eqns. (4.9) and (4.10) will not match because the convective heat transfer coefficient, h_c ,can be expected to have the same value as in the full-scale situation. Consequently good simulation of glaze ice shapes cannot be expected unless LWC and time, τ, are <u>each</u> matched. Anderson(1994) found that the shape of glaze ice deposits did indeed change substantially when LWC was varied while keeping the product (LWC • τ) constant.

Practice 2 (the "Swedish-Russian Law") allows testing at reduced scale. Droplet trajectories are approximately scaled by use of eqn. (4.1) with exponent $\lambda = 0$. Model LWC is required to equal the full-scale value and time and velocity are required to satisfy eqn.(4.4). Model and full-scale air temperatures are required to be equal. No attempt is made to scale heat transfer or surface tension effects and in reduced scale tests B, b, γ and Weber number (eqns. (4.9), (4.10) and (4.13)) cannot be expected to match full-scale values. In tests at full scale this practice would have the same problems as Practice 1 unless V and τ are <u>each</u> made equal to the full-scale

values. As seen earlier (Fig. 4.1-4) this scaling practice gave good results for rime icing. Some of Anderson's (1994) results for mixed and glaze icing are shown in Fig. 4.1-5. As expected, results are not entirely satisfactory for reduced-scale cases although they are quite good for the full-scale cases.

Practice 3 (the "French Law") also allows testing at reduced scale. Armand et al. (1977) present the derivation of the scaling laws used in this practice which was published by Charpin and Fasso (1972). Droplet trajectories are scaled using eqn. (4.1) with exponent λ = 0.39 . LWC is scaled on the basis of trying to match the relative heat factor of eqn. (4.10). Time and velocity are required to satisfy eqn. (4.4). The ambient air temperature is chosen in an attempt to match the model and full-scale freezing fraction, n. This is equivalent to trying to match the convective/latent heat ratio, B, of eqn. (4.9). The equation developed for this purpose assumes that the exponent x in the heat transfer correlation, eqn. (4.12), has a value of 0.8 No attempt is made to match surface tension effects. Figures 4.1-3 and 4.1-4 show that this Practice gives good results for rime icing. Results for mixed and glaze icing are included in Fig. 4.1-5; they are similar to those for the Swedish-Russian scaling law. Since this practice does attempt to scale convective effects it may be that the shortcomings seen in Fig. 4.1-5 are mainly due to improper scaling of surface tension effects and the associated water-caused roughness. Armand et al. remark that reproduction of ice accretions at reduced scale is much poorer when no scaling laws are followed.

Bongrand (1978) also outlines a scaling practice similar to that of the preceding paragraph. Since he is concerned with engine icing, length scale ratio is assumed to be unity but the effects of altitude differences between test and flight conditions are of interest. Droplet trajectories are scaled using eqn. (4.1) with exponent λ = 0.5. Equation (4.4) is satisfied and an effort is made to match the equivalent of the convective/latent heat ratio of eqn. (4.9). No detailed results for ice deposit shapes are shown.

It should be noted that the product of Velocity and Time for the reference cases of Figs. 4.1-4 and 4.1-5 gives horizontal extents much larger than the maximum realistic values suggested by Fig. 2.7 for the corresponding LWC values. Scaling discrepancies for shorter run times may be somewhat less than those seen in Fig. 4.1-5; nevertheless horned accretion shapes similar to the reference cases of Fig. 4.1-5 do actually occur in natural icing conditions and would have to be reproducible in sub-scale testing.

4.1.4 Recent Developments

Anderson (1995) presents results of comparative icing tests carried out to assess three scaling laws which differ somewhat from those outlined in Section 4.1.3.

The "Olsen Method" is a modification of Practice 1 of Section 4.1.3 . It only accomodates full scale testing. The requirement to match air temperature is dropped in favor of attempting to match the freezing fraction in the model and reference cases. That is, an attempt is made to properly scale convective heat transfer. The exponent, x, of eqn. (4.12) is assigned the value 0.5 This leads to an equation for the air temperature to be used in the model tests. The test results were much improved over those obtained by following the un-modified scaling practice. Three test runs using LWC ranging from 0.8 to 1.3 g/m^3 gave very similar ice deposit shapes; the deposits had pronounced horns.

The second set of results reported by Anderson (1995) is for a slight modification of the "French Law", Practice 3 of Section 4.1.3. The modification consists of using 0.5 instead of 0.8 for the exponent in the convective heat transfer relation, eqn. (4.12). This was motivated by speculation that the exponent value for laminar flow might be more appropriate for Anderson's test conditions. The modification had a substantial effect on ice deposit shapes but the results of half-scale tests were in little or no better agreement with the full-scale results than those based on the original "French Law".

Anderson (1995) also reported results obtained using the scaling analysis of Ruff (1986). This is basically the same as the "French Law", with some differences in the expressions used to evaluate certain parameters. 0.5 was used for the exponent, x, in the convective heat transfer relation. Quality of results was found to be about the same as for the "Modified French Law". Figure 4.1-6 shows one result. The results reported by Anderson (1995) support the importance of properly scaling convective heat transfer in glaze icing tests.

Bilanin and Anderson (1995) report results of comparative icing tests in which the Weber number was matched. That is, surface tension effects were properly scaled. Test conditions were chosen in an attempt to also satisfy all other scaling requirements, including convective heat transfer. The desired Weber number was achieved by choosing flow velocity and droplet size such that V^2d had the same value in the full- and reduced-scale tests. The surface tension of the spray water was not altered. Consequently the only parameter that was open to choice was the diameter of the model cylinder. The results of the tests were very encouraging, with good matching of glaze ice deposit shapes for tests at 1/3, 2/3 and full scale.

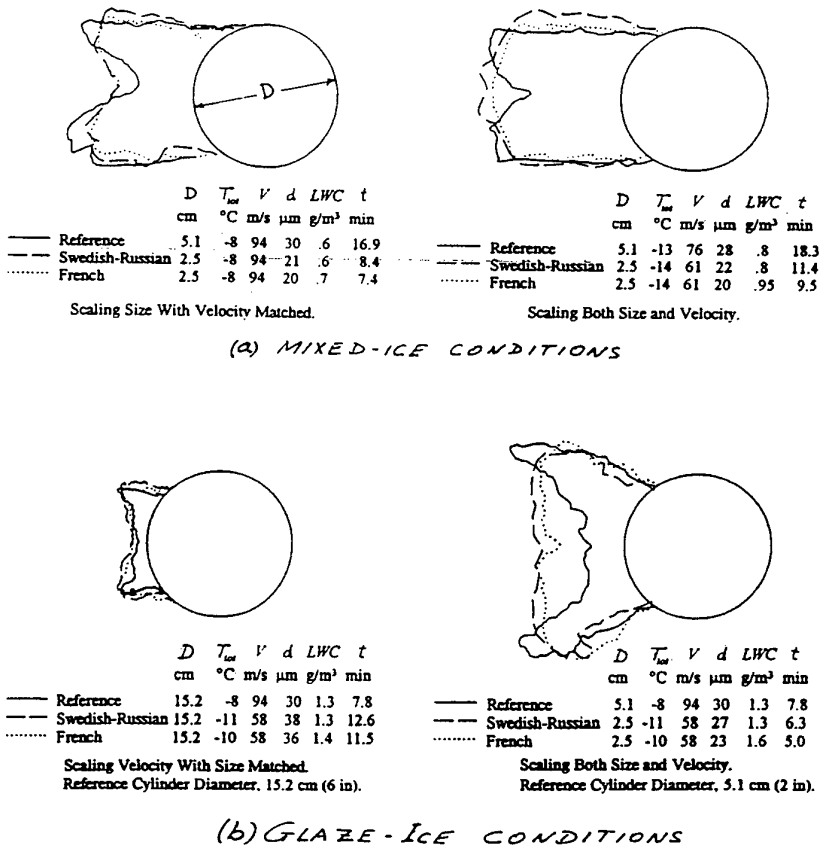

Fig. 4.1-5 Scaling with Swedish-Russian and French Laws for Mixed- and Glaze- Ice conditions (Anderson, 1994)

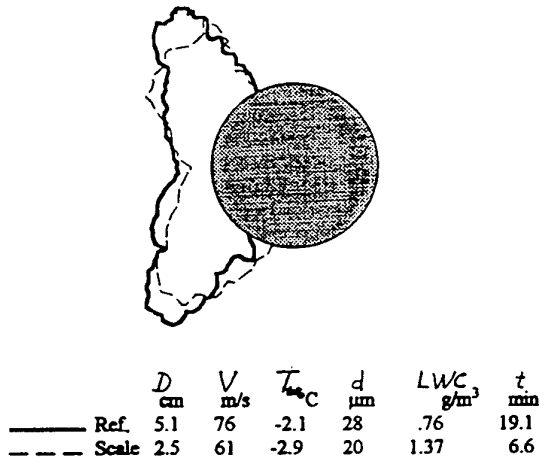

Fig. 4.1-6 Scaling with Ruff's (1986) Laws for Glaze Icing (Anderson, 1995)

Figure 4.1-7 shows some results. This indicates that good reduced-scale simulation of glaze ice accretion is indeed possible, provided that surface tension effects are correctly scaled. It would appear worthwhile to undertake a substantial effort to develop techniques for doing this over a wide range of conditions.

4.1.5 Concluding Remarks Regarding Similarity Requirements

The similarity requirements for rime icing are clear and can be satisfied without undue difficulty in both full and reduced scale testing. Good simulation of rime ice accretion, even at reduced scale, has been demonstrated when all the requirements are respected.

The experimental evidence indicates that convective heat and mass transfer and surface tension effects must be properly scaled in glaze icing tests. This is relatively straightforward in the case of full-size models but presents difficult challenges for tests at reduced scale. Some efforts have been made to scale convective effects.

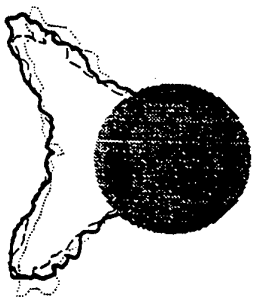

	D	V	T_{tot}	d	LWC	t
scale	cm	m/s	K	μm	g/m³	min
full	7.6	66.7	265.9	61.0	0.897	26.6
2/3	5.1	76.7	266.3	38.5	0.960	14.4
1/3	2.5	95.6	267.5	21.3	1.08	5.1

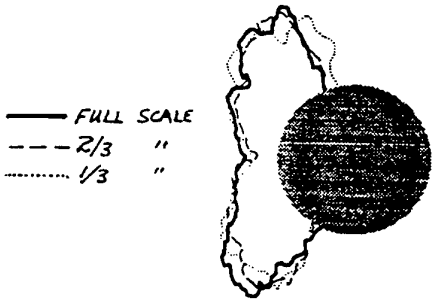

	D	V	T_{tot}	d	LWC	t
scale	cm	m/s	K	μm	g/m³	min
full	7.6	67.4	268.7	58.0	0.887	26.7
2/3	5.1	76.2	269.1	46.4	0.967	14.4
1/3	2.5	95.3	270.3	21.5	1.05	5.3

Fig. 4.1-7 Glaze Icing Test Results with Almost Matching Weber Number (Bilanin & Anderson, 1995)

Only one attempt to scale surface tension effects has been reported. Scaling laws for convective and surface tension effects are presented above; it appears to be possible, at least in principle, to satisfy them approximately, even in reduced scale tests. A substantial development effort would clearly be required. Although very recent results are promising, good simulation of glaze ice accretion at reduced scale has yet to be demonstrated for a wide range of conditions.

4.2 GROUND FACILITIES AND SIMULATION TECHNIQUES

Experimental simulations of ice accretion are understood to cover a wide range of test types. Some are intended to simulate natural in-flight icing situations, and others only to simulate certain aspects present in the complex ice accretion proccess. In each case some similarity requirements, as presented in Section 4.1, have to be met, but compromises must be accepted as the only possibility to obtain reliable data in the repeatable and controlled environments of ground test facilities.

To perform icing tests in prescribed conditions, complicated facilities are needed. They are specifically suited for different groups of tests:

1) Fixed-Wing Aircraft, 2) Rotorcraft and Propellers, and 3) Engines. Facility types and their specific characteristics are reviewed in the next Sections.

Once the external flow conditions are defined and depending on the objectives sought, different simulation techniques are employed.

In a first type of experiments, only dry air is needed. The ice shapes should be geometrically similar and objectives are either to measure global aerodynamic coefficients or to determine the characteristics of the flow field. Studies of this type include thermal measurements, since the local heat transfer coefficient is one of the most critical values in the determination of the ice accretion process. As is well known, surface roughness is a critical feature in heat transfer evaluation.

Since some of the accreted ice surfaces are characterized by large and irregular roughness elements, the measurement of the local heat transfer coefficients becomes a complicated matter.

A second type of simulations uses two-phase flows, made up of water droplets and dry air. These simulations are used to study water droplet trajectories, local impingement distributions, droplet splashing, surface runback water, thermal effects, etc. and include the presence of a liquid film that is deposited on the surface. The temperatures are above the freezing point and the experiments are aimed at understanding the role played by liquid water, and are applicable to glaze ice accretion cases.

The third type of simulations aims at complete similarity of all existing physical phenomena, maintaining air temperature below freezing values and including clouds of supercooled droplets. In many cases, the interest is only in the shape of the accreted ice, with its surface details and water phenomena, but there are also experiments undertaken to determine the flow field and the overall aerodynamic characteristics, as the ice accretion progresses with time. For these simulations, in which complete physical similarity is sought, direct measurements of important variables such as surface temperature distribution, droplet splashing, local convective heat transfer coefficients, etc. require specialized instrumentation and measuring techniques in addition to the proper test facility.

4.2.1 Ground Facilities

As already mentioned, experimental icing simulations are in many instances performed in specially designed ground facilities where natural icing conditions are to be reproduced. Such tests may be conducted with full-scale prototypes or sub-scale models. These tests are performed in cold airstreams, which contain icing clouds made up of supercooled droplets or ice particles. Similarity laws must be used to apply the results to the desired dimension, velocity and droplet-cloud conditions of the flight vehicle. In subsequent Sections, different types of ground icing facilities will be reviewed. Following Olsen (1981) they may be classified in three groups: 1) Icing wind tunnels, where normally sub-scale models are tested. 2) Engine test cells, specifically designed to simulate the relevant variables in engine icing tests. 3) Low velocity facilities where components or full-scale vehicles may be tested.

NASA's Icing Research Tunnel shown in Fig. 4.2-1 (Potapczuk and Reinmann, 1991).

Test section size ranges from intermediate dimensions of about 2m x 2m, to small ones of about 0.15m x 0.15m. The velocities usually cover only the low speed range (M=0 to 0.4), especially for the largest facilities, but there are some small icing tunnels that can reach high subsonic values (M=0.8).

As is the case in conventional dry air wind tunnels, flow quality is of utmost importance. In addition to requirements for uniformity of velocity and limits on flow angularity in the test section, temperature and droplet-cloud variables must have spatial uniformity. Also, the spray system must be capable of reproducing a wide range of values for liquid water content, droplet mean volume diameter (MVD) and droplet size spectra, in order to simulate nature.

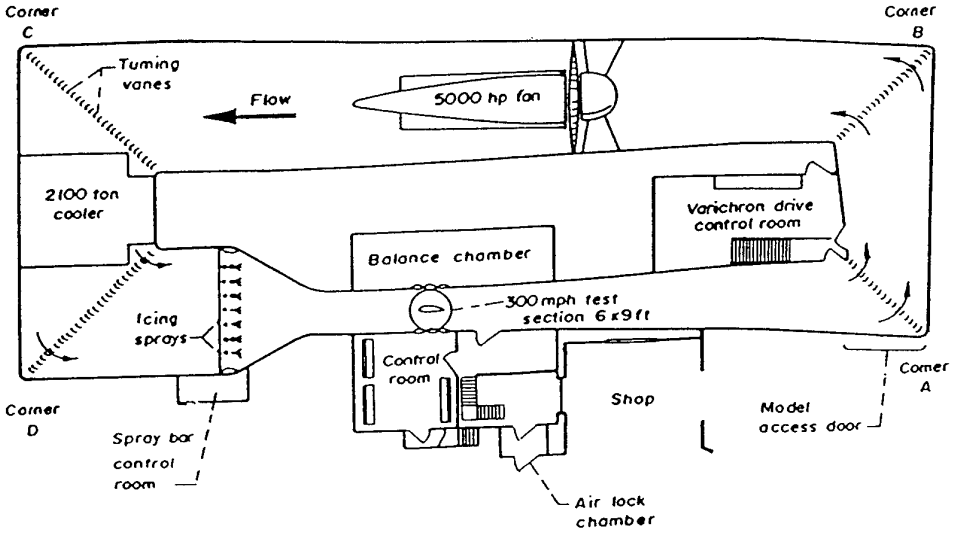

FIG. 4.2-1.- Schematic of the NASA Lewis Research Center Icing Research Tunnel (IRT)

4.2.1.1 *Icing Wind Tunnels*

These facilities have all the systems and are of similar configuration as conventional dry air wind tunnels, but they incorporate two additional features that make them special and unique.

First, they have a refrigeration system that cools the air to well below freezing temperatures and second, they have a water spray system that injects water droplets into the air stream creating a supercooled cloud. The typical configuration of a closed loop wind tunnel has the spray system located at the end of the settling chamber, before the tunnel contraction while the heat exchanger is in the leg upstream of the corner before the settling chamber. A classical example of an icing tunnel is offered by

As these facilities include a two-phase flow in the test section, specialized instrumentation is needed to measure the flow variables, in particular for the liquid phase.

A list of Icing Wind Tunnels, based mostly on AGARD AR-223 (1986), is shown in Table 4.2-1 at the end of this Subsection.

4.2.1.2 *Engine Icing Facilities*

Engine icing test cells try to simulate, as closely as possible, natural atmospheric icing conditions, and are used to evaluate ice accretion shapes that may form on engine inlets, to measure the effects on the operation and performance of the engine and to evaluate the engine's ice protection system.

These test cells are either of the "sea-level conditions" type or altitude test facilities. The first type are of large dimensions and have the advantage of enabling simulation of icing in crosswinds and tailwinds. This type of facility is shown schematically in Fig. 4.2-2 (Keller, 1978).

The second type are smaller facilities, but tests can be conducted over a wide range of Mach numbers, pressures, altitudes and inlet conditions and the variables defining the icing cloud can be accurately controlled and monitored during the test. Two possible configurations are illustrated in Figs. 4.2-3 and 4.2-4 (Hunt, 1978). This type of facility is described by Hunt (1978), Swift (1978) and Bongrand (1978). Due to their reduced size, tests are normally made at sub-scale and similitude plays an important role (Ruff, 1985; Bartlett, 1986).

A list of the most important Engine Icing Facilities, based on AGARD AR-223 (1986), is shown in Table 4.2-2.

One of these facilities is capable of testing full-size hovering helicopters in a wind-blown icing cloud. Table 4.2-3 includes existing Low Velocity Facilities, also based on AGARD AR-223 (1986).

4.2.2 Experimental Simulation Techniques

4.2.2.1 *Dry Air Simulations*

As ice accretes on the components of air vehicles, shape changes at the leading edges degrade their aerodynamic performance. One group of experimental simulations involves performing different types of tests in a dry air environment using detailed replicas of ice shapes. The ice shape at any desired stage of the icing process is supposed to be known and detailed replicas must be manufactured. Methods to obtain replicas from silicone rubber molds into which epoxy resins are poured, have been reported by Rehorst and Rictcher (1987).

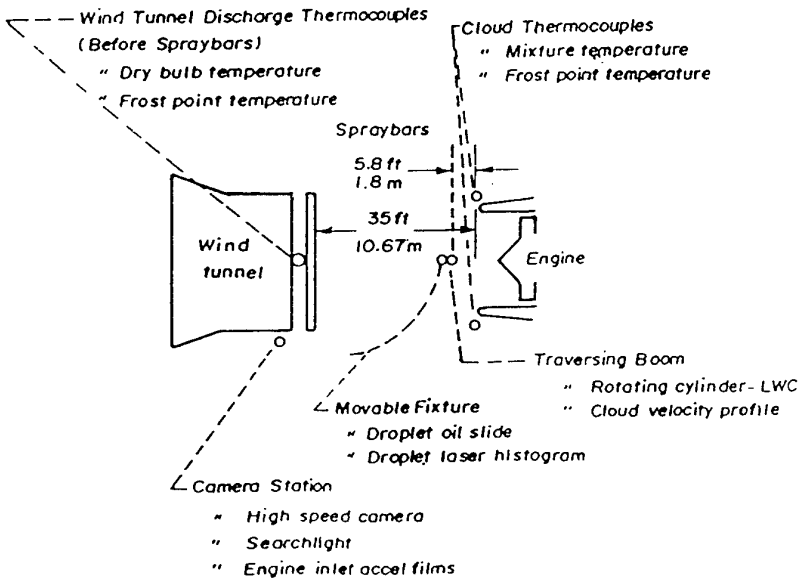

FIG 4.2-2 Schematic of the General Electric engine icing test facility in Peebles, Ohio, USA

4.2.1.3 *Low Velocity Facilities*

There is a group of facilities that are operated at low velocities (0-20 m/s) and generally have large dimensions. They either have refrigerated cold rooms or they are operated outdoors in cold climates. The icing cloud is produced by a spray system located in front of the test vehicle, as indicated in Fig. 4.2-5 (Olsen, 1981).

This group of simulations includes measurements made on airfoils to determine the effects of ice on their aerodynamic characteristics. At an early date tests were made by Gulick (1938), later by Clareus (1974) and more recently by Bragg (1982) and by Bragg and Coirier (1986). Measurements on a swept wing have also been made by Khodadoust and Bragg (1990).

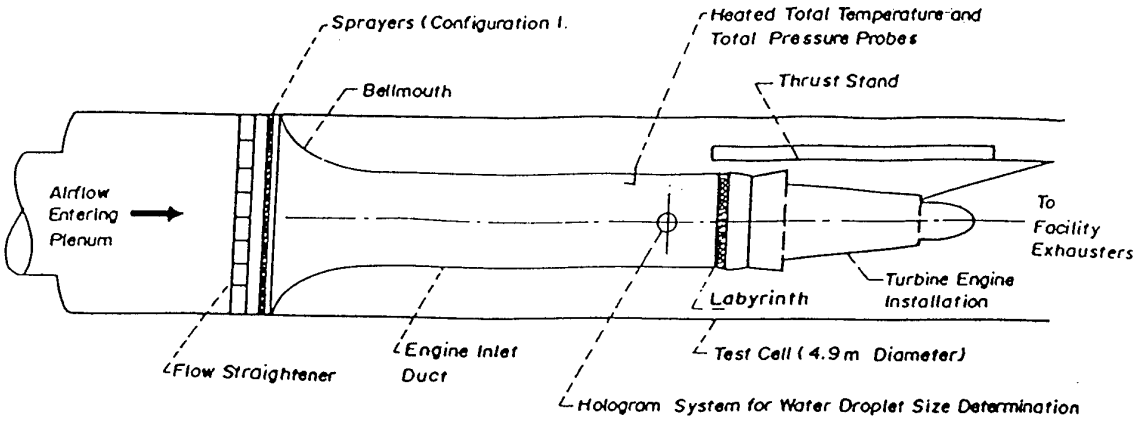

FIG. 4.2-3.- Direct-Connect Propulsion Engine Altitude Icing Test Cell Configuration

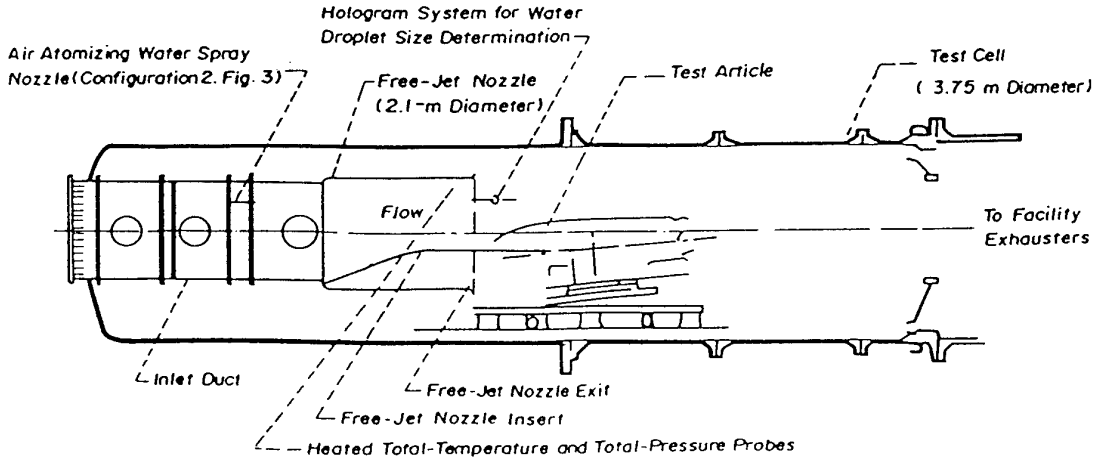

FIG. 4.2-4.- Free-Jet Propulsion Engine Altitude Icing Test Cell Configuration

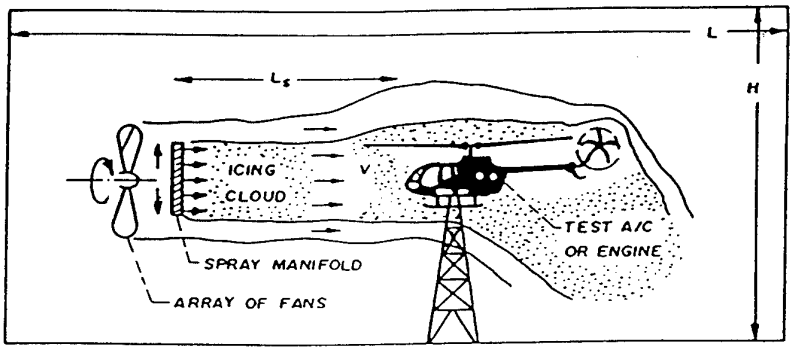

FAN BLOWN SPRAY BY A LARGE ROOM OR OUTDOORS

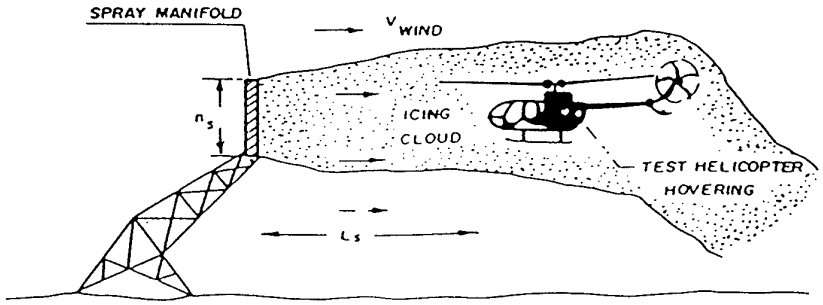

WIND BLOWN SPRAY OUTDOORS

FIG. 4.2-5 C. LOW VELOCITY FACILITIES

In glaze ice accretion cases, the leading edge geometry is completely modified and large changes in the flow field take place. Experimental studies of this type have been made by Bragg and Spring (1987), Spring (1988), Bragg and Khodadoust (1989) and Bragg et al. (1991). Among the different effects on the flow field, the formation of laminar separation bubbles stands as one of the most important, involving a number of complex flow phenomena such as laminar separation, shear layer transition, turbulent reattachment, flow recirculation, etc. Visualizations have been made by Khodadoust (1988) and Kerho and Bragg (1992) and measurements by Bragg and Khodadoust (1988), (1992). Advanced flow diagnostic LDV techniques have been employed by Bragg et al. (1993), to determine velocities on both straight and swept wings.

Glaze ice accretions are known to have rough surfaces with relatively large roughness elements. Evaluation of roughness effects, of ice accretion type, forms another group of simulation experiments. From early wind tunnel tests (Jones and Williams, 1936) it is known that airfoils with uniform upper surface roughness, experience maximum lift losses that are dependent on Reynolds number and roughness size. With small roughness elements the flow tends to remain attached and drag increases because of larger skin friction. If the roughness elements become large, in comparison to boundary layer thickness, their shape, orientation and distribution become important, leading to increased turbulence, thickened boundary layers and even to flow separation.

For simulating roughness effects it is important to geometrically characterize the different types of roughness that appear in nature, if the final objective is to extrapolate results obtained from sub-scale tests. Results from samples of different frost types have been reported by Kind and Lawrysyn (1991). Roughness height and spacing parameters determined from measurements of roughness geometry were in reasonably good agreement with effective values determined from zero pressure gradient boundary layer measurements.

Typical results for aerodynamic coefficient degradations on a wing due to uniform distributed roughness are shown by Wickens and Nguyen (1991) for different grit sizes and sandpaper covering about 30% of the chord from the leading edge.

Aerodynamic performance effects due to ice accretion related roughness have also been measured by Ljunstrom (1972), Boer and Van Hengst (1993) and Valarezo, Lynch and McGhee (1993). In most cases, results that are normally obtained at sub-scale are desired for full-scale applications. The scaling laws indicate that besides geometrical similarity, Mach and Reynolds numbers should be preserved. Since all of the laws can not usually be satisfied, care should be taken in extrapolations, because conventional procedures are not valid for these cases.

Numerical codes for the evaluation of glaze ice growth must predict the local freezing fraction which is a function of the local convective heat transfer coefficient h_c. Dry air simulations are employed to measure h_c and to translate it to the cases of real glaze ice growth. It should be pointed out that these simulations disregard some effects that directly influence h_c, for exemple, the presence of liquid water. Actual phenomena such as film dynamics, droplet impacts, etc. although affecting the heat interchange between surface and airstream, are not taken into account. Besides detailed geometrical similarity and equality of the flow parameters, the experimental techniques for measuring h_c must maintain thermal similitude. This means preserving the ratio of temperatures T_s and T_a (T_s being the surface temperature and T_a the airstream temperature), the T_s distribution and the Prandtl number

$$P_r = C_{pa}\,\mu_a / k_a$$

Usually, experiments deigned to measure h_c are made at temperatures a little above the ambient air temperatures, so that the temperature ratio is practically matched. The Prandtl number differences should then be small, and the surface temperature distribution is implicitly assumed to be $T_s \simeq$ constant.

Detailed geometrical similarity means, for glaze ice accretion, reproduction of the surface roughness, whose importance in convective heat transfer was first demostrated by Achenbach (1977). Van Fossen et al. (1984) made heat transfer measurements on a circular cylinder with four simulated ice accretion shapes, and their corresponding roughness. Measurements were made with heat transfer gages and their results, representative of 2 minutes glaze ice accretion, are presented in Fig. 4.2-6.

Similar measurements have been made by Pais and Singh (1988), using foil heaters beneath a rough skin. The technique employed is described in Pais and Singh (1987). In comparisons with Arimili and Keshok's (1984) results, they report values between 4% and 28% smaller, whereas in the comparisons with Van Fossen et al. (1984), increases between 21% and 58% are shown.

Heat flux gages have also been employed in convective heat transfer coefficient measurements on a NACA 0012 airfoil in flight, on smooth and roughened surfaces by Newton et al. (1988). When comparisons are made, for the smooth case, with other flight tests they are shown to be within 10% agreement. However comparisons with wind tunnel data from Pais et al. (1988), are reported to show differences in Froessling numbers ($Fr = N_u / R_e^{1/2}$) up to 300%.

It is indicated that the large differences could be due to wind tunnel turbulence or to some roughness present in the wind tunnel model tests. The same tests made by Poinsatte et al. (1990), in the NASA Lewis Icing Research Tunnel (IRT), give results in agreement with the flight data for the smooth case, whereas differences exist for the roughness configurations between the IRT Tunnel and the flight results.

4.2.2.2 *Two-phase Flow (Above Freezing) Simulations*

Liquid water exerts important influences on the determination of the shape of the accreting glaze ice. This sub-section presents a description of the combined effects of liquid water and air in a two-phase flow consisting of an airstream and a cloud of droplets. A review of representative experiments is also presented. Yurkanin (1993) has made a very specific classification of ice accretion, depending on the temperature of operation, and he includes five types. In order of decreasing temperature these are: 1) Film, 2) Glaze Runback, 3) Glaze, 4) Mixed, and 5) Rime. The first three types are presented as having features in which, in different manners, the liquid water present affects the ice accretion process.

Olsen and Walker (1986), in their detailed experiments made a number of above freezing observations. Their intention with these tests, was to partially describe the short initial time when there is water flowing over the surface at below freezing conditions and low freezing fractions. From photographic data, they were able to measure surface drop sizes and offer qualitative descriptions of the liquid water surface film and droplet splashing.

Hansman and Turnock (1989), conducted a number of experimental investigations in order to understand the factors that control the behavior of unfrozen surface water. They explain the ice accretion mechanisms influenced by surface water such as mass and heat transfer and study the microphysics of surface water behavior as influenced by surface tension and aerodynamic forces.

Droplet trajectories are a determining factor of the ice growth rate because of their infuence on the liquid inflow at any point. Given any aerodynamic shape, the impinging liquid mass flux distribution depends on the

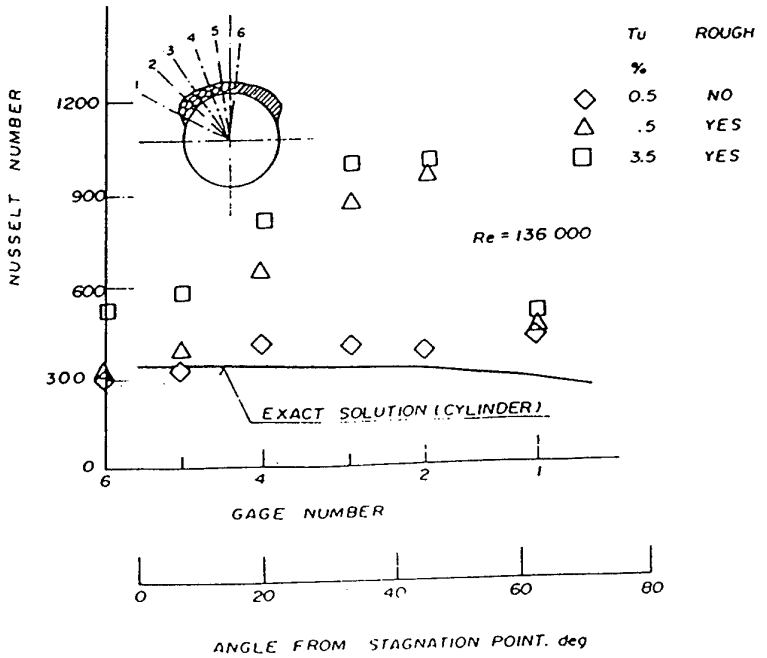

FIG 4 2-6 - Heat transfer distribution for two minutes accumulation of glaze ice.

characteristics of the droplet cloud and the Reynolds number, based on a characteristic body dimension. These variables are usually combined into a single parameter, called the accumulation parameter, which is a function of the cloud liquid water content and the collection but also efficiency. In practice, not only the liquid water content, its droplet size distribution, is important when estimating the impinging mass flux, as pointed out by Hansman (1985).

Studies of droplet trajectories are possible in facilities that do not have the capability of lowering the temperature below freezing, for measurements related to the accumulation parameter in ice accretion. Droplet impingement experiments have been carried out by Gelder et al. (1956) on two-dimensional airfoils and by Papadakis et al. (1987) on more general geometries.

Recently, a study has been made by Bragg and Wells (1994) in order to calculate the effect of wind tunnel walls on droplet impingement on airfoils. The effect is found to be small for reasonable height-to-chord ratios. Expanded studies, with corresponding experimental verification, are recommended. Experiments considering the droplet motion in wind tunnels should also address the issue of acceleration (Sartor and Abbot, 1975).

The freezing fraction is a variable that is not known with sufficient accuracy, especially for the cases where it is low (Bilanin, 1988). He argues that a more accurate consideration of the microphysics of the surface liquid water behavior is neccesary, and should include the phenomena of film dynamics, water bead formation and droplet splashing. All of these can be studied experimentally in two-phase flow conditions at sub-scale, if additional parameters such as the Weber number, We $= \rho_a U_\infty^2 c / \sigma_w$ and water/surface contact angle are preserved.

One possible source of error in the estimation of the freezing fraction is the existence of splash back in droplet impacts. Inclusion of this phenomenon in a theoretical prediction of performance degradation of airfoils in a water spray, purely from first principles, has been shown to be not feasible (Bilanin et al., 1989). The experimental determination of the velocities and sizes of the ejected droplets requires complex set-ups and has been considered by various authors. For the cases of impact velocities of interest in airfoil ice accretion, results are reported by Pavarov et al. (1975), Rockenback and Alexander (1980) and Feo (1987). However, there are no results in the size range that the supercooled cloud droplets are made of.

To experimentally measure the characteristics of the water film dynamics, special techniques are needed that are capable of detecting very small amounts of surface water accumulations and sensors that do not disturb the liquid flow at the point of interest. Film thickness measurements in water sprays, with larger drops than the ones present in ice accretion phenomena, have been reported by Hastings and Weinstein (1984) and by Feo et al. (1991).

Bilanin (1988) has estimated the effect of the liquid film, considering the heat transfer from the air to the film. In his order of magnitude analysis he finds small changes in the freezing fraction.

However, heat transfer measurements that include the presence of liquid films are nonexistent. These experiments would need the preservation of the non-dimensional parameters mentioned before, plus the water/air temperature ratio, thermal conductivities and specific heat ratios. An example of the influence of roughness beneath an impinging liquid jet on heat transfer is shown by Gabour and Lienhard (1994).

4.2.2.3 *Icing Simulations*

These are the experiments that attempt to reproduce all physical aspects present in natural ice accretion. For that purpose, ground facilities require air temperatures to be maintained below the freezing value, a cloud of supercooled droplets and specialized measurement techniques having the capability of yielding meaningful results. The main difference with the two preceeding simulations types is that the geometric shapes are not required in advance, but rather they are part of the desired end result.

Assuming that air and water are kept as test substances, a new parameter, the ratio of the air and local body surface temperatures should be matched in order to apply results from these simulations to the reference conditions.

It is very difficult in practice to match all the parameters existing in a reference condition and since ice accretion is a time-dependent proccess, cumulative differences appear in relatively short periods of time. Most probable candidates for important differences between the reference and simulated cases, due to mismatches in similarity parameters, are the local values of: 1) heat transfer coefficient. 2) impingement efficiency. 3) water-ice contact angle. The result is an increasing ice shape difference as time progresses.

Among these icing simulations we may form two sub-groups. The first has, at least in principle, the main objective of translating results to full-scale. The second sub-group is more research oriented, and the test measurements, in relation with the input variables, are the desired objective.

In the first sub-group one of the main concerns is the effects that ice formations have on performance. This is shown in the early works of Preston et al. (1948) and of Neel and Bright (1950), that present the effect of ice on propeller performance. Later, the works of Gray (1953) consider the effects of ice on a NACA 65-212 airfoil, on an unswept wing (Gray, 1957) and on various airfoils (Gray, 1964). He also correlated ice measurements with other icing variables (Gray, 1958).

The renewed interest in ice testing in the 70's shows in the work of Charpin and Fasso (1972), that presents wind tunnel icing tests on full and sub-scale aircraft models. Aircraft engine icing tests are reported by Kissling (1972) and by Berg and Wolff (1976).

In the 80's, there are the works performed at NASA on airfoil ice accretion drag degradation by Olsen et al. (1984) and by Potapczuk and Berkowitz (1989). The latter is an experimental investigation of performance degradation of a multi-element airfoil with ice accretion.

Model rotor icing wind tunnel tests are another group requiring specialized measurement techniques. Performance changes and the effects of droplet cloud variables are investigated. In this group there are the works of Guffond (1986) and Flemming et al. (1991). Effects of scaling relationships have been presented by Bond et al. (1990), Flemming et al. (1991) and by Armand et al. (1978).

The other sub-group of simulations are research experiments that are performed in icing wind tunnels for the purpose of understanding different phenomena present in ice accretion, and for the elaboration of physical mechanisms and theoretical models.

The simulation of conditions equivalent to natural icing in order to study ice protection systems, is reported by Bond et al. (1991). Also, examples of simulation of icing conditions to study the effects of roughness are contained in the works of Personne (1988) and of Shin and Bond (1993).

Simulation experiments of ice accretion were performed by Olsen and Walker (1986) with the objective of establishing new physical models. They used photographic techniques with the purpose of revising the conventional freezing fraction and heat transfer evaluations. Also close-up video observations from the stagnation line to the horn region of glaze ice have been made by Hansman (1993). Two types of horns are found and the formation of feathers are reported in the horn regions for some types of ice accretion. From simple experiments of ice accreted on a rotating cylinder, Bilanin (1992) has made an analysis to determine the mechanisms that result in ice roughness.

4.2.3 Concluding Remarks on Ground Facilities and Simulation Techniques

Experimental ground based ice accretion simulation techniques have been reviewed. They are categorized by test types, each of them duplicating parts or all the phenomena present in the ice accretion process.

The first simulation group uses model replicas of the real ice shape. Facilities and measuring techniques are the same as used in conventional dry air wind tunnels. Difficulties stem from the particular geometries, presenting irregularities and large roughness elements. Experiments dealing with representative local heat transfer values are lacking.

In the second group the model replicas are tested in a two-phase above-freezing flow. The applications of these

simulations are for glaze ice accretions with low freezing fraction values or for anti-iced aircraft surfaces. Quantitative results for surface water dynamics, splashing and local heat transfer values are lacking.

Finally, in the third group, ice is continously accreting on surfaces and all the similarity parameters and the air temperature should match to the reference conditions. Detailed quantitative experiments, dealing with the interactive microphysics of the ice surface, droplet cloud and surface water, including local heat transfer, are needed.

TABLE 4.2-1. WIND TUNNELS - NORTH AMERICA

FACILITY NAME (LOCATION)	TYPES OF ICING TESTS RUN (a)	WEATHER SIMULA-TED (b)	TYPE OF FACILITY	SIZE, m TEST CHAMBER	SIZE, m UNIFORM ICING CLOUD	RANGE OF PARAMETERS USED IN ICING TESTS (c) AIRSPEED Km/h	MINIMUM AIR TEMP. C	ALTITUDE m	LWC g/m³	VOL. MED. DROP SIZE	INSTRUMENTS USED FOR LOCAL DROP SIZE AND LWC
NASA-LEWIS RESEARCH CENTRE CLEVELAND, OH) A.IRT	FSC,I MS,R IA,P(d)	ICE, FR(d)	WIND TUNNEL	H=1.8 W=2.7 L=6	h_u=1.2 w_u=1.5	10 to 470	-30	0	0.5 to 3.0 (e)	5 to 50 (e)	ROT.CYCLS & VARIOUS MODERN INSTRUMENTS (ROT.CYL.)
LOCKHEED, (BURBANK, CA)	MS,FSC I	ICE	WIND TUNNEL	H=1.2 W=0.8	h_u=0.5 w_u=0.3	90 to 340	-20	0	0.7 to 4.0	10 to 25	ROT.CYLS., (ROT.CYL.)
BOEING (SEATTLE,WA)	MS,FSC, I	ICE	WIND TUNNEL	H=0.5 W=0.4 L=0.9	h_u=0.4 w_u=0.3	180 to 370	-30	0	0.3 to 5.0	10 to 50 (NOZZLES CHANGED)	ROT.CYLS., OIL SLIDE (SM.CYL.)
BOEING BRAIT a. Test Section 1	MS	ICE	WIND TUNNEL	H=2.41 W=1.52	h_u=2.13 w_u=1.22	277	-32	0	0.5 to 5.0	15 to 40	Phase Doppler Partical Analyzer
b. Test Section 2	MS	ICE	WIND TUNNEL	H=1.83 W=1.22	h_u=1.52 w_u=0.91	461	-32	0	0.5 to 5.0	15 to 40	Phase Doppler Partical Analyzer
c. Test Section 3 (Not planned and scheduled for near future)	MS	ICE	WIND TUNNEL	H=1.52 W=0.91	Not Available	648	-40	0	0.5 to 5.0	15 to 40	Phase Doppler Partical Analyzer
IAR (OTTAWA, CANADA)	MS,FSC	ICE	WIND TUNNEL	H=.55 W=.55	h_u=0.5 w_u=0.5	90 to M=0.3	-30	0 to 9,000	0.2 to 2	10 to 30	OIL SLIDE (ROT.CYL)& MODERN

FACILITY NAME (LOCATION)	TYPES OF ICING TESTS RUN (a)	WEATHER SIMULATED (b)	TYPE OF FACILITY	SIZE, m		RANGE OF PARAMETERS USED IN ICING TESTS (c)					INSTRUMENTS USED FOR LOCAL DROP SIZE AND LWC
				TEST CHAMBER	UNIFORM ICING CLOUD	AIRSPEED K_m/h_r	MINIMUM AIR TEMPERATURE °C	ALTITUDE m	LWC g/m^3	VOL. MED. DROP SIZE um	
ROSEMOUNT (MINNEAPOLIS MN) a. LOW SPEED	MS	ICE	WIND TUNNEL	H=0.15 W=0.1 L=0.3	h_u=0.1 w_u=0.07	90 to 170	-30	0	0.2 to 1.5	20 TO 40	OIL SLIDE (ROT.CYL.)
b.HIGH SPEED	MS	ICE	WIND TUNNEL	H=0.15 W=0.3 L=0.8	h_u=w_u=0.1	90 to 740	-25	0 to 3,000	0.1 to 3.0	10 to 40	OIL SLIDE (ROT.CYL.)
FROST TUNNEL (UNIV. OF ALBERTA CAN.)	MS, IA	ICE,	WIND TUNNEL	D=0.5 OCTAGONAL L=0.9	d_u=0.3	10 to 240	-20	0	0.4 to 3.0	20 to 50 (nozzles changed)	OIL SLIDE (ROT.CYL.)
UCLA CLOUD TUNNEL	MS, CP	ICE, R	VERTICAL WIND TUNNEL	H=0.15 W=0.15 L=0.5	h_u=0.1 w_u=0.1	0 to 55	-30	0	0.1 to 3	2 to 50	VARIOUS MODERN INSTRUMENTS
FLUIDYNE ENGINEERING (MINNEAPOLIS, MN)	MS, FSC	ICE	WIND TUNNEL	H=0.55 W=0.55 L=0.4	h_u=0.4 w_u=0.4	M=0.8(10min) M=0.25(40min)	-20 and lower	0	0.1 to 2.0	20	OIL SLIDE BLADE

TABLE 4.2-1. WIND TUNNELS - EUROPE

FACILITY NAME (LOCATION)	TYPES OF ICING TESTS RUN (a)	WEATHER SIMULATED (b)	TYPE OF FACILITY	SIZE, m		RANGE OF PARAMETERS USED IN ICING TESTS (c)					INSTRUMENTS USED FOR LOCAL DROP SIZE AND LWC
				TEST CHAMBER	UNIFORM ICING CLOUD	AIRSPEED K_m/h_r	MINIMUM AIR TEMPERATURE °C	ALTITUDE m	LWC g/m^3	VOL. MED. DROP.SIZE um	
AUSTRIA											
GROUND VEHICLES TEST STATION VIENNA		ICE	WIND TUNNEL	H=4.9 W=4.9		115	-18	0			
GERMANY											
VOLKSWAGEN WOLFSBURG	MS	N	WIND TUNNEL	H=5 W=7		180	-30	0			
PORSCHE	MS	N	WIND TUNNEL	H=1.5 W=1.0		170	-40				
FRANCE											
ETT TECHNIQUE BOURGES	FS, MS	ICE, FR	WIND TUNNEL	H=4.1 W=5.5 L=15	h_u=3 w_u=4	145	-40	0			A, B
LAMP			OPEN WIND TUNNEL	H=0.3 W=0.2	d_u=0.2	200	-10	1,500	0-2	10-20*	D
ONERA MODANE S-1	FS, MS, R	ICE	WIND TUNNEL	D=8	h_u= 2 w_u=2 or h_u= 1 w_u=4	540	-25	1,000 to 2,500	0.4 to 10	10-30	VARIOUS

(a) Types of icing and anti-deicing tests run: CPU = complete propulsion unit; EDC = engine direct connect; FSC = full-scale aircraft component (including wing, tail, fuselage, windshield, stores, gear, etec.); MS = model scale tests and instrumentation; IA = ice adhesion; CP = cloud physics; R = rotating experiments (e.g. helicopter rotor models and propellors); G = ground transport and installations in freezing rain; FS = full scale aircraft; FIT = flight tests of aircraft; I = Inlets with suction; P = complete propellor engines; H = humam physiological experiments.

(b) Weather simulated: ICE = Icing cloud environment; SI = solid ice particles; FR = freezing rain; R = rain; N = natural icing; S = snow.

(c) Instruments used for Drop Size and LWC.
A = olied slide; B = Rogeo spectrometer; C = Johnson and Williams moisture concentration meter; D = other devices (eg Knollenberg).

(d) Modification to do this has been seriously proposed.

(e) Tests are in progress to extend these limits.

ITALY											
CIRA*	FSC, MS, I	ICE	WIND TUNNEL	H=2.35 W=2.25 L=8.0 H=2.35 W=1.15 L=6.0		125 225	-32 -40	0 to 7000 0 to 7000	0.1 to 3 0.1 to 30	5 to 250 5 to 250	
UNITED KINGDOM											
DTEO BOSCOMBE DOWN BLOWER TUNNEL	FS, MS	ICE	WIND TUNNEL	OPEN BED	d=1.2 d=1.8	500 400	-30	0	0 to 3	20 to 1,000	A, C
AEROSPACE COMPOSITE TECHNOLOGIES ARTINGTON	MS, FSC	ICE, SI, FR	WIND TUNNEL	H=0.2 W=0.3 to H=0.5 W=0.5	80% OF CROSS-SECTION	660 215	-40	0	0.1-5 0.2-10 ICE	12-40 1mm ICE	A, D
ROLLS-ROYCE DERBY	MS, R	ICE	WIND TUNNEL	D=0.4	d_u=0.3	600	-70	0	0.2-3	20	D
NORWAY											
VHL SEA SPRAY ICING TUNNEL TRONDHEIM		ICE	WIND TUNNEL	D=1.4 L=9		108		0			
AERO-AND GAS DYNAMICS NTH/SINTEF TRONDHEIM			WIND TUNNEL	H=1.8 W=2.7 L=12.5		97		0			

* FACILITY AVAILABLE AT THE END OF 1998.

TABLE 4.2-2. ENGINE TEST FACILITIES - NORTH AMERICA

FACILITY NAME (LOCATION)	TYPES OF ICING TESTS RUN (a)	WEATHER SIMULATED (b)	TYPE OF FACILITY	SIZE, m		RANGE OF PARAMETERS USED IN ICING TESTS (c)					INSTRUMENTS USED FOR LOCAL DROP SIZE AND LWC
				TEST CHAMBER	UNIFORM ICING CLOUD	AIRSPEED K_m/h,	MINIMUM AIR TEMPERATURE °C	ALTITUDE m	LWC g/m^3	VOL. MED. DROP SIZE um	
AEDC (ARNOLD AFS, TN) A. ETF	EDC	ICE	DIRECT CONNECT d=1.5	D=3.7 or 4.5 L=11	SPRAY BARS SIZED TO ENGINE	0 to M=0.7+	-30	0 to 15,000	0.2 to 3+	15 to 30	VARIOUS MODERN INSTRUMENTS
B. FREE JET	CPU, FSC, I, MS	ICE	FREE JET d=1.5	D=3.7 or 4.5 L=11	SPRAY BARS SIZED TO ENGINE	0 to M=0.7+	-30 and lower	0 to 15,000	0.2 to 3+	15 to 30	VARIOUS MODERN INSTRUMENTS
C. ASTF	CPU, FSC I	ICE	FREE JET d +2.7	D=8 L=18	SPRAY BARS SIZED TO ENGINE	0 to M=0.7+	-30 and lower	0 to 15,000	0.2 to 3+	15to 30	VARIOUS MODERN INSTRUMENTS
DETROIT DIESEL ALLISON (INDIANAPOLIS, IN) A. COMP. TEST FACILITY	INLET & COMPRESSOR STAGE	ICE	FREE JET DIRECT CONNECT d=0.5	D=2.3 L=9	SPRAY BARS SIZED TO ENGINE	0 to M=0.7+	-30 AND LOWER	0 to 6,000	0.2 TO 3.5	15 TO 40	ROTATING CYLINDERS
B. SMALL ENGINE FACILITY	EDC	ICE	DIRECT CONNECT	D=0.45 L=1.2	SPRAY BARS SIZED TO ENGINE	0 to M=0.7+	-30 AND LOWER	0 to 6,000	0.2 TO 3.5	15 TO 40	ROTATING CYLINDERS
GE CROSS-WIND FACILITY (PEEBLES, OH)	CPU, P(d) R(d)	ICE	FREE JET OUTDOORS d=7.0	OUTDOORS	d_v=4.5	90	AMBIENT AIR TO -20	0	0.4 TO 3.5	15 TO 50	KNOLLENBERG SPECTROMETER (ROT. CYL.)
P&W ALTITUDE FACILITIES (E. HARTFORD, CT) A. LARGE	EDC, I	ICE	DIRECT CONNECT	D=5.5 L=10	SPRAY BARS SIZED TO ENGINE	0 to M=0.5	-25	0 to 6,700	0.2 TO 9	15 TO 40	OIL SLIDE
B. SMALLER	EDC, I	ICE	DIRECT CONNECT	D=3.7	SPRAY BARS SIZED TO ENGINE	0 to M=0.5	-30 AND LOWER	0 to 6,700	0.2 TO 9	15 TO 40	OIL SLIDE
C. P&W SEA LEVEL FACILITY	EDC	ICE	DIRECT CONNECT	VARIES WITH TEST CELL	SPRAY BARS SIZED TO ENGINE	0 to M=0.5	-20 (AMBIENT)	0	0.2 TO 9	15 TO 40	OIL SLIDE

FACILITY NAME (LOCATION)	TYPES OF ICING TESTS RUN (a)	WEATHER SIMULATED (b)	TYPE OF FACILITY	SIZE, m		RANGE OF PARAMETERS USED IN ICING TESTS (c)					INSTRUMENTS USED FOR LOCAL DROP SIZE AND LWC
				TEST CHAMBER	UNIFORM ICING CLOUD	AIRSPEED K_m/h_r	MINIMUM AIR TEMPERATURE °C	ALTITUDE m	LWC g/m^3	VOL. MED. DROP SIZE um	
MCKINLEY CLIMATIC LAB. ENGINE TEST CELL (EGLIN AFB, FL)	CPU, FSC	ICE, SI FRR, R	FAN BLOWS SPRAY INDOORS	H=7.5 W=9 L=40	h_u=3 W_u=6	0 to (30 TO 75)	-30 AND LOWER	0	0.1 TO 3	12 TO 60 800 TO 1500 (NOZZLES CHANGED)	PARTICLE INTERFEROMETER (ROT. CYL.)
NAVAL AIR PROPULSION FACILITY (TRENTON, HJ) A. FIVE SMALL ENGINE CELLS	EDC, CPU, I, FSC, MS	ICE, SI, FR, R	FREE JET d=0.6	H=3 W=3 L=6	SPRAY BARS SIZED TO ENGINE	0 to M=0.7+	-30 AND LOWER	0 to 15,000	0.1 TO 2	15 TO 50 (NOZZLES CHANGED)	KNOLLENBERG SPECTROMETER AND OAP (ROT. CYL.)
B. TWO LARGE SEA LEVEL CELLS	EDC, CPU, I, FSC, MS	ICE, SI, FR, R	FREE JET d=1.2	H=4.5 W=7 L=17	SPRAY BARS SIZED TO ENGINE	0 to M=0.7+	-30 AND LOWER	0	0.1 TO 2	15 TO 50 (NOZZLES CHANGED)	KNOLLENBERG SPECTROMETER AND OAP (ROT. CYL.)
C. THREE LARGE ALTITUDE CELLS	EDC, CPU, I, FCS, MS	ICE, SI, FR, R	FREE JET d=1.2	D=5 L=9	SPRAY BARS SIZED TO ENGINE	0 to M=0.7+	-30 AND LOWER	0 to 15,000	0.1 TO 2	15 TO 50 (NOZZLES CHANGED)	KNOLLENBERG SPECTROMETER AND OAP (ROT. CYL.)
TELEDYNE ALTITUDE CELLS (TOLEDO, OH) A. CHAMBER 1	CPU, EDC	ICE, SI, FR, R	FREE JET OR DIRECT CONNECT	D=2.7 L=5	SPRAY BARS SIZED TO ENGINE	0 to M=0.7+	-30 AND LOWER	0 to 15,000	UP TO 3	15 TO 25	OIL SLIDE
B. CHAMBER 2	CPU, EDC	ICE, SI, FR, R	d=0.2	H=2.5 W=2.5 L=4	SPRAY BARS SIZED TO ENGINES	0 to M=0.7+	-30 AND LOWER	0 to 15,000	UP TO 3	15 TO 25	ROTATING CYLINDERS
AVCO LYCOMING (STRATFORD, CT) A. COMPONENT FACILITY	EDC	ICE, FR	DIRECT CONNECT d=0.4	--------	SPRAY BARS SIZED TO ENGINE	0 to 370	-30 AND LOWER	0	0.1 TO 3	15 TO 40	OIL SLIDE (ROT. CYL.)
B. ENGINE TEST FACILITY	1EDC	ICE, FR	d=0.4 ----- d=1.2	W=3.7 H=2.7 -------- OUTDOORS	SPRAY BARS SIZED TO ENGINE	0 to 200	-30 AND LOWER ---------- -20	0	0.1 TO 3	15 TO 40	OIL SLIDE (ROT. CYL.)

TABLE 4.2-2. ENGINE TEST FACILITIES - EUROPE

FACILITY NAME (LOCATION)	TYPES OF ICING TESTS RUN (a)	WEATHER SIMULATED (b)	TYPE OF FACILITY	SIZE, m		RANGE OF PARAMETERS USED IN ICING TESTS (c)					INSTRUMENTS USED FOR LOCAL DROP SIZE AND LWC
				TEST CHAMBER	UNIFORM ICING CLOUD	AIRSPEED K_m/h,	MINIMUM AIR TEMPERATURE °C	ALTITUDE m	LWC g/m^3	VOL. MED. DROP SIZE um	
FRANCE											
CEPR SACLAY R2 CELL	CPU, FS	ICE	FREE JET	D=3.5	d_u=1.15	540	-60	0	0-6	15-30	A
CEPR SACLAY R4 CELLS	CPU, FS	ICE	FRE JET	D=3.5	d_u=1.30	500	-60	0	0-6	15-30	A
CEPR SACLAY R5 CELL	CPU, FS	ICE	FREE JET	D=5	d_u=3	260	-60	0	0-10	15-30	A
UNITED KINGDOM											
DTEO PYESTOCK CELL 3	EDC, CPU IA, I, R	ICE	DIRECT CONNECT OR FREE JET	D=6.1	ENGINE DIA OR d_u= 1.4	TO SUIT ENGINE OR 820	-70	0 to 15,000	0.2-10	15-30	D
DTEO PYESTOCK CELL 3 WEST	FSC, EDC, CPU, FS, MS, IA, I, P, R	ICE, FR	DIRECT CONNECT OR FREE JET	D=7.6	ENGINE DIA OR d_u=2.6	TO SUIT ENGINE OR 770	-40	0 to 15,000	0.2-10	15-30	D
AERO AND INDUSTRIAL TECHNOLOGY BURNLEY	EDC, MS	ICE	DIRECT CONNECT OR FREE JET	D=4 L=13	d_u=0.7	TO SUIT ENGINE OR 250	-55	0 to 15,000	0.2-10	15-40	D
ROLLS-ROYCE ATF DERBY	CPU, EDC MS, R	ICE	DIRECT CONNECT OR FREE JET	D=3.7	d_u=1.2	TO SUIT ENGINE OR 600	-70	0 to 15,000	0.2-3	20	D

(a) Types of icing and anti-deicing tests run: CPU = complete propulsion unit; EDC = engine direct connect; FSC = full-scale aircraft component (including wing, tail, fuselage, windshield, stores, gear, etec.); MS = model scale tests and instrumentation; IA = ice adhesion; CP = cloud physics; R = rotating experiments (e.g. helicopter rotor models and propellors); G = ground transport and installations in freezing rain; FS = full scale aircraft; FIT = flight tests of aircraft; I = Inlets with suction; P = complete propellor engines; H = humam physiological experiments.

(b) Weather simulated: ICE = Icing cloud environment; SI = solid ice particles; FR = freezing rain; R = rain; N = natural icing; S = snow.

(c) Instruments used for Drop Size and LWC.
A = olied slide; B = Rogeo spectrometer; C = Johnson and Williams moisture concentration meter; D = other devices (eg Knollenberg).

(d) Modification to do this has been seriously proposed.

(e) Tests are in progress to extend these limits.

TABLE 4.2-3. - LOW VELOCITY FACILITIES - NORTH AMERICA

FACILITY NAME (LOCATION)	TYPES OF ICING TESTS RUN (a)	WEATHER SIMULATED (b)	TYPE OF FACILITY	SIZE, m TEST CHAMBER CLOUD	SIZE, m UNIFORM ICING	RANGE OF PARAMETERS USED IN ICING TESTS (c) AIRSPEED K_m/h,	MINIMUM AIR TEMPERATURE °C	ALTITUDE m	LWC g/m^3	VOL.MED. DROP SIZE	INSTRUMENTS USED FOR LOCAL DROP SIZE AND LWC
NRC HELICOPTER SPRAY RIG (OTTAWA, CANADA)	FLT (HELICOPTERS IN HOVER)	ICE, FR	WIND BLOWN SPRAY OUTDOORS	D=∞	SPRAY MANIFOLD h_s=4.5 w_s=23	AMBIENT WIND, 20 TO 45 (GUSTY)	-20 AMBIENT	0	0.1 to 0.8	30 to 60	OIL SLIDE (ROT. CYL.)
G.E. CROSS WIND FACILITY (PEEBLES, OH)	CPU, P(d), R (d)	ICE, FR	FREE JET OUTDOORS	D=∞	d_u=4.5	90	-20 AMBIENT	0	0.4 to 3.6	15 to 50	KNOLLENBERG SPECTROMETER (ROT. CYL.)
MCKINLEY CLIMACTIC LAB (EGLIN AFB, FL) A. MAIN CHAMBER	FS, R (d)	ICE, SI	FAN BLOWN SPRAY INDOORS	H=21 W=76 L=76	SPRAY MANIFOLD h_s= 3 w_s= 9	0 TO (30 TO 75) (e) (DEPENDING ON L_n)	-30 AND LOWER	0	0.1 to 3	12 to 60 800 to 1,500 (NOZZLES CHANGED)	PARTICLE INTERFEROMETER (ROT. CYL.)
B. ENGINE TEST CELL	CPU, FSC	ICE, SI	FAN BLOWN	H=7.5 W=9 L=4.0	MANIFOLD h_s=3 w_s=6	0 TO (30 TO 75) (DEPENDING ON L_n)	-30 AND LOWER	0	0.1 to 3	12 to 60 800 to 1,500 (NOZZLES CHANGED)	PARTICLE INTERFEROMETER (ROT. CYL.)
C. ALL WEATHER ROOM	FSC	ICE, SI	FAN BLOWN SPRAY INDOORS	H=4.5 W=6.5 L=12	MANIFOLD h_s=3 w_s=3	0 TO (30 TO 75) (DEPENDING ON L_n)	-30 AND LOWER	0	0.1 to 3	12 to 60 800 to 1,500 (NOZZLES CHANGED)	PARTICLE INTERFEROMETER (ROT. CYL.)
US ARMY CRREL COLD ROOM (HANOVER, NH)	FSC, MS R, LA	ICE, SI FR, R	FAN BLOWN SPRAY INDOORS	H=1.1 W=0.7 L=1.5	-------- -	0 TO 20	-30 AND LOWER	0	1 to 2.5	10 to 60	CASCADE IMPACTOR
MT WASHINGTON OBSERVATORY (GORHAM, NH)	FS, CP, MS	NATURAL ICING OF TIED DOWN EQUIPMENT ON TOP OF MOUNTAIN				0 TO 80 (GUSTY)	-20 AND LOWER	1800	GENERALLY SEVERE NATURAL CONDITIONS		ROTATING CYLINDERS
US NAVY FMTC (PT MUGU) CLIMATIC HANGAR	FSC, FS G	R, FR	FAN BLOWN SPRAY INDOORS	H=7.6 W=18 L=18	h_s=1.2 w_s=1.2	0 TO 75	-30 AND LOWER	0	30 CM RAIN/HR 5 CM SNOW/HR	500 TO 4,500 50 TO 100	OIL SLIDE (RAIN GAUGE)

TABLE 4.2-3. - CONCLUDED

FACILITY NAME (LOCATION)	TYPES OF ICING TESTS RUN (a)	WEATHER SIMULATED (b)	TYPE OF FACILITY	SIZE, m		RANGE OF PARAMETERS USED IN ICING TESTS (c)					INSTRUMENTS USED FOR LOCAL DROP SIZE AND LWC
				TEST CHAMBER	UNIFORM ICING CLOUD	AIRSPEED K_m/h,	MINIMUM AIR TEMPERATURE °C	ALTITUDE m	LWC g/m^3	VOL.MED. DROP SIZE	
ACTON ENVIRONMENTAL TEST CORP. (ACTON, MA)	G	R, FR S(d)	FAN BLOWN	H=6 W=4.5 L=7.5	d_s=2.5	0 to 45	-30 AND LOWER	0	10 CM RAIN/HR	1,000 TO 4,000	NOT MEASURED (RAIN GAUGE)
IAR (OTTAWA, CANADA) CLIMATIC ENG'S FACILITY	G, FS	FR, S(d)	FAN BLOWN SPRAY INDOORS	H=6.1 W=6.1 L=30.5	d_s=1.2 to 2.5	0 to 55	-30 AND LOWER	0	0.3 CM RAIN/HR	500 TO 1,000	SCREEN METHOD (ACCUMULATION RATE)
COLD CHAMBER #2	G, FS	FR	FAN BLOWN SPRAY INDOORS	H=5 W=5 L=7	d_s=1.8	0 to 55	-30 AND LOWER	0	0.3$_4$ CM RAIN/HR	500 TO 1,000	SCREEN METHOD (ACCUMULATION RATE)
WYLE LABS (NORCO, CA) COLD ROOM	G, FSC	FR	FAN BLOWN SPRAY INDOORS	H=5 W=4.5 L=11	--------	0 to 35	-30 AND LOWER	0	12 CM RAIN/HR	--------	----------
ARCTEC CANADA Ltd (OTTAWA, CANADA) COLD ROOM	G, IA	FR (d) S (d)	FAN BLOWN SPRAY INDOORS	H=3.7 W=5.5 L=9	--------	0 to 35	-30 AND LOWER	0	--------	--------	----------

(a) Types of icing and anti-deicing tests run: CPU = complete propulsion unit; EDC = engine direct connect; FSC = full-scale aircraft component (including wing, tail, fuselage, windshield, stores, gear, etec.); MS = model scale tests and instrumentation; IA = ice adhesion; CP = cloud physics; R = rotating experiments (e.g. helicopter rotor models and propellors); G = ground transport and installations in freezing rain; FS = full scale aircraft; FIT = flight tests of aircraft; I = Inlets with suction; P = complete propellor engines; H = humam physiological experiments.

(b) Weather simulated: ICE = Icing cloud environment; SI = solid ice particles; FR = freezing rain; R = rain; N = natural icing; S = snow.

(c) Instruments used for Drop Size and LWC.
A = olied slide; B = Rogeo spectrometer; C = Johnson and Williams moisture concentration meter; D = other devices (eg Knollenberg).

(d) Modification to do this has been seriously proposed.

(e) Tests are in progress to extend these limits.

4.3 IN-FLIGHT ICING TESTING

4.3.1 Artificial Ice Shapes

4.3.1.1 *Scope*

The certification with ice protection provisions must show that the airplane is able to operate safely in the continuous maximum and intermittent maximum icing conditions under FAR and JAR icing envelopes.

The effects of ice accretion on aircraft handling qualities and aerodynamic performance are critical for an airplane. The significance of these effects depends on the airplane configuration, size, and design features. For large transport airplanes, aircraft handling characteristics cannot be assessed in ground facilities. In-flight testing with artificial ice shapes is one of the methods used to demonstrate and evaluate aircraft handling performance.

During the early 1950's, certification of transport category aircraft in icing involved 100 per cent protection of the wing and empennage leading edge surfaces. In recent years, as a result of the introduction of super computers, technological advancement, research on aerodynamic effects due to ice accretion on lifting surfaces and validated computational methods, civil transport airplanes are designed more efficiently and are certified with ice protection provision on as little as 50 per cent of the aerodynamic leading edge areas.

To support the design effort and verification, in-flight testing with artificial ice shapes has become more important in evaluating aircraft performance. Also, the use of artificial ice shapes in flight tests provides improvement in certification safety and reduces time and cost compared with flight test in actual icing conditions.

4.3.1.2 *Ice Shape Description*

The ice shape definition is determined from icing tunnel tests of full-scale leading edges or from analytical computations of the accretion. The shapes on unheated surfaces are based upon the flight critical conditions within icing envelopes of meteorological conditions defined in Appendix C of reference (FAR 25). It is generally assumed that the glaze type ice accretion would cause larger degradation in aerodynamic performance than rime ice accretion. The artificial ice shapes have been manufactured using rigid urethane or wood, covered with fiberglass, and molded plastic. The roughness of ice may be simulated by adding epabond or epoxy adhesive to the surface. The cross-sectional definition of typical ice shapes is given in Figure 4.3-1.

4.3.1.3 *In-Flight Test*

The airplane with the artificial ice shapes installed on the unprotected portion of the wing and empennage leading edge surfaces is normally flight tested to encompass all

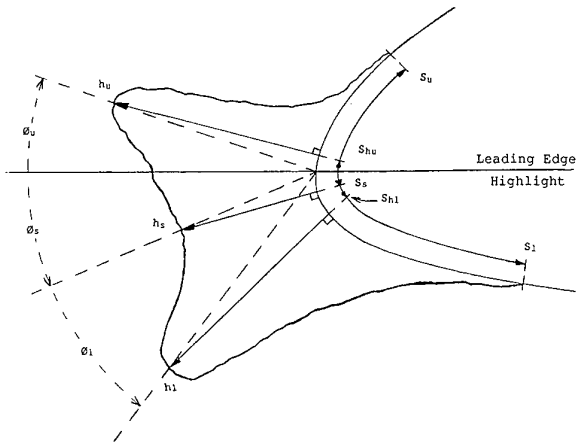

Legend:
- h_u = Upper ice horn height perpendicular to leading edge surface
- h_s = Stagnation ice height perpendicular to surface at stagnation point
- h_l = Lower ice horn height perpendicular to leading edge surface
- $Ø_u$ = Angle between highlight and upper ice horn
- $Ø_s$ = Angle between highlight and stagnation point
- $Ø_l$ = Angle between highlight and lower ice horn
- S_u = Leading edge surface distance from highlight to upper impingement limit
- S_{hu} = Leading edge surface distance from highlight to upper ice horn
- S_s = Leading edge surface distance from highlight to stagnation point
- S_{hl} = Leading edge surface distance from highlight to lower ice horn
- S_l = Leading edge surface distance from highlight to lower impingement limit

Figure 4.3-1 Typical Ice Shape Dimensions

flight maneuvers which would indicate any degradation of aircraft handling qualities. No rigidly set program of tests is established. Listed below are the test conditions generally considered in the certification program. Some test conditions may be satisfied by using wind tunnel data in conjuction with flight test trim data.

- Longitudinal Control
- Directional Control
- Stalls-Flaps Up/Flaps Down
- Pushover from Initial Buffet
- Trim Characteristic
- Lateral/Directional Stability
- Longitudinal Stability-Approach Regime
- Tailplane Stall

The extent of the tests performed is tailored to the magnitude of the unprotected area and significance of areas to the aircraft's flight handling characteristics. The stability and control characteristics are evaluated within the aircraft's entire speed range envelope. Past experience shows that the glaze type accretions are conservative for lift loss.

4.3.1.4 *Shortcomings*

The size and shape of the simulated ice accretion is limited to predetermined critical icing conditions and a flight scenario. This allows only qualitative aircraft evaluation of aircraft handling. In-flight airplane performance data with the ice shapes have been used to substantiate the wind tunnel data at the most important

flight conditions. Then, interpolation or extrapolation of data from the tunnel simulation on a scale model may be required to estimate airplane performance penalty for other flight conditions.

4.3.2 Artificial Icing Tests Using Spray Tanker

A special aircraft fitted with an icing spray system and the capability of providing a closely controlled in-flight artificial icing environment is required for an artificial icing test. In general a test aircraft is flown behind the tanker aircraft which is equipped with an icing spray system. Also a chase aircraft is usually used to photograph events and for external observation of the test.

4.3.2.1 *Scope*

The primary objectives of the artificial icing test are:

- to demonstrate satisfactory ice protection system operation
- to evaluate engine operation in icing
- to evaluate ingestion capability of the engine
- to evaluate icing characteristics of the test article, and
- to show aircraft certification compliance in icing conditions.

The icing spray tanker aircraft may be classified into three categories for test purposes.

1. Transport size aircraft, e.g. Government in-flight icing tankers such as USAF NKC-135 and USAF C-130.

2. Rotorcraft, e.g. Government in-flight icing tankers such as USA CH-47 Helicopter.

3. General Aviation, e.g. Industry in-flight icing tankers such as Cessna 404, Piper Cheyenne, Flight Systems T-33

Table 4.3-1 lists the availability of tankers and their characteristics. Tankers differ in the shape, size, and location of the spray system. The point of contact is also listed wherever available.

In-flight icing occurs when an aircraft flies through clouds in which water droplets are in the supercooled state. The spray cloud produced by a spray tanker aircraft should be representative of natural icing clouds. The primary parameters that characterize an icing cloud are: Cloud Temperature, Liquid water content(LWC), and the droplet size distribution. No testing can truly be valid unless the artificial icing cloud is measured by instrumentation throughout the testing process.

The artificial cloud generated by a spray system is a function of flow rates and distance behind the spray nozzle array. The latter can be characterized by decrease in LWC and increase in MVD with increasing distance from the spray nozzle array. Miller(1975) in his study on a numerical solution for the LWC in icing spray concluded that the relative humidity, the droplet number density distribution and the bleed-air mass flow rate were critical variables affecting the final LWC in the spray clouds. Flight test measurements indicate that relative humidity greater than 70% prevents the rapid evaporation of small droplets, giving a smaller average droplet size throughout the spray cloud.

Rotorcraft tankers are capable of producing icing cloud at lower altitude and desired temperature and provide a safe environment for testing. They also allow icing tests to be performed in any season and time of the year. American rotorcraft manufacturers rely heavily on in-flight tanker test for evaluating adequacy of the ice protection systems for the airframe, engine and rotorblades.

The use of tankers in simulating icing cloud for large transport-type aircraft is severely limited for certification of the total aircraft due to small coverage. The cost of tanker use and difficulties in controlling icing cloud characteristics make this test method less desirable than tests in icing wind tunnels or in-flight natural icing tests for such purposes.

4.3.2.2 *Description of Several Spray Tanker Systems*

NKC-135 Tanker

The NKC-135 water spray tanker (Figure 4.3-2) has been used to demonstrate system performance while flying through an artificial cloud. The tanker aircraft has been modified to hold an aggregate total of approximately 4000 gallons of water in aft body fuel tanks number 1, 2, and 3.

Bleed air from the aircraft engines is ducted to the boom where it passes through the boom to the spray rig. The spray rig has five concentric circular rings with 100 nozzles in total. In the spray rig nozzles, the bleed air mixes with the water and atomizes it into the atmosphere. The artificial cloud produced by the spray rig is approximately 10-12 feet in diameter. The resulting droplets are directed onto the aircraft surface to be tested. Sometimes a yellow dye has been added to the tanker water so ice accumulation can be seen and photographed by observers in the spray tanker and T-38 chase aircraft.

Calibration of liquid water content in the cloud can be accomplished by measurement with a chase aircraft or the measuring equipment installed on the test airplane.

The NKC-135 tanker operates at high altitude with an operating speed range of 200-300 knots. This may limit ice testing of a slower test aircraft to lower altitudes.

Table 4.3-1 TANKERS CHARACTERISTICS

Tanker Aircraft	Weather Simulated (a)	Time in Icing @ High LWC, min.	Size of Spray, m at Nominal Distance L	Range of Parameter used in Icing Tests (b)					Test Season (Find temperature at altitude)
				Air speed, km/h IAS	Min. Air Temperature, C	Altitude, m x 10^3	LWC, gm/m^3	VMD size, μm	
USAF KC-135 (Edwards AFB, CA.)	Ice, N	60	L = 60 D = 3	300 to 650 (370 nom.)	-20 ambient	1.2 to 8.0	0.05 to 1.5	28 to 35	All year
	R, FR						0.5 to 32	200 to 800	
USAF KC-135 (Edwards AFB, CA.)	Ice, N	60	L = 60 D = 5	190 to 390 (280 nom.)	-20 ambient	1.2 to 8.0	0.05 to 1.5	28 to 35	All year
	R, FR						0.5 to 32	200 to 800	
CH-47 HISS (Edwards AFB, CA.)	Ice, N	30	L = 50 H = 3 W = 12	110 to 140 (120 nom.)	-20 ambient	0.6 to 3.5	0.1 to 1.0	25 to 30	Normally winter
Cessna 404 (Wichita, KS.)	Ice, N	60	L = 150 D = 6	165 to 330 (260 nom.)	-20 ambient	3.0 to 8.0	0.05 to 4.0	20 to 49	All year
Piper Cheyenne (Lock Haven, PA.	Ice, N, R, FR	14	L = 30 H = 3 W = 5	200 to 300 (240 nom.)	-20 ambient	3.0 to 8.0	0.1 to 1.7	30 to 50	Not summer
Flight Systems T-33 (Mojave, CA.)	Ice, N, R, FR	45	L = 60 D = 2.5	230 to 420 (370 nom.)	-20 ambient	3.0 to 8.0	0.1 to 1.0	17 to 50	All year
Dornier 228-212, Deutsche Aerospace, Germany	Ice, N	30	L = 40 D = 1.75-2.0	up to 300	-15 ambient	0.5 to 6.0	0.1 to 1.5	29 to 35	All year
	FR							180-200	

NOTES:
(a) ICE = Icing Cloud Environment; N = Natural Icing; R = Rain; FR = Freezing Rain
(b) Parameter ranges vary with conditions.

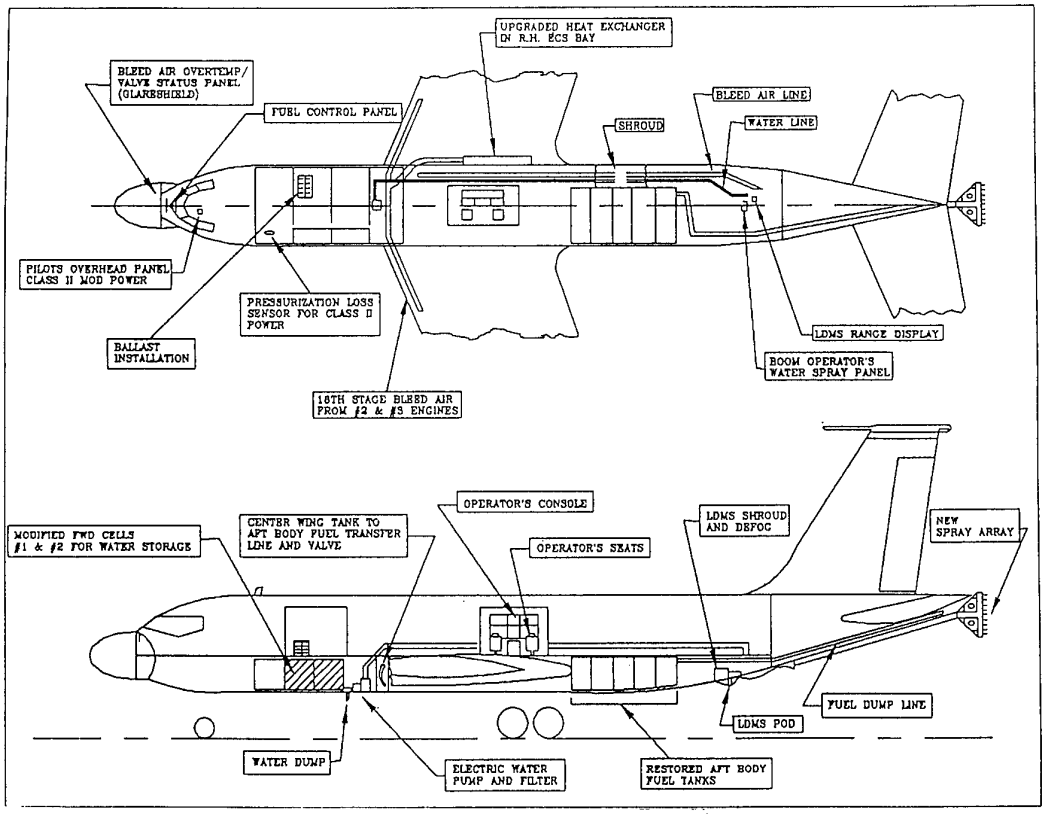

Figure 4.3-2 NKC-135A Tanker Aircraft

Recently, the spray system was modified to simulate icing cloud with large supercooled droplets consistent with those measured in the natural environment. Ashenden and Marwitz (1995) reported tanker icing cloud calibration. Cloud calibration was performed with an instrumented Learjet. They used three laser spectrometers and a Jonson and William's LWC probe to measure droplet size distribution and LWC in the cloud. Figure 4.3-3 and Figure 4.3-4 show a mass-weighted

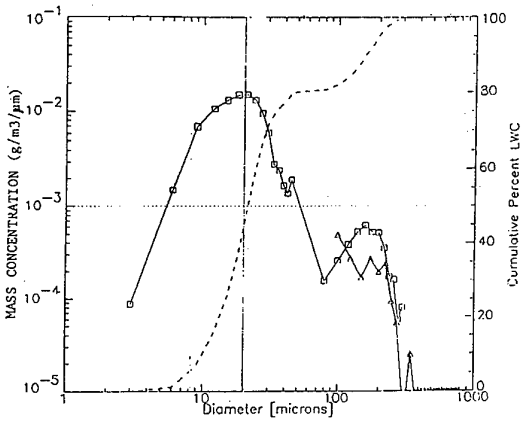

Figure 4.3-3 Mass-Weighted Tanker Distribution FAR Part 25 Conditions

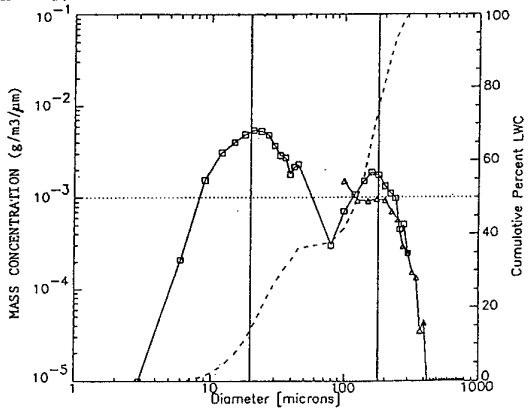

Figure 4.3-4 Mass-Weighted Tanker Distribution, Larger Droplet Test Condition

tanker distribution for a FAR Part 25, Appendix C test condition and distribution for a large droplet simulating condition, respectively. The artificial cloud droplet distribution favorably compares with distribution found in the natural environment.

CH-47 Helicopter Icing Spray System (HISS) Tanker

The HISS tanker has been used mainly to test rotorcraft in icing (Figure 4.3-5). The HISS consists of an internally mounted large water tank (1500 gal. capacity) in a CH-47 helicopter, an external spray assembly, a calibrated static air temperature probe, a dew point hygrometer and a radar altimeter. The spray assembly generates an icing cloud by pumping water at measured flow rate through the nozzles. High pressure bleed air

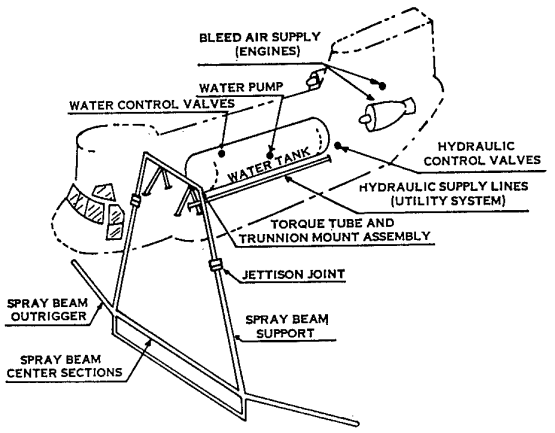

Figure 4.3-5 HISS Tanker

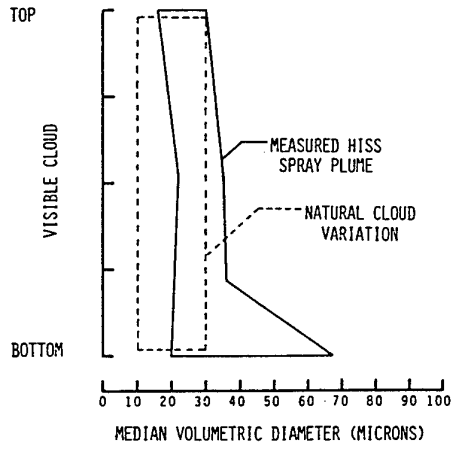

Figure 4.3-6 Vertical Variation-Droplet MVD

from the engine is used to atomize the water into fine droplets. The temperature probe and hygrometer provide accurate cloud humidity and temperature measurements (Belte,1980).

The 60 ft wide dual trapeze assembly, lowered 20 feet beneath the aircraft provides cloud depth and also minimizes turbulence and down wash at the test aircraft. The current 1984 HISS configuration (Chambers and Adams,1986) has the following operating characteristics:

LWC $\Rightarrow$ 0 to 1.3 g/m^3

MVD $\Rightarrow$ 17-30 micron @ the top of cloud

20-65 micron @ the bottom of cloud

Temperature range $\Rightarrow$ 0-20 C

Altitude range $\Rightarrow$ up to 12,000 ft (3,658 m)

Airspeed range $\Rightarrow$ 80-130 kts.

Cloud depth $\Rightarrow$ 8 ft (2.4 m)

Cloud width $\Rightarrow$ 36 ft (11 m)

The size of the cloud produced by the spray assembly is approximately 8 feet deep x 36 feet wide. The depth of the spray cloud is inadequate for exposing the entire ice-protection system to the same icing environment for comprehensive aircraft testing.

The variation of droplet MVD and LWC with vertical position in the cloud is shown in Figures 4.3-6 and 4.3-7 respectively. The measured MVD and LWC varies greatly from top to bottom of the cloud. Increased concentration in the lower part of the cloud is consistent with the larger droplet MVD measured at the bottom.

Figure 4.3-8 shows representative droplet size spectra measured in the HISS spray plume. The cloud contains droplets larger than 100 microns. The typical drop size distribution in a natural cloud is also given for comparison.

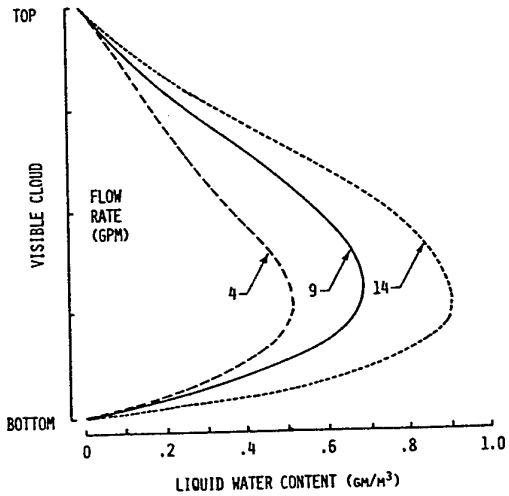

Figure 4.3-7 Vertical Variation-Cloud LWC

Dornier Icing Tanker (DIT)

The DIT is a Dornier 228 aircraft (Figure 4.3-9), equipped with a 61 nozzle spray mast located behind the tail. The 61 nozzles are installed on a rake of hexagonal shape. The nozzles are supplied with water from tank of 210 gallons (800 liters) volume. The supply pressure for the water can be varied from 435 psia to 1160 psia (30 to 80 bar). The maximum spray time is 30 minutes.

The DIT spray rig has been calibrated with the measuring aircraft equipped with the laser spectrometer FSSP-100 to measure the droplet size, the Johnson-William's hot wire sensor to measure the LWC, and a distance view finder to define the distance between the DIT and the measuring aircraft.

The measured mean volumetric diameter (MVD) in the icing cloud is between 29 and 35 micron. The LWC is between 0.1 g/m^3 and 1.5 g/m^3. The high value of LWC

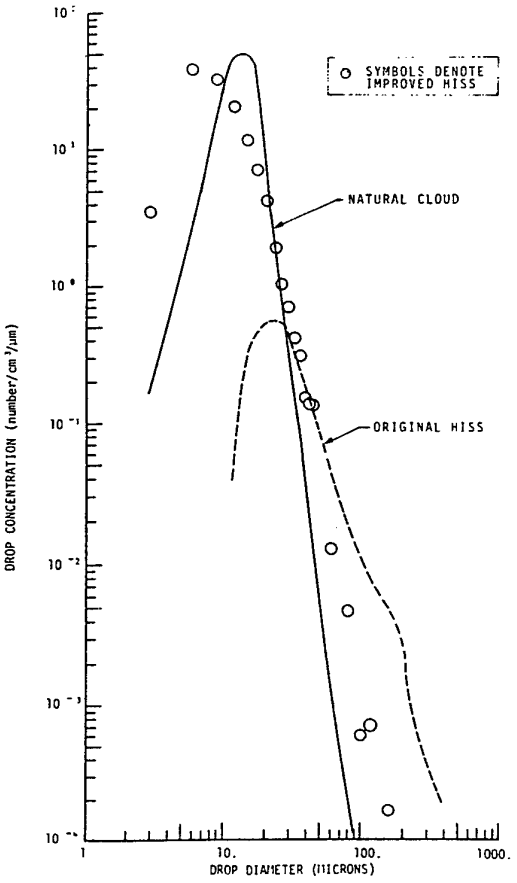

Figure 4.3-8 Drop Size Spectra

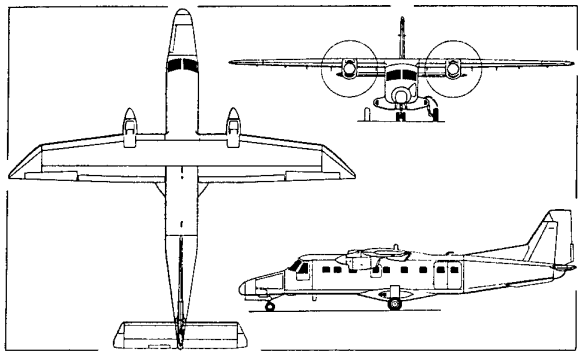

Figure 4.3-9 Deutsche Aerospace Dornier 228-12 (Garrett TPE331-5-252D turboprops)

is at a distance of approximately 65 ft (20 m) with a pressure of 1015 psia (70 bar) and the low value is at approximately 200 ft (60 m) with a pressure of 435 psia (30 bar). The cloud produced by the spray rig is approximately 6-7 ft (2-3 m) in diameter.

The maximum speed of the DIT is 210 KTAS at 22,000 ft altitude.

The DIT can be equipped in the with alternate nozzles producing droplets of 180-200 micron diameter for simulating freezing drizzle (large droplet) conditions.

4.3.2.3 *Testing*

Testing behind an icing spray tanker requires careful planning for both of the aircraft. Generally, a chase plane is also required to photograph areas exposed to simulated icing.

The usefulness of tanker testing has been recently demonstrated in a series of tests conducted as a result of the fatal crash of an American Eagle ATR72 in Roselawn, Indiana, on 30 October 1994. An ATR aircraft was exposed to icing conditions simulating freezing rain behind the tanker. These tests showed that a peculiar shape of ice can build up on the wings behind the de-icing boots in freezing rain with very large droplet size. From these tests, a new operational procedure was established based upon the observation of icing on side windows in conditions with large droplets. This is a unique sign of freezing drizzle or rain for this particular aircraft. Also, data from extensive flight tests provided the basis for a new deicer for the ATR aircraft.

This demonstrates a benefit of such simulated icing flight testing and the usefulness of spray tanker aircraft for icing tests.

4.3.2.4 *Shortcomings*

Aircraft icing simulation behind an icing spray tanker suffers from various shortcomings due to limitations in the testing environment. The coverage of the test aircraft is relatively small, hence only a very small area of the aircraft or only a single component can be fully tested. Generally, the simulation exposure is of a short duration due to limitations in the water capacity of the tanker aircraft. The tanker spray rig usually produces lower LWC than the LWC levels required by FAR 25, Appendix C. The tanker spray system has shortcomings in MVD drop size. The typical size is larger than the MVD found in natural icing clouds. The cloud drop size distribution is somewhat unknown and hence the MVD can not be precisely established. The large drop size results in higher catch efficiency tending to result in a more severe test than required. This can potentially show inadequacy of the icing protection system and hence may lead to wrong conclusions and over sizing of the system.

LWC in tanker spray clouds varies as a function of distance from the spray rig to the aircraft being tested.

In addition to the above shortcomings, helicopter tankers have limitations on altitude. Because of limited altitude capability, the icing test may have to be performed in the winter months.

In general, icing spray tankers have suffered in large part from:

1) Small icing cloud size so that only a portion of the aircraft can be tested,

2) Uncontrolled variables- water droplet size, liquid water content level, supercooling, and freeze out,

3) High turbulence levels trailing behind the tanker,

4) Effects of changes in atmospheric relative humidity causing large shifts in drop size and distribution between test runs,

5) Inconsistency-Lack of consistent icing cloud and continuous measuring instruments,

6) Large variety of weather conditions making it difficult to duplicate test conditions,

7) Simulation exposure of a short duration due to limited water capacity of the tanker aircraft,

8) Deficiencies in correlation between artificial and natural icing cloud characteristics.

4.3.3 Tests in Natural Icing

4.3.3.1 *Scope*

The air worthiness regulations require, if certification for flight in icing conditions is desired, tests in natural icing to demonstrate that the aircraft is able to operate safely in all operational conditions within Federal Aviation Regulations (FAR's) and Joint Aviation Regulations (JAR's), Appendix C icing envelopes. In-flight testing along with analysis and icing simulation in ground facilities such as icing tunnels or outdoor spray rigs have been used to demonstrate compliance with FAR's/JAR's.

By 1962, ice protection had been deleted from the tailplanes on some jet transports. This was the result of in-flight testing (there were no supercomputers then), and took advantage of the performance attributes of jet transports. In-flight testing in natural icing is a realistic means of checking effects of icing on aircraft. Effectiveness of the aircraft's ice protection system can also be demonstrated for full scale conditions. The natural icing environment provides conditions that are difficult to simulate in ground facilities or in in-flight simulation such as behind a spray tanker. However, the specific performance-critical conditions needed to demonstrate the adequacy of the systems are extremely difficult to find, and such testing is very costly and perhaps dangerous.

4.3.3.2 *Natural Icing Environment*

Aircraft icing occurs in clouds of supercooled liquid water droplets at temperatures ranging from 0 to -40 C. Three major atmospheric parameters are associated with aircraft icing: supercooled liquid water content (SLWC), cloud temperature, and droplet size distribution. Ice generally accretes on leading edges such as on wing and empennage.

In the early 1950s, measurements of icing clouds and icing encounters were made by Lewis and Jones (1949). These meteorological data provided the basis for system design and requirements. The icing envelopes were constructed as a combination of three variables having the assigned exceedence probability. The FAR icing envelopes have the exceedence probability of one in 1000 icing encounters.

4.3.3.3 *Testing*

Instrumented natural icing tests are conducted to demonstrate the effectiveness of an aircraft's ice protection systems. Additionally, it provides verification and validation of the analysis procedures used to calculate system performance for the entire icing envelope conditions. The test vehicle is generally a production aircraft. The ice protection systems are instrumented sufficiently to obtain system performance data in icing conditions and to allow comparison between predicted and observed test results. This includes high speed video or photography of ice accretion. This is extremely useful in recording the events associated with a particular test condition for ice shedding. Time correlation of the video record with other data is essential. The types of instruments used for natural icing testing are discussed in sub-chapter 4.4, Instrumentation for Icing Tests. The following is a checklist of measurement requirements normally necessary for natural icing tests:

1) Airspeed

2) Altitude

3) Ambient Temperature

4) Time

5) Attitude

6) Engine Data

-Engine Power Setting

-Exhaust Gas Temperature

7) System Data

-Airflow

-Pressures

-Temperatures

8) Meteorological Data

-Droplet Size (Median Volume Droplet, MVD)

-Liquid Water Content

9) Photographic Data

10) Ice Accretion Data

Operational regimes such as climb, cruise, hold and descent are usually investigated at various altitudes. The testing procedure checks out system functionality and the indication system in the cockpit. Surface temperature measurements in dry air and wet conditions indicate the system's potential for de-icing and anti-icing.

During the testing, icing conditions may not be at the critical design point. The procedure requires an extended period of exposure to build up predetermined ice thickness on the unprotected areas and selected protected areas with the ice protection system turned off. Then the aircraft is flown out of the icing into dry air conditions to perform aircraft operating and handling tests with accreted ice. The aircraft's ice shedding characteristics and de-icing time are also recorded and observed with its ice protection systems operating.

4.3.3.4 *Shortcomings*

The major concerns with natural icing testing are: 1) Finding suitable natural icing conditions for tests, 2) Flight safety during natural icing testing in stormy weather, and 3) Measurement and recording of dynamic icing conditions and effects during the exposure. The nature of the testing and the requirement of testing at a given design point necessitate staying in icing conditions for an extended period in order to fully test all systems. This can result in cases where ice build up on unprotected parts becomes excessive, thus increasing the possibility of hazardous ice shedding into the engines or other critical aircraft components. Generally, testing is off-site and is limited to certain locations. Finding even a reasonable encounter for a short time period can require many flight hours.

4.3.4 Research Aircraft for Icing Tests

A specially equipped Convair 580 twin-engine, long-range turboprop aircraft operated by the National Research Council (NRC) of Canada's Institute for Aerospace Research is being used as a multi-purpose flying laboratory supporting projects in atmospheric studies. Recently, research projects have been undertaken to increase knowledge of cloud physics, cloud chemistry and major storms. The aircraft is fitted with specialized instrumentation to detect the accretion of ice on the aircraft and to monitor the aircraft response to icing. The instruments include laser probes and holographic camera to record the size and concentration of cloud droplets, ice particles, and precipitation, ice detectors for ice detection, liquid water content, and dual dropsonde system for wind, temperature and humidity profiling. Currently, a Canadian research team is conducting a unique study to measure and document the formation of freezing drizzle and its effect on aircraft aerodynamics.

4.3.5 Concluding Remarks on In-Flight Icing Tests

Testing in natural icing conditions need not be a major part of certifying or qualifying the aircraft. However, because of limited analytical capabilities, lack of large ground icing simulation facilities and small coverage of test aircraft by icing spray tanker aircraft, testing in natural icing is currently a major part of an icing certification or qualification program. It is necessary that the results of tests in simulated conditions be compared with those obtained in natural icing so that the test facility either can be validated or the necessary techniques developed to enable extrapolation to natural conditions. The current in-flight tanker's inability to produce sufficiently large clouds limits the usefulness of artificial icing testing for fixed wing aircraft. However, military aircraft and rotorcraft have been successfully tested using icing spray tankers for demonstrating airworthiness. A systematic approach to validate analytical techniques is highly recommended. Experimental studies to further the development of icing scaling rules should be funded. A good correlation between scaled and prototype icing test results would significantly reduce the cost of aircraft certification and produce better understanding of in-flight ice accretion in general.

4.4. INSTRUMENTATION FOR ICING TESTS

The adequacy of an ice protection system may be examined by the use of icing simulation techniques. These techniques, both analytical and experimental, help to identify only some of the critical icing design points for an aircraft and/or its components; the experimental techniques may be used to demonstrate compliance with Federal Aviation Administration (FAA) regulations or to understand basic problems.

In the following we shall present the instrumentation requirements for the two main experimental methods used for icing simulation:

- Icing Wind Tunnel (IWT)
- Spray Tanker Simulation

and the type and the accuracy of the data obtainable from each technique.

4.4.1 Instrumentation for Measurement of the Environment

In icing simulation studies it is necessary to measure many parameters which characterize the environment, including static and total pressures, temperatures and properties of the icing cloud.

Measurements of cloud droplet distributions and Liquid Water Content (LWC) are critical to understand the physical processes in clouds.

The Median Effective/Volumetric Diameter of the water droplets [MED/MVD, i.e. the droplet diameter which divides the total water volume present in the distribution in half] , the LWC and the distributions, in space and in time, within icing clouds are the parameters of interest.

Instruments for measuring droplet diameters within icing clouds can be considered to be of three types:

1. Optical techniques based on the light scattering properties of the particles;
2. Vaporization of droplets based on the balance of the exchange of energy between heated wires and two phase-flow;
3. Mechanical systems based on the mechanical collection of droplets [for example by multicylinders, grids or blade] or systems based on the impact of droplets on a reference soot-coated slide, for example the cloud gun.

The accurate determination of the liquid water content and droplet size of an icing cloud is important in icing research, in the development of ice protection systems and in certification testing. It is still, nowadays, a difficult task due to the primary problem of a lack of accurate calibration methods that can provide droplet populations with known distributions under conditions similar to those that the instrument might encounter during testing.

In the following only a brief description of the main measurement systems for cloud characterisation will be given. More information can be found in Olsen (1983), where different types of icing cloud instruments have been compared in the NASA 6 x 9 foot Icing Research Tunnel (IRT), and in SAE (1993) where a large number of modern and old-style instruments have been compared.

4.4.1.1 *Static and total pressure measurements*

Conventional instrumentation, such as Pitot tube and wall static pressure taps, are used in Icing Wind Tunnels (IWT) for these types of measurements. The main differences between the IWT and conventional wind tunnel applications are due to possible ice accretion on the orifices of the probes; these must be avoided by using suitable heating systems.

4.4.1.2 *Temperature measurements*

Thermocouples are the devices most commonly used for temperature measurements. For measuring the ambient static temperature, thermocouples must be installed in the flow by using a special immersion device with de-icing systems. The error due to de-icing is more or less ± 0.5 C and is considered acceptable.

The static temperatures can be measured by using the total temperature measurement device in conjunction with the measurement of the air speed under the hypothesis of adiabatic transformations. The air speed can be determined in the usual way from measurement of total and static pressure.

4.4.1.3 *LWC instrumentation*

The Leigh and Rosemount LWC sensors

These sensors are automatic ice accretion detector instruments that sense the ice as it builds up on the sensing surface. When a critical amount of ice is exceeded, the sensing surface is electrically heated to remove the ice; then the build-up cycle is repeated over and over again. Each instrument accomplishes the sensing somewhat differently. The LWC is related to the cycle time and to the airspeed.

The Leigh sensing surface is a small tube that is mounted across the inside of small inlet tube. When the ice build-up on the sensing tube exceeds a pre-set thickness, an infrared light beam, aimed across the sensor tube at a photo detector, is interrupted and commands the de-icing cycle to start; heated compressed air, used to aspirate the air flow through the inlet, keeps it free of ice.

The Rosemount LWC sensor uses electronics which detect the changes in the resonant frequency of the small vibrating sensor tube as ice builds up on the surface.

The Johnson-Williams (J-W) LWC Instruments

The J-W is basically a hot wire probe; it uses the correlation between LWC and the increase of heat transfer that occurs when droplets strike the hot sensing surface. The operation of the J-W is based on the principle that droplets hitting and evaporating from the heated wire will cool the wire.

A wire, whose resistance is a function of temperature, is mounted perpendicular to the air flow. A second wire is mounted parallel to the air flow; this wire is not subjected to droplet impingement and it is used only for temperature compensation. The diameter of the sensitive wire is $\approx$ 0.6 mm, whereas the diameter of the compensating wire is $\approx$ 0.3 mm.

The J-W probe has an accuracy of only ±20%.

The CSIRO King Probe

The sensing element of this instrument is a coil of copper wire, approximately 4.25 cm long and 1.8 mm in diameter (sizes vary for different models). An electric current, passing through the coil, maintains it at a constant temperature. The electric power needed to maintain this temperature is monitored. Droplets striking the wire will cause cooling. The increase in power, needed to offset the cooling effect of evaporation, is related to the measure of the liquid water content (Hovenac, 1986). The King probe has been reported to have an accuracy of ±5% (Baumgardner, 1983).

The Blade Instrument

The blade is manually operated and de-iced, and its data are manually reduced. A thin blade (made of aluminium bar stock 0.3 cm thick x 1.9 cm wide and 25 cm long) is attached to a manual actuator and mounted inside a shield. The unit is suspended from the ceiling of the icing tunnel test section.. The shield is removed for 30 seconds to expose the thin edge of the blade to the icing cloud in the center of the test section; the thickness of the ice accretion on that surface is then measured with a micrometer and the LWC is calculated by accounting for the collection efficiency.

The Rotating Multi-Cylinder

This is also a manually operated instrument. Five rotating cylinders, with various diameters ranging from 0.35 cm to 11.0 cm, are stacked (one on top of the other with transition pieces) to make the cylinder array. This instrument gives data for LWC and for MDV. The LWC is determined from the weight of the ice on each of the cylinders. Theoretical relations involving droplet size, cylinder diameter, collection efficiency, and airspeed, are used to derive average liquid water content and median effective droplet diameter (Brun, 1955).

4.4.1.4 *Droplet sizing instruments*

The Forward Scattering Spectrometer Probe (FSSP)

This is an optical droplet sizing instrument used for the measurement of water droplet diameters in natural and artificial clouds and it is the most widely used droplet sizing instrument for cloud research. The probe contains a 10 mW helium-neon laser, optics, and electronics. The FSSP has two probe arms that are connected by a flow straightening tube. One probe arm contains the laser beam transmitting optics and the other contains the receiving optics. A flow straightening tube is used to insure mechanical stability between the probe arms and also to provide a path to the droplets contained in the airflow. The mirror and the prism, that are located in the probe arms, are open to the airflow and, therefore, are heated to reduce contamination. The forward section of the flow straightening tube is also heated to keep ice from blocking the inlet of the tube.

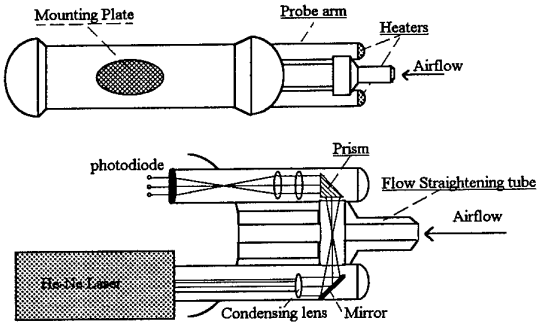

The FSSP has five droplet size ranges:

0.5	-	8	μm
1	-	16	μm
2	-	32	μm
2	-	47	μm
5	-	95	μm

Each range in the FSSP has 15 size bins so that, for example, the 2 to 47 μm range, which is used for most icing applications, has 3 μm bin width.

There are two major environmental factors that can effect the accuracy of the FSSP's droplet measurement: the droplet number density and the droplet velocity.

The upper limit of droplet number density for the FSSP is governed by the size of the probe volume and by the speed of the electronic circuitry in the instrument. Typically the droplet number density limit is 500 droplets/cc. At droplet number densities above this value, multiple droplets in the probe volume can cause counting and sizing errors. There is also a lower limit to droplet number density: as the number density decreases, it takes longer and longer for the FSSP to measure enough droplets to get a statistically valid sampling at any given velocity.

The FSSP's error in the measurement of the MVD is approximately 10% in an icing wind tunnel. Measurements of high droplet number densities tend to be smaller than the true values, and the measured LWC can be either larger or smaller than the true values, depending on whether counting errors or sizing errors dominate.

The FSSP can make errors if droplets pass through the probe volume at high velocities (electronic limitation). Errors in FSSP can begin to occur at velocities of 80 m/s.

The FSSP also has a lower limit to droplet velocity of 10 m/s.

Other error sources that have been identified in the FSSP include calibration errors (5% to 10% predicted as sizing error for larger droplets) and laser beam illumination errors.

The measurement time (not including transit time) for one particle is about 6 μsec.

Axial Scattering Spectrometer Probe (ASSP)

The ASSP was a predecessor of the FSSP and is no longer used. Like the FSSP, this instrument measures the intensity of the light scattered by the droplets. The scattered light intensity is theoretically related to the droplet size. The number of droplets counted in each size channel is then periodically sampled and the MVD, the LWC and drop size distribution are automatically calculated.

The Optical Array Probe (OAP)

The OAP is the most widely used instrument to measure the diameter of particles larger than 100 μm. The OAP comes in 1D and 2D models. The 1D model measures only diameter, but the 2D version also provides images so that the shape of the particles can be viewed.

As with the FSSP, the OAP is a self-contained probe that is approximately 1 m in length. The probe contains a small (5 mW) laser. An external data acquisition system is needed for displaying, manipulating, and saving data, and also for viewing the images. The OAP has two probe arms but does not have a flow straightening tube. One probe arm contains the laser beam transmitting optics and the other arm contains the receiving optics, both of which are heated.

The OAP can measure droplets as small as 10 μm or as large as several millimetres and can have 15, 30 or 62 size bins.

There are several factors to consider when assessing the accuracy of the OAP. These include the counting errors, spectral broadening due to forms of the droplets, coincidence errors, velocity errors, and statistical uncertainties.

Both experimental and theoretical studies have been done for the estimation of the sizing error: droplets can be undersized or oversized by as much as 15%; this leads to a broadening of the size spectrum.

The size range and the resolution of the OAP depend on the magnification of the lens systems and on the size of the photo diode array. The minimum size is limited by diffraction effects and is usually no less than 10 μm. The maximum size can be factory adjusted to several millimetres.

The Phase Doppler Particle Analyser (PDPA)

The Phase Doppler Particle Analyser was developed in the early 1980s for spray and combustion analysis in laboratory environments or in small wind tunnels. Papers describing the phase Doppler technique appeared in 1984 by W. Bachalo et al. , who founded *Aerometrics, Inc.*, which currently manufactures the PDPA. Recently the PDPA has been modified to allow measurements in large icing wind tunnels or from research aircraft .

The PDPA is a single particle counter that can make size and velocity measurements of a droplet as it crosses the instrument's probe volume.

A beam from a low power laser is split into two beams, then focused by a lens. The two beams intersect and form an interference pattern of bright and dark fringes. As a droplet crosses these fringes it scatters more or less light, depending on its position relative to the fringes. This periodic fluctuation in the scattered light from a droplet is known as a Doppler burst. The frequency of the Doppler burst is proportional to the droplet's velocity normal to the fringes. To measure the Doppler burst, the scattered light is collected by a lens system. The lens system is set up so that it images the beam intersection region onto a spatial filter. The purpose of the spatial filter is to pass only the scattered light that comes from droplets in the beam intersection region. This filtering method defines the probe volume of the PDPA. The light that passes through the spatial filter is collected by a lens and transferred to three detectors. One of the detectors is used to measure the Doppler burst and other two detectors are needed for making a size determination. The size of droplet is determined by analysing the scattered light from the droplet. As the droplet passes through the probe volume the scattering pattern shifts and the alternating bands of light and dark pass over the detectors. Since the detectors are located at slightly different locations relative to one another, they measure Doppler bursts that are slightly out of phase from one another (hence the term phase Doppler). Since the spacing between the detectors is known, the spatial frequency and the droplet size can be determined from the phase difference measured by any two detectors. A third detector is used as an additional phase check.

The velocity and size range of the PDPA can vary depending on its optical configuration. In one configuration used for cloud measurements, the manufacturer lists the velocity range as 20 to 350 m/s and the diameter range as 1 to 150 μm with 50 size bins (Hovenac, 1986).

One area of possible concern is the effect of non spherical particles on the PDPA measurement. All PDPA measurements are made with the assumption that the droplets are spherical. Any deviation from sphericity can lead to measurement errors. The actual effect on the

measurement of the droplet distribution by the presence of non spherical particles in a cloud is not well documented.

Malvern particle Size Analyser (MPSA)

The Malvern particle size analyser was designed as a laboratory type instrument and has been widely used for fuel spray droplet size analysis. The Malvern has unique attributes that make it attractive for measurement of high density sprays.

This instrument consists of a transmitter which contains a 5 mW helium-neon laser and the receiver has a lens, a detector, and sampling electronics. A microcomputer is provided for data acquisition and storage.

The MPSA instrument is not designed to be exposed to the severe environment of an icing facility. In order to make such measurements, it must be protected, while having optical access to the cloud. Two windows are needed for this access: one for the transmitter and one for the receiver. The windows should be anti-reflection coated and angled slightly to avoid unwanted reflections on the detector. The working distance from the cloud to the lens should be less than the focal length of the lens. Thus, the MPSA can only be used in tunnels with a very small test section.

The MPSA is unique in that it does not have any limitations on the velocity of the droplets in the laser beam. It is assumed that the overall droplet distribution in the laser beam does not change over time. If the actual droplet distribution changes during the measurement period, then the MPSA will measure an average of the distribution.

The size bins in the MPSA are logarithmically spaced and depend on the focal length of lens used. Prior to making measurements with the MPSA it is necessary to take a background reading with no spray present. When the spray measurement is made, the background reading is subtracted from the reading with the spray present.

The MPSA does have a feature that allows the signal to be integrated over time and this will decrease the effect of random noise fluctuations. This feature, however, assumes that the spray does not change over the integration period. In most tunnels this is a valid assumption.

The MPSA is sensitive to window or lens contamination, stray reflections, room lights, and misalign optics. Although the background reading can be used to compensate all of these effects, to a certain degree, in practice the user must be meticulous about care and operation of the MPSA in order to get the best possible data.

Holography System

A holography system is used to obtain holograms of the water droplets. The holograms contain three-dimensional water droplet data. The holograms are reconstructed to obtain particle size, particle size distribution, and in some instances, by using a double laser pulse, particle velocity.

The system is semi-automatic in that the operator must first recognise a particle image then bring the image into focus by traversing the hologram with respect to the laser beam. The image size and its location are recorded on tape for later data reduction.

With this system, droplets as small as 8 μm can be resolved, and the location of the droplet images can be ascertained to within ±0.01 mm.

Measuring uncertainties in recorded values of LWC, MED, and engine inlet gas temperature (Hunt,1978) are, in general, dependent on the particular installation ; values are as follows:

Parameter	Uncertainty percent
LWC, g/m3	±15%
MED, μm	±36%
Engine Face Temp., K	±1.2%

The advantages of using a holocamera, as a particle diagnostic tool, are that it provides three-dimensional viewing of the particle field,. allowing also the analysis of the flow field (holographic PIV).

The Oil Slide Technique

An oil covered slide is put into the airstream and exposed to the cloud droplets. The droplets hit the slide and are captured in the oil. The slide is then placed under a microscope and the resulting image is analysed by computer to measure the size of individual droplets.

This measurement assumes that the captured cloud droplets retain their mass during and after impact and that the sample is representative of the cloud. The width of the slide is 2.5 mm. The slide's collection efficiency at 50 m/s for 5 μm droplets is approximately 60%.

There is some difficulty in controlling the time exposure of the oil slide in the cloud. This is a problem for several icing conditions because of the very short exposure time needed. Manual exposure is too slow, so an automatic exposure device is required. The accuracy of this system is dependent on the sample exposure, the image analysis calibration, and the MVD calculation.

The image measuring software is calibrated with the use of a reticule whose image is brought into focus. A manual check of the calibration typically shows a measured repeatability to one micron.

The MVD calculation finds the droplet size distribution using a bin width of two microns: 0 to 2 μm, 2 to 4 μm, 4 to 6 μm and so on. This MVD resolution gives a size tolerance of ± 1 μm.

The overall repeatability of this method was checked by making multiple measurements of the same cloud. The results show that this method is very repeatable in measuring the MVD of a cloud.

The Soot Gun Technique

This is a mechanical device, of similar operation to the oil slide technique and provides a snapshot of the droplet spectrum and hence MVD of an icing cloud. The device consists of a small target slide which is coated with a thin layer of soot. The slide, in its housing, is covered by a rotating shutter driven by a torsion spring which operates when a trigger is depressed. As the shutter rotates it momentarily exposes the slide to the cloud particles. The marks left by the impacted droplets are analyzed with image processing software to obtain an estimate of the cloud MVD. The device is a much simpler and lower cost design than a Knollenburg Nephelometer (FSSP,OAP) but requires both a degree of manual processing to analyse the data and cannot provide a display of the MVD in real-time. The device provides only a spot reading of the cloud MVD, rather than the continuous record which is available with a nephelometer. A soot gun has proven useful during UK military helicopter icing trials for checking the accuracy and calibration of Knollenburg probes.

The advantage of the soot slide over the oil slide technique is that the droplet impact image can be retained, without degradation, for long time periods. There is however a slight disadvantage in that the measured diameter of the impacted droplet must be corrected to allow for the spread of the droplet which occurs on impact.

4.4.1.5 *Comparison between instruments*

In the test program reported in Olsen(1983), a large number of modern and old-style icing cloud instruments were compared in the NASA Icing Research Tunnel (IRT): the instruments tested were for LWC and drop size (both MVD and distribution measurements). The purpose of the tests was to determine the relative accuracy of these instruments over a broad range of conditions.

The instruments tested were:

LWC Instruments:

- the Blades
- the Leigh Sensing Surface
- the J-W LWC sensor
- the Rotating Multi-Cylinbder
- the Rosemount LWC sensor

Droplet Sizing Instruments

- Forward Scattering Spectrometer Probe (FSSP)
- Four Axial Scattering Spectrometer Probes (ASSP)

For the two best performing instruments, in the IRT, repeatability of LWC was about 13 % and 15 %, over many different repeats at the same cloud conditions; this per cent variation is one standard deviation of the readings about the average LWC reading.

The values of percent error for the LWC instruments, compared to IRT calibration data, are reported in the following Table 4.4-1 over a large range of velocity but at low temperature to avoid thermal errors (i.e. run-off) which cause ice accretion on the instruments. In the Table

$$X^* = \frac{LWC_{indicated} - LWC_{IWT}}{LWC_{IWT}} \times 100$$

The scatter shown in the above table is due mainly to two causes:

- the repeatability of the instrument and the IRT;
- the inability of the instrument to properly account for the effect of MVD, LWC and airspeed over a large range of test conditions.

From the results in the table it appears that the laser spectrometer instruments tested (the ASSP's and FSSP) are too inaccurate to be used as LWC instruments.

All the droplet sizing instruments were similarly tested in the IRT and the indications of LWC and MVD were compared. The median volume droplet size (MVD) and LWC of the spray cloud are set according to the old IRT calibration, which is a function of the air and water pressure to the spray nozzles and the airspeed. All the instruments were immersed in exactly the same cloud of 16 μm MVD and 1.02 g/m^3 LWC and at an airspeed of 89 m/s. The table below (Olsen, 1983) shows the results for repeatability, in percent of variation (± one standard deviation), of the instruments, and the repeatability of the instruments, and the repeatability of the IRT spray cloud.

The first column of the Table 4.4-2 shows that the percent variation during a given spray is about ± 3 percent , which corresponds to less then ± 1 μm.

Table 4.4-1 LWC Measurement Accuracy

PROBE	AVERAGE OF X*	STANDARD DEVIATION OF X*	NUMBER OF TEST CASES
Blade	-3 %	± 19%	25
Leigh	-1 %	± 18%	111
J-W	-4 %	± 22%	33
Rotating Cylinder	-11 %	± 15%	25
Rosemount	-11 %	± 13%	23
FSSP 1	-68 %	± 15%	68
ASSP 1	+11 %	± 25%	23
ASSP 2	+3 %	± 79%	19
ASSP 3	-7 %	± 33%	41
ASSP 4	+25 %	± 28%	29

Table 4.4-2 Droplet Size Measurement Accuracy

PERCENT VARIATION IN DROP SIZE (MVD) IN THE IRT - Same Airspeed and Spray Nozzle Pressure -		
Laser Spectrometer	Samples during a given spray	Samples from sprays during the test period
FSSP 1	± 3 %	± 4 %
ASSP 1	± 2 %	± 3 %
ASSP 2	± 3 %	± 3 %
ASSP 3	± 2 %	± 7 %
ASSP 4	± 3 %	± 7 %
± one standard deviation of the MVD indications as a percent of mean value for that probe		

The second column is the percent variation during different spray but at the same sprays settings; again the variation with a given instrument is less than ± 1 μm.

4.4.2 Flight Test Instrumentation

During an icing test behind a spray tanker or in a natural cloud, the following data and instruments are required:

1. Pressure altitude; altimeter
2. Airspeed, indicated airspeed (usually Pitot-static tubes);
3. Outside air temperature; calibrated temperature probe;
4. Dew point; hygrometer;
5. Liquid water content; LWC meter;
6. Median volume droplet diameter (MVD); droplet sizing spectrometer (or other)(*This is the most difficult measurement)*;
7. Photographs of the critical components; still or motion picture or video cameras.

The LWC and MVD instrumentation has been described earlier. These data are required as a function of flight time in the icing cloud, so time correlation of photographic data with the other data is essential. A data acquisition system is needed to collect and reduce the data for display in near-real-time.

A typical data acquisition system would include a micro-processor, a data recording system, a printer or CRT for near-real-time output, and an operator control panel.

Regarding limitations, according to the Aircraft Icing Handbook (1993), with a maximum icing cloud width of 35 to 40 feet, all parts of an aircraft cannot be tested simultaneously. Therefore, the icing sensors for LWC and droplet size must be located on the test aircraft near the tested components in order to measure cloud conditions during the test. The artificial cloud conditions (such as liquid water content and mean droplet diameter) are dependent upon location in the cloud.

LWC and drop diameter varies as a function of location in the cloud of the tanker. Maintaining a fixed position behind the tanker is a challenge for the pilot. The median droplet size is generally larger in artificial clouds than natural clouds due to the difficulty of maintaining small water droplets. This is due to the rate of evaporation of

droplets which changes the cloud's droplet distribution. The evaporation rate varies with local atmospheric humidity from hour to hour. For droplets with diameters less than 25 microns, the evaporation time at 90 KIAS (167 Km/hr) may be about 1.5 seconds or less, depending on the humidity.

Increasing the water flow rate may produce smaller droplets but it will also result in an undesirable droplet distribution and excessive ice accumulation in parts of the cloud. Evaporation of small droplets makes it very difficult to simulate ice accretions of shapes and types that occur in natural icing when small droplet impingement is predominant.

Turbulence is almost always high in the spray cloud due to propeller wakes and lifting surface vortices. The turbulent eddies are "*large*" since the tanker is usually larger than the test aircraft, causing the coalescence of some droplets into larger drops.

4.4.3 Test Article and Aircraft Instrumentation

4.4.3.1 *Icing Article Instrumentation*

Here we shall present a brief description of the systems that are in use to make measurements during model tests in icing wind tunnels.

Ice Thickness Measurements

During the testing of de-icing systems, physical measurements of the ice thickness on the airfoil could be made with a laser beam depth micrometer.

Two laser beam depth micrometers could be placed at two sections, above and below the chord of the wing model. Each micrometer will measure the clean model and then the model contaminated with the ice. Thus the distribution in time of ice thickness can be found.

Shed Ice Particles Measurement by Image Processing Technique

An important application of particle size measurement was made at NASA during wind tunnel testing to obtain information on thickness and size of ice shed from an eddy-current deicer system (EDS) (Smith,1994). In this work 58 test runs were made in the Icing Research Tunnel (IRT) at NASA Lewis. Post-cycle ice thickness remaining on an airfoil was measured. Aerodynamic penalties associated with ice build-up was correlated with ice layer thickness and ice layer distribution.

Shed ice particle size was recorded with a high speed imaging system. Knowledge of the path and size of these particles can be used to avoid possible damage to engine inlets, windshields, lights, etc. operating downstream of the EDS. Particle sizes were recorded with a high-speed videography system. Two intensified imaging cameras recorded the shed ice particles as they were swept away by the airstream. One camera looks down from the top of the tunnel to capture the shed ice particles as they move over a 25 mm grid painted on the floor of the IRT. The second camera records, at 1000 frames/second, the shed ice from the control room looking at the pressure side of the airfoil. The images from the camera are stored on magnetic media tapes and can be later downloaded in a

digital format to a computer workstation. NASA has developed computer software for digitally processing each frame. The image of the iceless airfoil is subtracted from each frame, leaving only white shed ice particles captured on a still, black background. Each pixel is 1.7 mm high by 1.4 mm wide. A complete description of the particle size imaging is given in Shin (1992).

4.4.3.2 *Icing Detector Instruments*

Ice detection instruments for aircraft are available in several types including those which detect ice and provide a visual display in the cockpit and those that automatically activate ice protection systems. Currently, most of the ice detectors are only certified for use as an advisory backup system to visual crew monitoring of ice condition. More information can be found in the Aircraft Icing Handbook (1993).

Hot Wire Ice Detectors

Hot wire ice detectors transform the ice into liquid water at constant temperature. Typically, the detector has a thermal sensor made of nickel or nickel-alloy wire wound on a mandrel that is exposed to the airstream. The wire is subjected to a periodic current pulse which causes the wire to heat up. If there is no ice on the wire, its resistivity will change linearly with time as the wire heats up. If ice has accreted, the wire temperature will remain constant at the melting point of the ice. After all the ice is converted to water, the wire resistivity will again increase. The resistance plateau at the ice melting point is electronically sensed and an ice signal is generated by the electronics. When ice is detected, the probe is de-iced by an internal cartridge heater. The probe is then allowed to cool down and the sensor is again ready to accrete ice.

Vibrating Probe Ice Detectors

This detector works on the principle of a vibrating rod or probe whose natural frequency is known. The probe is typically mounted on an aerodynamic strut. As ice accretes on the probe, the natural resonant frequency decreases. At a specified frequency shift, which is related to the ice mass on the probe, an output signal is generated and probe heaters are energised to remove the ice. The heater is then de-energised, the probe cools down, and it is again ready to accrete ice. Icing severity is determined by measuring the overall cycle rate with respect to time. The ice detection and measurement capability of the vibrating probe range up to 2 g/m^3 and ice thickness from 0.01 to over 0.10 inches. Accuracy of this type of detector, in measuring icing severity, is within ± 15%.

Pressure Array Detectors

These devices sense a decrease in ram air pressure whenever ice accretes over a row of holes drilled into the leading edge of a small strut. The detectors have seven small holes about 1/32 inch in diameter located in-line near the tip, and one ¼ inch diameter hole located about one third of the way in from the tip of the strut. A differential pressure sensor monitors the ram pressure difference between the large hole and the set of the small holes. In the absence of any ice accretion the ram pressure is balanced and independent of the airspeed. Any ice accumulation on the strut will block the small holes first, and the resulting unbalance in ram pressure can be used to activate a warning light.

Light Beam Interruption Ice Detectors

The operational principle of this detector is that the ice accreted on a probe occludes a light beam (normally infrared) crossing the central area of the probe at an oblique angle with a light sensitive receiver placed on the opposite side. The degree of occlusion is determined by the amount of ice on the probe. When the light occlusion reaches a predetermined level, representing the maximum permitted ice thickness, a heating cycle is initiated to remove the ice from the low thermal inertia probe. The time taken to accrete ice between two predefined levels is used as a measure of the icing rate from which LWC can be calculated.

Beta Beam Interruption Ice Detectors

A Beta beam interruption detector works in a similar way to the light beam device. The main disadvantage of the beta beam detector is that a radioactive source is required (usually Strontium 90). This detector is capable of detecting as little as 0.015 inches of ice thickness.

Rotating Disk Ice Detectors

This device is an obstruction type instrument where a disk is exposed perpendicular to the airstream.

Ice accreting on the rotating disk is shaved off by a scraper; the torque required to remove the ice is used to activate a warning system.

Pulse Echo Ice Detectors

This system operates on the principle of using pulsed ultrasonic waves to measure ice thickness over a small transducer mounted flush with an aircraft surface. The system produces a real-time ice thickness signal. Ice accretion rate may be determined by electronically differentiating ice accretion with respect to time.

In operation an ultrasonic transducer containing a piezoelectric element emits a pulse (2-10 MHz) which travels through the ice in a direction parallel to the transducer emitting axis. When the pulse reaches the ice/air interface it is reflected back into the ice layer. This "*echo*" returns to the aircraft surface where it is detected by the transducer which now acts as a receiver. The velocity of the pulse-echo signal through the ice

(approximately 3800 m/s) is determined by the ice density and elastic constants. By measuring elapsed time between the pulse emission and the echo signal return the ice thickness may be calculated

The operational accuracy achievable depends primarily on the transducer specifications (frequency and element diameter) and the transducer location. An accuracy of ± 0.02 inches (± 0.5 mm.) has been obtained for ice thickness measurements from 0.04 to 1.2 inches. The ultrasonic pulse-echo technique also allows the presence or absence of liquid water on the iced surface to be uniquely determined by examining the echo signal time variations received from the ice surface.

Microwave Ice Detectors

This system measures both icing rate and accumulated ice thickness. It consists of three major components:

- A microwave transducer
- A data transmitter located near the transducer
- A cockpit-mounted microprocessor and display

The microwave transducer consists of a resonant surface wave guide embedded flush in the surface on which ice accretes. The wave guide is constructed of dielectric material (polyethylene) having almost the same dielectric properties as ice. When ice accretes on the surface, the ice behaves as if it is part of the surface wave guide, by effectively thickening it, and causing its resonant frequency to shift downward in proportion to the thickness of the ice layer. The frequency shift is electronically related to ice thickness by means of a pre-established empirical equation stored in the computer. Ice growth with time is stored in the computer from which icing rate is obtained by differentiating ice thickness with respect to time. Icing rate change is also computed from the second derivative of the ice thickness with time.

References

Achenbach , E.(1975), "Total and Local Heat Transfer from a Smooth Circular Cylinder in Cross-Flow at High Reynolds Number," *Int. J. Heat Mass Transfer*, Vol.18, pp. 1387-1396.

Achenbach, E.(1977), "The Effect of Surface Roughness on the Heat Transfer from a Circular Cylinder to the Cross Flow of Air," *Int. J.Heat Mass Transfer*, Vol.20, pp. 359-369.

AGARD-AR-166.(1981), "Rotorcraft Icing-Status and Prospects", 136p.

AGARD AR-223.(1986), " Rotorcraft Icing-Progress and Potential,".

Anderson, D. N.(1994), "Rime-, Mixed- and Glaze-Ice Evaluations of Three Scaling Laws," *AIAA 94-0718.*

Anderson, D. N.(1995), "Methods for Scaling Icing Test Conditions," *AIAA 95-0540.*

Arimili, R.V. and Keshok, E.G. (1984), "Measurements of Local Convective Heat Transfer Coefficients on Ice Accretion Shapes," *AIAA 84-0018.*

Armand, C., Charpin, F., Fasso, G. and Leclere, G.(1977), "Techniques and Facilities at the ONERA Modane Centre for Icing Tests," *AGARD Advisory Report No.127*, 1977.

Ashenden R. and Marwitz, J. D.(1995), "A Comparison of the Air Force Water Spray Tanker Artificial Drizzle Cloud Distributions to the Natural Environment," Publication Unknown.

Barlett, C. S.(1986), "An Analytical Study of Icing Similitude for Aircraft Engine Testing," *AEDC-TR-86-26 (AD-A 173713), DOT/FAA/CT-86-35.*

Baumgardner, D. (1983), "An Analysis and Comparison of Five Water Droplet Measuring Instruments," *Journal of Climate and Applied Meteorology*, Vol. 22,1983.

Belte, Daumants(1980), "Helicopter Icing Spray System," *Proceedings of the Eleventh Annual Symposium.*

Berg, A. L. and Wolff, H. E.(1976), "Aircraft Engine Icing Test Techniques and Capabilities at the AEDC," *Paper presented at AIAA 14th Aerospace Sciences Meeting*, Washington, D.C.

Bilanin, A. J.(1991), "Proposed Modifications to Ice Accretion/Icing Scaling Theory," *J.Aircraft*, Vol.28, pp. 353-359.

Bilanin, A.(1992), "Mechanisms Resulting in Accreted Ice Roughness," *AIAA 92-0297.*

Bilanin, A. J. and Anderson,D.N.(1995), "Ice Accretion With Varying Surface Tension," *AIAA 95-053.*

Bilanin, A. J., Quackenbush, T.R., and Feo, A.(1989), "Feasibility of Predicting Performance Degradation of Airfoils in Heavy Rain," *NASA CR-181842.*

Boer, S.N. and Van Hengst, J. (1993), "Aerodynamic Degradation Due to Distributed Roughness on High Lift Configuration," *AIAA 93-0028.*

Bond, T. H., Flemming, R. J., and Britton, R. K.(1990), "Icing Tests of a Sub-scale Model Main Rotor," *Proceedings of the 46th Annual American Helicopter Society Forum* pp. 267-281.

Bond, T. H., Shin, J., and Mesander, G.(1991), "Advanced Ice Protection Systems Test in the NASA Lewis Icing Research Tunnel," *NASA TM 103757.*

Bongrand, J.(1978), "Etude Theorique et Experimentale de l'Influence de Divers Parametres Sur le Givrage d'un Profil," *Paper 10 in AGARD CP 236.*

Bragg, M. B.(1982), "A Similarity Analysis of the Droplet Trajectory Equation," *AIAA Journal*, Vol.20, pp.1681-1686.

Bragg, M.B. and Coirier, W.J.(1986), "Aerodynamic Measurements of an Airfoil with Simulated Glaze Ice," *AIAA Paper 86-0484.*

Bragg, M. B, Kerho, M. F. and Khodadoust, A.(1993), "LDV Flowfield Measurements on a Straight and Swept Wing with a Simulated Ice Accretion," *AIAA 93-0300.*

Bragg, M. B. and Khodadoust, A.(1988), "Experimental Measurements in a Large Separation Bubble due to a Simulated Glaze Ice Accretion," *AIAA 88-0116.*

Bragg, M.B. and Khodadoust, A.(1989), "Effect of Simulated Glaze Ice on a Rectangular Wing," *AIAA 89-0750.*

Bragg, M. B. and Khodadoust, A.(1992), "Measurements in a Leading-edge Separation Bubble due to a Simulated Airfoil Ice Accretion," *AIAA Journal*, Vol. 30, No. 6.

Bragg, M. B. and Spring, S. A.(1987), "An Experimental Study of the Flow Field about an Airfoil with Glaze Ice," *AIAA Paper 87-0100.*

Bragg, M. B. and Wells, S. L.(1993), "Effect of wind Tunnel Walls on Airfoil Droplet Impingement," *Journal of Aircraft,* Vol. 31. No. 1.

Brun, R., Lewis, W., Perkins, P., and Sacrafini, J. (1955), "Impingement of cloud droplets on a cylinder and procedure for measuring liquid water content and droplet sizes in supercooled clouds by rotating cylinder method," *NACA Report 1215*, 1955.

Chambers, H. W. and Adams, J. Y.(1986), "Summary of Artificial and Natural Icing Tests Conducted on U. S. Army Aircraft from 1974 to 1985," *DOT/FAA/CT-85/26*; *TR-85-F-11*, 223p.

Charpin, F. and Fasso, G.(1972), "Icing Testing in the Large Modane Wind Tunnel on Full Scale and Reduced Scale Models," *l'Aeronautique et l'Astronautique, no.38*; English translation published as *NASA TM-75373.*

Clareus, U.(1974), "Ice Simulation: A 2-Dimensional wind Tunnel Investigation of a NACA 65_2 A2515 wing Section with Single Slotted Flap," *Report FFA AU-995 Part 2.*

DOT/FAA/CT-88/8-1, "Aircraft Icing Handbook," - Vol. 1, 2.

Etkin, B.(1971), "Interaction of Precipitation With Complex Flows," *proc. Third International Conference on Wind Effects on Buildings and Structures*, Tokyo, 1971, pp. 135-143.

Federal Aviation Regulations, *Part 25 (FAR 25), Air worthiness Standards: Transport Category Airplanes, Appendix C*, (Code of Federal Regulations, Title 14, Chapter 1, Part 25, Appendix C), Superintendent of Documents, Government Printing Office, Washington, DC 20402.

Feo, A.(1987), "Rotating Arms Applied to Studies of Single Angular drop Impacts," *AIAA 87-0257.*

Feo, A., Rogles, F., and Urdiales, M.(1991), "The Measurement of Water Film Thickness on Airfoils in Heavy Rain Conditions Using Conductance Sensors," *AGARD CP 496*, p.16.

Flemming, R. J., Bond, T. H., and Britton, R. K.(1991), "Model Rotor Icing Tests in the NASA Lewis Icing Research Tunnel," *AGARD Specialists Meeting, Effects of Adverse Weather on Aerodynamics*, Toulouse, France.

Flemming, R. J., Bond, T. H., and Britton, R. K.(1991), "Results of a Sub-scale Model Rotor Icing Test," *AIAA 91-0660.*

Gabour, L. A. and Liehard V, J. H.(1994), "Wall Roughness Effects on Stagnation-point Heat Transfer Beneath an Impinging Liquid Jet," *ASME Journal of Heat Transfer*, Vol. 116 pp. 81-87.

Gelder, T.F; Smyers, W.H., and von Glahn, U.(1956), "Experimental Droplet Impingements on Several Two-dimensional Airfoils with Thickness Ratios of 6 to 16 Percent," *NACA TN 3839.*

Guffond, D. P.(1986), "Icing and De-Icing Test on a 1/4 Scale Rotor in the ONERA S1MA Wind Tunnel," *AIAA 86-0480*, AIAA 24th Aerospace Sciences Meeting, Reno.

Gulick, B. G.(1938), "Effects of Simulated Ice Formation on the Aerodynamic Characteristics of an Airfoil," *NACA WRL-292.*

Gray, Vernon H.(1964), "Prediction of Aerodynamic Penalties Caused by Ice Formations on Various Airfoils," *NASA TN D-2166.*

Gray, Vernon H.(1958), "Correlations Among Ice Measurements, Impingement Rates, Icing Conditions, and Drag Coefficients for Unswept NACA 65A004 Airfoil," *NACA TN 4151.*

Gray, Vernon H. and von Glahn, Uwe H.(1957), "Aerodynamic Effects Caused by Icing of an Unswept NACA 65A004 Airfoil," *NACA TN 4155.*

Gray, Vernon H. and von Glahn, Uwe H.(1953), "Effect of Ice and Frost Formations on Drag of NACA 65-212 Airfoil for Various Modes of Thermal Ice Protection," *NACA TN 2962.*

Hansman, R. J.(1985), "Droplet Size Distribution Effects on Aircraft Ice Accretion," *Journal of Aircraft,* Vol. 22, No. 6.

Hansman, R. J., Breuer, K.S., Hazan, D., Reehorst, A., and Vargas, M.(1993), "Close-up Analysis of Aircraft Ice Accretion," *NASA TM 105952 and AIAA Paper 93-0029.*

Hansman, R. J., Jr.(1993), "Microphysical Factors Which Influence Ice Accretion," *proc. First Bombardier International Workshop: Aircraft Icing, Boundary-Layer Stability and Transition*, Ecole Polytechnique de Montreal, Montreal, Sept.1993, pp. 86-103.

Hansman, R. J. Jr., Yamaguchi, K., Berkowitz, B., and Potapczuk, M.(1991), "Modelling of Surface Roughness Effects on Glaze Ice Accretion," *J.Thermophysics*, Vol.5, pp. 54-60.

Hansman, R. J. Jr. and Turnock, S. R.(1989), "Investigation of Surface Water Behavior During Glaze Ice Accretion," *J. Aircraft*, Vol.26, No. 2, pp. 140-147.

Hastings, E.C. and Weinstein, L.M.(1984), "Preliminary Indications of Water Film Distribution an Thickness on an Airfoil in a Water Spray," *NASA TM-85796.*

Hovenac, E. A. (1986), "Calibration of Droplet Sizing and Liquid Water Content Instrumentation: Survey and Analysis," *NASA CR 17 5099.*

Hunt, J. D. (1978), "Engine Icing Measurement Capabilities at the AEDC," *AGARD CP 236.*

Jones, R. and Wiliams, D.H.(1936), "The Effect of Surface Roughness on the Characteristics of Airfoils," *RAE R&M 1708.*

Keller, R. G.(1978), " Measurement and Control of Simulated Environmental Icing Conditions in an Outdoor, Free Jet," Engine Ground Test Facility. *AGARD CP-236.*

Kerho, M.F. and Bragg, M.B.(1992), "Helium Bubble Visualization of the Spanwise Separation on a NACA 0012 with Simulated Ice Shape," *AIAA 92-0413.*

Khodadoust, A.(1988), "A Flow Visualization Study of the Leading Edge Separation Bubble on a NACA 0012 Airfoil with Simulated Glaze Ice," *NASA CR 180846.*

Khodadoust, A. and Bragg, M.B.(1990), "Measured Aerodynamic Performance of a Swept Wing with a Simulated Ice Accretion," *AIAA 90-0490.*

Kind, R. J., Gladstone, D. H., and Moizer, A. D.(1983), "Convective Heat Losses From Flat-Plate Solar Collectors in Turbulent Winds," *ASME J. Solar Energy Eng.*, Vol.105, pp. 80-85.

Kind, R.J. and Lawrysyn, M.A.(1991), "Effects of Frost on Wing Aerodynamics and Take off Performance," *AGARD CP-496.*

Kind, R. J. and Lawrysyn, M. A.(1992), "Aerodynamic Characteristics of Hoar Frost Roughness," *AIAA J.*, Vol.30, pp. 1703-1707.

Kirchner, R. D.(1983), "Aircraft Icing Roughness Features and Its Effect on the Icing Process," *AIAA Paper 83-0111.*

Kissling, H. H.(1972), "Aircraft Engine Anti-Icing Test and Evaluation Technology," *Paper presented at AIAA 10th Aerospace Science Meeting,* San Diego, California.

Kreith, F.(1965), *Principles of Heat Transfer*, second ed., International Textbook Co., Scranton, Pennsylvania, pp. 550-560.

Langmuir, I. and Blodgett, K. B.(1946), "A Mathematical Investigation of Water Droplet Trajectories," *Army Air Forces Tech. Rept. 5418,* Contract W-33-038-ac-9151.

Lewis, W. and Jones, A. R.(1949), "Recommended Values of Meteorological Factors to be Considered in the Design of Aircraft Ice-Prevention Equipment," *NACA TN 1855.*

Ljungstrom, B. L. G.(1972), "Wind Tunnel Investigation of Simulated Hoar Frost on a 2-Dimensional wing Section with and Without High Lift Devices," *Report FFA AU-902.*

McPherson, R. L.(1972), "Pilot Handbook for Critical and Exploratory Flight Testing," *Society of Experimental Test Pilots*, pp . 173-176.

Messinger,B.L.(1953), "Equilibrium Temperature of an Unheated Icing Surface as a Function of Air Speed," *J.Aero. Sci.*, VOl.20, pp. 29-42.

Miller, C. M.(1975), "Numerical Method for Liquid Water Content Prediction in the Air Force Flight Test Center Icing Spray Cloud," Towards More Effective Testing; *Proceedings of the Sixth Annual Symposium, Society of Flight Test Engineers*, pp. 335-346.

Neel, C.B., Jr. and Bright, L.G.(1950), "The Effect of Ice Formations on Propeller Performance," *NACA TN 2212.*

Newton, J. E., Van Fossen, G. J., Poinsatte, P.E., and Dewitt, K.J.(1988), "Measurement of Local Convective Heat Transfer Coefficients from a Smooth and Roughened NACA-0012 Airfoil: Flight Test Data," *AIAA 88-0287.*

Olsen, W., Shaw, R., and Newton, J.(1984), "Ice Shapes and Resulting Drag Increase for a NACA 0012 Airfoil," *NASA TM 83556.*

Olsen, W., Takeuchi, D., and Adams, K.(1983), "Experimental Comparison of Icing Cloud Instrumentation," *NASA TM 83340*, and *AIAA-83-0026.*

Olsen, W. and Walker, E.(1983), "Close up Suction Pictures of the Icing Process," *NASA Lewis Research Center Film.*

Olsen, W., and Walker, E.(1986), "Experimental Evidence for Modifying the Current Physical Model for Ice Accretion on Aircraft Structures," *NASA TM 87184.*

Pais, M. and Singh, S. N.(1987), "Local Heat Transfer Coefficients of Simulated Smooth Glaze Ice Formations on a Cylinder," *J. of Thermophysics and H.T.*, Vol. 1. No. 2.

Pais, M. R. and Singh, S. N.(1988), "Fourier Analysis Approach for Surface Definition and the Effect of Roughness on the Local Convective Heat Transfer Coefficient as Related to Ice Accretion," *AIAA 88-0117.*

Pais, M.R., Singh, S.N., and Zou, L.(1988), "Determination of the Local Heat Transfer Characteristics on Glaze Accretions on a NACA 0012 Airfoil," *AIAA 88-0292.*

Papadakis, M., Elangovan, R., Freund, G.A. Jr., and Breer, M.D.(1987), "Experimental Water Droplet Impingement Data on Two-dimensional Airfoils, Axisymmetric Inlet and Boeing 737-300 Engine Inlet," *AIAA 87-0097.*

Pavarov, O.A., Shal nev, K. K., Navarov, O.I. and Shalovasov, I.A.(1975), "Collision of Droplets with a Moving Plane Surface," *Trans. in Soviet Physics-Doklady (USA),* Vol. 20, no. 11, pp. 782-783.

Personne, P.(1988), "Effect de la Rugosité sur la Croisance du Givre a Faible Vitesse: Resultats Experimentaux et Modelisation," *D. Sc. Thesis. L'Universite Blaise-Pascal* (Clermont-Ferrand II).

Potapczuk, M. G. and Reinmann, J. J.(1991), "Icing Simulation: A survey of Computer Models and Experimental Facilities," *AGARD CP-496.*

Potapczuk, M.G. and Berkowitz, B.M.(1989), "An Experimental Investigation of Multi-element Airfoil Ice Accretion and Resulting Performance Degradation," *NASA TM-101441.*

Preston, G. Merritt and Blackman, Calvin C.(1948), "Effect of Ice Formations on Airplane Performance in Level Cruising Flight," *NACA 1598.*

Reehorst, A. L. and Rictcher, P.G.(1987), "New Methods and Materials for Molding and Casting Ice Formations," *NASA TM 100126.*

Reich, A.(1994), "Interface Influences Upon Ice Adhesion to Airfoil Materials," *AIAA 94-0714.*

Rockenback, F.A. and Alexander, D.R.(1980), "An Experimental Study of Angular Collisions Between Drops and Moving Liquid Films," *Proceedings of ASME-ANS. Nuclear Reactor Thermal Hydraulic Topical Meeting*, Saratoga, New York.

Ross, R. (1986), "Electro-Impulse Deicing of NASA Lewis Altitude Wind Tunnel Turning Vanes," *J. Aircraft, vol. 25, no. 6*, June 1986.

Ruff,G. A.(1986), "Analysis and Verification of the Icing Scaling Equations," Volume 1 Revision (U), *Arnold Engineering Development Center AEDC-TR-85-30-V-1-REV.*

SAE : (1993), "Droplet Sizing Instrumentation Used in Icing Facility," *International AIR-4906,* 1993.

Sartor, J.D. and Abbott, C.E.(1975), "Prediction and Measurement of the Accelerated Motion of Water Drops in Air," *J. Appl. Meteo.* Vol. 14, pp. 232-239.

Scott, W. B.(1983), "Icing Tankers Aid Aircraft Certification," *Aviation Week & Space Technology.*

Shin, J. and Bond, T. H.(1993), "Surface Roughness Due to Residual Ice in the Use of Low Power Deicing Systems," *NASA TM 105971.*

Shin, I., Bond, T.H., and Meesander, G. A.(1992), "Result of a Low Power Ice Protection System Test and a new Method of Imaging Data Analysis," *NASA TM 105745*, June 1992.

Simpson, R. L.(1973), "A Generalized Correlation of Roughness Density Effects on the Turbulent Boundary Layer," *AIAA J.*, Vol.11, pp. 242-244.

Stallabrass, J. R.(1977), "Helicopter Ice Detection, Icing Severity and Liquid Water Content Measurements," *AGARD AR 127.*

Smith, S. O.(1994), "Ice Thickness and Particle Size from an Eddy Current Deicer," ELECTROIMPACT Inc.

Spring, S.A.(1988), "An Experimental Mapping of the Flow Field Behind a Glaze Ice Shape on a NACA 0012 Airfoil," *NASA CR 180847.*

Stokes, G. G.(1851), "On the Effect of the Internal Friction of Fluids on the Motion of Pendulums," *Cambridge Phil. Trans.*, Vol.9, pp. 8-106.

Swift, R. D.(1978), " Icing Test Facilities at the National Gas Turbine Establishments," *AGARD CP-236.*

Valarezo, W. O., Lynch, F. T., and McGhee, R. J. (1993), "Aerodynamic Performance Effects Due to Small Leading-edge Ice (Roughness) on Wings and Tails," *Journal of Aircraft*, Vol. 30. No. 6.

Van Fossen, G.J., Simoneau, R. J., Olsen, W.A., and Shaw, R. J.(1984), "Heat Transfer Distributions Around Nominal Ice Acretion Shapes Formed on a Cylinder in the NASA Lewis Icing Research Tunnel," *AIAA 84-0017.*

Von Karman Institute for Fluid Dynamics (1994), "Measurement Techniques in fluid dynamics - an introduction,".

Wickens, R. H. and Nguyen, V. D.(1991), "Wind Tunnel Investigation of a Wing Propeller Model Performance Degradation Due to Distributed Upper Surface Roughness and Leading Edge Shape Modifications," *AGARD CP-496.*

Yamaguchi, K. and Hansman, R. J., Jr.(1992), "Heat Transfer on Accreting Ice Surfaces," *J.Aircraft*, Vol.29, pp. 108-113.

Yurkanin, D. J. (1993), "Microphysical Models for Simulating Realistic Ice Accretions," *AIAA 93-0025.*

Zamorski, A. D.(1944), "Meteorological Conditions For Ice Formation," *NAVER 50-IR-106* , April 1944.

Zumwalt, G. W., Schrag, R. L., Bernhart, W. D., and Friedberg, R. A.(1985), "Analysis and Tests for Design of Electro-Impulse De-Icings System," - *NASA CR 174919*, May 1985.

5. REVIEW, VALIDATION, AND EXTENSION OF ICE ACCRETION PREDICTION CODES

Icing is a meteorological hazard that may affect aircraft and helicopter operations due to supercooled droplets that impinge on aircraft structures. The impinging water freezes and the resulting ice deposit produces high aerodynamic degradation. Manufacturers have to demonstrate, during the certification process, that their aircraft can fly in icing conditions. This may be achieved by flight tests or modeling. As flight tests are expensive and the icing conditions obtained during the tests are not always as severe as required, computer models are often used to determine the ice shape deposit in failure cases and on the unprotected parts of the aircraft. The computed shapes are then reproduced and applied to a real aircraft in order to justify the absence of protection and/or analyze the aircraft behavior when the existing protection is out of order. Two-dimensional and three-dimensional icing models have been developed at ONERA (France, Guffond et Brunet, 1985), DRA (UK, Gent, 1990), NASA (USA, Wright, 1995), Boeing (USA), École Polytechnique (Canada, Brahimi et al., 1994), CIRA (Italy) and the FFA (Sweden).

Initial efforts at icing simulation took place in the late 1920's and early 30's. World War II precipitated an urgent need for research into icing simulation and ice protection system design. In the United States, this led the National Advisory Committee for Aeronautics, NACA, to build the Icing Research Tunnel (IRT) at the Lewis Research Center in Cleveland, Ohio during the early 1940's. Initial activities in the IRT covered a broad range of icing problems. Many of these included the development of ice formations on aerodynamic surfaces and the evaluation of aerodynamic performance degradation. A complete bibliography of the NACA research activities during this period is available as a NASA TM (ANON. 1981).

Icing simulation activities have increased dramatically during the period from the late 1970's to today. Wind tunnel and flight research has been conducted by many organizations in North America and Europe. In addition, the advent of high speed computer systems has allowed the development of sophisticated computer simulations of ice accretion processes and resulting performance degradation. As a result, a new role has been created for wind tunnel and flight research, that is development of code validation databases.

Despite the long history of icing research, there still remains a significant number of unresolved issues in the process of icing simulation. These issues range from the fundamental physics of the icing process to the mechanisms underlying the ice removal process. The ability of the aerospace community to predict the effects of aircraft icing and the performance of potential ice protection systems will be strengthened by addressing these issues and incorporating an increased understanding of the icing process into simulation efforts.

Two-dimensional icing models have been under development for some time. They have been used to calculate ice growth on airfoil surfaces and to simulate ice protection system performance. More recently, three-dimensional icing models have been developed with the purpose of having a tool for calculating ice accretion shapes on such profiles as finite swept wings, aircraft noses or air intakes for which two-dimensional icing codes are inadequate. This chapter describes current 2D and 3D ice accretion modeling methods and the codes, currently in use, based on those methods.

5.1 OUTLINE OF PREDICTION METHODOLOGY

Analytical icing simulation has been based on a combination of correlations, computer codes, and theoretical models of the icing process and its consequences. This section will discuss some of the current methods used for modeling the ice accretion process.

5.1.1 Aerodynamic Flow

In both 2D and 3D cases, the first step in icing simulation is to compute the flow field around the body. Currently, there are two different ways that are in common practice to obtain the flow field around a body. These are panel methods or methods using a spatial grid around the body (i.e. Euler/Navier-Stokes methods).

For 2D ice accretion calculations, the panel method approach to flow field calculation has several advantages. Panel methods are quite fast and codes based on this approach can be easily run on personal computers. Additionally, since panel methods do not use grids to determine off-body velocities, such codes can easily adapt to the changing geometry of the ice accretion. As such, for 2D ice accretion calculations, panel methods form the basis of most ice accretion codes. There is some concern over the use of panel methods for evaluating the flow field associated with complex multi-element airfoils. Research is currently underway, focussed on the need for alternate flow codes in ice accretion prediction on multi-element high-lift airfoils.

The panel method also saves computer time for 3D flow field calculations, but can be time-consuming for calculating droplet trajectories. This is because the velocity at any point in the flow, needed for the droplet trajectory calculation, requires the evaluation of the contribution of each panel to the velocity value at that point. In large 3D models, containing many thousands of panels, this can require a great deal of computer time. As such, several alternatives have been used to evaluate 3D flow fields in ice accretion simulation codes.

One approach is to use the panel method for computing the flowfield and then calculate the local aerodynamic values on a spatial grid. In that case, the grid need not cover the space all around the body, but only the regions where the impacting droplet trajectories could be located. Moreover, grid generation can be achieved so as to avoid the position where the flow field is not accurately calculated (i.e. close to the body). The droplet trajectory code then determines the value of the velocity at any arbitrary point in the flow through an interpolation process. This takes considerably less time than the direct calculation of the velocity from the panel code.

The other approach is to use a grid based flow code directly. The trajectory code still must employ an interpolation scheme as in the above approach. The trade-off is that the grid based code should provide more accurate velocity values as input to the interpolation process.

5.1.2 Trajectories And Collection Efficiency

The flow field velocities around the body are used to integrate the trajectories of supercooled water droplets, and subsequently to calculate the collection efficiency on the body. In order to compute the trajectories, the local flow field velocity in a region around the body is used as input to an evaluation of the equations of motion governing droplets subjected to the forces of drag and gravity.

5.1.2.1 Two-dimensional Calculation Methods

The following assumptions are generally made when formulating the equations of motion for super-cooled water droplets:

- droplet size is so small that droplets remain spherical;
- the flow field is not affected by the droplets;
- gravity and aerodynamic drag are the only forces affecting droplet motion.

These assumptions were verified in 2D cases, either by sensitivity tests or by comparison with experimental data. As there is no reason to think otherwise, they are generally considered to be true in the 3D cases as well.

The above assumptions are considered valid for droplet radii of less than 500 μm. The governing equations are thus,

$$m\ddot{x} = -\vec{D}\cos\gamma + mg\sin\alpha$$

$$m\ddot{y} = -\vec{D}\sin\gamma - mg\cos\alpha$$

where

$$\gamma = \tan^{-1}\frac{\dot{y}_p - V_y}{\dot{x}_p - V_x}$$

$$\vec{D} = C_d\frac{\rho_a V^2}{2}A_p$$

$$V = \sqrt{(\dot{x}_p - V_x)^2 + (\dot{y}_p - V_y)^2}$$

and where C_d is the drag coefficient, α is the angle of attack, Vx and Vy are the components of the flow field velocity at the droplet location and $\dot{x}_p$, $\dot{y}_p$, $\ddot{x}_p$ and $\ddot{y}_p$ are the components of the droplet velocity and acceleration, respectively.

Some formulations consider the gravity term to be negligible and hence the governing equations are reduced to,

$$m\ddot{x} = -\vec{D}\cos\gamma$$

$$m\ddot{y} = -\vec{D}\sin\gamma$$

The pattern of droplet impingement on the body surface determines the amount of water that hits the surface and becomes part of the ice growth process. The ratio of the actual mass that impinges on the surface to the maximum value that would occur if the droplets followed straight-line trajectories, is called the total collection efficiency, E_m. The total collection efficiency for the body is found by integrating the local collection efficiency, β, between the upper and lower limits of droplet impingement. The local collection efficiency is defined as the ratio, for a given mass of water, of the area of impingement to the area through which the water passes at some distance upstream of the airfoil. Taking a unit width as one dimension of both area terms, the 2D local collection efficiency can then be defined as,

$$\beta = \frac{dy_o}{ds} = \frac{\Delta y_o}{\Delta s}$$

where dy_o is the spacing between water droplets at the release plane and ds is the distance along the body surface between the impact locations of the same two drop-

lets. The local collection efficiency is illustrated in Figure 5-1.

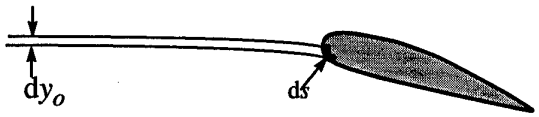

$$\beta = \frac{dy_o}{ds}$$

Figure 5-1. Local Collection Efficiency for a 2D Airfoil.

Considering that the water flux remains constant within a tube defined by two (or four trajectories in 3D) we have:

$$LWC_o \cdot V_o \cdot \Delta y_o = LWC_i \cdot U_i \cdot \Delta s$$

So the impinging water $LWC_i \cdot U_i$ can be calculated using the formula:

$$LWC_i \cdot U_i = \beta \cdot LWC_o \cdot Y_o$$

In the 2D code, we assume that the trajectories can be very close to each other and then $\beta = dy_0 / ds$. Thus, the local collection efficiency is equal to the slope of the curve that fits the initial position of the droplets to their impact positions. The local collection efficiency calcula-

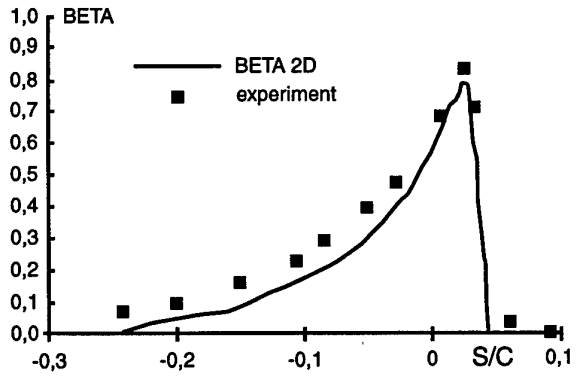

Figure 5-2. Collection Efficiency for a NACA 65018 Airfoil, chord=0.33m, d=20μm, a=8°, T=94.5kPa, M=0.24

tions can be checked by comparison to experimental curves, as was done by Guffond and Hedde (1994) on a NACA 65018 airfoil with an angle of attack of eight degrees. The result of the 2D calculation is quite good

The small differences found in this plot are due to the use of the droplet median volumetric diameter in the computation.

5.1.2.2 Three-dimensional Calculation Methods

In 3D codes, such simplification is not always possible, and the collection efficiency value is obtained directly by calculating the ratio of the area delimited by four trajectories away from the body (in the free stream) to the corresponding impact area. There are two possibilities for this calculation:

- trajectories are computed until four of them impinge on the four corners of a panel: the impinging area is immediately calculated, but the number of calculated trajectories is quite high. Moreover if the limits of impingement are inside a panel, it is impossible to impinge on the four corners and these limits are less precisely determined.
- the coefficient is given directly by the ratio of the area delimited by four trajectories away from the wing over the corresponding impact area. Only four trajectories are required to obtain one value of the collection efficiency, but the impact area is not easily calculated. This second method is used by DRA, NASA, and ONERA.

Figure 5-3 illustrates the collection efficiency calculation for a 3D geometry.

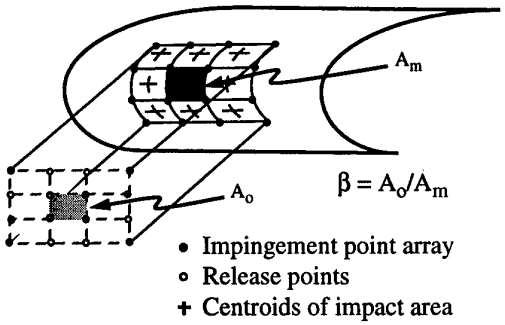

Fig. 5-3. Illustration of starting point and impaction point arrays.

Regardless of which of the above procedures is used, the collection efficiency calculation is essentially the same once the impacting trajectories are determined. If the release area delimited by four adjacent trajectories is given by A_o and the areas on the body surface defined by those same trajectories is given by A_m, then the collection efficiency for that surface is given by the relationship,

$$\beta(s) = A_o / A_m$$

Once these values are determined for the area of interest on a body, the collection efficiency values must be manipulated in order to provide the information needed for the ice accretion calculation. Normally, this means

that the collection efficiency values obtained for the surface areas delimited by the trajectories are interpolated onto the panels or surface grid faces used in the control volume based ice accretion calculation. The interpolation procedures employed in this process are not standardized nor have they been validated. There is some need for validation efforts in 3D droplet trajectory calculations, especially for complex geometries.

There are some corrections required in 3D droplet trajectory calculations to account for pitch, sideslip, and rotation. If the flux tube is defined by four adjacent trajectories in the release matrix (Fig. 5-3), then the collection efficiency at the surface can be written as shown in the following relationship, where corrections for angle-of-attack and yaw have been made.

$$\beta(i,j) = \frac{\cos\Psi \cdot \cos\alpha \cdot \bar{A}_o(i,j)}{A_m(i,j)}$$

In this expression, the collection efficiency, $\beta(i,j)$, is said to be located at the center of the impact region mapped out by the four impacting particles. The angles Ψ and α refer to the sideslip and pitch angle of the geometry relative to the free stream flow vector (Fig. 5-4).

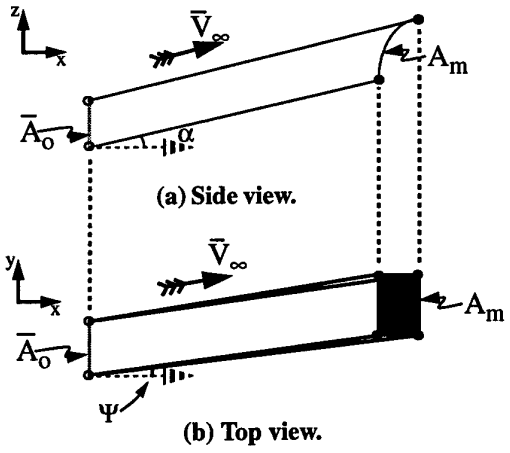

Figure 5-4. Pitch and sideslip corrections for 3D collection efficiency calculation.

5.1.2.3 Approximate Methods

In swept wing calculations, a 2D collection efficiency calculation can approximate a 3D value with corrections made to account for sweep angle. Calculation of collection efficiency using these "pseudo 3D" methods is based on the standard 2D methods with corrections for angle-of-attack, yaw angle, sweep angle of the surface and deformation of the flux tube (Fig. 5-5). The resulting collection efficiency equation is then

$$\beta(i) = \frac{\cos\psi \cdot \cos\alpha \cdot \cos\nu \cdot DS_o(i)}{DS_m(i)}$$

where the collection efficiency is said to occur at the center of the impacting points of the two trajectories. The distances $DS_o(i)$ and $DS_m(i)$ represent the distance between the upstream release point and the impact points respectively for two adjacent trajectories (Fig. 5-5). As for the 3D case, the angles α and Ψ represent the pitch and sideslip angles, respectively. Angle ν represents the rotation angle of the droplet trajectory pair relative to the sweep of the leading edge of the airfoil.

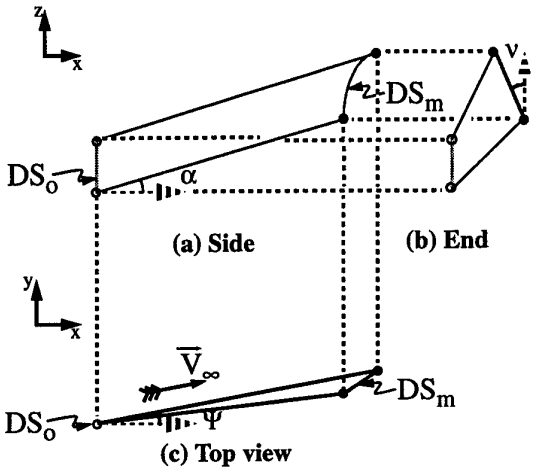

Figure 5-5. Corrections for pitch, sideslip, and rotation for "pseudo 3D" collection efficiency calculation.

5.1.3 Thermodynamic Balance & Accretion Rate

The goal of these models is to determine the ice growth rate at every location of a body, as governed by the heat and mass balance analyzed by Messinger (1953). The codes use a control volume approach to study the heat and mass balance: the bodies are discretised into a number of small surfaces over which the control volume will be defined. In this volume, temperature and the other physical variables are assumed to be constant so that the heat transfer balance can be studied. Figures 5-6 and 5-7 depict mass and energy control volumes, respectively.

The following assumptions are generally made about the heat transfer balance:

- the physical transformations are instantaneous,

- the radiative heat flux is negligible, and heat transfer by conduction within the ice is negligible. (This assumption is generally acceptable during ice growth, ice conductivity being relatively low).

The heat balance is obtained when the equality between sink and source quantities is achieved. The main heat fluxes are:

- convective heat transfer;
- evaporation/sublimation;
- heating of the impacting water
- cooling or heating of the running water from a neighboring surface
- cooling of ice
- latent heat obtained during the freezing of the water;
- and droplet kinetic energy.

Positive terms are considered to be "sources", and negative ones "sinks".

The following discussion outlines the Messinger approach to the energy balance for the ice accretion process.

The equations governing the mass balance are,

$$\dot{m}_c + \dot{m}_{r_{in}} - \dot{m}_e - \dot{m}_{r_{out}} = \dot{m}_i$$

where $\dot{m}_c$ is mass flow rate of incoming water, $\dot{m}_{r_{in}}$ is the mass flow rate of runback water from the previous control volume, $\dot{m}_e$ is the mass flow rate of evaporated water, $\dot{m}_{r_{out}}$ is the mass flow rate of water running back to the next control volume, and $\dot{m}_i$ is the mass flow rate of water leaving the control volume due to freeze-out.

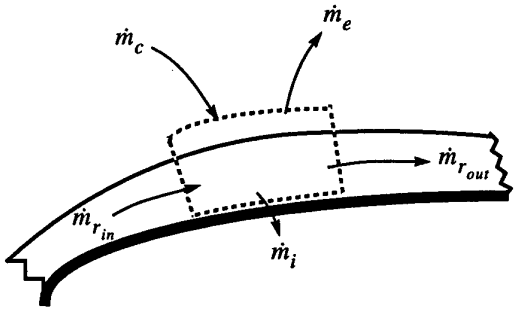

Figure 5-6. Mass Balance Control Volume.

The equations governing the energy balance are,

$$\dot{m}_c i_{w,T} + \dot{m}_{r_{in}} i_{w,sur(i-1)}$$
$$= (\dot{m}_e i_{v,sur} + \dot{m}_{r_{out}} i_{w,sur} + \dot{m}_i i_{i,sur} + q_c \Delta s + q_k \Delta s)$$

where $i_{w,T}$ is the stagnation enthalpy of the incoming water droplets, $i_{w,sur(i-1)}$ is the enthalpy of the water flowing into the control volume from upstream, $i_{v,sur}$ is the enthalpy of the vapor leaving the control volume due to evaporation, $i_{w,sur}$ is the enthalpy of the water running back to the next control volume, $i_{i,sur}$ is the enthalpy of the ice leaving the control volume, q_c is the heat transfer due to convection, q_k is the heat transfer due to conduction at the bottom of the control volume, and Δs is the length of the surface covered by the control volume.

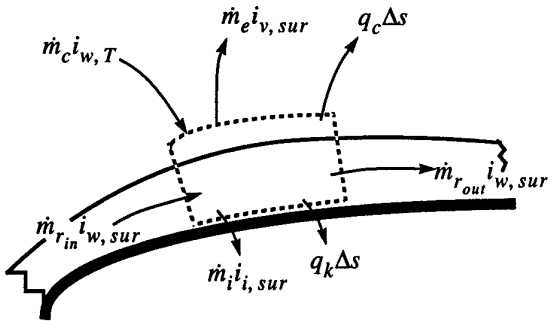

Figure 5-7. Energy Balance Control Volume.

The convective heat transfer coefficient, q_c, can be obtained through several different methods. Correlation equations, boundary layer calculations, and Navier-Stokes calculations have all been used to determine this parameter. Currently, the determination of convective heat transfer values for most ice accretion codes is based, in some form, on correlations of heat transfer for rough surfaces. However, these correlations are usually for 'sand-grain' roughness which does not capture the true nature of ice shape roughness. Thus, an area of current research is in the determination of how ice accretion roughness affects the convective heat transfer process.

The relative magnitudes of the various heat transfer values in the ice accretion energy balance are shown in Figure 5-8, taken from Guffond and Hedde (1994), for typical flight conditions.

In this example, the major source is the latent heat flux and there are three sinks of equal level to counterbalance it; the convective heat flux, the evaporation or sublimation latent heat flux, and the sensible heat flux between the impinging water and the underlying surface. It should be noted that the parameter *s/c* is measured from the stagnation point and not from the leading edge. This sensible heat flux is important in the situation where the outside air temperature (i.e. the droplet temperature) is low (-30°C). We can see that the heat transfer coefficient has a major importance in the balance as the convective heat flux and the evaporation/sublimation flux

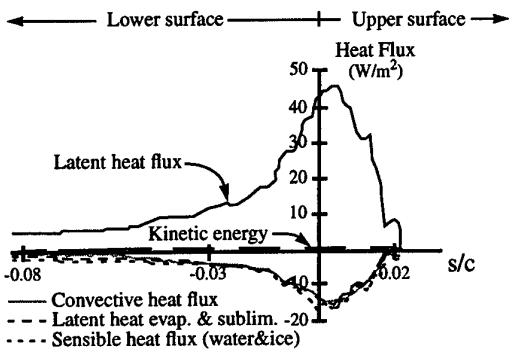

Figure 5-8. Relative Heat Transfer Levels for Typical Flight Conditions.

depend on it (60% of the sinks are affected by this coefficient).

In the process of performing the mass and energy balance for the ice accretion calculation, the concept of freezing fraction is developed to provide an additional relationship among several of the independent variables. The "freezing fraction" is defined as the fraction of liquid water that freezes in a given control volume. The following expression describes the freezing fraction,

$$f = \frac{\dot{m}_i}{\dot{m}_{r_{in}} + \dot{m}_c}$$

The heat balance is achieved by varying the freezing fraction and the equilibrium temperature. When the freezing fraction has a value between 0 and 1, that is when all the water does not freeze in the given control volume (glaze ice), the remaining water runs back into the following control volume, where a new heat and mass balance is solved. When the freezing fraction is equal to 1, there is no runback (rime ice).

This mass and energy balance procedure is performed in each control volume on the surface, starting at the stagnation point and marching downstream along the upper and lower surfaces. In the LEWICE3D code, the mass and energy balance is performed along 2D cuts or following surface streamlines. In the ONERA3D code the procedure is similar except it is performed between two adjacent streamlines. The latter approach thus seems to account for streamline convergence or divergence on complex geometries.

Currently, there are no 3D ice accretion codes which perform a complete 3D mass and energy balance over an entire surface. This complexity may not be required in simple 3D geometries such as wing surfaces. However, as more complex 3D bodies are examined, the need for a complete 3D solution may become necessary.

5.1.4 Ice Shape Calculation and Geometry Modification

In the 2D case, the ice shape is simulated by adding an ice thickness to each control volume, based on the mass of ice frozen during the time period of consideration. Using $\dot{m}_i$ and the density of ice to determine the ice volume, the following equation for the height of ice deposited within a control volume can be formulated.

$$d_{ice} = \frac{\dot{m}_i \Delta t}{\rho_i A_{sur}}$$

The thickness is then considered to be uniform over the entire panel for determination of the new geometry. The new coordinates for the panel are obtained from the relation,

$$x_i = x_i + d_{ice}\hat{x}_i$$

where x_i is the coordinate of the center of the panel in the i-direction and $\hat{x}_i$ is the i-component of the unit normal vector for the panel.

Wright and Bidwell (1995) have investigated the ice growth or geometry modification process and have devised a robust scheme for ice growth calculations. Their scheme is conservative, fast, and independent of time step or grid size selected by the user. The formulation of the geometry modification procedure for ice growth simulation is critical to the accuracy of any ice accretion code. Small variations in geometry modification procedures can eventually lead to large inaccuracies in ice shapes regardless of the validity of the underlying trajectory and energy balance calculations.

Additionally, Wright and Bidwell (1995) have developed a geometry modification procedure which allows specification of arbitrary ice growth direction. Thus ice growth can occur along the surface normal direction or along a tangent to the droplet trajectory at the surface. This allows more realistic simulation of glaze and rime growth patterns.

In the 3D case, the ice shape calculation is achieved by deforming the surface grid (Fig. 5-9), either by making the new grid run along the runback direction or, by interpolating the icing rate, using the original geometric grid. Deforming the original grid enables re-use of the grid in the icing code thus allowing a simple multi-stepping ice growth procedure.

The grid is deformed by moving each node along the normal vector **n** on the profile surface.

$$\mathbf{n} = (OO_1 - OO_3) \times (OO_2 - OO_4)$$

where OO_1, OO_2, OO_3, and OO_4 are the sides of the cells containing the node.

The displacement length is the average ice height in the cells sharing the node:

$$\mathbf{ht} = (ht1 + ht2 + ht3 + ht4)/4 \cdot \mathbf{n}/|\mathbf{n}|$$

where $ht1$, $ht2$, $ht3$, and $ht4$ are the ice growth heights in the cells surrounding the node.

This process is repeated for all of the nodes connected to cells which have some ice accumulation. The new iced surface is then created by connecting the iced grid cell surfaces, such as the one shown in Figure 5-9.

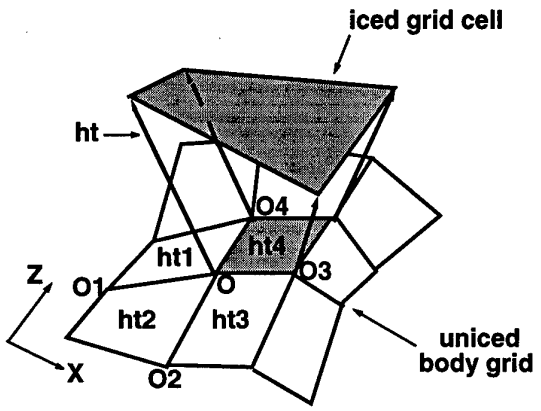

Figure 5-9 Ice Growth on a 3D Grid Cell.

5.2 ICE PROTECTION SYSTEM SIMULATION

Simulation of ice protection systems can be an important design tool for airframe manufacturers and ice protection system manufacturers as well. As such, ice protection systems have also been modeled computationally. Analysis methods for thermal systems are the most advanced. Both hot air systems and electrothermal systems have been modeled successfully. There have been fewer reported results from analysis efforts for mechanical systems. However, some recent activity in this area suggests that these systems will also be modeled computationally in the future.

Al-Khalil, et al. (1989) used a 3D potential flow code, a 3D particle trajectory code, and a control volume energy analysis to evaluate a hot air anti-icing system for an engine inlet. ONERA also has a code, called MAPAC, for evaluation of hot air ice protection systems. These methods hold the potential for optimization of hot air ice protection systems.

Electrothermal systems have been modeled using finite-difference methods by Keith, et al. (1988). An electrothermal system consists of an array of electric heater elements embedded under the outer skin of the wing surface. The heater elements are activated during an icing encounter with enough current to melt the ice that may form on a wing surface. A typical 2D model of an electrothermal heater element is shown in Figure 5-10. The model simulates the thermal behavior of the composite structure and ice layer. Results indicate that temperature traces at the ice-skin interface, heater base, and substrate base agree well with measured values. Current work by Wright, et al. (1991) in this area is centered on combining this analysis with ice accretion predictions in order to provide a tool for the evaluation of electrothermal anti-/de-icing system performance. Similar codes have been developed by DRA (HRB2D) and ONERA (MAD).

Development of methods for evaluation of mechanical ice protection systems is just beginning with some initial work on ice structural properties as described by Scavuzzo, et al. (1987). Computational methods to predict FOD (*i.e.* shed ice) damage to engine blades are also under development. The ability to determine the damage resulting from various sizes and shapes of shed ice will greatly enhance de-icing system design.

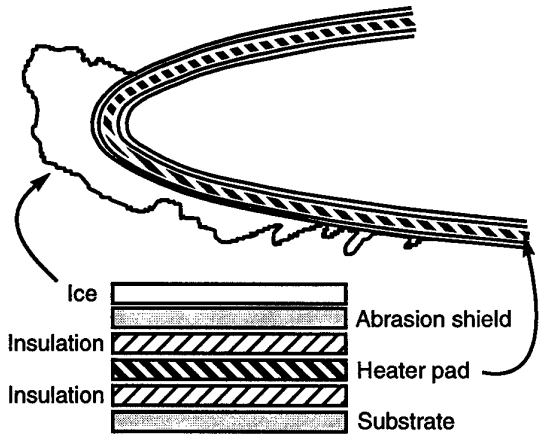

Figure 5-10 Two-dimensional finite-difference model of an electrothermal heater.

Ramamurthy, et al. (1991) have evaluated computationally the Pneumatic Impulse Ice Protection (PIIP) system. The PIIP system relies on rapid inflation of pneumatic tubes embedded in the wing surface. The pneumatic impulse causes a displacement of the surface which combined with the surface acceleration, cracks, debonds, and expels the ice. The PIIP system is described more fully by Martin and Putt (1990). Ramamurthy, et al. (1991) used a time dependent, compressible flow model for

internal duct flow to model this ice protection system. Results to date have been encouraging however further work is required.

In general, the development of ice protection system analytical tools is not as advanced as icing simulation codes. The use of computational methods for ice protection simulation in the design and certification process could greatly benefit manufacturers and the development of such tools deserves increased attention.

5.3 DEFINITION OF TEST CASES AND VALIDATION OF COMPUTER CODES

Typically, the 2D ice accretion code results are compared to experimental ice shape tracings, in order to determine the accuracy of the code. Additionally, individual subsystems of the code can be compared to measured values of pressure distribution, collection efficiency, and heat transfer coefficient. Ice shape comparisons can be difficult to interpret, as there is always the question of repeatability and quantification of the differences in geometry.

In the following comparison, the ONERA 2D accretion code was used to predict the ice shape for various experimental configurations. The prediction agrees quite well with the experimental data (Fig. 5-11).

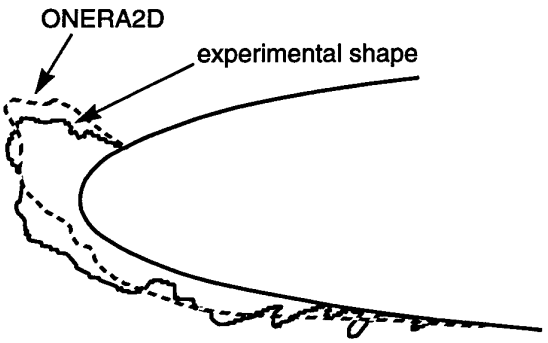

Figure 5-11. Comparison between ONERA 2D code and experimental shape.

The conditions used for the 2D calculation were the following:

airfoil = NACA 0012

chord = 0.53m

α = 4 degrees

T_∞ = 266.45 K

P_∞ = 95.61 kPa

Mach = 0.177

LWC = 1.3 g/m^3

icing time = 480 s

droplet diameter = 20 μm

Some comparisons were then performed on the same experimental shape with the 3D code, to check whether the results were at least as good as those yielded by the 2D icing code.

The 3D icing code was applied to an unswept wing of one meter span with a NACA 0012 profile. The results are given at mid-span. The local catch efficiency is calculated using the 2D code because the leading edge is perpendicular to the flow.

One can see in Figure 5-12, that the 2D and 3D icing codes give essentially the same shape using a single time step calculation (i.e. a calculation based on the clean airfoil, without allowance for the effect of the ice on the airflow or the ice accretion process). Compared with the experimental shape the results are good. Thus, in some cases, a 2D calculation can be used to approximate the results of a 3D problem.

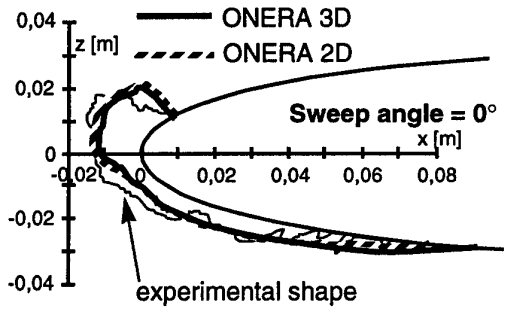

Figure 5-12. Comparison of ONERA 2D code, ONERA 3D code, and experimental shape.

Several ice shape comparison studies such as these have been performed by researchers at Dornier, DRA, NASA, and ONERA. Most recently, a joint study by DRA, NASA, and ONERA investigated the comparison of each organizations code results to the same set of experimental data. That study, reported by Wright, et al. (1997), suggests that each code has about the same degree of agreement with the measured results.

Most evaluations of the level of agreement that code simulations exhibit with respect to measured ice shapes are qualitative. There is a need for some sort of quantitative measure of this quantity. Perhaps, the cross-sectional area of an ice shape, the perimeter length, the orientation of major horn growths, and the upper and lower icing limits could figure into a quantitative value.

5.4 EVALUATION OF PREDICTION CODE CAPABILITIES

The discussion in the previous section suggested that current capabilities are quite good especially for simple, single element geometries and cold temperature, low LWC conditions. In general, the ice accretion codes have more difficulty in accurately reproducing warm temperature, high LWC conditions. This is due to inadequate modeling of several processes important to ice shape development under those conditions. The processes have been identified as the following:

- the surface physics associated with ice-water-substrate interaction
- ice growth on swept wing surfaces
- ice roughness development
- boundary layer behavior over surfaces with roughness on the order of the boundary layer height
- convective heat transfer rates and evaporative cooling rates over such rough surfaces

5.4.1 Surface physics

Investigators are examining the physics of ice growth with an eye to improve on the Messinger model and thus produce more reliable ice shape predictions under a wide range of icing conditions.

Olsen and Walker (1986) observed the icing process in the NASA IRT with close-up movies. These movies revealed accretion phenomena for glaze ice quite different from that contained in the currently used analytical model for ice accretion. Some of the differences noted were the possibility of splashing and the absence of runback under typical glaze ice conditions. Their work led to a number of investigations regarding the micro-physical aspects of ice accretion.

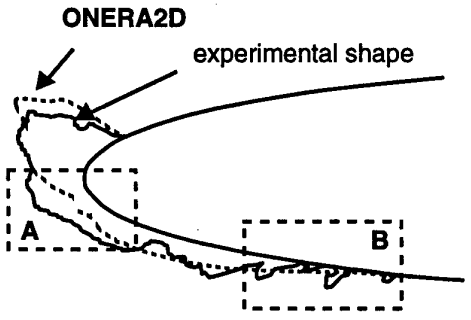

Figure 5-13. Limits of the Messinger model in a 2D simulation.

Guffond and Hedde (1994) have suggested that the latter observation may explain why computational results many times predict less ice near the stagnation point than is found in actual measured ice shapes (see Figure 5-13, part A).

Recent close-up analysis of aircraft ice accretion by Hansman et al. (1993) points out that ice growth can start from discrete initial growth sites giving feathers along the flow direction. These feathers correspond to square B in Figure 5-13, and a continuum approach does not allow modeling this kind of ice growth. Velazquez et al. (1995) have attempted to model feather growth behavior by using a two zone approach for ice growth. One zone models the ice feathers while the other zone models the underlying ice growth. In 2D cases however, when the LWC is large, the ice shapes have generally a continuous macroscopic aspect and the Messinger approach yields acceptable results in first approximation.

5.4.2 Ice growth on swept wing surfaces

In 3D cases, this feather growth can produce a shadow effect and the final ice deposit is not uniform at all, giving rise to shapes known as "lobster tails". In that case, the simulated shapes are underestimated (Figure 5-14). The experimental shape shown here was taken from flight test information obtained by Reehorst (1992).

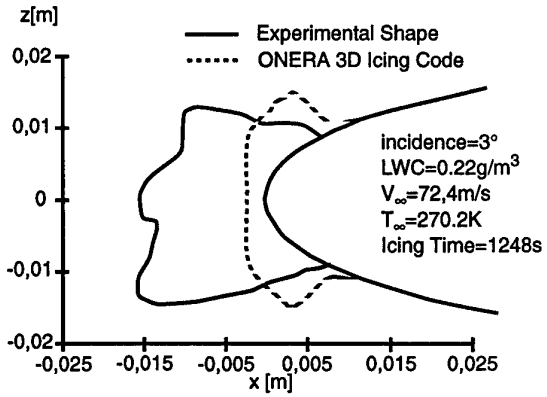

Figure 5-14. Lobster tail effect on an actual ice shape.

The effect of a "lobster tail growth" is to increase the volume of the deposited ice, since the filling ratio is not equal to 1. In the certification requirements, the maximum ice quantity is not determined by icing time, but by a maximum height of ice (3 inches). Assuming that the filling ratio is equal to 1 makes the simulation difficult because the ice time becomes longer.

The development of lobster tail ice growth is currently being investigated by several groups. According to Personne (1988), when droplets freeze before another drop-

let impinges at the same place, the freezing process needs to be considered individually for each droplet. On the other hand, when the time between two impacts at the same place is shorter than the droplet freezing time, this forms of a water film; thus the droplets loose their individuality.

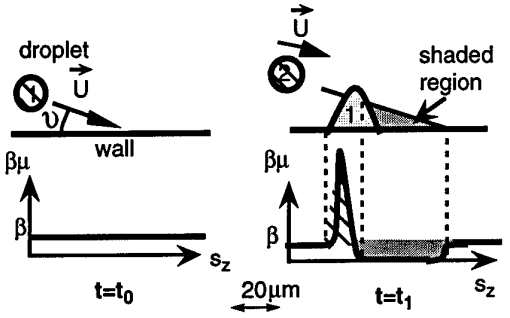

Figure 5-15. The 1st frozen droplet modifies the impingement probability (βμ) of a 2nd droplet. This explains how a non uniform ice deposit starts growing.

When a droplet freezes before another one impinges at the same place, the frozen droplet forms a small hummock of ice on the wall. Due to the shadowing of the hummock, the impingement probability of a 2nd droplet is then modified. Thus, the microscopic scale catch efficiency increases on the front side of the hummock while it decreases on the rear side and even downstream (Fig. 5-15). With the impingement of more droplets, either the hummock grows faster than its downstream region or the downstream region is filled up, depending on the size of the shadow.

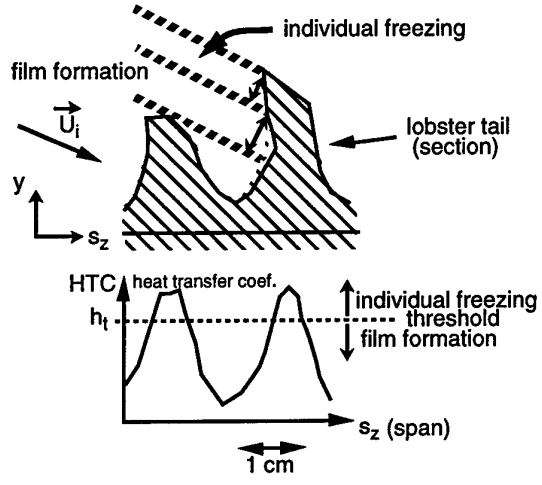

Figure 5-16. Macroscopic growth of the lobster tails is explained by film formation in the regions where heat transfer is lower.

Although the conditions described above are necessary for lobster tail growth, they are not sufficient to induce macroscopic lobster tail growth. As a matter of fact, such a totally individual growth would give rise to quite a uniform, low-density ice shape (i.e. $\rho << 917$ kg/m^3).

But, the lobster tail ice seems to have a high density close to that of glaze ice (i.e. $\rho \cong 917$ kg/m^3). Obviously, heat transfer is modified by hummock growth: it increases on top and decreases at the bottom (Fig. 5-16). Now, freezing time increases as heat transfer decreases; therefore, one can observe individual freezing at the top while there is film freezing at the bottom (Fig. 5-16). It is in this way that the lobster tail can grow macroscopically.

One measure of the severity of a lobster tail growth is the filling ratio, Ξ. The filling ratio is the area occupied by ice at a given height divided by the total area at that same location. Figure 5-17 shows the values of the filling ratio versus the contact angle and the impingement angle.

The impingement angle is the angle between the incoming droplet trajectory path and the surface of the body. The contact angle is the angle between the water droplet on the surface and the surface itself. When there are no lobster tails Ξ is close to 1 (the value does not reach 1 because of the ice roughness). As Ξ decreases, the lobster tails become larger.

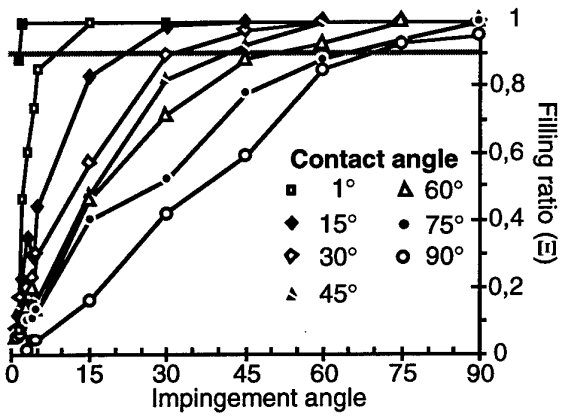

Figure 5-17. Filing ratio Ξ as a function of impingement angle and contact angle.

5.4.3 Roughness

Personne (1988) examined the effects of roughness on the type of ice developed on cylinders. He found that for low airspeeds (less than 20 m/s) surface roughness increases the droplet collection efficiency. He also suggests that rime ice roughness levels are due to the random nature of droplet trajectories caused by increased airstream turbulence near the surface.

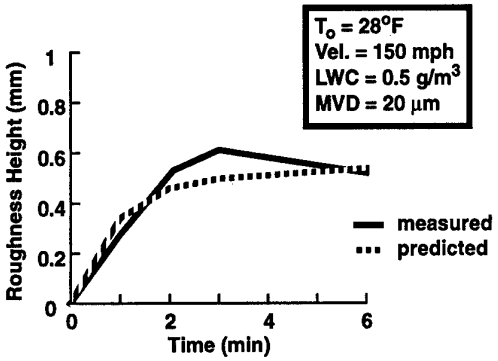

Figure 5-18. Variation of Roughness with Time in LEWICE Code.

Wright and Bidwell (1995) have incorporated a roughness prediction model into the LEWICE code, based on evaluation of the aerodynamic and surface tension forces working on the liquid water film on a glaze ice surface. Their model, based on the work of Al-Khalil (1991), predicts the average roughness height to be used in the LEWICE code. This eliminates the need for input of the roughness height into the code. The variation of roughness with time using this model is shown, in Figure 5-18, compared to the measured values of Shin (1994) for a NACA 0012 airfoil model test in the NASA Icing Research Tunnel.

As a result of the observations of Olsen and Walker (1986), Personne (1988), Hansman et al. (1993), and Shin (1994), current thinking on ice roughness development suggests that the roughness becomes larger than the boundary layer height. Since most roughness models used in heat transfer calculations are based on much smaller roughness levels, further study of heat transfer augmentation due to roughness is required.

5.4.4 Boundary layer behavior

Bragg et al. (1995) has evaluated the boundary layer development over artificial roughness elements of the size observed in the close-up photographic studies described previously. Their results suggest that these large roughness elements cause the boundary layer transition process to start further upstream on the airfoil and to persist for a longer distance along the airfoil than occurs for either a clean airfoil or for an airfoil with small roughness levels.

5.4.5 Convective heat transfer

In a related study, Dukhan et al. (1995) measured the convective heat transfer rate for an aluminum plate cast from an actual ice shape. In that experiment the plate was cut into several sections in order to measure the variation in heat transfer as a function of position along the plate. Although the measurements are an average heat transfer rate for the small section, they do indicate how the convective heat transfer varies with respect to the development of the boundary layer.

5.4.6 Additional areas of potential research

An area related to the ice growth process itself that has become of greater concern recently is the simulation of ice accretion during freezing rain or drizzle. These processes are similar to the standard ice accretion scenario except they are complicated by the physics associated with large droplet (i.e. droplet clouds with MVDs greater than 50 μm) impact, thermodynamics, and surface physics. Recent studies by Ashenden (1995), Addy et al. (1996), and others suggest that there is a greater potential for splashing, the possibility of droplet break-up, enhanced impact on surface boundary layer development, and the potential for movement of the accreted ice along the surface of the aircraft.

Since the accretion physics associated with these conditions are even less understood than for ice formations associated with the standard icing envelope and they have been identified to have a catastrophic effect on aircraft performance, it is necessary for additional research to be performed on the resulting ice growth process to augment the current research in the identification of meteorological conditions leading to their formation.

Another aspect of ice accretion prediction requiring further attention is the application of ice accretion prediction methods to more complex aircraft geometries than have been studied to date. There is a need to develop ice accretion prediction methods or to validate current methods for geometries such as:

- multi-element, high-lift airfoils, wings and control surfaces
- highly swept delta-wings with vortical flow structures on the upper surface
- engine inlets and ducts
- rotating systems

Wright and Bidwell (1995) have adapted LEWICE to calculate ice accretions on a multi-element body. The use of the current potential flow code in LEWICE for such cases requires further investigation. Likewise, Brahimi et al (1995) have adapted an ice accretion code for use with supercritical and multi-element airfoils. Although these efforts are promising further work is certainly required for validation as many issues relating to such flow cases are not well understood currently.

Additionally, the present standard of codes do not appear to predict accurate ice shapes for accretions formed under conditions of medium to high values of incidence. It is believed that the present codes are unable to account for the aerodynamic stall due to the ice accretion. This limitation is believed to manifest itself in a predicted accretion which is centered too far aft on the lower surface. Potapczuk, et al. (1993) combined a Navier-Stokes code in with LEWICE, which has the potential for use in such conditions.

The development of successors to the Concorde and the TU-144 are currently under development in Europe and the US. Certification of any such vehicle will require the use of ice accretion simulation codes. The vortical flow structures that can develop over such vehicles have the potential to deposit super-cooled water droplets on surfaces well behind the leading edge. Thus, icing simulation tools must be developed which can deal with such flow structures. Additionally, ice accretion tests must be performed to provide validation information for such codes.

The use of ice accretion codes for analysis of engine inlets and ducts is another area requiring attention. Bidwell and Mohler (1995) have completed some calculations for a few representative geometries. They used the grid based version of the LEWICE3D code along with flow field calculations from the NPARC Navier-Stokes code to evaluate an axisymmetric inlet and a Boeing 737-300 inlet. Their results are encouraging.

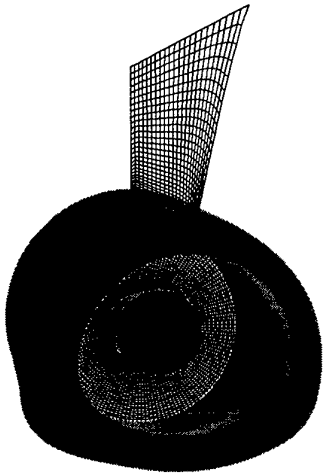

Figure 5-19. Grid model for a Boeing 737-300 engine inlet.

Figure 5-18 shows the grid used for the Boeing inlet geometry. The grid used for this calculation consisted of two blocks with an x-z plane of symmetry. One of the two blocks was an O-H grid with 42x42x25 grid points and extended from the rear of the inlet to the free stream. The second block was a C-O grid which modeled the inlet geometry and consisted of 80x30x73 grid points. Their results indicated ice shapes developing along the inside or outside surfaces of the inlet depending on the angle of attack and the mass flow rate condition.

Ice accretion on rotating systems has been modeled by Britton, as described in the paper by Flemming, et al. (1994) as well as by Gent (1991), and Gent, et al (1987). Britton and Gent employ a similar approach which is focussed on the creation of a method of modeling rotor performance degradation via use of rotor performance codes. In both methods, an evaluation of the ice shape present on the rotor is calculated based on the cloud and flight conditions and this ice shape data is used with a correlation for changes in lift and drag for the rotor. A standard rotor performance code is then used to estimate the likely torque rise that would be experienced by the rotor.

The approach used by Gent, et al (1987) is to modify a basic steady state 2D ice accretion code to run in a pseudo-unsteady mode, by allowing for cyclic varying pitch and speed appropriate to a helicopter in forward flight. The aim of the code is to find the equilibrium conditions for the azimuthal variation of temperature and surface growth rate. The ice growth rates are then averaged over a complete revolution which allows an ice shape prediction to be made, as in the steady 2D icing models.

Results from these methods have been promising, as indicated in the referenced articles. However, there is certainly need for continued research in these areas.

5.5 RECOMMENDATIONS

In order of priority, the following improvements to the current standard of ice accretion prediction models is recommended;

- A set of reference ice accretions should be established for the use of agencies seeking to validate their codes. This would provide valuable evidence to show certificating authorities who are increasingly being asked to consider predicted ice shapes in support of an icing clearance.
- The codes being developed for multi-element aerofoils, bodies of revolution, and three-dimensional flow conditions should be further developed and validated.
- More research is required to understand the basic physics of ice accretion and, more specifically, to understand better the development of individual

crystals and the evolution of surface roughness. The aim will be to advance the theory beyond the control volume approach adopted by all of the existing models. This work is believed to be essential for the accurate prediction of rime feather and lobster-tail ice.

- The conditions of freezing rain or freezing drizzle should be examined in order to understand the additional physics that must be incorporated into current ice accretion simulation methods.
- More research should be undertaken into the phenomenon of droplet splash and to investigate water shedding under high liquid water concentration conditions.
- More research is required to understand the accretion of ice under conditions of aerodynamic stall which is likely to occur with aerofoils at medium to high values of incidence (e.g. > 6 degrees)
- Further work is required to understand the physics of water runback and of the motion of ice on the surface. These phenomena should be introduced into ice accretion models and validated.

REFERENCES

Addy, H.E., Miller, D.R., and Ide, R.F. (1996), "A Study of Large Droplet Ice Accretion in the NASA Lewis IRT at Near-Freezing Conditions; Part 2," NASA TM 107424

Al-Khalil, K.M., Keith, T.G., DeWitt, K.J., Nathman, J.K., and Dietrich, D.A. (1989), "Thermal Analysis of Engine Inlet Anti-icing Systems," AIAA Paper 88-0759.

Al-Khalil, K., Keith, T., and Dewitt, K. (1991), "Further Development of an Anti-icing Runback Model," AIAA-91-0266.

Anon. (1981), "Selected Bibliography of NACA-NASA Aircraft Icing Publications," NASA TM-81651, NASA Lewis Research Center, Cleveland, OH.

Ashenden, Russell A. (1995), "Conducting Artificial Tailplane Icing Evaluations at the Air Force Flight Test Center," AIAA Paper 95-0450

Bidwell, C.S. and Mohler, S.R. (1995), "Trajectory and Ice Accretion Calculations for a Swept NACA 0012 Wing, a Swept MS-317 Wing, an Axisymmetric Inlet, and a Boeing 737-200 Inlet," AIAA-95-0755

Bragg, M.B., Kerho, M.F., and Cummings, M.J. (1995), "Airfoil Boundary Layer Due to Large Leading-Edge Roughness," AIAA-95-0536.

Brahimi, M.T., Tran, P., and Paraschivoiu, I. (1994), "Numerical Simulation and Thermodynamic Analysis of Ice Accretion on Aircraft Wings," Centre de Développment Technologique de l'École Polytechnique de Montréal, C.D.T. Project C159, Final Report prepared for Canadair.

Brahimi, M.T., Tran, P., Paraschivoiu, I., and Tezok, F. (1995), "Prediction of Ice Accretion on Supercritical and Multi-Element Airfoils," AIAA-95-0754.

Dukhan, N., Masiulaniec, K.C., and DeWitt, K.J. (1995), "Experimental Technique and Assessment for Measuring the Convective Heat Transfer from Natural Ice Accretions," AIAA-95-0537.

Flemming, R.J., Britton. R.K., and Bond, T.H. (1994), "Role of Wind Tunnels and Computer Codes in the Certification and Qualification of Rotorcraft for Flight in Forecast Icing," NASA TM 106747, October 1994 (also Paper Number 53, proceedings of the Twentieth European Rotorcraft Forum, October 4-7, 1994.)

Gent, R.W., Markiewicz, R.H., and Cansdale, J.T. (1987). "Further studies of helicopter rotor Ice Accretion and Protection". *Vertica*, Vol. 11, No. 3, pp. 473-492.

Gent, R.W. (1990), "TRAJICE2 - A combined water droplet and ice accretion prediction code for aerofoils," Royal Aerospace Establishment TR 90054.

Gent, R.W. (1991), "A review of icing research at the Royal Aerospace Establishment", AGARD Conference Proceedings 496.

Guffond, D. et Brunet, L. (1985), "Validation du programme bidimensional de captation", ONERA, RT n° 20/5146 SY.

Guffond, D. and Hedde, T. (1994), "Prediction of Ice Accretion: Comparison Between the 2D and 3D Codes", La Recherche Aérospatiale, No. 2, pp. 103-115.

Hansman, R.J., Breuer, K.S., and Hazan, D. (1993), "Close-up Analysis of Aircraft Ice Accretion," AIAA-93-0029.

Keith, T.G., DeWitt, K.J., Wright, W.B., and Masiulaniec, K.C. (1988), "Overview of Numerical Codes

Developed for Predicting Electrothermal De-Icing of Aircraft Blades," AIAA Paper 88-0288.

Martin, C. and Putt, J. (1990), "An Advanced Pneumatic Impulse Ice Protection System (PIIP) for Aircraft," AIAA-90-0492.

Messinger, B.L. (1953), "Equilibrium Temperature of an Unheated Icing Surface as a Function of Airspeed," Journal of the Aeronautical Sciences, Vol. 20, No. 1, pp. 29-42.

Olsen, W.A. and Walker, E. (1986), "Experimental Evidence for Modifying the Current Physical Model for Ice Accretion on Aircraft Surfaces," NASA TM-87184.

Personne, P. (1988), "Effect de la Rugosite sur la Croissance du Givre a Faible Vitesse: Resultats Experimentaux et Modelisation," D.Sc. Thesis, L'Universite Blaise Pascal (Clermont-Ferrand II).

Potapczuk, M.G., Al-Khalil, K.M., Velazquez, M.T. (1993), "Ice Accretion and Performance Degradation Calculations with LEWICE/NS," NASA TM-105972, AIAA-93-0173.

Ramamurthy, S., Keith, T.G., DeWitt, K.J.Putt, J.C. Martin, C.A., and Leffel, K.L. (1991), "Numerical Modeling of an Advanced Pneumatic Impulse Ice Protection System (PIIP) for Aircraft," AIAA 91-0555.

Reehorst, A.L. (1992), "Prediction of Accretion on a Swept NACA 0012 Airfoil and Comparisons to Flight Test Results," AIAA-93-0004.

Scavuzzo, R.J., Chu, M.L., and Olsen, W.A. (1987), "Structural Properties of Impact Ices Accreted at Aircraft Surfaces," NASA CR-179580.

Shin, J. (1994), "Characteristics of surface Roughness Associated with Leading Edge Ice Accretion," AIAA-94-0799.

Velazquez, M.T. and Hansman, R.J. (1995), "Implementation of Combined Feather and Surface Normal Models in LEWICE/X," AIAA-95-0753.

Wright, W.B., Keith, T.G., and DeWitt K.J. (1991), "Numerical Simulation of Icing, Deicing, and Shedding," AIAA Paper 91-0665.

Wright, W.B. (1995), "Users Manual for the Improved NASA Lewis Ice Accretion Code LEWICE 1.6," NASA CR 198355.

Wright, W.B. and Bidwell, C.S. (1995), "Additional Improvements to the NASA Lewis Ice Accretion Code LEWICE," NASA TM-106849, AIAA-95-0752.

Wright, W.B., Gent, R.W., and Guffond, D. (1997), "DRA/NASA/ONERA Collaboration on Icing Research, Part II - Prediction of Airfoil Ice Accretion," NASA CR-202349.

6. CONCLUSIONS, RECOMMENDATIONS AND OUTLOOK

Ice Accretion Effects on Aircraft. If supercooled water droplets exist in the atmosphere, they can impinge on the airframe surface and they may freeze on it. This process is accreting ice on lifting and control surfaces as well as in engine inlets and on rotors and propellers which often seriously affects performance and handling qualities of aircraft. Ice accretion statistically leads to a considerable number of hazards per year. Depending on the actual meteorological situations, we distinguish for in-flight icing between rime ice conditions, occurring at temperatures well below 0 C in combination with low LWC and causing immediate freeze of all impinging water, and glaze ice conditions present at temperatures close to 0 C or at high LWC and leading to a more complicated freezing process and often to rather dangerous ice shapes with respect to performance, stability and control. Recently, also very adverse weather conditions as freezing drizzle with extremely large droplets were recognised to occur repeatedly causing a more serious danger than previously expected. Therefore, research in aircraft icing remains an important topic in order to improve flight safety and to reduce efforts for certification/qualification of aircraft in icing conditions.

Besides description of the related in-flight icing phenomena and the corresponding degradation effects, the present report aims on warnings for aircraft designers and manufacturers and it provides some design recommendations for improving performance and handling under icing conditions. Continuation of work in the fields of ice protection, ice accretion detection, ice shape influence on aircraft performance and handling, and suitable design improvements is indispensable for improving safety for flights in icing environment, especially under conditions outside the meteorological envelope valid up to now for certification.

Certification/Qualification Regulations. The current regulations FAR/JAR § 25.1419 concerning certification of aircraft for flight into known icing conditions offer clear guidance on the certification of ice protection equipment. However, these regulations appear to be less specific on the flight test procedures for determining the safety against leading edge ice with respect to degradation of performance and even less with respect to degradation of handling qualities. The proposed changes by JAA embodied in the Advisory Material Joint AMJ 25-1419 offer more specific procedures, but these procedures are not yet all accepted by the national certifying authorities. In the military field the situation is quite similar since the military demands usually evolve in parallel to the civil ones at least for military transport. Therefore certification of a new transport aircraft is still an elaborate, expensive and time consuming process for each aircraft manufacturer. The corresponding efforts need to be reduced by use of improved simulation techniques and facilities - experimental ones as well as theoretical ones. For example the worst ice shapes can be predicted by experimental or computational means and can then be applied as artificial ice shapes for most of the in-flight tests during certification.

Meteorological Data on Icing Conditions. Some interesting, new ideas are coming out on better ways to characterise the icing atmosphere, based on graphing LWC averages vs. horizontal extent. This is in answer to longstanding complaints about the limitations of the present LWC vs. dropsize characterisations. The new characterisations are more flexible and permit easier comparisons of measurements, test points, and design points. The new ideas remain to be explored by the users and to be refined by trial and application. Nevertheless, they are already helpful for simulation purposes because they provide more useful information, new insights, and open new ways of thinking about selecting and graphing icing variables.

Recent aircraft accidents and incidents apparently related to freezing drizzle have brought renewed interest and concern about 'large droplet' icing conditions. Little data exist on the details of these icing conditions and on the ice accretions and aerodynamic effects that they cause. Some simulation efforts are already being attempted with airborne spray rigs and in wet wind tunnels. It is expected that research into freezing rain and freezing drizzle conditions will be increased to supply further guidance.

Scaling and Similarity Laws. The limited size and capabilities of icing tunnels often dictate the use of reduced scale models or substitute conditions when testing aircraft or components in simulated icing environments. In natural icing flight tests too, one usually has to accept conditions that are different from the desired test values. Both of these situations require the use of scaling or similarity laws in order to extrapolate test exposures to full scale or design value conditions.

The straightforward application of similarity theory to the icing problem leads to numerous scaling laws which cannot all be satisfied in practice, unless the testing is done at full scale. Less restrictive sets of scaling laws can be derived if the key physical processes are carefully considered and if certain approximations are made. These scaling laws can usually be satisfied in practice for rime icing conditions and it appears that good results can be obtained for such conditions even from subscale tests. Glaze icing presents more of a challenge, especially for subscale tests. More scaling laws apply than for rime icing; it would only be possible to satisfy all of them in subscale tests if surface tension properties of the spray water and model surface can be suitably adjusted. The feasibility of doing this and of obtaining correct results including, for example,

correct roughness of the ice accretion, has yet to be demonstrated. Work on scaling of icing needs to continue, including exploration of the sensitivity of ice shapes to deviations from the scaling and similarity laws, especially for glaze ice conditions.

Icing Windtunnels and Airborne Spray Rigs. There are about twenty icing windtunnels and about twenty engine test cells for icing presently available in North America and Europe. Only four of the windtunnels are 'large' - having test section areas exceeding one square meter. Most are considerably smaller. At this writing, Italy is planning the latest, large, icing windtunnel for international use. It will have a test section measuring 2.2 m × 2.2 m.

Airborne spray rigs are an endangered species. Few of them exist because of the expense of outfitting and operating them. At this writing, the largest, the NKC-135A spray tanker operated by the U.S. Air Force, is scheduled for retirement in 1996. It figured prominently in recent tests of an ATR-72 turboprop aircraft in large droplet conditions.

A new challenge for both the windtunnel and airborne rigs is to produce sprays simulating freezing drizzle conditions. This requires a whole new or modified set of spray nozzles, different air and water pressure settings, and a new calibration of the spray in terms of drop sizes and water concentrations.

However, flight tests in natural icing conditions cannot be avoided for certification/qualification although reasonable experimental facilities exist for testing in laboratories and in flight through artificial icing atmospheres. At least it has to be shown to the authorities in some certification flights that all experiments simulating icing atmospheres or ice accretion effects do produce effects equivalent to natural icing or worse.

Instrumentation for Icing Tests. Accurate measurements of dropsize distributions and water concentrations in the sprays remains a problem for both the windtunnels and the airborne rigs. Modern, electro-optical, droplet-size probes are preferred these days because of their size resolution capabilities and the convenience of continuous, digital recording. But, unfortunately, they continue to be plagued with frustrating uncertainties at both the large and small droplet ends of their range of sensitivity. Because the water content (mass) of the droplet varies with the cube of the droplet radius, small uncertainties in droplet size or in large droplet counts can have a large effect on the resulting water concentration. This problem has received new concern as the need to measure larger droplets has arisen. New, accurate, bulk water concentration meters are needed for the large droplet conditions. Presently available hot-wire LWC probes begin to lose sensitivity to droplets larger than about 40 μm diameter. This is an urgent problem for the calibration of large droplet sprays.

Ice Accretion Prediction Codes. Sophisticated computer routines for predicting two-dimensional ice shapes have been available for several years. The use of CFD codes for predicting droplet trajectories and limits of impingement, ice shapes of rime and glaze type, and ice protection system layouts is reasonably widespread now and further refinement of the codes along with experimental calibration and validation is recommended. Further enhancements and validations are especially required for predictions in glaze ice conditions. The codes should be extended and validated for a wider range of icing conditions, especially for large droplet conditions. In particular, the development of three-dimensional ice accretion codes acceptable for certification purposes is urgently needed. At present these codes are at an early stage of development.

Also recommended is the development of flow codes that can predict how the aeroperformance of aircraft components will be affected by ice accretion - i.e. by ice horn shapes or by surface roughness. However, it cannot be expected that the degradation of handling qualities for a complete aircraft may reliably be predicted by computational methods within the foreseeable future, although reasonable progress for prediction of performance degradation might be possible.

An important need is to intercompare the prediction of codes with each other and with ice shapes produced in various icing research tunnels and in flight. This work has been proposed as an immediate follow-on effort to the work of FDP Working Group 20, documented in this report. Demonstrated consistency between the codes and experimental results is urgently needed in order for the codes to be accepted as reliable by civilian certification and military qualification officials.

Related Research. The deficiencies of computational methods are in many respects closely related to weaknesses in experimental knowledge for specific physical aspects, e.g. for the effects of surface roughness due to ice accretion, effects which usually exceed the effects of conventional types of roughness by orders of magnitude. Therefore, systematic experimental studies are needed to investigate the roughness effects in combination with large Reynolds number variations; extending the present experimental knowledge base is essentially the only way to improve predictions of glaze ice. Also ice shape prediction in the case of very large droplets - usually characterised by 'freezing drizzle' and 'freezing rain' - must be made more reliable with the help of more systematic experiments.

On the other hand experimental facilities and techniques could profit from systematic numerical simulations. For example the questions regarding applicability of similarity laws for subscale model experiments may be elucidated by calculations, and shortcomings in ice-tunnel and in-flight experiments may be assessed by analysis. Also, theory should be used in every way possible to enhance the credibility of in-flight icing tanker

tests and their acceptance by the certification authorities to the maximum possible extent.

The next generation of high bypass turbofan engines will provide little or no excess bleed air for thermal ice protection systems. Therefore, some emphasis has to be put on the development of efficient alternate de-icing systems for turbofan driven transport aircraft. Alternative new systems may also solve the existing, well known ice protection problems of turboprop aircraft. Intensified research, development and certification efforts in this area are definitely recommended.

APPENDIX A: AERODYNAMIC EFFECTS OF DE/ANTI-ICING FLUIDS AND A DESCRIPTION OF A FACILITY AND TEST TECHNIQUES FOR THEIR AERODYNAMIC ACCEPTANCE

M. Carbonaro*

S. Özgen†

Aeronautics/Aerospace Department-Von Karman Institute for Fluid Dynamics
Chaussée de Waterloo, 72
B-1640 Rhode-St-Genèse
Belgium

1 INTRODUCTION

Since 1950's operating regulations state that no aircraft may take-off when frost, ice or snow is adhering to the wings, controls surface and the propeller.

European airlines have worked together as the association of European Airlines (AEA) to establish procedures and specifications for materials and equipment for the appropriate de/anti-icing of aircraft on ground. Historically, the newtonian de/anti-icing type I fluids were the first ones to be used. In the 1980s, non-newtonian type II fluids started to become widely used especially by European airlines with the thought that they were offering significant operational advantages over type I fluids. The most important difference between newtonian and non-newtonian fluids is in the parameters affecting their viscosity. For newtonian fluids, viscosity is dependent on temperature alone whereas for non-newtonian fluids it is dependent on both the temperature and the shear rate. This means that when the aircraft is at rest or moving with a small velocity (e.g. taxiing), the viscosities of these fluids are very high and thereby they remain on the wing for much longer durations of time hence providing an almost unlimited duration of protection compared to newtonian fluids. However, when the aircraft accelerates for take-off on the runway, due to the increasing shear, the viscosity of a non-newtonian fluid drops rapidly (becoming comparable to that of type I newtonian fluids at take-off and climb speeds or even lower) and the fluid should flow off the wing to leave a clean surface at the time of lift-off. The usual procedure in the application of these fluids is taken in two steps. First the wing surface is de-iced with a type I newtonian fluid and then the type II anti-icing fluid is sprayed on the clean surface so that the plane can wait a significant time before take-off without the danger of ice reforming on the wings.

However, until the early 1980's the adverse aerodynamic effects of these fluids themselves were considered to be negligible or the adverse effects were thought to be within the operational safety margins of airworthiness regulations for dry, uncontaminated wings. However, efforts towards the understanding of such effects, which started in 1982 by the pioneering work of Boeing [1] revealed that these fluids may also have considerable and transitory adverse effects on airplane performance, although it is accepted that these effects are far less severe than those caused by ice, frost or snow adhering on the wings.

Research on the aerodynamic effects of de/anti-icing fluids was started in 1982 by the Boeing company [1]. In this work, type II de/anti-icing fluids on model airfoils having one-foot chord have been tested at ambient laboratory temperatures which is high above the normal operating conditions of the fluids used. To simulate the viscosities of these fluids at freezing or subfreezing temperatures, additives have been used. In these tests, it was seen that the wavefronts of the fluid form close to the leading edge and propagate towards the trailing edge as the airspeed increases. Photographs of the fluid motion revealed that almost no fluid leaves the wing until the wavefront reaches the trailing edge. Considering that at the time of the rotation maneuver the wavefront has still not reached the trailing edge, it is likely that most of the fluid is still on the wing at this moment. It is indicated that the fluid that has accumulated on the aft portions of the airfoil causes significant losses in lift (could be as high as 10%) and increases in drag.

The results of [1] initiated a reaction of several European airlines and in early 1983, the Von Karman Institute (VKI) was approached by SABENA with a request to further study the phenomena. The VKI was asked to verify whether the fluid would indeed have the time to flow-off the wing before the rotation maneuver and to determine what was the effect of the fluid on the lift at take-off. This request resulted in a three-year VKI research program carried out from 1984 to 1987 under the funding of Association of European Airlines (AEA). The main idea was to remove the two scaling limitations of the earlier study by using chord lengths similar to those of real wings and conducting the tests at real subfreezing temperatures. The research program was handled in three phases. Each of these phases will be described separately below.

2 FLOW OF DE/ANTI-ICING FLUID ON A FLAT PLATE

The first phase of the research [2] required the design and construction of a special facility at VKI in 1984 which is the Cold Wind Tunnel, CWT-1 (Figure 1). It is a closed circuit wind tunnel cooled by liquid nitrogen and the insulation permits stable temperatures as low as $-30°C$ to be attained. The test section was designed to have 2.2m. length, 0.3m. width and 0.1m. height. The upper and

* Professor
† Doctoral Candidate

lower walls of the test section were made of glass for the optical setup. Provision was made to deposit a thin layer of fluid, precooled to the test temperature, on the bottom test section wall. The tunnel could be accelerated manually from 0 to the maximum speed of 65 m/s in approximately 30 seconds. This regime corresponds to the real take-off run of a commercial transport aircraft.

During the experiments it was seen that soon after the airflow started two phenomena were occurring, namely, surface waves form on the fluid surface and the fluid starts moving downstream. The instantaneous thickness profile of the fluid layer was measured using an optical technique. As shown in Figure 2, a video camera, located above the test section, was used to record the images of the moving wavy fluid layer. This method is explained in Appendix A. A typical example of the thickness profile obtained during these experiments is shown in Figure 3. It shows the initial layer having a thickness of about 3 millimeters, and 15 seconds after the start, the formation of surface waves and the overall decrease in thickness. This trend continues and 30 seconds after the start the fluid layer has a smaller thickness and the amplitudes of the waves are also smaller. However 30 seconds roughly corresponds to the time at which the rotation maneuver would take place and at this time it is seen that there is still about 1 millimeter of fluid left on the surface which is a rather extreme one. Even after 60 seconds, there is still a residual fluid film of about 0.5 millimeter thickness and which according to what was observed during these tests does not seem to evolve anymore.

About 100 sets of thickness profiles similar to the one shown were measured to compare five different fluids which were: an ethylene/propylene glycol mixture as described by Military Specifications 8243-D which is a newtonian fluid, and four additional non-newtonian anti-icing fluids, none of which is in production any more (Kilfrost ABC, SPCA AD 84, Hoechst 1704/83, Union Carbide ADF 2.2). The tests were conducted at four different temperatures ($-20°C, -10°C, 0°C$ and ambient) and for three different initial thicknesses of the fluid layer (1, 2 and 3 millimeters). Figure 4 summarizes the results of several tests conducted on a specific anti-icing fluid at various temperatures with layers of different initial thickness. It shows that the final thickness at 30 seconds is independent of the initial layer thickness. Already at about 15 seconds the various curves merge. This result is typical for other fluids too and it is quite important as it demonstrates that one of the test parameters, the initial thickness, does not influence the final fluid layer thickness. But in contrast to this, some fluids showed remarkable dependence on temperature. On the other hand for newtonian fluids, the behaviour of the liquid film did not show noticeable dependence on temperature but its residual film thickness was influenced by its initial value, measured indirectly from the pressure drop along the test section. Another remarkable variation between the newtonian fluid and the non-newtonian fluids tested was in their wall shear stress values. The values obtained were fundamentally different for each type of fluid but in all cases were above the value obtained from a dry surface.

3 EFFECTS OF DE/ANTI-ICING FLUIDS ON A LARGE AIRFOIL MODEL AT EXTREME CONDITIONS

Following a suggestion of Boeing, who collaborated to the definition of the test program, the same airfoil shape, previously used in [1] was again used for this phase of the research [3]. The model used for this work is shown in Figure 5. This airfoil corresponds to the one at 66% spanwise position of the wing (normal to the leading edge) at 5° flap position of a Boeing 737-200ADV airplane. For simplicity, as in [1], it had no slot at the flap.

One of the goals of the research was to remove the limitation associated with the fact that the scaling parameters for the flow around the model and for the wavy fluid film are different. Indeed, surface roughness of an airfoil scales down with the chord while the surface waves on the fluid film are independent of this parameter. The waves are influenced by parameters like surface tension, viscosity or elasticity of the non-newtonian fluid which are temperature dependent and do not scale down with the chord.

Therefore it was decided to choose a model chord close to the real chord and this resulted in a 1.5 m. chord, 2.2 m. span model as shown in Figure 6. The model was fitted with an internal strain gauge balance designed and manufactured at VKI to measure lift, drag and pitching moment. The model was enclosed in a wind tunnel test section insert as shown in Figure 7. The wing model, built by British Airways, was made of three parts. The center portion, 0.3 m. wide, was connected to the internal balance.

Tests were conducted in 1986 both in the VKI 3 meter diameter, low speed (72 m/s peak) L-1A wind tunnel to check the setup and the instrumentation at ambient conditions and in another wind tunnel located in Wien at the Bundesversuch-und-Forschung Arsenal (BFA). This tunnel designed to be used for the testing of trains, has a test section of 2.4x2.2 meters, a maximum speed in excess of 77 m/s and can be cooled down to $-50°C$.

Tests were conducted with the airfoil either clean or covered with various fluids. Several clean airfoil tests, repeated frequently throughout the test program, served the purpose of providing a reference baseline to determine fluid induced effects, as well as allowing a repeatability check. The same fluids used for [2] were used again.

The test procedure was as follows: at temperatures of $-20°C, -10°C$ and $0°C$, a sufficient amount of unsheared, dyed fluid was poured on the airfoil model so that its center portion would be completely wetted. Excess fluid was left to drip off. Then the tunnel was started and accelerated linearly to reach a velocity of about 55 m/s (107 knots). After about 30 seconds the airfoil was pitched up to simulate the rotation maneuver. Recordings of the balance measurements were made at a 5 Hz. sampling frequency and fluid motion was continuously recorded on videotape. Photographs of the upper surface were taken every 3 seconds.

A sample sequence of such photographs is reproduced in Figure 8. It shows the formation of surface waves soon after the flow initiation (a). A typical triangular shape is apparent as the initial surface perturbation widens laterally when it is convected downstream. Some time later, the perturbations have merged to form a wavefront (b) propagating downstream. This wavefront has almost reached the trailing edge when the rotation maneuver starts (c). At the end of the rotation, it was seen that there was still some fluid present at the trailing edge, an observation which is in agreement with the reported results of [1]. The forward part of the airfoil seemed to be relatively clean but there was still some fluid present, as revealed by close visual inspection and by use of a mechanical depth gage.

Figure 9 shows the different formation of waves for a newtonian and a non-newtonian fluid. For the newtonian fluid, almost two-dimensional small surface riddles due to capillary forces appear, whereas in non-newtonian fluids much larger waves appear.

Figure 10 shows another unexpected phenomenon, the appearance of a second wave front during the rotation

maneuver. Its existence had been controverted for some time. However in these tests, it was understood clearly that the second wavefront appeared when the airfoil pitch-up angle was large, but it did not when this angle had a moderate value. The reason for its formation is due to the increase of shear stress over the forward part of the airfoil upper surface, which is associated with the change of incidence. The second wavefront sweeps some additional fluid on the forward part of the airfoil towards the trailing edge.

As a result of the second phase of the VKI/AEA research, the aerodynamic characteristics of the fluid-contaminated airfoil were measured at extreme conditions, i.e relatively low velocity (about 55 m/s) and high incidence (10-14 degrees) which are close to stall. This was the most unfavorable case and it indicated the existence of a lift loss as high as 17% and of intermittent stall, when testing a specific anti-icing fluid, which is not in production any more.

Among the non-newtonian fluids tested in 1986, those with lower viscosity seemed to yield lower lift losses and a tentative correlation showing this dependence was established. However, also the newtonian Mil-Spec fluid unexpectedly yielded substantial lift losses, up to 10% at the lowest testing temperature $-20°C$. These results triggered the third phase of the research, directed to repeat the experiments at lower incidence and higher velocities as encountered during a real take-off maneuver.

These results also encouraged fluid manufacturers, at the request of AEA, to stop production of the existing fluids and to develop new products with reduced viscosity to improve their flow-off behaviour and thereby their aerodynamic characteristics and to make them available during the coming winter 1986/87.

4 EFFECTS OF FLUIDS ON LARGE AIRFOIL MODEL AT CONDITIONS CLOSE TO OPERATIONAL

The same airfoil model, with some improvements on the setup to allow higher test velocities and a variable pitch-up angle was again used for the third phase of the VKI/AEA research [4]. Tests were again conducted at BFA in May 1987 following the same procedures as in the previous work [3] but with test conditions simulating those of a normal Boeing 737-200 take-off as well as those of a one-engine take-off. Thus a wind tunnel speed of 75 m/s (145 knots) and a pitch-up angle of 4 degrees were used for the first case and of 67 m/s (130 knots) and 7 degrees for the latter.

The fluids that were tested were the three new products developed following the results of the second VKI/AEA research phase [3], i.e. Kilfrost ABC-2, Hoechst 1704 LTV-87 and SPCA AD-99/6, the usual newtonian Mil-Spec fluid and one of the non-newtonian fluids tested in the previous work. Four additional experimental products were supplied by Union Carbide, Canada, among which was the UCAR 250/3 fluid.

During the third phase of the research, the effect of solid roughness on the wing upper surface was also examined. According to the procedures defined by Boeing [5], this roughness, which simulates the presence of frost, was obtained by gluing an adhesive anti-slip safety walk sheet on the wing surface. This product was commercially available from the 3M company. Two-different roughnesses were tested: 3M stock No. 61-2091-5102-8 and No. 61-2080-3073-6, named Frost 1 and Frost 2 respectively. These corresponded to roughness heights of 0.36 and 0.48 millimeters. A rougher coverage (Frost 3) of about 1.3 mm was obtained as done in [5] by applying an epoxy putty material to the Frost 1 safety walk and then roughening it with a paint roller.

Results of the tests with solid roughness contamination are shown in Figure 11, where the lift coefficient versus incidence curve shows a progressive decrease with increasing roughness, as expected. A decrease in stall angle and in maximum lift coefficient is also apparent. This test demonstrated the validity of the measurements because the measured losses of lift agreed with the results of flight tests previously carried out by Boeing [6] on a Boeing 737-200 using artificially roughened wings to simulate two frost cases, named Frost A (similar to Frost 1 and Frost 2) and Frost B (similar to Frost 3).

Tests were run with or without fluid on the smooth model and similar results were obtained (Figure 12). Losses of lift coefficient were again found to be present for all fluids and test temperatures (Figure 13). However, these lift coefficient losses are lower than those found in the previous research phase. This is due to the improvements in the fluids achieved by the manufacturers and to the less critical test conditions (lower wing incidence, higher tunnel speed) which are closer to the real case values.

However, these wind tunnel tests indicated that the reduction of lift loss was not as important as could be expected by the reduction of viscosity of the new fluids tested. Indeed it was noticed that lift loss was not correlated with viscosity alone, as fluids of high viscosity could yield lower losses than other fluids with lower viscosity. This means that a quality control of the de/anti-icing fluids cannot be made by a viscosity check only, but an aerodynamic test is required at least until the mechanism of fluid flow-off and lift loss is fully understood and modeled.

Just after the third phase of the VKI/AEA was over, the Union Carbide Co. of Canada requested the VKI to test of four of its development fluids, one of which was newtonian and the other three were non-newtonian [7]. The objective was to assess the effects of fluid presence on the wing upper surface on the wing aerodynamics. For the test the same airfoil model used before in [1], [3] and [4] was used. Also the procedures followed in the previous VKI/AEA research phases were used. Tests were done at two different temperatures, namely at $-10°C$ and $-20°C$. The take-off was simulated at three different incidences, at 4, 7 and 12 degrees. The fluids yielded quite low aerodynamic losses (less than 5% for lift coefficient) which are much less than the losses caused by earlier generation fluids. A surprising result of this work was that one of the non-newtonian fluids, the one which had the highest viscosity, yielded the least aerodynamic losses. This showed that the losses are not correlated with viscosity alone a conclusion which is in agreement with the results of [4].

At this stage the research on airfoils was taken over by Boeing who conducted wind tunnel tests in NASA Lewis Icing Research Tunnel (IRT) and flight tests on a Boeing 737 in Kuopio (Finland), to extend these results to a real 3D case and to validate the wind tunnel studies [8]. A quite reasonable agreement of the wind tunnel results on the 2D airfoil, as obtained by VKI/AEA and by Boeing/NASA-IRT is shown in Figure 14. Both in wind tunnel and flight tests a newtonian deicing and three non-newtonian anti-icing fluids were used. In the wind tunnel experiments a 2D airfoil model and a 3D half model of a Boeing 737 airplane were used. In these experiments, it was again observed that the fluids remain on the wing after lift-off and cause a measurable lift loss and drag increase. It was noticed that the fluid effects were maximum at configurations with the high lift leading edge devices at the maximum lift conditions. However, when these high lift devices were not deployed, the effect was small. It was also found out that the fluid effects are de-

pendent on the fluid roughnesses particularly in the first 30% chord. Both in the wind tunnel and and in the flight tests, a secondary wavefront was seen to form and propagate downstream at the time of the rotation maneuver.

5 ANALYSIS OF THE LIFT LOSS MECHANISM

After the conclusion of the three phases of the VKI/AEA research program described above, another problem was addressed by VKI in an independent, self supported venture. This effort was towards the definition of a simplified test for aerodynamic acceptance of de/anti-icing fluids [9]. In this work the same fluids used in [4] were used at the same temperatures. But instead of using a 2D wing model a flat plate was used. The objective was to determine whether any correlation existed between the boundary layer displacement thickness measured on a flat plate and the lift loss on a 2D wing. Boundary layer displacement thickness measurements were done by the blockage method (described below) and these were correlated with the lift losses available from [4] at the same conditions. The validity of this approach will be further emphasized below.

This work resulted towards the end of 1988 in a proposal of an original test methodology that was presented to AIA and AECMA member companies and further investigated in 1989 by VKI under the sponsorship of Airbus, British Aerospace and Fokker.

The fundamental question refers to the nature of the mechanism of lift loss of a contaminated airfoil. It can be recognized that the wavy fluid layer produces an increase of the aerodynamic roughness of the wing surface thus thickening the airflow boundary layer. Also in order to entrain the liquid, energy is transferred from the boundary layer to the fluid which again results in the thicknening of the boundary layer. This in turn modifies the effective shape of the airfoil as felt by the external inviscid flow, by an amount which is the boundary layer displacement thickness. Therefore this last quantity must be related to the variation of the aerodynamic characteristics of the airfoil.

To investigate this concept, a numerical model was developed [10], [11] using an inviscid panel method for the external airflow based on Hess-Smith approach coupled with a simple integral boundary layer calculation based on Head's entrainment approach, proposed long ago by Dvorak [12] for turbulent flow over a rough surface. In this approach, the usual Ludwig-Tilmann formula for skin friction, valid for smooth walls, was replaced by another one, proposed by Betterman [13] for walls with periodic roughness. In this formula, the periodic roughness is characterized by a roughness height and wavelength. This model was selected because of its analogy with the periodic waves on the fluid surface. Its applicability was verified with pitot probe boundary layer surveys over a periodically rough flat plate [14].

In the context of [10] the roughness parameters (height of roughness and roughness density distribution) were measured in the experiments for each of the de/anti-icing fluid studied and these were given as an input to the boundary layer calculations via Dvorak's correlation. The displacement thickness values calculated by the boundary layer solver (which now includes the effects of surface roughness) were fed into the inviscid panel program. This program calculates the lift and the drag coefficients for configurations in which the fluid presence is accounted for. Calculations were done for the test airfoil and the lift coefficient loss was an increasing function of the displacement thickness over a rough airfoil surface, independent of the roughness wavelength.

6 DEFINITION OF AN AERODYNAMIC ACCEPTANCE TEST

As explained, one could characterize the aerodynamic effects of a fluid layer deposited on an airfoil by the displacement thickness of the airflow boundary layer above it. Furthermore, a basic simplifying assumption was made: to assess these effects by measuring the boundary layer displacement thickness over a flat plate, not over an airfoil. The two situations are of course different, but may be related to one another, and a study supported by Airbus, British Aerospace and Fokker was carried out at the VKI in 1989 and 1990 to investigate the correlation between the boundary layer thickness over a flat plate covered with fluid and the lift loss experienced by a contaminated airfoil as determined by the wind tunnel tests of [4] and [8].

For this study, the VKI CWT-1 Cold Wind Tunnel was again used. However it had to be improved in terms of flow quality and test procedures [10]. An important modification was that the electrical motor driving the tunnel fan was made computer controlled. This ensured a repeatable velocity-time sequence. The tunnel was cooled by injecting liquid nitrogen (manually adjusted) like in the cryogenic wind tunnels and the tunnel test section length was reduced to 1.6 meters to avoid the merging of the boundary layers developing on the top and bottom walls. Figure 1 illustrates the modified and the current state of CWT-1. The test setup is illustrated in Figure 16. Wall pressures are measured in the settling chamber and at the inlet and the outlet of the test section. Figure 15 shows the boundary layer profiles measured in the CWT-1 test section, at ambient conditions, on the top and the bottom walls, when the bottom plate is either smooth or covered with three different roughness. The effect of roughness in increasing the bottom wall boundary layer thickness is evident, as expected.

However, it would have been quite difficult to measure the time dependent airflow boundary layer with a pitot probe measurement during an actual test with moving fluid, so an alternative method, based on the wind tunnel blockage concept was used. This method was developed in the VKI in 1985 [2] and is based on the fact that the increase in boundary layer displacement thickness causes the inviscid flow outside the boundary layer to accelerate, and this in turn causes a variation of the static pressure difference along the test section. The details of the method are described in Appendix B. These measurements are carried out continuously during the test run and a graph like that shown in Figure 17 is plotted for each case. The graph gives the velocity variation with time, increasing linearly for about 25-30 seconds and then remaining constant, as it would happen in a take-off velocity history of an airliner. The graph also shows the boundary layer displacement thickness history which at first increases abruptly and then starts decreasing steadily. The large increase in this quantity in the first few seconds of the run is due to the formation of large surface waves causing a great perturbation. Once the flow has well established, the fluid is entrained downstream and the disturbances decrease steadily. Also shown on the same figure is the displacement thickness history of a flat plate which becomes independent of time after approximately 20 seconds. Two histories, one for a fluid with good flow-off properties and one for bad qualities are also shown on the same figure for comparison.

Figure 18 refers to a non-newtonian fluid, and demonstrates that the effect of different initial fluid thicknesses

tend to disappear very quickly (time corresponding to the rotation maneuver), a result which was also reported earlier in [2].

Such histories are used to extract the value of the displacement thickness at the 30^{th} second, which is a critical instant during the take-off. This value is plotted against the temperature which fully characterizes the flow-off behaviour of a given fluid. Such a plot is shown in Figure 19 which compares two non-newtonian fluids: an old generation fluid yielding high displacement thickness (thus high lift losses), and another one with quite good flow-off properties.

The effect of diluting an anti-icing fluid with water was also examined by testing the pure and diluted fluids. Dilutions of 25% and 50% with demineralized water were tested. Results shown in Figure 20 indicate that the dilution rate may either yield better or worse flow-off properties. A reason to this may be that the rheological properties of non-newtonian fluids are altered significantly by even small amounts of additives.

Finally, it was possible to correlate these measured boundary layer displacement thickness values over a flat plate to the lift loss of an airfoil under the same flow conditions. Such a correlation for the fluids that were tested by VKI at BFA in 1986 is shown in Figure 21. The correlation looks reasonable and was also made for other products tested by Boeing in the NASA-IRT (Figure 22). There is some scatter for a few products which is attributed to the fact that the samples used during the two groups of tests were belonging to different production batches.

On the basis of these results and as a result of extensive discussions with American and European airframe manufacturers carried out in the context of the Aerospace Industries of America (AIA) Transport Committee (TC) Project 218-4, a procedure was agreed upon [15] and the VKI CWT-1 facility and the test procedures were recognized as being suitable for aerodynamic certification of fluids to be used on grounded aircraft. The idea was to compare the displacement thickness behaviour of a candidate fluid with respect to temperature with that of a dry and smooth wall and that of a reference newtonian fluid. The reference fluid should have a well-defined composition like the propylene glycol fluid described by the Military Specification 8243-D. Appropriate factoring of the curve for the Mil Spec fluid allows to define a limit curve below which a candidate fluid should fall in order for it to pass the aerodynamic acceptance test.

Such a limit was defined by the Boeing Company on the basis of a tolerable lift coefficient loss at take-off, inferred from the the minimum lift-off velocity mentioned in FAR 25. In agreement with this the maximum tolerable lift loss was determined to be $\Delta C_l/C_l = 5.24\%$ [16]. The formulation of this limit has undergone some modifications since the time it was first proposed due to the growing database of the VKI CWT-1 fluid tests and the availability of new data, as well as the use as reference of the displacement thickness for the dry runs of the specific test series considered.

The present formulation of the limit of acceptability is defined as [16]:

$$at \quad -20°C \quad {\delta_L}^* = \delta^*_{ms} - 0.18\left(\delta^*_{ms} - \delta^*_{dry}\right)$$
$$at \quad 0°C \quad {\delta_L}^* = \delta^*_{ms} + 0.71\left(\delta^*_{ms} - \delta^*_{dry}\right)$$

where the suffix ms refers to the values obtained for the Mil-Spec fluid. At temperatures between $-20°C$ and $0°C$ the limit is the linearly interpolated value between the above values. At temperatures below $-20°C$ the limit is taken to be the limit value at $-20°C$. The acceptance limit, defined on the basis of the dry run and the tests on the reference Mil-Spec fluid is shown in Figure 20 for the fluid with code name 5.1.

Knowing this, the criteria for a fluid to be acceptable will be mentioned. A de/anti-icing fluid is acceptable if no more than 10% of the independent boundary layer thickness measurements exceed the acceptance criterion boundary layer displacement thickness envelope. The allowable test points shall not exceed the acceptance criterion boundary layer thickness by more than 10%. If a fluid specimen is found unacceptable over a range of temperatures, the manufacturer should be explicitly informed. Any fluid intended for commercial use should pass the aerodynamic acceptance test. An existing fluid should also undergo the test each two years. Any modification in the composition of an existing fluid also makes the renewal of the aerodynamic acceptance test necessary. An important point is that , the aerodynamic acceptance test is the minimum requirement for the adequateness of a fluid intended for operational purposes. Airframe manufacturers may impose additional requirements [16]. The specifications of the aerodynamic acceptance test were incorporated in the AEA Recommendation Issues since September 1990 [17]. They are fully described in [16] which prescribe the important test parameters among which are the wind tunnel flow quality (velocity and temperature uniformity), the fluid identification, precooling, handling and laying the fluid on the bottom wall and the general test procedure: test temperatures, relative humidity inside the wind tunnel and the velocity versus time speed-up sequence.

Test temperatures should be as uniform as possible ($\pm 1°C$ of the target temperature for the gas, $\pm 2°C$ between gas and fluid) and is monitored by the help six thermocouples. Three of these thermocouples measure the temperature of the fluid at three locations, one measures the temperature of the glass plate on which the fluid is laid and two of them measure the gas temperature at the inlet and outlet of the test section. The temperature uniformity is achieved by opening or closing the liquid nitrogen injection valve manually.

Relative humidity (RH) should be at $70\% \pm 30\%$ to avoid water loss from the fluid by evaporation which can be significant below RH 40% which in turn can alter the rheological properties of the fluid. Fluid water content variation is monitored by measuring the fluid index of refraction before and after a run and using a water content/refraction index calibration. A water loss study [18] indicated that the value of relative gas humidity for which there is no transfer of water between the gas and the fluid depends on the water contents of the fluid and varies approximately between 50% (for a fluid with 12% water) and 70% (for a fluid with 40% of water).

It is worth mentioning that in a wind tunnel like CWT-1 which is cooled by liquid nitrogen injection, one would think that the relative humidity drops to very low values because the liquid nitrogen would evaporate to form dry nitrogen. However, this is not the case and the relative humidity remains around $50 - 80\%$ because of three reasons: the amount of water required to saturate air (or nitrogen) decreases sharply with temperature. Ambient air of high humidity (typical of Belgium) is continuously brought into the tunnel by opening the test section repeatedly to lay the fluid to be tested. The used fluid from previous runs accumulates in the tunnel diffuser where it is trapped and could evaporate if the humidity is too low. The tunnel speed-up sequence is prescribed in [16]. The starting speed, in the first two seconds can be comprised between 0-5 m/s (zero speed or idle speed which is the speed at which the precooling of the tunnel is done). Then the speed should increase to a speed of 65 ± 5m/s in 25 ± 2 seconds. Once this speed is achieved, the speed should remain constant until the end of the one-minute duration run. The influence of such a variation in tunnel speed was studied [19] and the results indicated that this

variation should be reduced because it may lead to variances as high as 20% in the boundary layer displacement thickness measurements.
During these research activities, the CWT-1 tunnel and the data acquisition methods were being continuously improved. In [20] the modifications on the insulation, the diffuser, the liquid nitrogen injectors, temperature measurements, the test section and the data acquisition system are summarized together with the related improvements. The data acquisition was made completely automatic by the help of a data acquisition computer. Acquired data is processed in the VAX-4000 computer.
In [21] the boundary layer measurements in the wind tunnel were performed and the method for displacement thickness measurement described in Appendix B was well defined.
Boeing company was also following up with the testing of de/anti-icing fluids on two and three dimensional models in NASA-IRT tunnel. The objective of the study reported in [22] was to supplement earlier reported flight and wind tunnel tests and to support the development of aerodynamic acceptance criteria for aircraft ground de/anti-icing fluids. Three newtonian, four non-newtonian and a reference Mil-Spec fluid were used during the tests. Both the neat and the diluted versions of the fluids were used. Upon dilution (75:25), the aerodynamic effects of the Type II were seen not to change but there was a substantial reduction in the adverse aerodynamic effects of Type I fluids. Boundary layer displacement thickness measurements made with the fluid on a two dimensional model showed excellent correlation with lift loss due to the fluids at maximum lift and at operating angles of attack (Figure 23) and with the boundary layer displacement thickness measured on a flat plate in the VKI CWT-1 tunnel. Using these two correlations it was possible to establish a correlation between the boundary layer displacement thickness on a flat plate and the lift loss (Figure 24). The establishment of this correlation validated the use of a flat plate boundary layer displacement thickness measurement as a criterion for the aerodynamic acceptability of a fluid.
In 1992 the VKI was approached by the European Regional Airliners Association. The question was, how would the aerodynamic acceptance tests would be extended to the performance characteristics of commuter airplanes which have quite different speeds, lift-off times, accelerations compared to the large transport aircraft which were the only types of airplanes addressed until then [23]. The objectives were to:

- derive trends for the parameters for fluid flow-off using the boundary layer displacement thickness as an indicator of fluid presence and perturbation,
- correlate if possible the boundary layer displacement thickness results with the wind tunnel lift coefficient loss measurements carried out by Boeing-De Havilland in the NASA-IRT with clean or contaminated airfoils [24].

The tests were carried out for a reference Mil-Spec fluid and two anti-icing fluids commercially available at the time of the work. The flow conditions used were closer to the flight conditions of commuter airplanes which meant reduced tunnel speed, different tunnel speed-up time and model chord length. The tests were done for maximum tunnel velocities of 35 ± 5m/s, 45 ± 5m/s and 65 ± 5m/s. The testing temperatures were $-20°C$, $-10°C$ and $0°C$. Values of the displacement thickness were determined at 20 and 30 seconds after the test start both at the mid and end of the test section length.

The results indicated that a correlation between the lift coefficient loss and any one of the four measured boundary layer displacement thickness value indeed exists (Figure 25). The best choice to establish such a correlation seemed to be the values taken at the end of the full length of the model, either at the 20^{th} or the 30^{th} seconds. These values seemed to be more convenient because they provided a more obvious correlation. The choice of the acceptable value of the displacement thickness is dependent on the tolerable lift loss and as previously done for the case of the transport aircraft the decision on the acceptable level of loss has to be made by airplane manufacturers. The losses in lift coefficient caused by fluid presence ranged between $3 - 18\%$.

7 WIND TUNNEL STUDY OF THE INTERACTION BETWEEN A RIBLET SURFACE AND AN AIRCRAFT DE-/ANTI-ICING FLUID

Although it was known for a long time that riblet coated surfaces yielded less drag in flight, not much was known about the behaviour of de-/anti-icing fluids applied on such a material. Airbus Industries requested from the VKI to investigate and compare the behaviour of a fluid applied on a smooth or on a riblet surface. The following aspects were considered during this study [25]:

- the influence of riblets on fluid behaviour,
- the influence of fluids on riblets,
- whether the flow-off of a fluid is different on a smooth or riblet surface,
- the fluid residual on the riblets at the end of the test,
- whether a difference between a smooth and riblet surface can be detected,
- whether a difference between clean riblet and fluid contaminated riblet surface can be detected,
- whether the free stream velocity had any effect on any one of the above characteristics.

The same techniques used for the previous research activities were used again, and the boundary layer blockage technique was employed to assess the effects of riblets on the flow and fluid flow-off behaviour. Two fluids were used, one being a Type I de-icing fluid and the other one being a Type II anti-icing fluid. Three different flat plate models were used. The first one was the usual flat plate model used in the aerodynamic acceptance tests. The second one was again a flat plate model covered with the riblet material in which the riblets were aligned with the airflow (riblet1 configuration). The last model was also covered with riblet material but this time the riblets made an angle of $30°$ with the free stream (riblet2 configuration). Tests were done at $-20°C$, $-10°C$ and $0°C$. In addition to the usual one-minute aerodynamic acceptance tests, there were also several five-minute extended duration runs, aimed at investigating the fluid flow-off properties with deeper insight. The tunnel speeds used in these tests were 56, 65 and 70 m/s.
It was seen that, the riblet1 configuration yielded a slight improvement both in terms of the aerodynamical perturbation and from the fluid flow-off properties with respect to the smooth surface. On the other hand, the riblet2 configuration showed a substantial penalizing effect from

all points of view. The difference between the riblet1 configuration and the riblet2 configuration in terms of their performances in the aerodynamic acceptance tests is clearly visible in Figure 26. Figure 27 shows a displacement thickness history at $-20°C$ for the surface configurations with different fluids applied on them. At this temperature the anti-icing fluid seems to have better flow-off properties. But at elevated temperature like $0°C$ (not shown) the de-icing fluid flows off much easier hence causing less aerodynamical perturbation. There was also a slight improvement of the riblet1 configuration in dry cases over the two other surface configurations. The improvements were in the order of 10% in the best case which is on the limit of the uncertainity of the experimental results. On the other hand, free stream velocity variation (at least in the region considered) does not have a considerable effect on these properties.
The phenomenon of drag reduction for riblet surfaces has been investigated both experimentally and numerically by other scientists also [26], [27]. In [26], the results of DNS calculations on a riblet surface have been reported. One of the important results of the study is that the drag reduction is observed only when riblet spacing is less than 25-30 wall units. For such configurations it is observed that wall shear is reduced substantially over most of the riblet surface; only near the riblet tip the wall shear is larger than on the flat wall. These regions of high shear are often associated with the downwash region of strong streamwise vortices which typically have diameters of about 30 wall units. It is seen that these streamwise vortices are more likely to be found inside the grooves of riblets with high spacing (larger than 30-40 wall units). When the vortex moves into the riblet valley, a larger area is exposed to the downwash of the vortices, resulting in a higher friction coefficient. Conversely, when the spacing is smaller than the average vortex diameter, vortices are forced to remain above the riblet tips, which results in a smaller region near the tip being exposed to downwash. Currently an Airbus 340 aircraft is flying with riblet material coated on its wings, vertical stabilizer, tailplane and part of its fuselage for evaluation purposes [28].

8 EXPERIMENTAL AND NUMERICAL EFFORTS TOWARDS THE UNDERSTANDING OF THE FORMATION OF SURFACE WAVES AND INSTABILITIES

The experimental research has focused on the effect that the wavy liquid film has on the turbulent airflow. The mechanism of appearance of surface instability on the fluid film and the parameters governing the phenomena have to be well understood. The optical method, previously described is used. The variation of the thickness of the fluid with time and space can be measured during a wind tunnel test. The observed wave patterns have been found to be quite obvious for newtonian de-icing fluids, whereas different patterns were encountered for the initial instability of anti-icing fluids with non-newtonian behaviour [29], [30]. In [31], the non-intrusive optical method was further developed and explained. The surface instabilities of de-icing and anti-icing fluids were further investigated and it was seen that the initial surface instability of of anti-icing fluids seemed to be a solitary wave with a triangular wake. Figure 28 shows two examples of surface instabilities of de-icing fluid films. These aspects may lead to future determination of the effect of the fluid film on aircraft airfoil performance using the height and spatial frequency of the surface waves.
To complement these investigations, efforts have also been undertaken for the theoretical study of the basic phenomena of formation of interfacial waves and their growth in two-layer flows from the hydrodynamic stability point of view [32], [33]. Here a Blasius boundary layer flow over a dense viscous fluid (newtonian or non-newtonian) on a flat plate is considered. The parameters effecting the phenomena have been found to be numerous: the viscosity ratio of the two fluids (m), the density ratio (r), the relative thickness of the liquid layer (l), surface tension (S), gravity (F:Froude number) and the rheological characteristics of the non-newtonian fluid. The stability characteristics of the two-layer problem are governed by an eigenvalue problem and the eigenvalues are:

- α: the wavenumber of the disturbance waves,
- C_r: the propagation speed of the disturbance waves,
- C_i: the amplification factor of the disturbances,
- Re: Reynolds number based on the Blasius length scale of the boundary layer.

A very interesting result of this study turned out to be that a different mode exists other than the classical Tollmien-Schlichting mode which has growth rates and propagation speeds an order of magnitude smaller than the latter (therefore this new mode is called the soft mode and the classical T-S mode the hard mode). The presence of the soft mode was first reported in [34], [35]. The significance of this mode to the current de/anti-icing fluid aerodynamic perturbation problem is currently under investigation. Figure 29 shows the stable and unstable domains enclosed by the two mentioned modes and Figure 30 shows the effect of viscosity stratification on the amplification factors of these modes. As can be seen increased viscosity stratification makes the soft mode amplification rates smaller and smaller and even indistinguishable after a certain value of it. Thinking that the viscosity ratios in a de/anti-icing application would be very large (about 500000), it seems that the newly found mode may not be very relevant to this particular flow situation.
Efforts towards the understanding of interfacial waves and their influence on the wing performance have been taken up by other scientists as well. In [36] a similar method to the one mentioned in [33] has been employed for a de/anti-icing application. In agreement with the results of [33], it was seen that the flow instabilities are governed by the classical Tollmien-Schlichting mode for the range of parameters considered.

A LIGHT ABSORPTION METHOD

The fluid film thickness measurements were conducted using a non-intrusive measurement technique based on the light absorption. This is a technique which has been used in the VKI since many years. The method is based on the very well known relation:

$$I = I_o e^{-\lambda h} \tag{1}$$

where h is the film thickness, I_o the incident light, I the transmitted light and λ the light absorption coefficient. The relation reduces to:

$$\log\left(\frac{I_o}{I}\right) = \lambda h \tag{2}$$

Measuring the incident and transmitted light intensity on a point and knowing the absorption coefficient for the liquid, the previous relation is used to calculate the fluid thickness at that point.

To obtain the absorption coefficient of the fluid a calibration device must be used. This is done with a wedge filled with the fluid to be tested with a thickness varying from 0 to about 8 millimeters. To enhance the absorption characteristics the fluid was dyed with an adequate dye fluid which did not alter the rheological properties of the fluids used. Knowing the fluid thickness at a certain point and knowing the incident and the transmitted light, the absorption coefficient can be calculated. The incident light is obtained by diffusing and reflecting light below the test section. The images are treated using the Digital Image Processing unit of the VKI. This unit is composed of a video camera, a MATROX image acquisition board and a C2I PCSCOPE software. The images are digitized, on a frame of 512x512 pixels in the computer via the camera or the VCR. A value corresponding to the brightness of that pixel is attributed to each pixel. Then the images were treated using a specific software.

B CALCULATION OF THE BOUNDARY LAYER DISPLACEMENT THICKNESS

The following procedure to measure the instantaneous value of the boundary layer displacement thickness on a flat plate was developed in 1985 in the VKI and is described in [2]. It is based on the test section blockage due to the boundary layer growth.
Referring to Figure 16, from the measurement of static pressure differences between the settling chamber and the inlet of the test section:

$$p_{12} = p_1 - p_2 \tag{3}$$

as well as between the inlet and the outlet of the test section

$$p_{23} = p_2 - p_3 \tag{4}$$

it is possible after some approximations to calculate the boundary layer displacement thickness.
It is clear that the growth of the boundary layer restricts the effective cross sectional area of the test section. The effective cross sectional areas after accounting for the boundary layer displacement thicknesses are:

$$S_{2eff} = S_{2g} - c_2\delta_2^* \tag{5}$$

$$S_{3eff} = S_{3g} - c_3\delta_3^* \tag{6}$$

where c_2 and c_3 are the perimeters of the test section at the inlet and outlet respectively and g denotes geometrical values. One can employ the Bernoulli equation for the inviscid core between location 1-2 and 2-3:

$$p_1 + \frac{1}{2}\rho V_1^2 = p_2 + \frac{1}{2}\rho V_2^2 \tag{7}$$

$$p_2 + \frac{1}{2}\rho V_2^2 = p_3 + \frac{1}{2}\rho V_3^2 \tag{8}$$

Conservation of mass between stations 1 and 2 state that:

$$\frac{V_1}{V_2} = \frac{A_2}{A_1} \tag{9}$$

Knowing that $A_2/A_1 = 1/10$, it is immediately seen that $V_1^2 << V_2^2$, so one can write for V_2:

$$V_2 = \sqrt{\frac{2}{\rho}(p_1 - p_2)} \tag{10}$$

Using 10, from 8, one can derive:

$$V_3 = \sqrt{\frac{2}{\rho}((p_1 - p_2) + (p_2 - p_3))} \tag{11}$$

Moreover, the continuity equation for the inlet and outlet of the test section yields:

$$\frac{V_2}{V_3} = \frac{S_{3eff}}{S_{2eff}} \tag{12}$$

Combining 10, 11, 12, the displacement thickness from 6 becomes:

$$\delta_3^* = \frac{1}{c_3}\left(S_{3g} - S_{2eff}\sqrt{\frac{p_{12}}{p_{12} + p_{23}}}\right) \tag{13}$$

However, S_{2eff} is not yet known. From a previous study [21], it is known that the value of the displacement thickness $\left(\delta_3^*\right)$ over the CWT-1 flat plate in dry conditions at 65 m/s is 2.7 mm. The value of S_{2eff} is fixed to a value such that the data reduction program which calculates $\left(\delta_3^*\right)$ values using the pressure measurements, yields a value of 2.7 mm for the smooth, dry cases. This value of S_{2eff} is used for all cases regardless of the temperature and surface configurations. Applying 13, one can calculate the displacement thickness at the outlet of the test section during a dry test with a smooth surface. However, for a wet configuration things change. When de-/anti-icing fluid is sprayed on the bottom wall, during the run, waves appear on the fluid surface. Since these waves transform a smooth surface into a rough one, a thicker boundary layer develops. Hence the thickness of the boundary layer is not the same at all four walls of the test section. Hence for the wet configurations, using 13, one can only compute the average displacement thickness of the four walls. Nevertheless, it can easily be derived that:

$$\delta_{3,ave}^* = \frac{c_3 - b_3}{c_3}\delta_{3,smooth,dry}^* + \frac{b_3}{c_3}\delta_{3,wet}^* \tag{14}$$

Manipulating this equation, one ends up with:

$$\delta_{3,wet}^* = \frac{c_3}{b_3}\left(\delta_{3,ave} - \frac{c_3 - b}{c_3}\delta_{3,smooth,dry}\right) \tag{15}$$

REFERENCES

[1] T. Nark. Wind tunnel investigation of the aerodynamic effects of type II anti-icing fluids when applied to airfoils. Document D6-37730, Boeing Commercial Aircraft Co., December 1983.

[2] M. Carbonaro, C. Locatelli, C. Mantegazza, C. Mcspadden, and I. Moller. Experimental study of the flow of a film of aircraft anti-icing fluid during a simulated take-off at subfreezing temperatures. CR 1985-02, VKI, May 1985.

[3] M. Carbonaro. Experimental study of the aerodynamic chracteristics of a two-dimensional wing model covered with de/anti-icing fluid during a simulated take-off at subfreezing temperature. CR 1986-22, VKI, August 1986.

[4] M. Carbonaro. Further study of the aerodynamic performance of a two-dimensional wing model covered with simulated frost or with de/anti-icing fluid during a wind tunnel simulated take-off at subfreezing temperatures. CR 1987-29, VKI, July 1987.

[5] T.A. Zierten and E.G. Hill. Effects of wing simulated frost on aeroplane performance. In *VKI LS 1987-03 on Influence of Environmental Factors on Aircraft Wing Performance,*, Rhode-St-Genèse, Belgium, February 1987.

[6] A.R. Mulally, M.D. Shirkey, and C.R. Higgins. Winter operations: keep it clean. *Boeing Airliner*, (October-December 1983), 1983.

[7] M. Carbonaro. Aerodynamic performance of a 2D wing model covered with various experimental de/anti-icing fluids during a simulated take-off at subfreezing temperatures. CR 1988-01, VKI, October 1987.

[8] L.J. Runyan, T.A. Zierten, and E.G. Hill. Flight and wind tunnel investigation of aerodynamic effects of aircraft ground deicing/anti-icing fluids. In *Flight in Adverse Environmental Conditions, AGARD CP-470*, Gol, Norway, May 1989.

[9] L. Macri and M. Carbonaro. Tentative correlation between loss on fluid contaminated wing and boundary layer modifications. SR 1988-33, VKI, September 1988.

[10] B. Moyaux and M. Carbonaro. Aerodynamic effetcs of aircraft anti-icing fluids. PR 1989-15, VKI, June 1989.

[11] P. Godrie and M. Carbonaro. Etude de l'aerodynamic de voiles de bateau. Graduation thesis, ULB, 1989.

[12] F.A. Dvorak. Calculation of turbulent boundary layer on rough surfaces in pressure gradient. *AIAA J.*, 7(9), September 1969.

[13] D. Bettermann. Contribution a l'étude de la couche limite turbulent le long de plaque rugueness. Raport 65-6, Laboratoire d'Aerothermique du C.N.R.S., 1965.

[14] P.G. Spazzini and M. Carbonaro. Boundary layer measurements over a 2D discrete roughness wall. SR 1991-05, VKI, November 1990.

[15] M. Carbonaro. Proposed specification for aerodynamic acceptance tests of aircraft de/anti-icing fluids. In *AIA TC Project 218-4 / AECMA Meeting*, number VKI PP 1990-20, Amsterdam, The Netherlands, April 1990.

[16] T.A. Zierten and E.G. Hill. Aerodynamic acceptance test for aircraft ground deicing/anti-icing fluids. Technical Report D6-55573, Boeing Commercial Airplane Company, March 1992.

[17] AEA Task Force on De-/Anti-Icing Aircraft on Ground. Recommendations for de- anti-icing of aircraft on the ground. Technical Report G.6807/R, AEA, March 1993.

[18] F. Gioia and M. Carbonaro. Evaluation of the aerodynamic penalties on an airfoil covered by de/anti-icing fluids and problems due to the test procedures. SR 1991-41, VKI, September 1991.

[19] T.C.G. Van Der Burght and M. Carbonaro. Testing of a modified fluid in the CWT-1 and analysis of several data reduction procedures. SR 1993-08, VKI, December 1992.

[20] L. Bluszez and M. Carbonaro. New data acquisition and processing on the CWT-1 facility. SR 1990-31, VKI, September 1990.

[21] E. Sardi and M. Carbonaro. Further analysis of procedures for aerodynamic acceptance tests of aircraft de/anti-icing fluids in the VKI cold wind tunnel CWT-1. SR 1991-25, VKI, July 1991.

[22] T.A. Zierten and E.G. Hill. Wind tunnel investigation of the aerodynamic effects of aircraft ground deicing/anti-icing fluids and criteria for aerodynamic acceptance. In *Effects of Adverse Weather on Aerodynamics, AGARD CP-496*, Toulouse, France, April 1991.

[23] P. Godrie and M. Carbonaro. Study of aerodynamic effects of ground de-/anti-icing fluids for commuters. CR 1992-31, VKI, August 1992.

[24] N. Ellis. Aircraft ground de-icing/anti-icing fluids with wind tunnel tests. 2nd entry in NASA Lewis IRT. In *ERA De/Anti-icing Task Force Meeting*, Frankfurt, Germany, September 1990.

[25] S. Özgen, M. Carbonaro, and R. Voets. Wind tunnel study of the interaction between a riblet surface and an aircraft de-/anti-icing fluid. CR 1996-21, VKI, February 1996.

[26] H. Choi, P. Moin, and P. Kim. Direct numerical simulation of turbulent flow over riblets. *Journal of Fluid Mechanics*, 255, 1993.

[27] M.J. Walsh. Drag characteristics of v-groove and transverse curvature riblets. In *Viscous Drag Deduction (G. R. Hough, ed.)*, AIAA, 1980.

[28] M. Mecham. 3M thin skin tested by airbus. *Aviation Week & Space Technology*, (December 2), 1996.

[29] F.S. Cunha and M. Carbonaro. Surface wave instability on aircraft de/anti-icing fluid films. In *First European Symposium: The Mechanics of Film Coating*, number VKI PP 1995-40, Leeds, United Kingdom, September 1995.

[30] J. Johansen and M. Carbonaro. Surface waves on de/anti-icing fluids. PR 1995-05, VKI, June 1995.

[31] F.S. Cunha and M. Carbonaro. A non-intrusive measurement technique for the study of surface waves on de/anti-icing fluids. Aeronautics/Aerospace Department, VKI, Belgium.

[32] O. Rumberg and G.S.R. Sarma. Two-layer flow instability. PR 1995-15, VKI, June 1995.

[33] S. Özgen and G.S.R. Sarma. Stability of parallel non-newtonian flows. PR 1995-22, VKI, June 1995.

[34] C.S. Yih. Instability due to viscosity stratification. *Journal of Fluid Mechanics*, 27(2), 1967.

[35] C.S. Yih. Wave formation on a liquid layer for deicing airplane wings. *Journal of Fluid Mechanics*, 212, 1990.

[36] O.J. Boelens, P.J.J. Moeleker, H. de Jong, and H.W.M. Hoeijmakers. Numerical methods for simulating the flow over an airfoil covered with a thin layer of liquid. Department of aerospace engineering, Delft Institute of Technology, The Netherlands, 1996.

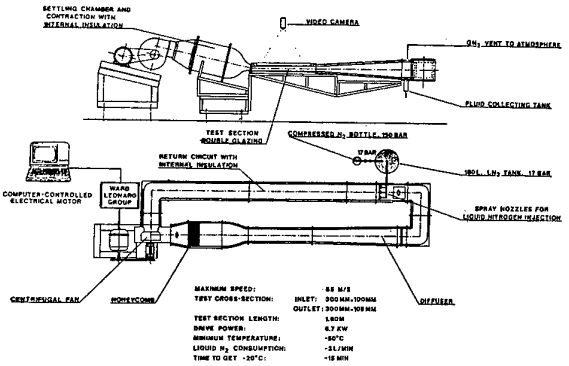

Fig. 1 : The VKI Cold Wind Tunnel

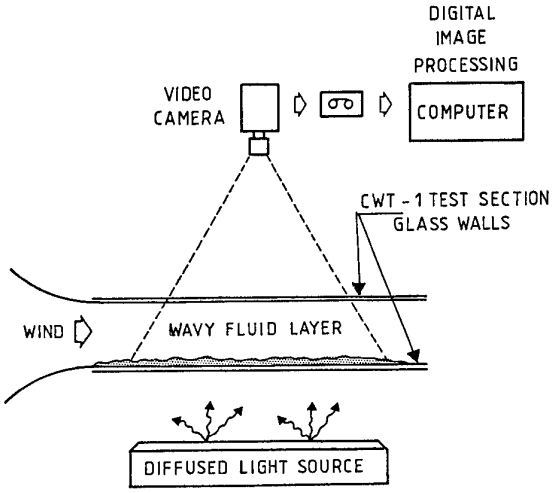

Fig. 2 : Set-up for measurement of local thhickness of a dyed fluid layer by a light absorption technique

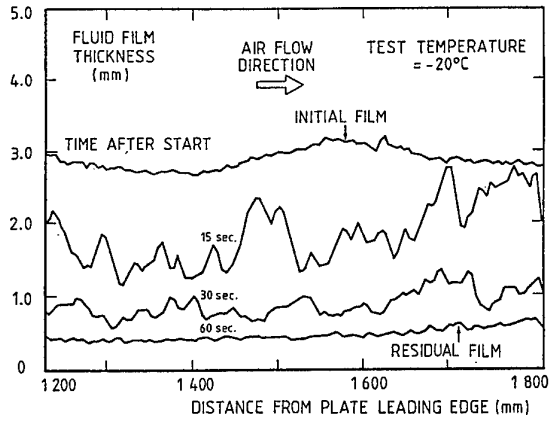

Fig. 3 : Time-dependent thickness profile of a layer of a specific anti-icing fluid on a flat plate under the effect of an accelerating motion

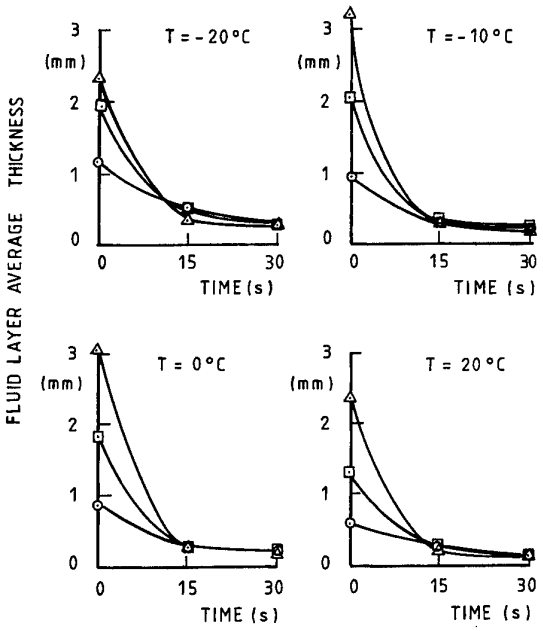

Fig. 4 : Variation with time of space-averaged thickness of an anti-icing fluid layer for various initial thicknesses and test temperatures

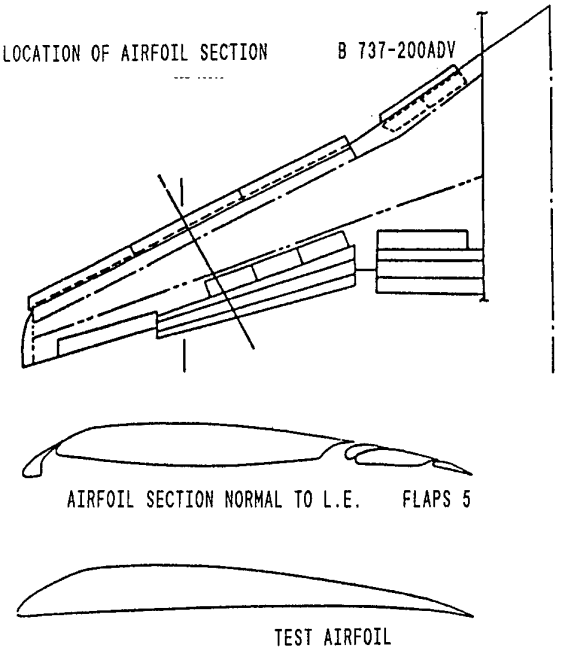

Fig. 5 : Section of the B737 wing selected as test airfoil

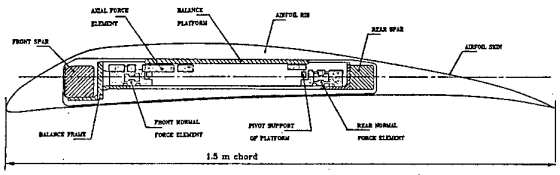

Fig. 6 : Test airfoil model and internal balance arrangement

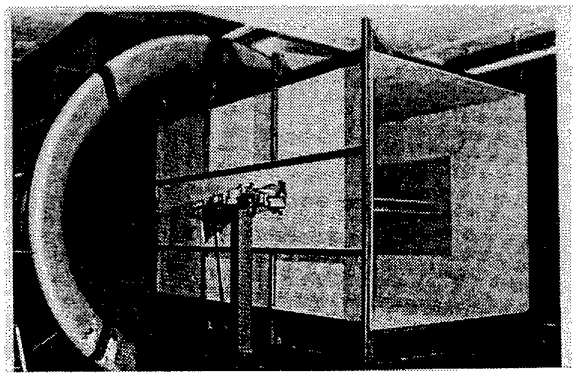

Fig. 7 : Airfoil model in test section insert for VKI L1-A and BFA wind tunnels

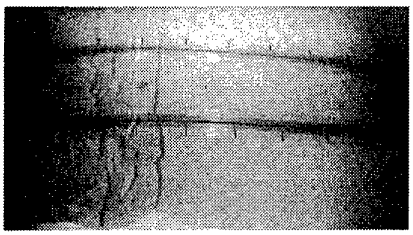

a) Initial wave formation

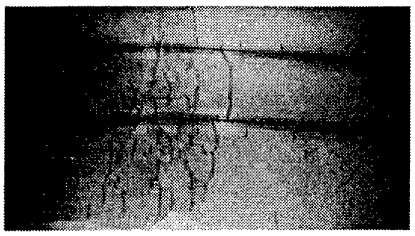

b) Merging of waves to form a single front

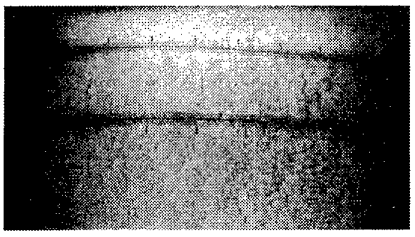

c) Wave front approaching trailing edge

Fig. 8 : Wind-induced surface waves on an anti-icing fluid layer deposited on upper wing surface

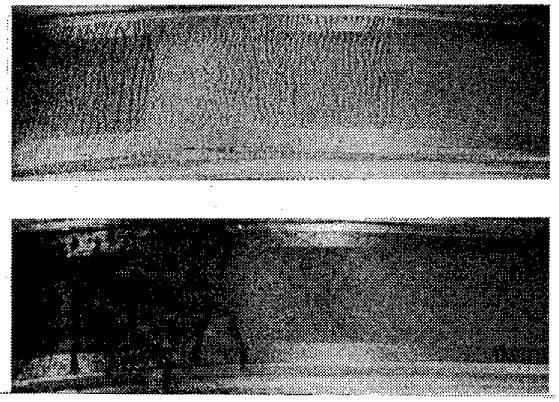

Fig. 9 : Difference in wind-induced surface waves for a newtonian de-icing fluid (upper) and a non-newtonian anti-icing fluid (lower)

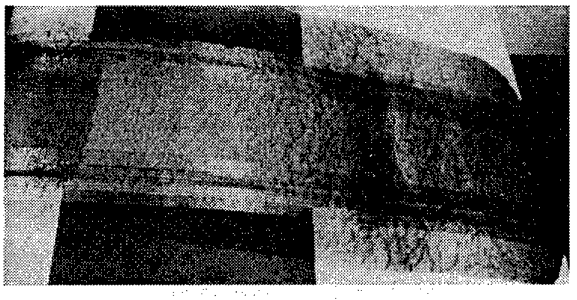

Fig. 10 : Second wave front appearing after the wing rotation maneuver

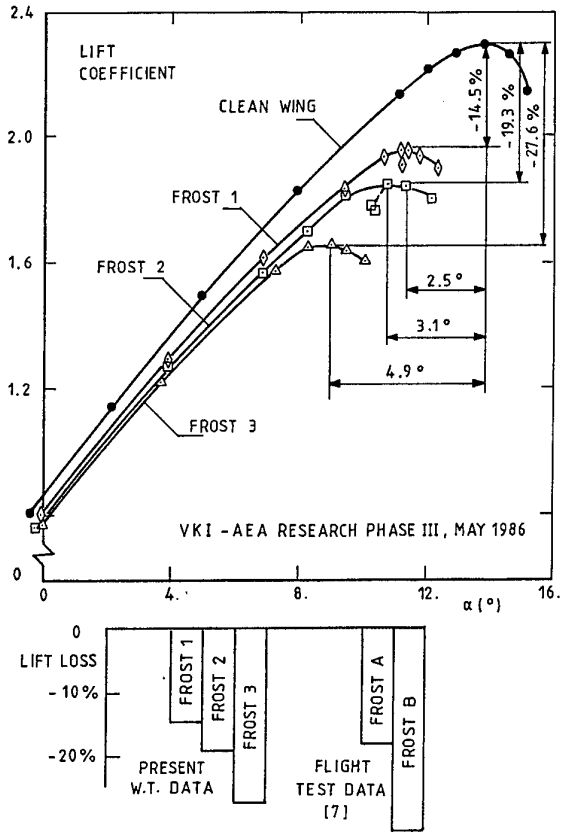

Fig. 11 : Lift vs. incidence curve of wing, clean or with roughness-simulated frost on upper surface

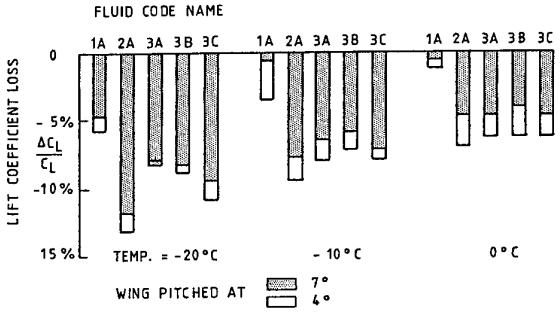

Fig. 13 : Loss in wing lift coefficient at two post-rotation incidences, for various fluids and temperatures

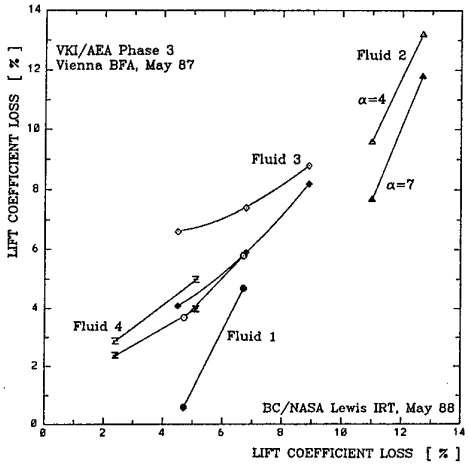

Fig. 14 : Comparison of lift coefficient losses measured in BFA and NASA-Lewis icing tunnels

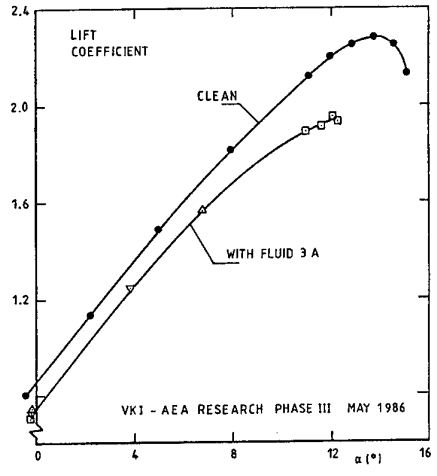

Fig. 12 : Lift vs. incidence curve of wing, clean or with an anti-icing fluid deposited on upper surface

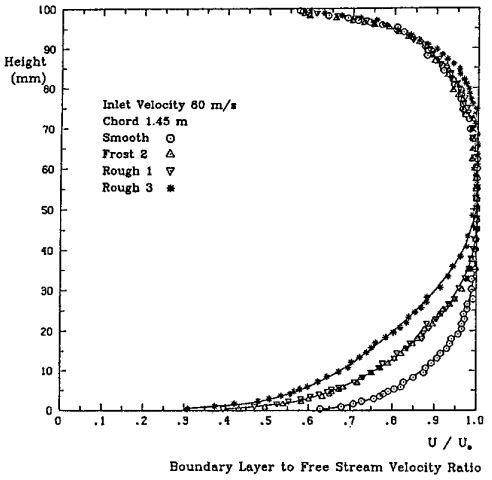

Fig. 15 : Vertical profile of velocity at the exit of the test section of the VKI CWT-1 facility

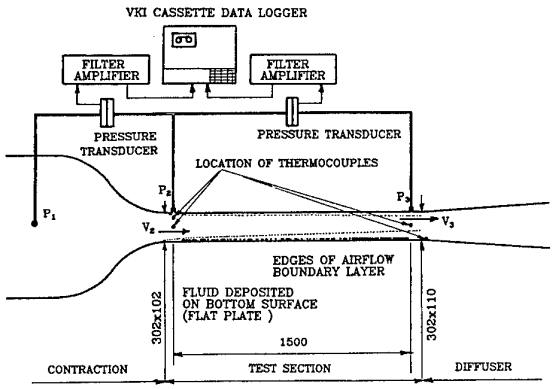

Fig. 16 : CWT-1 test section and instrumentation setup

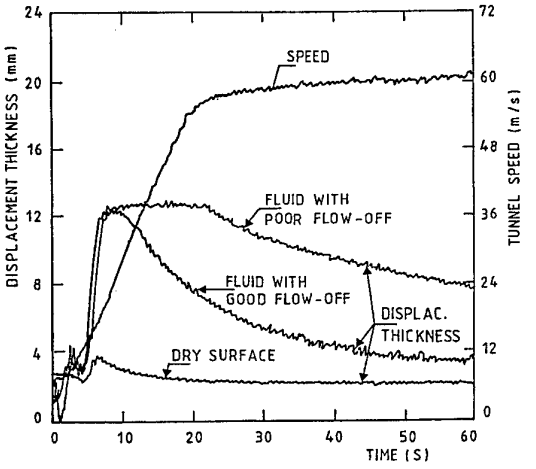

Fig. 17 : Typical results of CWT-1 flow-off tests, with bottom flat wall of test section clean or covered with fluid

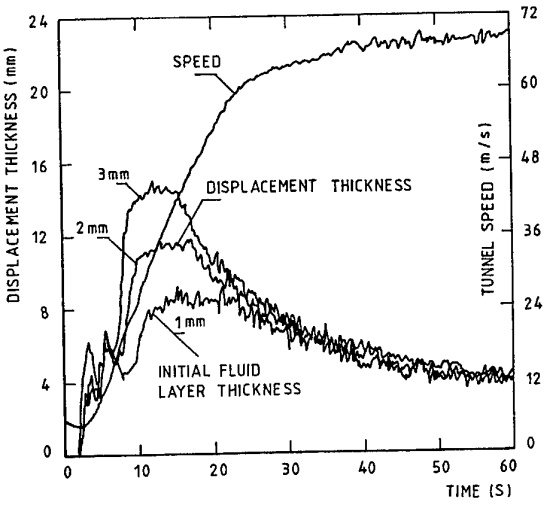

Fig. 18 : Effect of initial thickness of fluid layer on the measured boundary layer displacement thickness

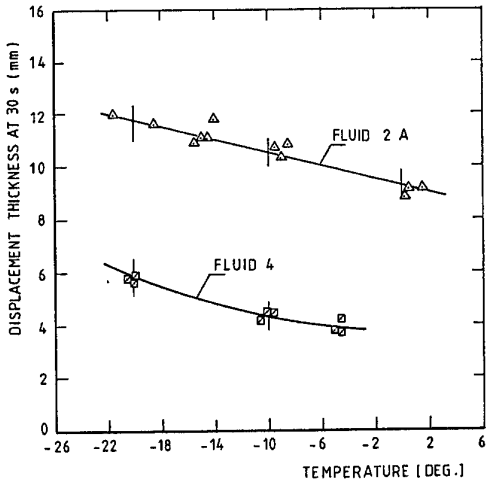

Fig. 19 : Characterization of the temperature-dependent flow-off behaviour of a fluid

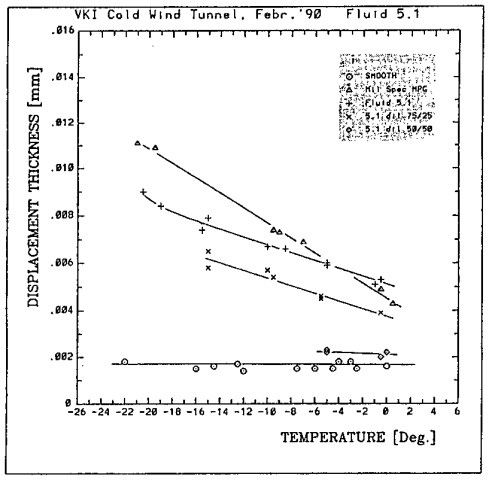

(a)

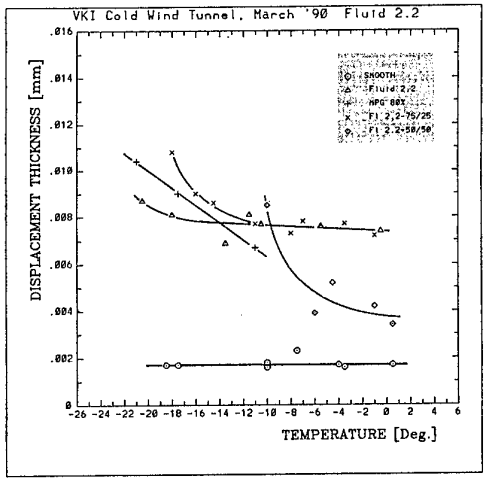

(b)

Fig. 20 : Effect of water dilution on the flow-off behaviour of two different anti-icing fluids

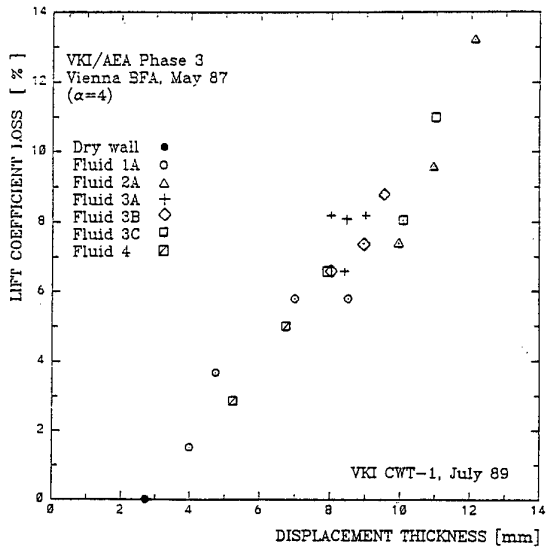

Fig. 21 : Correlation between boundary layer displacement thickness in CWT-1 and airfoil lift coefficient loss measured in BFA icing tunnel

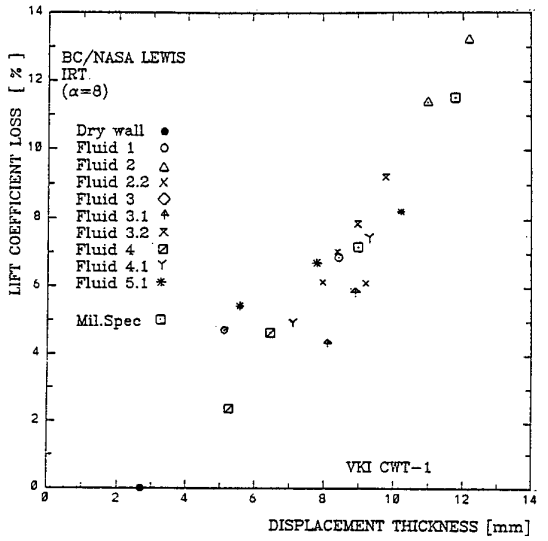

Fig. 22 : Correlation between boundary layer displacement thickness in CWT-1 and airfoil lift coefficient loss measured in NASA Lewis icing tunnel

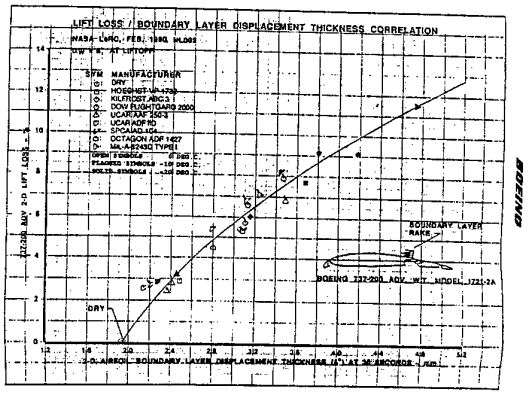

Fig. 23 : Correlation between 2-D airfoil boundary layer displacement thickness and 3-D lift loss

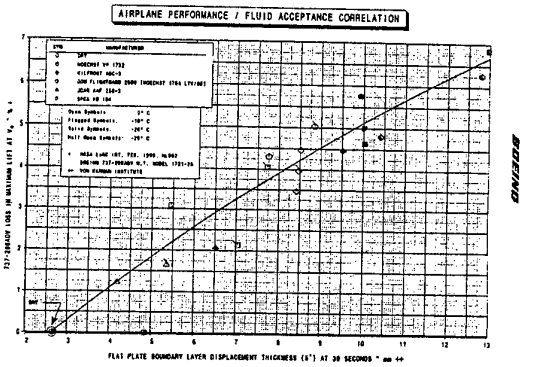

Fig. 24 : Correlation between flat plate boundary layer displacement thickness and 3-D lift loss

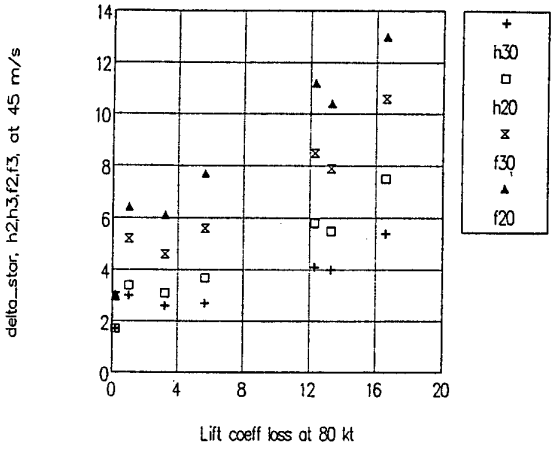

Fig. 25 : Correlation of boundary layer displacement thickness measured at various locations and times with lift loss

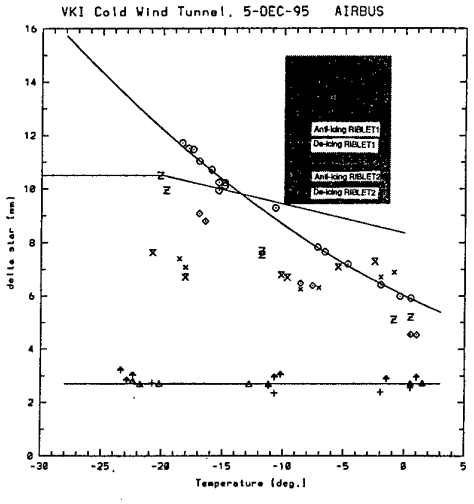

Fig. 26 : Comparison of the aerodynamic acceptance test results of riblet1 and riblet2 configurations

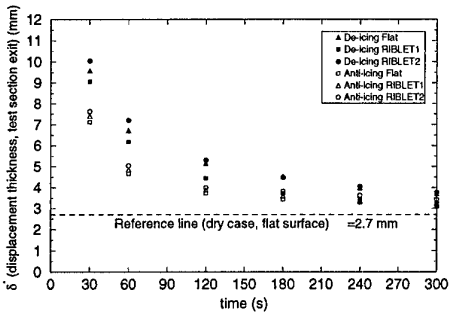

Fig. 27 : Displacement thickness histories for the three different surface configurations in clean or fluid contaminated conditions (V=65m/s)

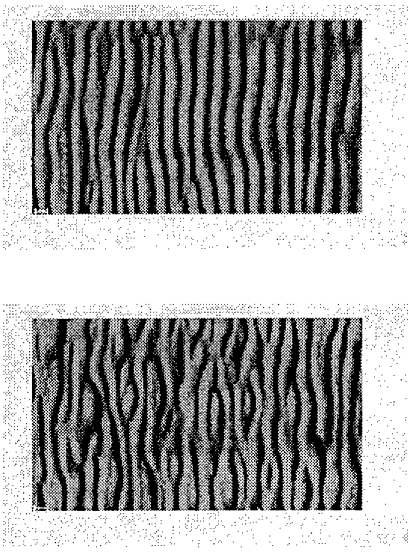

Fig. 28 : 2-D sinusoidal surface instability on a de-icing fluid film (top), 3-D surface instability breakdown on a de-icing fluid film (bottom)

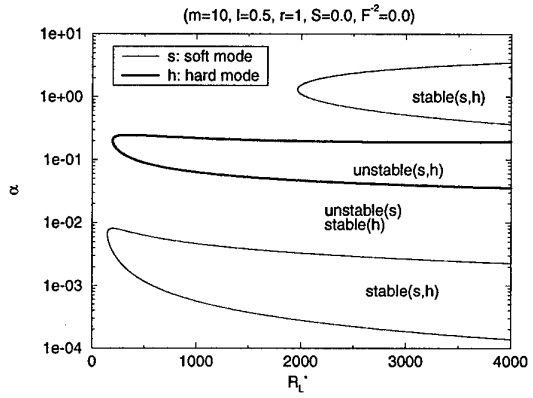

Fig. 29 : Two-fluid boundary layer stability modes (thick line belongs to the hard mode)

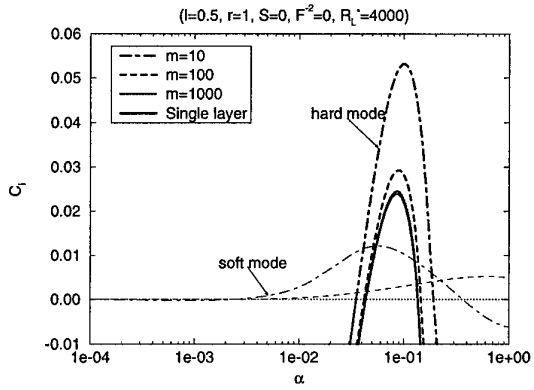

Fig. 30 : The effect of viscosity stratification on hard and soft modes (thick line belongs to the hard mode)

"APPENDIX B"

EFFECT OF HEAVY RAINFALL ON AIRCRAFT PERFORMANCE

by

A. Feo
INTA
EXPERIMENTAL AERODYNAMICS DPT.
28850 TORREJON DE ARDOZ (MADRID)

Lecture presented at the
von Karman Institute for Fluid Dynamics
Lecture Series Entitled
"Effect of Icing, De-icing and Heavy Rain on Aircraft Performance"
February 1997

I. INTRODUCTION

Studies of weather related aircraft accidents have shown that a considerable number in which low altitude wind shear has been a contributing factor, have been classified as intense or heavy rain encounters. They have led to reconsider high-intensity, short duration rainfall as a potential aircraft safety hazard, particularly for the take-off or approach phases of flight. As a consequence, interest in aircraft performance degradation due to heavy rain has been growing in recent years.

An early investigation of the effect of rain [(1)] dealt with the case of a moderate altitude flight (5000 ft) heavy rain encounter. The conclusion of this study was that although the torrential rain had a significant effect on airplane performance, was insufficient to force a cruising vehicle to the ground. No new studies were performed until attention was focused onto the fact that heavy rain was present in a number of aircraft accidents in take-off and/or landing phases of flight. Approximate estimates of the different effects present in heavy rain, showed that an airplane in landing configuration does not have a wide margin of performance in which to overcome the aerodynamic penalties of rain[(2)].

Heavy rain affects the aerodynamics of the airplane acting through: a) a continuous surface film that interacts with the boundary layer, including its break down into run-off streams; b) water drop cratering associated with an equivalent surface roughness; c) Momentum exchange between ejected droplets from incoming drop impacts and air boundary layer. These phenomena act simultaneously, presenting a complex fluid dynamics problem, whose general solution will lead to the understanding of the causes of the airfoil aerodynamic degradation by a low quality, two component, two-phase flow.

In this paper, studies done to the present time in this area are reviewed complementing previous overviews [(3), (4)]. Here is included, a discussion of the nature of heavy rain, the analytical work on airfoil rain effects and the results of different experimental methods and techniques, paying particular attention to scaling considerations. Complete understanding of the influence of heavy rain and associated issues, still requires considerable additional effort in both, the analytical and experimental side of the problem, before a comprehensive assessment of the hazard to aircraft flight operations can be established with confidence.

II. CHARACTERISTICS OF HEAVY RAIN

Natural rain needs to be understood if analytical models and representative experiments are to be developed. To adequately assess the safety hazard, rain parameters such as rainfall rate, its drop size distribution and frequency of occurrence needs to be known

The rainfall rate (RR) is the water accumulated measured in length units at ground level per unit time. This is alternatively measured by another variable called the liquid water content (LWC), which is the mass of water in a unit volume of air. There is a direct relationship between these two variables in the absence of vertical wind velocity, through the terminal drop velocity which is the drop's fall velocity at ground level. In metric units RR is normally measured in mm/hr and LWC in g/m^3, being the expression for an idealized situation with uniform drop size distribution:

$$RR\ (mm/hr) = 3.6 \times V_t\ (m/s) \times LWC\ (g/m^3)$$

where V_t is terminal drops velocity

In natural rain the drop size distribution is given by [5]:

$$N(D) = N_o e^{-ID}$$

where N(D) is the number of drops per cubic meter of air per unit interval, D is the drop diameter $I = nR^m$, where n, m and N_o are empirically determined constants, depending on the type of precipitation considered and R is the rainfall rate. For light continuous rain values for these variables are [5] : $N_o = 8 \times 10^3$, n = 4.1 and m = -0.21 In References 6 and 7 , values for a heavy thunderstorm are: $N_o = 1.4 \times 10^3$; n = 3.0 and m = - 0.21.

Given a drop size distribution, LWC can be calculated by the expression:

$$LWC = \frac{\pi}{6}\rho_w \int_o^\infty D^3 N(D) d(D)$$

ρ_w being the density of water. After integration we have:

$$LWC = \frac{\pi \rho_w N_o}{n^4 R^{4m}}$$

once the substitution of $I = nR^m$ has been performed. Introduction of numerical values of References 5 and 6 for light continuous rain and storm rain conditions, the following are obtained respectively:

$LWC = 0.08894\ R^{0.84}$ (Light Continuous Rain)

$LWC = 0.0540\ R^{0.84}$ (Thunderstorm)
which are represented in Fig. 1.

The range of rainfall rate an airplane may be expected to encounter varies from light rain of 5 mm/hr to very large values in rain storms. The ground level world record is 30.5 mm in one minute [8], equivalent to 1830 mm/hr. However, significantly higher liquid water concentrations exist inside thunderstorms, probably in convergence regions of the storm. Reference 9 shows values that when converted to rainfall rates range from 400 mm/hr to 2920 mm/hr. At the same time, ground radar measurements indicated considerable lower rainfall rates.

The potential frequency for encountering a given rainfall rate at a given climatic zone may be obtained from the work reported in Reference 10. A frequency distribution was measured in different world zones and an average was obtained for each climate zone (Fig. 2). The probable number of minutes in a year, a given rainfall rate can be expected for each of the considered zone, can be obtained by converting the percentage ordinate to fractional and then multiplying by 5.2596×10^5 (number of minutes in a year). From this Figure, for about two

minutes, every year in the maritime subtropical zone a rate of at least 200 mm/hr may be reached.

A recent review of the methods to obtain instantaneous rainfall rates, have determined that the obtained measurements masks the short-duration high-intensity rainfall characteristics [11], [12]. In the new technique, data is taken at short time intervals and has verified the existence of high-intensity rainfall rates at ground level. In Fig. 3, data are presented as percentage of the total number and is observed that one quarter percent of events measured were above 508 mm/hr, and sustained up to 10 seconds per event.

III. ANALYTICAL WORK

The computation of the aerodynamic characteristics of airfoils immersed in a rain environment is not yet a mature technology due to the interaction of the complex existing phenomena. The environment consists of water drops with certain size distribution, whose local impingement efficiencies should be calculated. The physics of the drop impacts on a wet surface is to be understood to supply data of the crown, filament and droplet ejecta characteristics. The drops are partly deposited as a liquid water film breaking down into rivulets that interact with the airfoil's air boundary layer. Modification of the transition and separation locations pose a new challenge not yet solved, although some studies have been performed, directed at the understanding of some partial aspects of the problem.

Rhode [1] was one of the first to address the problem of possible performance degradation of an airplane due to a rain encounter. He calculated the drag increase in a cruise flight when encountering a rain of liquid water content of 50 g/m^3. He found a reduction of 18% in airspeed due to drag increase. The effects of heavy rain on landing or take-off was not considered.

The calculation of drop trajectories around an airfoil has been done for small droplets from 10 to 100 microns for the purposes of studying ice accretion (References 13 to 17). In a rain flow field, drops as large as 7 mm have to be considered. Haines and Luers [18], [19] estimated the skin friction increase due to drop cratering and film waviness. The drop cratering effect was equated to an equivalent sand grain roughness. Calculations for both wing and fuselage of a large airplane, gave increases in total drag ranging from 1.6 to 5.9 percent for rainfall rates form 100 mm/hr to 2000 mm/hr. The waviness effect estimate was from 2.1 to 4.6 percent for the same rainfall rates. The combined drag penalty was estimated to be from 10% to 50%.

They also hypothesized that the roughness effect gave changes in maximum lift and stall angle of attack. Decreases in C_{Lmax} for drop cratering and waviness ranged for each one from about 10% to 50% and corresponding to decreases in stall angle of attack from 1 to 6 degrees for each effect. They considered that these penalties are serious to attract consideration for a landing aircraft in a thunderstorm. Since these were rough estimates, they also recommended experimental validation of their results.

Calarese and Hankey [20] studied numerically droplet drag acting as a body force in the Navier-Stokes equations on a NASA 0012 airfoil neglecting interfacing effects as cratering, splash-back and water-film formation. For coarse rain (large drops and large Reynolds number) they obtained little change in pressure distribution. For fine rain (small drops and small Reynolds number) significant changes in airfoil pessure distribution were predicted showing small increases in lift with increasing liquid water content.

Kisielewski [21] did a 3-D Euler analysis to investigate momentum and energy exchange between the rain and the air flow field. The conclusion was that there was little effect on the calculated lift on an airfoil.

The conclusions from these last two works is that the major influence of rain on airfoil aerodynamic characteristics must probably come from viscous effects within the air boundary layer interacting with the resultant drop phenomena after impacting with the airfoil surface, which were not considered in their models.

Anderson and Chappidi [22], established a computational model of a two-phase boundary layer and estimated the water film thickness that forms due to rain on an airfoil surface. The air boundary layer is coupled with the water film, including the pressure gradient due to airfoil curvature. However, effects such as surface tensions, waviness and cratering are not considered in this theoretical model.

Donaldson [23] and Donaldson and Sullivan [24], took into consideration the effects of variations in momentum deposition of droplets that are splashed back into the air stream upon striking the airfoil surface. They modified a computational code to allow splashed back droplets to affect the separation location at high angles of attack and see under what conditions stall could be induced. Also, it was intended to obtain information on how to conduct properly scaled tests of airfoils in heavy rain. They estimated the ejected droplet's diameter to be inversely proportional to the square of the incident velocity, an adjustment length proportional to that diameter and a mixed Weber number formed by density of air and surface tension of water, having an effect similar to rainfall rate. The examination of NASA-Langley experimental data showed that Clmax decreased with increasing Rainfall Rate (RR) for a given mixed Weber Number (N_D) and also decreased for increasing N_D for a fixed RR. Calculations with the computational code for a NASA 64-210 airfoil $\alpha = 12^0$; of critical RR showed a decrease with N_D increasing at fixed Re and an increase with Re, for a fixed N_D.

Bilanin et al. [25] studied the feasibility of estimating the degradation of performance of airfoils from first principles. The analytic effects were supplemented by a droplet splashback test program in order to understand the physics of impact and the generation of ejecta. The modelling of the coupling of drop impingement and splash-back was made via the imposition of a drag force in the momentum equation near the surface. A given flux of rain is assumed to penetrate a layer of specified thickness. This influx was then assumed to splash into droplets of pre-determined radius and drag coefficient and to remain trapped within the specified layer for the remainder of the calculation. The model required the selection of a number of parameters, such as the droplets radius resulting from the impact, liquid water content, incident drop speed and incidence angle. The droplet layer thickness and air reference velocity within the thickness were also needed. Sample calculations were made which included the free stream pressure gradient and surface slope of an NACA 64210 airfoil. Velocity profiles obtained in the boundary layer are noticeably flatter than the "dry" case, indicating that the separation process is anticipated by the presence of heavy rain. The values of the estimated parameters were confirmed from observations of the conducted experiments. It was concluded that given the complexity of the physics of drop impact and splashback, it is not likely that in the near future, it will be possible to predict performance degradation of airfoils in heavy rain directly from first principles.

IV. EXPERIMENTAL METHODS AND RESULTS

The experimental investigation of rain effects on aircraft aerodynamics requires the elaboration of new instrumentation and test techniques.

Full-scale flight research programs need the measurements to be made while the airplane is inside a rainstorm presenting hazards to the pilot and the extraction of accurate flight results and environmental parameters are difficult and costly and of impossible repeatability. Ground model tests are faced with different challenges, one being the proper simulation of the rain environment. To simulate and measure any rain effects three types of facilities have been used depending on the purposes sought. They are: 1) Rotating arms, 2) Conventional wind tunnels and 3) Large-scale acceleration tracks.

Rotating arms have been used to analyze specific rain effects, when centrifugal forces can be shown not to be important. To determine performance degradation parameters, wind tunnels and acceleration tracks are necessary. In conventional wind tunnels, when supplemented with the rain simulation hardware, special attention should be paid to preserve flow quality and to generate a uniform water distribution in the test volume. The acceleration tracks need very elaborate and extensive water manifolds to allow for sufficient test time inside the rain to reach a steady state in which to perform the measurements.

IV.1 Non-Dimensional Analysis

Being the computational models of airfoils immersed in heavy rain inexistent, experiments are primarily the tool to supply information in this complex problem. Due to the large number of variables involved, dimensional analysis is necessary to obtain a reduced number of non-dimensional parameters under which experimental results may be generally applicable. Bilanin [26] has addressed the scaling problem of an airfoil in heavy rain. He has estimated the condensation and evaporation effects on an airfoil lift curve slope, concluding that thermodynamic variables could be discarded in the problem.

The airfoil surface was considered smooth and gravity effects neglected. Under theses conditions, the variables controlling the force exerted on an airfoil immersed in a two phase flow, consisting of water drops moving at the same velocity as the air, are:

Symbol	Variable	Units
F	Force	MLT^{-2}
c	Airfoil chord	L
l	Model Span	L
α	Model angle of attack	radians
U_∞	Air speed	LT^{-1}
D	Average drop diameter	L
λ	Mean drop spacing	L
ρ_a	Density of air	ML^{-3}
ρ_w	Density of water	ML^{-3}
ν_a	Kinematic viscosity of air	L^2T^{-1}
ν_w	Kinematic viscosity of water	L^2T^{-1}
$\sigma_{w,s}$	Surface tension water-solid	MT^{-2}
$\sigma_{a,s}$	Surface tension air-solid	MT^{-2}
$\sigma_{w,a}$	Surface tension water-air	MT^{-2}

The non-dimensional force coefficient $\frac{F}{\rho_a U_\infty^2 cl}$ is dependent on the following non-dimensional parameters

1) $\quad Rea = \frac{U_\infty c}{\nu_a}; \frac{l}{c}; \alpha$

These are the air Reynolds number, the length to chord ratio and the angle of attack. All of them are present in the corresponding dry tests.

2) $$\frac{\rho_a}{\rho_w};\mathrm{Re}\,w=\frac{U_\infty c}{\nu_w}$$

If air and water conditions are preserved between experiments, the first parameter is automatically kept. In this condition if Rea is kept so is Rew.

3) $$\frac{D}{c};\frac{\lambda}{c}$$

They indicate that both relative mean drop size and mean drop spacing should be preserved. Generally these two parameters are reduced to only one, this being the liquid water content (LWC).

4) $$W_e=\frac{\rho_w U_\infty^2 D}{\sigma_{w,a}};\frac{\sigma_{w,s}}{\sigma_{w,a}};\frac{\sigma_{a,s}}{\sigma_{w,a}}$$

The first is the Weber number and the other two are surface tension ratios. Note that adding to the water a surface tension reducing agent, changes in the three parameters are produced.

The importance of an analysis of this type in heavy rain is mainly for the scaling of reduced size model tests, as it will permit, once the behaviour of the parameters is known, the establishment of a methodology used for simulation and experimental extrapolation to full scale values.

IV. 2 Some measurements on single drop impacts and surface water films

To understand the various individual phenomena that influence heavy rain airfoil aerodynamics, the development of test methods and techniques is necessary. They are important not only for the physical interpretation of the overall performance degradation but for the establishment of theoretical models to predict it.

Drop impacts are micro-second occurrences, needing accurate synchronization systems, to capture its details and evolution. Depending on its angle of incidence, they are classified as 1) Low, for the impacts with all the ejecta taking place on the upstream side, approximately for $\beta \leq 12°$ (Fig. 4). 2) Intermediate, with ejecta taken place all around the crown, but most of it from the upstream side $12°\leq\beta\leq 45°$. 3) High incidences, where ejecta is quasi-symmetrically distributed all around for $\beta>45°$. Cases 1) and 2) are treated in Ref 27. Schematics, photographs and results are shown in Fig. 5 to 14. Case 3) is treated in Refs. 28 and 29. Schematics, photographs and results are shown in Fig. 15 to 17. This case is relevant to impacts taking place on the airfoil leading edge and conditions the subsequent boundary layer evolution, particularly near the stall angle. Evaluation of these results have led to the following considerations:

a) The ejected droplets have diameters of a few microns, their velocities are initially much larger than the incident velocity, are directed at large cone angles and interact very effectively with the air boundary layer.

b) More mass of water remains on the surface than is ejected and the airfoil performance degradation is complicated by film dynamics, impact cratering and surface waviness.

c) The final airfoil aerodynamics degradation is the product of interaction of the several mentioned phenomena (ejecta, cratering, film-dynamics and waviness), and is unlikely that predictions from first principles can be established.

Drop impact investigations have been supplemented with surface water film waviness measurements on airfoils. Evaluation of the results helps the understanding of the aerodynamic performance loss and in the establishment of film dynamics theoretical models.

Some initial film thickness measurements were made in a small (0.3m chord)

NASA 0012 airfoil [30]. The general results showed an increase in thickness with increased LWC, thicker films on the lower surface and a general decrease in thickness for increasing angle of attack.

Later, tests on an NACA 64-210 airfoil with 0.75 m chord were made in the 4m x 7m Low Speed Wind Tunnel at NASA - Langley [31]. For the cruise configuration a continuous film on the upper surface with a maximum in thickness at $x/c \simeq 0.3$ location, is measured. Complementary tests done in the same facility have shown similar trends for the different conditions tested [32]. In Fig. 18 is shown the increase in film thickness with LWC. The Reynolds number effect is shown in Fig. 19 for α =-2° and LWC = 39 g/m^3. The increase in angle of attack shows a general decrease in film thickness on the upper surface up to the stall angle (α=14^0) and abrupt increase after this angle (Fig. 20). Evaluation of these results, tells that the upper surface water film may be responsible for increased skin friction and premature boundary layer separation. On the lower surface, the air boundary layer is mostly laminar and early transition is the probable cause of a decrease in performance.

For the high-lift configuration tests (Fig. 21), the film thickness on the upper surface is again thinner than on the lower surface (Fig. 22 and 23). In these Figures it is observed that an increase in Reynolds number produces an increase in film thickness on the lower surface and a decrease on the upper. Evaluation of the available data tells that the performance decrements may be due to water flowing through the gaps at large angles of attack.

Water film thickness measurements have also been made on a large scale wing section model. They were conducted in a NASA-Langley's Acceleration Track, on an NACA 64-210 airfoil. Two sensors were located at x/c=0.1 on a 3 m chord, 3.9 m span wing section. Circular end plates of 4.5 m diameter were placed at each side of the model that was equipped with leading and trailing edge high lift devices. For rain rates of 1000 mm/hr, time dependent film thickness is shown in Fig. 24 and 25 for both upper and lower surface locations. For rain rates of 482 mm/hr, lower surface location indicates the values for 82 m/s and 52 m/s and several angles of attack (Fig 26 and 27). Results for the upper surface location and same speeds are shown in Fig. 28 and 29. From the lower location values is possible to observe some trends that tend to confirm the wind tunnel results. For α = 13.5° and 82 m/s the increase in LWC increases the thickness. However for α = 15.5° and rain rate of 482 mm/hr a decrease in Reynolds number show an small increase in film thickness.

All the film thickness measurements have been made with conductance sensors installed flush to the surface [33].

IV. 3 Low Reynolds number and laminar airfoils

General aviation and sport aviation airplanes use airfoil sections designed for significant amounts of natural laminar flow. As part of a -general aviation stall/spin research program the sensitivity associated with early transition due to rain was investigated by NASA [34]. A full-scale model was installed in the 30 by 60-feet low speed wind tunnel at the NASA-Langley Research Center. The rain was sprayed only on the starboard canard surface at a velocity of 68 mph, and an LWC of 3.6 g/m^3 (Fig 30). Test results for the lift and drag on the canard surface are shown in Fig. 31. It is observed that the water effect was about one half as severe as the effect of tripping the laminar boundary layer. For this configuration and the conditions mentioned the effect of rain appeared equivalent to fixing transition.

Similar results have been obtained at MIT [35]. In those tests a 6 inch chord

Wortmann FX-67-K170 natural flow airfoil was studied in a 1-foot by 1-foot low speed wind tunnel. The Reynolds number was 3.1 x 10^5 and LWC was 14.6 g/m^3. The data shown in Fig 32 indicates that the effects of simulated rain and fixed transition may be compared directly. Transition fixed at 25% chord agreed with water spray data, but fixing transition near the leading edge produced a more severe effect. This work also showed the performance degradation dependence on surface wetting characteristics, as indicated in Fig. 33. A non-wettable surface is one on which an spherical drop of water remains the same, whereas a fully wettable surface is one on which a drop flows to form a thin uniform film. In reality, surfaces fall between these two extremes. The data show that a waxed surface produced the largest lift loss and was comparable to changes noted for fixing transition near the leading edge.

A number of wind tunnel tests have been conducted to determine the influence of rain on the aerodynamic performance of a Wortmann FX 63-137 wing at Reynolds number from 10^5 to 3 x 10^5. Results reported in Reference 36, show an improved performance at the lowest speed and general deterioration at higher speeds. The primary effect is a decrease of lift at high angles of attack and elimination of stall hysterisis, characteristic of the Wortmann's performance at low Reynolds numbers. Also tests were performed using a waxed wing surface and the results showed that waxing produced increased beading, further reducing the lift.

Another group of tests at low Reynolds number are reported in Reference 37 on an NACA 4412 airfoil at rain rates of 77 to 137 mm/hr, mean drop size of 18 μm and a chord Reynolds number of 2.5 x 10^5 . Results are presented as increments of lift, drag and moment coefficient for clean, grit-tripped and wire-tripped wings. Emphasis is placed in correlating these rain induced increments with the surface water film behaviour. Four regions of surface flow are identified, each one covering the airfoil surface and changing with the angle of attack. One important result is that transition fixing for wings in rain does not represent an effective increase in Reynolds number and would not represent a proper simulation between flight and wind-tunnel data in rain conditions.

IV. 4 Conventional airfoils and high-lift systems

NASA has developed new test techniques, procedures and conducted a series of tests, both in a wind tunnel and in a large-scale acceleration track, to determine degradation of aerodynamic characteristics of conventional airfoils and high-lift systems.

IV. 4 .1 Wind Tunnel Tests

Tests were performed in the NASA-Langley 4 by 7 meters subsonic tunnel with a 50 ft. long test section. Typical set-up and schematic of the test technique employed are shown in Fig. 34 and Fig. 35. The water spray distribution manifold shown in Fig. 36, was located approximately 10 wing chord lengths upstream of the model location, directing the spray horizontally while aerodynamic forces were obtained. Shape and location of the spray manifold were selected to minimize interference effects and to allow time for stabilization of the accelerating water drops. Also, the system was aligned above the chord plane to account for gravity effects of the drops. Comparisons of model aerodynamic data in and out of the rain environment were made with the spray manifold in position at the all times.

The characteristics of the simulated rainfield was quantified in terms of LWC, drop size distribution and drop velocity. The Jet Propulsion Laboratory, under contract to NASA [38], developed a nozzle system,

consisting of a series of hypodermic tubes around a plenum which would provide control on drop size and rain intensity independently. (Fig. 37).

Exploratory tests were initially conducted on a wing with an NACA 0012 airfoil section fitted with full span trailing edge flap for Reynolds numbers ranging from 1.2 to 1.7 x 10^{6}[3]. Transition was fixed at 5 percent chord for all tests. Lift and drag data are shown in Fig 38 for the higher Reynolds number and LWC from 13.1 to 22 g/m^3. All spray concentrations caused about the same reduction in lift coefficient, the measured reduction in maximum lift was not as pronounced for the lower velocities. Drag increase was noted for all spray concentrations and speeds. The airfoil was fitted with a simple full-span trailing edge flap having a chord equal to 30-percent of the mean aerodynamic chord. The lift and drag coefficient data for this configuration with flap deflection of 20 degrees is shown in Fig 39 for the same rain intensity as before. All rain concentrations resulted in approximately the same amount of reduction in lift; the maximum lift coefficient being reduced about 15 percent for both the flapped and unflapped wings.

A cambered airfoil representative of the type used on commercial transport airplanes has been also tested in the Langley Research Center 4 by 7 meters subsonic tunnel [39], as shown in Fig. 40. The model has an NACA 64-210 airfoil section. of rectangular planform , and is mounted between two endplates. Wing chord is 2.5 feet and span between endplates is 8 feet. A 1 foot span section in the center of the model is supported separately from the outer panels by an external strain gauge balance that measures forces and moments. The model was equipped with leading edge slat and double slotted flap as shown in Fig. 41. Tests were conducted at Reynolds numbers ranging from 1.8 to 3.2 x 10^{6} based on chord length. Transition was fixed at the 5 percent chordline. Liquid water content varied from 16 to 47 g/m^3.

Lift and drag measurements for the basic 64-210 airfoil section are shown in Fig. 42 and 43. For the indicated conditions there was little effect of the water spray on lift but there was a noticeable increase in drag. For the 64-210 wing with flaps and slat deployed a reduction in maximum lift was measured for all test velocities and all spray intensities. Results are shown in Fig. 44 and 45.Sensitivity to test speed and spray concentration are observed for this data set. Transition was fixed, the data indicating a sensitivity that is not accounted for in normal Reynolds number scaling. This particular configuration caused about a 20 percent reduction in maximum lift and a reduction in stall angle of about 8° for the lower Reynolds number.

Additional tests were conducted using the same configuration with an NACA 64-210 airfoil to explore the sensitivity of this configuration to surface tension effects. A surface tension reducing agent was mixed with the water prior to injecting the water spray into the wind tunnel. Lift and drag results have been obtained for dynamic pressure of 30 and 50 lb./ft^2. Comparisons with the corresponding results obtained with plain water show only small differences. Comparing with wettability effects obtained for laminar airfoils although made with different methods, it appears that the sensitivity to surface tension may be different for rain effects on laminar flow airfoils as compared to turbulent boundary layer, high lift configured airfoils.

In Reference 40 results are shown for a modified NASA 65_2215 airfoil with leading edge slat and two element trailing edge fowler flap and two different surface treatments. One was an epoxy painted surface and the other was a base metal surface. Although surface contact angle for the surfaces was not reported, there was a

significant difference between surface tension characteristics of the two surfaces. The results show an small but measurable difference in performance degradation between the two sets of results.

Visualization photographs show the water flow on the upper surface of the wing in different attitudes. In Fig. 46 the view was taken with the optical axis 18° displaced from the vertical and for an angle of attack of 8° and 45 g/m^3. A thin water film with run-off rivulets can be observed on the aft of the upper surface and the upper surface of the flap appear to have higher concentrations than the wing. Some of the water appears to be coming from the underside through the flap gap openings. The results of the water film measurements have indicated that the film is thicker on the lower surface than on the upper surface.

Fig. 47 is for α = 20°, LWC = 45 g/m^3 and dynamic pressure of 30 $lb./ft^2$. It shows the wing having a large three dimensional region of separated flow indicating that it was stalled due to premature flow separation.

IV. 4.2 Large-scale tests

Because the extrapolation of results from sub-scale wind tunnel tests is uncertain, it has been necessary to conduct experiments at full scale in order to evaluate rain effects. For that purpose a large-scale ground testing capability has been developed at the NASA-Langley Research Center. Fig. 48 shows a facility which was equipped to acquire aerodynamic data on large-scale wing sections immersed in a simulated natural rain environment [41,42,43]

A wing section was mounted on a test vehicle and propelled along a track through a simulated rain, which was produced by a number of spray nozzles suspended above the track. The generation of rain environment in the vertical direction allows the water drops to achieve a size distribution and terminal velocities near to those found in severe rainstorms. The simulation system developed was capable to obtain rainfall conditions from 50 to 1016 mm/hr of intensity. Details of the design, development and operation of the Aircraft Landing Dynamics Facility (ALDF) at the Langley Research Center is given in references 41, 42 and 43. The (ALDF) is composed of: test carriage, a propulsion system and an arrestment system. A high pressure water jet is directed into a turning bucket located at the back end of the carriage, to provide its thrust. When the carriage attains its peak velocity it coasts to the arrestment system. The large-scale wing section is mounted above the central bay area, as shown in Fig. 49.

The wing section had an NACA 64-210 airfoil with rectangular planform mounted between circular endplates. It was equipped with leading-edge and trailing-edge high lift devices simulating a landing configuration, Fig. 50. The wing chord was 3.05 m, corresponding to an scaling factor of 4 when compared to the wind tunnel model chord. The wing span was constrained to a width of 3,96 m imposed by the location chosen. The wing surfaces were painted with commercially available aircraft paint to model a full-scale prototype properly. The angle of attack remained fixed during each launch and could be varied from 7.5° to 19.5° in 2° increments.

The ALDF Rain Simulation System (RSS) was approximately located 152 m downstream of the propulsion system, providing uniform simulated rain of approximately 9.1 m wide by 152.4 m long (Fig. 51). The system consists of three commercially manufactured irrigation pipes positioned length-wise along the track in 30.5 m sections, being supported at both ends by a structural support frame. One leg of the frame was piping which allow the flow of water to travel from the supply

system to the three irrigation pipes. Feeding off each irrigation pipe was an array of nozzles whose spacing was dependent upon the desired rainfall rate.

Most of the data obtained [44] was for a rain rate of 1016 mm/hr for angles of attack from 7.5° to 19.5°. The raindrop size to model chord ratio was 0.0009, approximating to the ratio that was tested in the wind tunnel and to meet one of the test objective which was to investigate the significance of scale effects. Aerodynamic data was also obtained for rain rates of 229 mm/hr and 483 mm/hr for angles of attack from 9.5° to 19.5°. The carriage exiting the RSS is shown in Fig. 52.

Dynamic pressure data was measured by a standard aircraft pitot static tube mounted on the forward extremity of the carriage. Also wind speed, direction, temperature and barometric pressure were systematically recorded. Because of the carriage deceleration, the air Reynolds number varied from 11 to 18 x 10^6. Time dependent data were averaged to provide a single lift coefficient for each angle of attack. As it was in the sub-scale tests, the effect of rain reduced the maximum lift coefficient and the angle of attack for stall (Fig. 53). It reflects the fact that the wing has stalled prior to 13.5° and has its maximum lift at 11.5° with reduction of lift capability of about 15 percent. Comparisons of lift coefficients, angle of stall for maximum lift, and loss of maximum lift with the wind tunnel results at equivalent rain rates, is given in Fig. 54, 55 and 56 respectively. It should be noted that, besides differences in speed and aspect ratios, that have been corrected, air Reynolds number and Weber number are different in the large scale tests when compared to the wind tunnel tests.

IV 4.3 Application of results to full scale aircrafts

Results from the large-scale testing and wind tunnel have been used to estimate the effects of heavy rain on a full scale airplane, in particular for a Boeing 437-100 [45]. The data have been integrated over the wing planform of the airplane. The aerodynamics, including the effect of the rain, were modelled as a change in lift and drag with liquid water content from the integrated dry baseline aerodynamic model, using a vortex lattice method. A sample of these results is shown in Fig 57. In Fig. 58 is shown the rain effect on the climb performance of the airplane in a landing configuration as a function of liquid water content. The reductions in performance do not present a serious hazard unless combined with another performance degradation hazard such as wind shear. In Fig. 59 are shown the results of heavy rain combined with a wind shear. The wind shear considered in this case has a maximum flow of 37 knots at an altitude of 36.6 m and a radius of 728.8 m, which represents a wind shear that has caused some aircraft accidents. The rain was modelled as an step input when the aircraft enters the 728.8 m radius. The wind shear was located at a distance of 1219.2 m from the intended landing point. The wind shear recovery modeled the Federal Aviation Administration (FAA) recommended procedure. When the wind shear is encountered, the throttles are moved to take-off power and the airplane pitched to an initial altitude of 15 degrees. The pitch altitude was limited throughout the encounter to the airplane's stick shaker angle. It is observed that the aircraft can safely recover from the shear, if the rain is not present. Increasing the rain rate decreases the safety margin and at very heavy rain rates the combined hazard rain-wind shear is not recoverable.

V. CONCLUDING REMARKS

Application of two-dimensional large-scale and wind tunnel sub-scale experimental data, has shown that normal aircraft operations for transport aircraft would not be affected by heavy rain, because most operations avoid high angle of attack maneuvers. However, when heavy rain encounters occurs during a severe low altitude wind shear, the piloting procedures recommended to counter the wind shear result in operating at higher than normal angle of attack. Analytical considerations have shown that combined effects of heavy rain and wind shear may significantly reduce the capability of an aircraft to escape the combination of both hazards.

Considerable amount of analytical and experimental work is still required to fully understand the various mechanisms involved in the lift loss and drag increase produced on an airfoil immersed in a two-component, two-phase flow. Wind tunnel tests of a complete aircraft configuration should be a top priority.

Basic airfoil analytical studies must incorporate in the existing numerical models the effects of water film dynamics including the detailed physics of: 1) Ejecta fog and water deposited due to drop impacts, 2) Film changes due to cratering, waviness, film instability and rivulet formation, 3) Water gap blockage in high-lift systems. Analytical models of these phenomena for the conditions present in airfoil heavy rain aerodynamics do not exist and data must rely on appropriate experiments. To support the data that need to be introduced into the numerical models more experiments are required. In particular in the area exploring the physics of drop impacts the existing results should be supplemented with others for different drop sizes and film thickness. Experimental techniques for the accurate determination of the characteristics defining the splash are needed. In the group of experiments for water film determination, complete measurements along the airfoil chord for different values of the parameters and different techniques should be made, including measurements of water flow across the gaps in high-lift configurations. Along with new tests, more work is required in order to generate and control the injection of drops of varying size in the wind tunnel stream, specially in the range of above 2 mm. Care is to be exercised in the spatial LWC uniformity along with the development of new and efficient techniques for its measurement.

The validation of future theoretical results will need a broad data base of aerodynamic coefficients at different values of the non-dimensional parameters. These tests are necessary to cover sensitivities to different variation mainly to LWC, and Reynolds and Weber numbers. Direct force measurements and indirect methods using surface pressure distributions will be needed. For these last measurements a new measuring technique has to be developed.

First steps at the clarification of the scaling issue have been given. For the 64-210 in the range of results from about 3 x 10^6 to 10^7, little effect of scale has been noticed. However, comparison of the large-scale with the wind tunnel tests, differ not only on the air and water Reynolds numbers but on the Weber number, via the mean drop size. The results of wind tunnel tests with water containing surface-tension reducing agent not only changes the Weber number but also the $\frac{\sigma_{w,s}}{\sigma_{a,s}}, \frac{\sigma_{a,s}}{\sigma_{w,a}}$ between both set of experiments. The most reasonable interpretation of all available results for the 64-210 airfoil rain effects is that the scale effect for the high-lift configuration is small.To rigorously reach conclusions on the scale effect, more experiments are needed where only one parameter at a time is changed, not only for this but for other airfoil types.

REFERENCES

1. Rhode, R.V. Some Effects of Rainfall on Flight of Airplanes and on Instrument Indications. NACA TN803. April 1941.

2. Haines, P. and Luers, J. Aerodynamics Penalties of Heavy Rain on Landing Airplanes. J. of Aircraft. Vol, 20, No. 2. February 1983.

3. Dunham, R. E. Jr. The Potential Influence of Rain on Airfoil Performance. Lecture presented at the Von Karman Institute for Fluid Dynamics. February 1987.

4. Dunham, D.J. ; Dunham, E. R. Jr. and Bezos, G. M. A Summary of NASA Research on Effects of Heavy Rain on Airfoils. AGARD CP-496. April 1991.

5. Marshall, J. S. and Palmer, W. McK. The Distribution of Raindrops with Size. Journal of Meteorology, Volume 5, 1948, pg. 165-166.

6. Joss, J. and Waldvogel, A. Raindrop Size Distribution and Sampling Size Errors. Journal of the Atmospheric Sciences, Vol. 3, 1969, pg. 566-569.

7. Markowitz, A.H. Raindrop Size Distribution Expressions. Journal of Applied Meteorology, Vol. 15, September 1976, pg. 1029-1030.

8. Riordan, P. Weather Extremes Around the World, Earth Sciences Laboratory TR-70-45-ES. January 1970.

9. Roys, G. and Kessler, E. Measurements by Aircraft of Condensed Water in Great Plains Thunderstorms. National Sever Storms Laboratory Publication, TN-49 NSSP-19. 1996.

10. Jones, D.M. and Sims, A.L. Climatology and Instantaneous Rainfall Rates. Journal of Applied Meteorology, Vol. 17. August 1978, pg. 1135-1140.

11. Melson, W.E., Jr. Heavy Rain Characteristics and Ground Measurement Comparisons. Presented at the WHO IAHS 8th International Workshop on Precipitation Measurement. December 1989.

12. Melson, W.E., Jr. Observation and Comparison of Rainfall Measured at High Sample Rate. Proceedings of the American Meteorology Society, 41st Annual Meeting, January 13-18, 1991. New Orleans, Lousiana.

13. Bergrun, N.R. A Method of Numerically Calculating the Area and Distribution of Water Impingement on the Leading Edge of an Airfoil. NACA TN 1397. 1947.

14. Bergrun, N.R. An Empirically Derived Basis for Calculating the Area, Rate and Distribution of Water-Drop Impingement on Airfoils. NACA Report 1107. 1952.

15. Dorsch, R.G. and Brun, R.J. A Method for Determining Cloud Droplet Impingement on Swept Wings. NACA TN 2913. 1953.

16. Morsi, S.A. and Alexander, A.J. An Investigation of Particle Trajectories in Two-Phase Flow Systems. Journal of Fluid Mechanics, vol. 56, pg. 193-208; 1972.

17. Bragg, M.B. A Similarity Analysis of the Droplet Trajectory Equation. AIAA Journal, Vol. 20 pg. 1681-1686, December 1982.

18. Haines, P.A. and Luers, J.K. Aerodynamic Penalties of Heavy Rain on Landing Aircraft. NASA CR 156885. July 1982.

19. Haines, P. and Luers, J. Aerodynamic Penalties of Heavy Rain on Landing Airplanes. Journal of Aircraft, Vol. 20, No. 2. February 1983.

20. Calarese, W. and Hankey, W.L. Numerical Analysis of Rain Effects on an Airfoil. AIAA 84-0539. January 1984.

21. Kisielewski, K. A Numerical Investigation of Rain Effects on Lift Using a Three-Dimensional Split Flux Vector. Form of Euler Equations. Master Thesis, Dpt. of Aerospace Engineeering Mississipi State University. May 1985.

22. Anderson, L.A. and Chappidi P.R.. A Study of Roughness Effects Caused by Cratering and an Estimation of the Water Film Thickness. EIES College of Engineering, University of Central Florida. July 1985.

23. Donaldson, C. du P. On the Scaling of the Effect of Heavy Rain on the Maximum Lift of Airfoils. A.R.A.P. Tech. Memo. 85-33. August 1985.

24. Donaldson, C du P. and Sullivan, R.D. The Effect of Heavy Rain on Airfoil at High Lift NASA CR 178248, 1987.

25. Bilanin, A.J.; Quackenbush, T.R and Feo, A. Feasibility of Predicting Performance Degradation of Airfoils in Heavy Rain. NACA CR 181 842. June 1989.

26. Bilanin, A.J. Scaling Laws for Testing of High-Lift Airfoils Under Heavy Rain. AIAA-85-0259. January 1985.

27. Feo, A. Rotating Arms Applied to Studies of Single Angular Drop Impacts. AIAA 87-0257. January 1987.

28. Feo, A. and Rogles F.. Single Drop Perpendicular Impact Experiments. INTA N/221/510/87.013. August 1987.

29. Feo, A. Waterdrop Splashback Characteristics of a Perpendicular Impact Near an Air Stagnation Point. INTA N/221/501/89025. September, 1989.

30. Hastings, E.C.. and Weinstein L. M. Preliminary Indications of Water Film Distribution Thickness on an Airfoil in a Water Spray. NASA TM 85796. 1984.

31. Hastings, E.C. and Manuel, G. S. Measurements of Water Film Characteristics on Airfoil Surface from Wind Tunnel Tests with Simulated Heavy Rain. AIAA 85-0259. January 1985.

32. Feo, A. and Gonzalez, P. Water Film Thickness Measurements on an Airfoil Surface in a Water Spray from NASA-Langley's 4x7 Meter Wind Tunnel Tests. INTA N/221/510/89.004. December 1988.

33. Feo, A , Rogles, F. and Urdiales M. The Measurement of Water Film Thickness in Heavy Rain Conditions Using Conductance Sensors. AGARD CP-496. April 1991.

34. Yip, L.P. Wind-Tunnel Investigation of a Full-Scale Canard-Configured General Aviation Airplane. NASA TP-2382. Marach 1985.

35. Hansman Jr., R.J. and Barsotti, M.F. The Aerodynamic Effect of Surface Wetting Characteristics on a Laminar Flow Airfoil in a Simulated Heavy Rain. AIAA 85-0260. January 1985.

36. Marchman III, J.F.; Robertson, E.A. and Emsley, H.T. Rain Effects at Low Reynolds Number, Journal of Aircraft, Vol. 24, No 9, pg 638-648. 1987.

37. Thompson, B. E, Jang J. and Dion, J. L.. Wing Performance in Moderate Rain. Journal of Aircraft , Vol 32, No 5, pg 1034-1039. September-October 1995.

38. Hernán, M. A.; Gharib, M.; Parikh, P. and Sarhoía V. Simulation and Analysis of Natural Rain in a Wind Tunnel Via Digital Image Processing Techniques JPL D-2231. Jet Propulsion Laboratory. CALTEH October 1984.

39. Bezos, G. M.; Dunham, R. E. Jr; Gentry, G. L. and Melson, W. E. Jr. Wind Tunnel Test Results of Heavy Rain Effects on Airfoil Performance. AIAA 87-0260. January 1987.

40. Tang, F. C. Experimental Investigation of Heavy Rainfall Effects on a 2-D High Lift Airfoil. AGARD CP-496. April 1991.

41. Taylor, J.T.; Moore, C.T. III; Campbell, B.A.; and Melson, W.E. Jr The Development of a Facility for Full-Scale Testing of Airfoil Performance in Simulated Rain. AIAA 88-0055. January 1988.

42. Bezos, G.M.; Campbell, B.A. and Melson, W.E., Jr. The Development of a Capability for Aerodynamic Testing of Large-Scale Wing Sections in a Simulated Natural Rain Environment. AIAA 89-0762. January 1989.

43. Campbell, B.A. Bezos, G.M.; Dunham, R.E., Jr. and Melson, W.,Jr. Operational Considerations for Aerodynamic Testing of Large-Scale Wing Sections in a Simulated Natural Rain Environment. AIAA 89-0485. January 1990.

44. Bezos, G.M.; Dunham, R.E, Jr.; Campbell, B.A. and Melson, W.E., Jr. Results of Aerodynamic Testing of Large-Scale Wing Sections in a Natural Rain Environment. AIAA 90-0486, January 1990.

45. Vicroy, D. .D The Aerodynamic Effect of Heavy Rain on Airplane Performance AIAA 90311. September 1990.

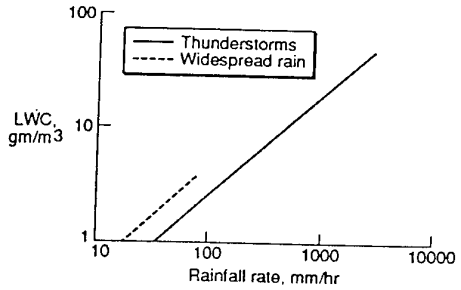

FIG. 1 LIQUID WATER CONTENT AS A FUNCTION OF RAIN RATE.

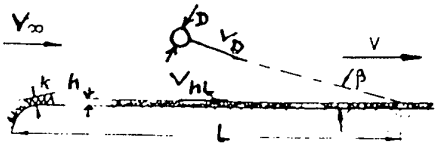

FIG. 4. SINGLE ANGULAR DROP IMPACT. INCIDENCE VARIABLES.

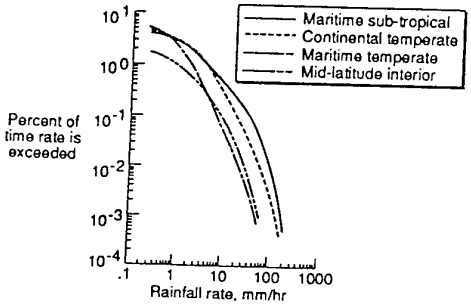

FIG. 2. CLIMATOLOGY OF INSTANTANEOUS RAIN RATES.

FIG.5. PHOTOGRAPH OF A LOW INCIDENCE SPLASH.

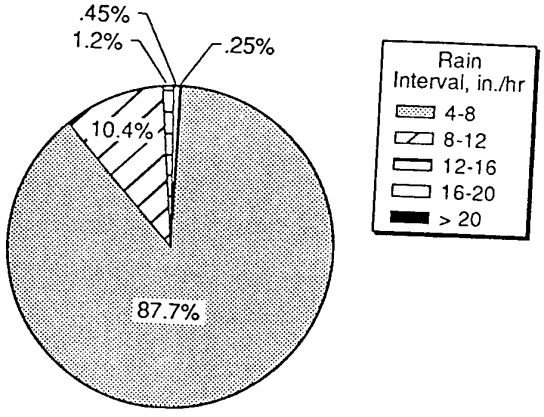

FIG. 3. DISTRI BUTIONS OF RAINFALL RATES MEASURED FOR LESS THAN 10 SECS.

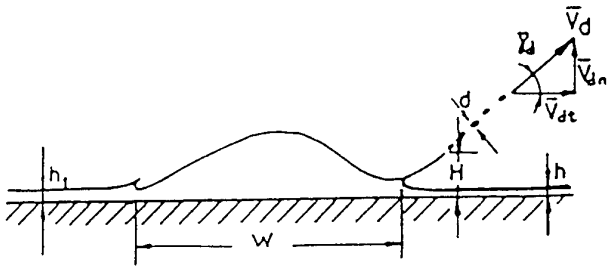

FIG. 6. SCHEMATICS OF A LOW INCIDENCE SPLASH. (DROP COALESCENCE STAGE)

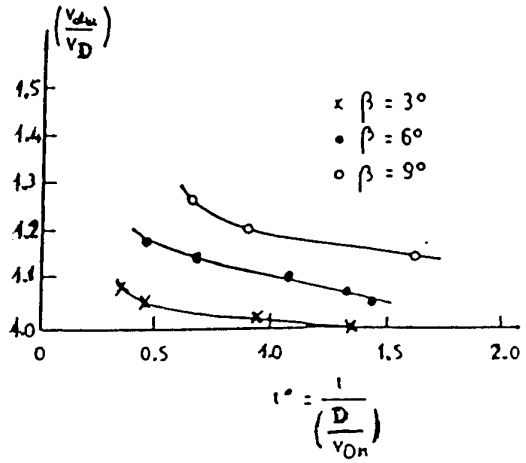

FIG. 7 LOW INCIDENCE EJECTION VELOCITIES.

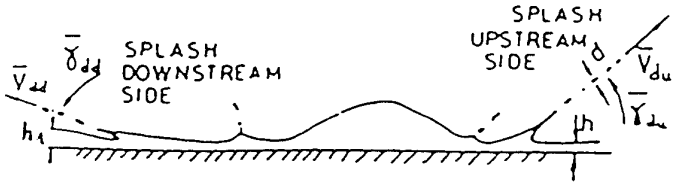

FIG. 10. SCHEMATICS OF AN INTERMEDIATE INCIDENCE SPLASH. (DROP COALESCENCE STAGE).

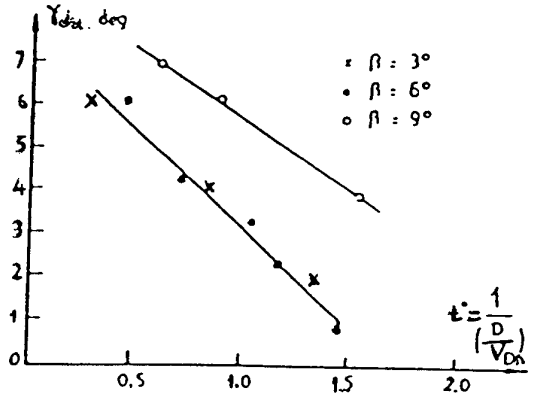

FIG. 8. LOW INCIDENCE EJECTION ANGLES

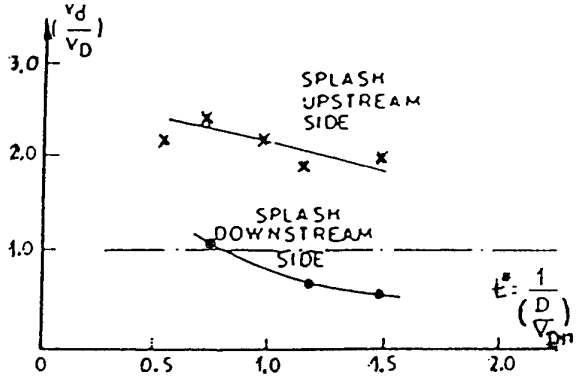

FIG.11 INTERMEDIATE INCIDENCE EJECTION VELOCITIES. $\beta=24^0$

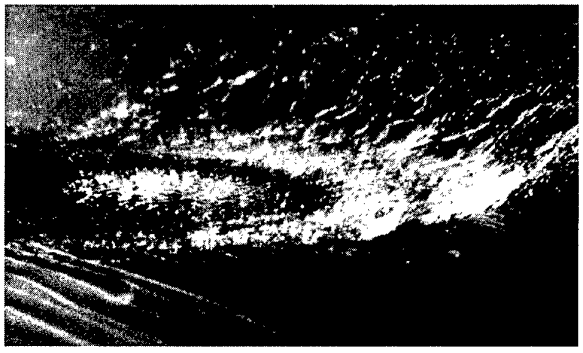

FIG. 9 PHOTOGRAPH OF AN INTERMEDIATE INCIDENCE SPLASH.

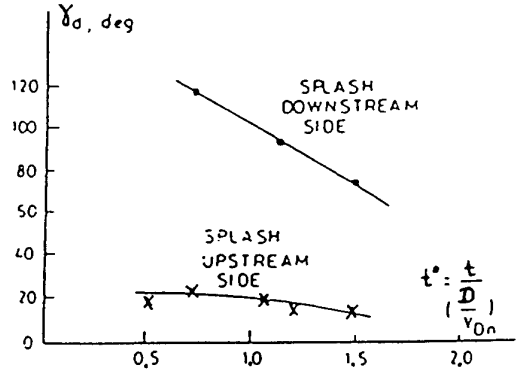

FIG. 12. INTERMEDIATE INCIDENCE EJECTION ANGLES. $\beta=24^0$

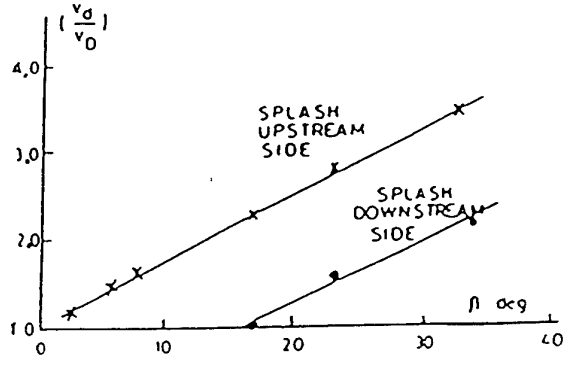

FIG. 13. INITIAL EJECTION VELOCITIES ($t \simeq 0$)

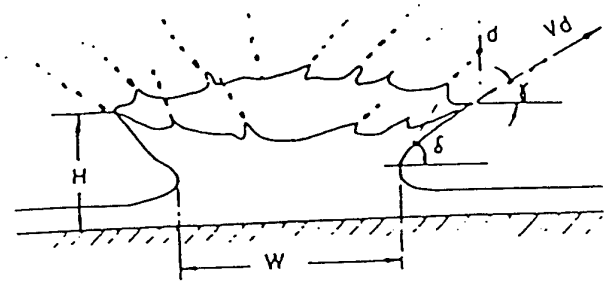

FIG. 16. SCHEMATICS OF A PERPENDICULAR IMPACT.

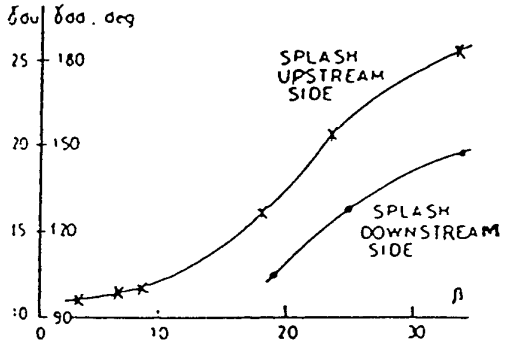

FIG.14. INITIAL EJECTION ANGLES ($t \simeq 0$)

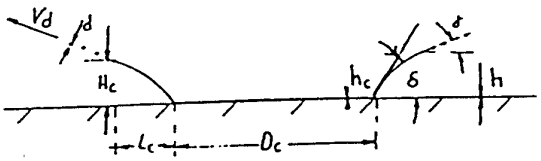

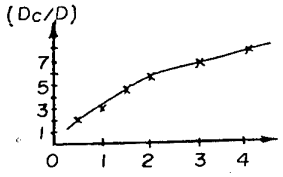

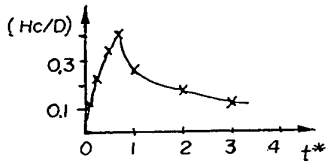

$t^* = t/(D/V_D)$

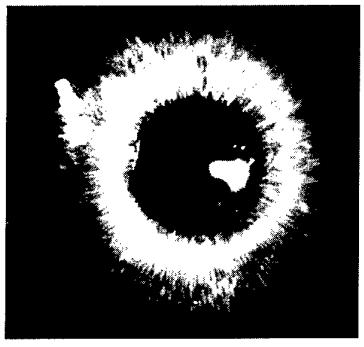

FIG. 15. PHOTOGRAPH OF A PERPENDICULAR IMPACT.

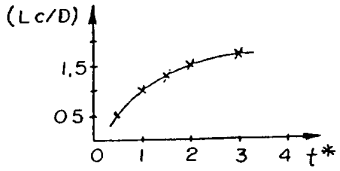

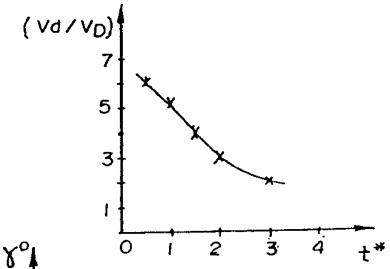

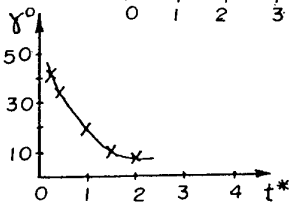

FIG. 17. SPLASHBACK CHARACTERISTICS OF A PERPENDICULAR IMPACT

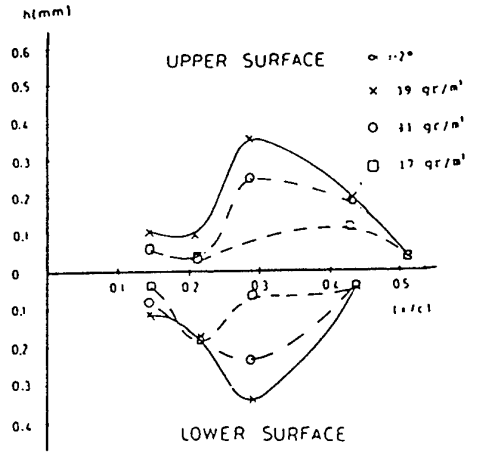

FIG. 18. EFFECT OF LWC ON FILM THICKNESS DISTRIBUTION.
CRUISE CONFIGURATION
$\alpha = -2^0$: v_∞= 48 m/s

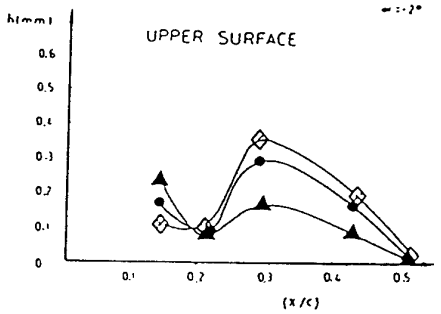

FIG. 19. EFFECT OF REYNOLDS NUMBER ON FILM THICKNESS DISTRIBUTION.
CRUISE CONFIGURATION; $\alpha = -2^0$;
LWC = 39 gr/m^3, ◊ Re=2.1x10^6
•Re= 2.8 x 10^6, ▲ Re= 3.4 x 10^6

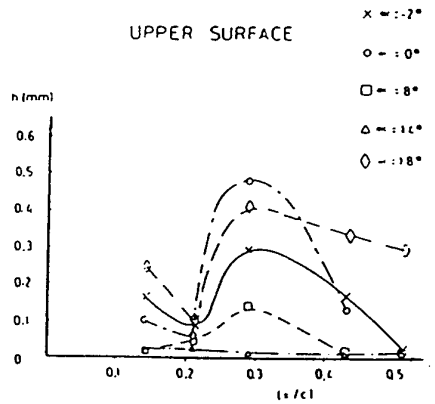

FIG. 20. EFECT OF ANGLE OF ATTACK ON FILM THICKNESS DISTRIBUTION.
CRUISE CONFIGURATION
LWC = 39 gr/ m^3 ; v_∞= 62 m/s

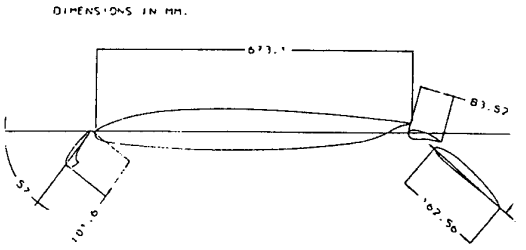

FIG. 21. AIRFOIL MODEL.
HIGH-LIFT CONFIGURATION.

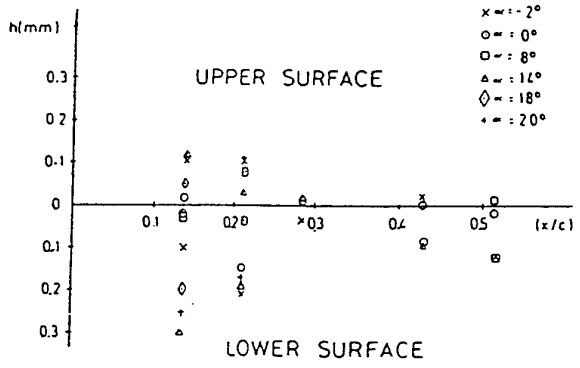

FIG. 22. EFFECT ON ANGLE OF ATTACK ON FILM THICKNESS DISTRIBUTION.
HIGH-LIFT CONFIGURATION.
LWC= 39 gr/m^3. v_∞= 48 m/s

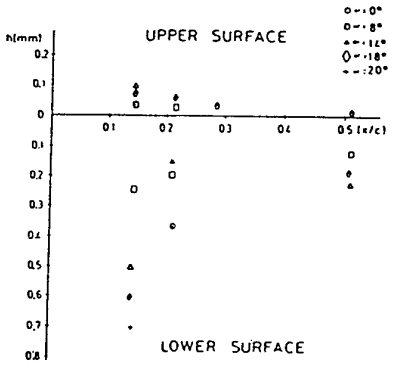

FIG. 23. EFFECT OF ANGLE OF ATTACK ON FILM THICHNESS DISTRI BUTIONS.
HIGH-LIFT CONFIGURATION
LWC= 39 gr/m^3 ; v_∞= 78 m/s

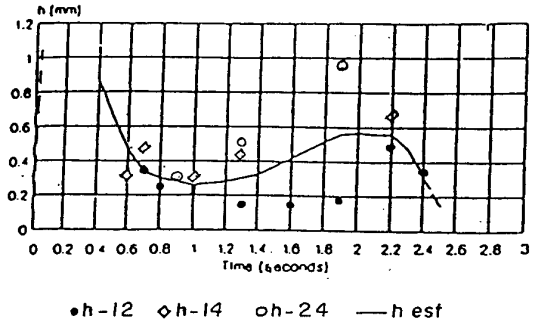

FIG. 24. UPPER SURFACE TIME-DEPENDENT FILM THICKNESS . α=13.5 ^{0}; v_∞= 82 m/s ; RR=1000 "/hr

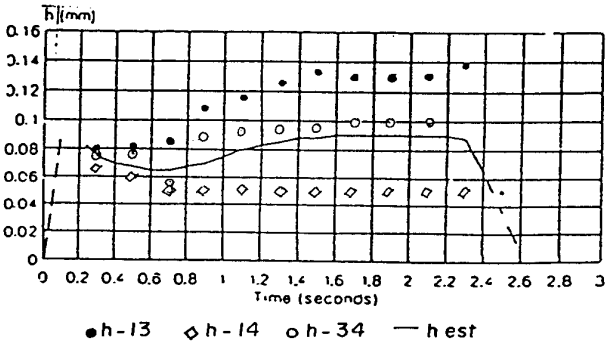

FIG. 25. LOWER SURFACE TIME-DEPENDENT FILM THICKNESS. α=13.5 ^{0}; v_∞= 82 m/s; RR=1000 "/hr

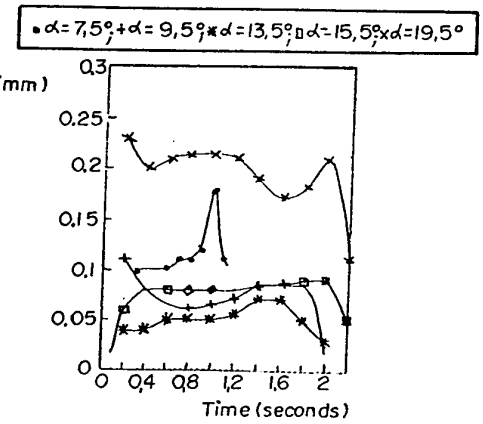

FIG. 26. LOWER SURFACE TIME-DEPENDENT FILM THICKNESS. v_∞= 82 m/s; RR=482 "/hr

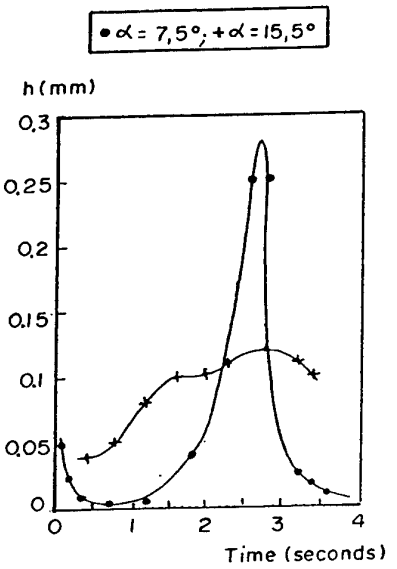

FIG. 27. LOWER SURFACE TIME-DEPENDENT FILM THICKNESS. v_∞= 52 m/s; RR = 482 "/hr

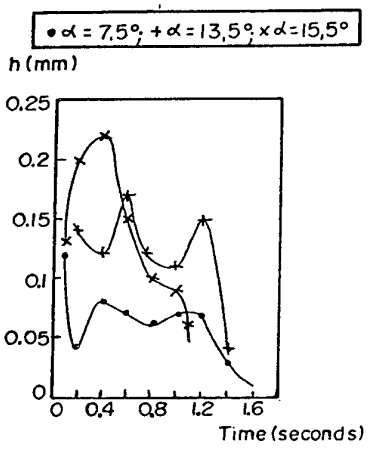

FIG. 28. UPPER SURFACE TIME-DEPENDENT FILM THICKNESS. v_∞ = 82 m/s : RR = 482 "/hr

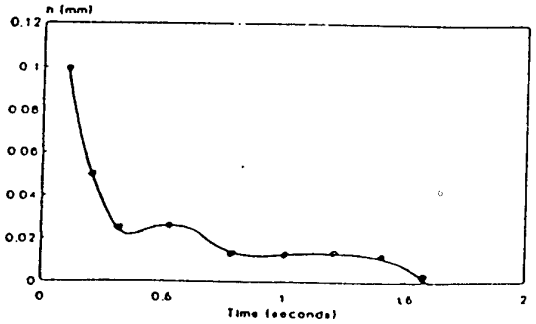

FIG. 29. UPPER SURFACE TIME-DEPENDENT FILM THICKNESS. v_∞ = 52 m/s ; RR = 482 "/hr; α=7.5^0

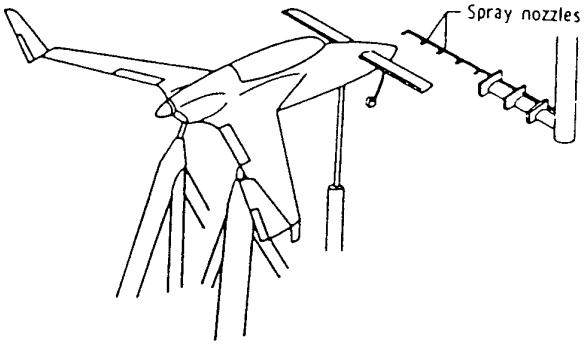

FIG. 30. SPRAY NOZZLES USED IN THE CANARD STUDY.

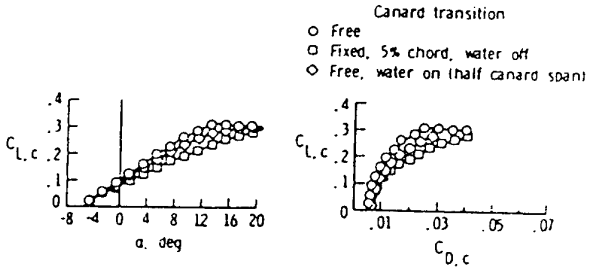

FIG. 31. CANARD TEST DATA.

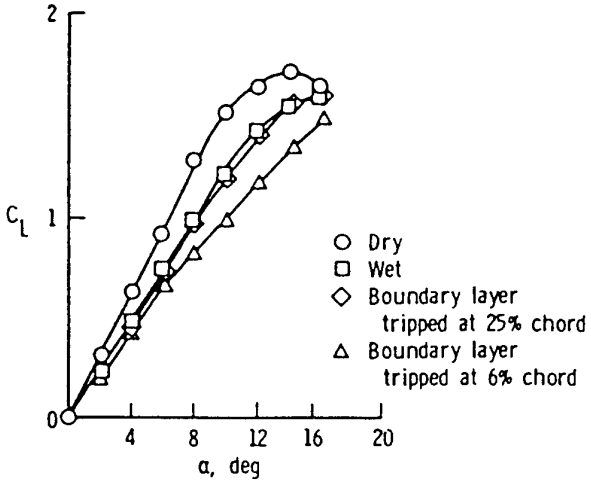

FIG. 32 WATER SPRAY EFFECTS WITH FIXED TRANSITION ON NATURAL LAMINAR FLOW AIRFOIL.

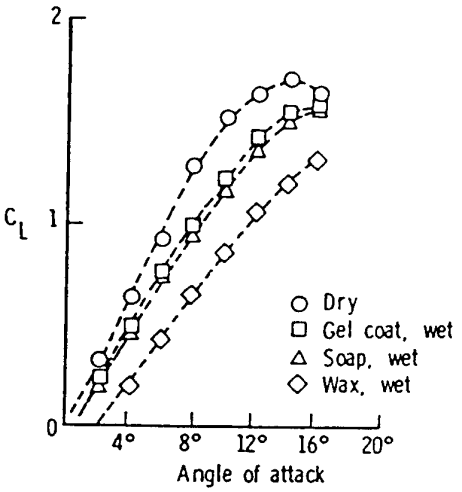

FIG. 33. EFFECT OF SURFACE WETTABILITY ON A NATURAL LAMINAR FLOW AIRFOIL.

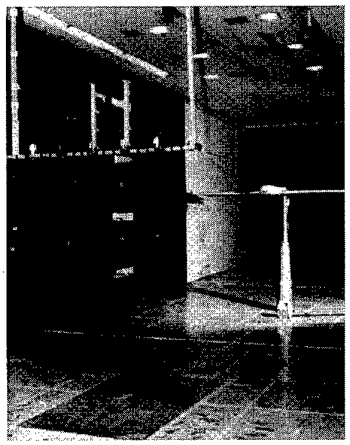

FIG. 34. RAIN SIMULATION SYSTEM IN LANGLEY 4 BY 7 METER SUBSONIC TUNNEL.

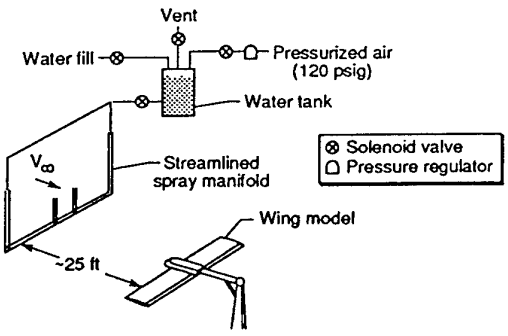

FIG. 35. SCHEMATIC OF WIND TUNNEL TEST SET-UP FOR RAIN EFFECTS STUDIES.

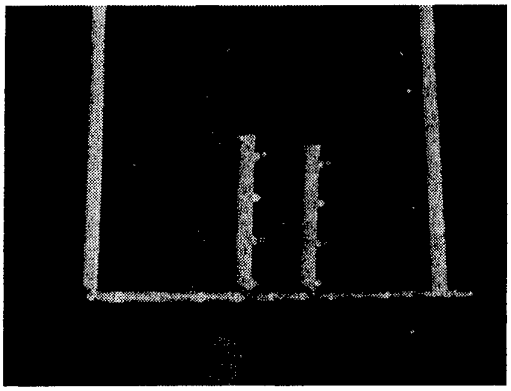

FIG. 36. WATER SPRAY MANIFOLD IN WIND TUNNEL.

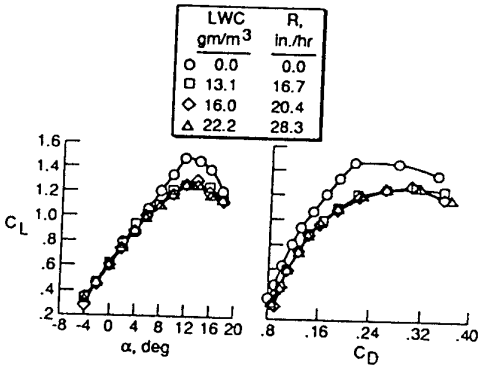

FIG. 39. RAIN EFFECT ON A NACA 0012 WING MODEL WITH 30% CHORD FLAP DEFLECTED 20^0

FIG. 37. NOZZLES USED TO VARY SPRAY CHARACTERISTICS.

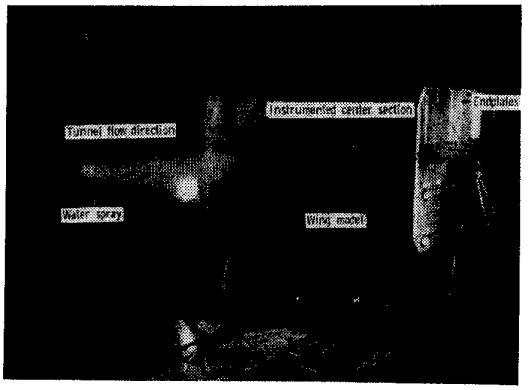

FIG. 40. PHOTOGRAPH OF NACA 64-210 AIRFOIL MODEL IN NASA LANGLEY 4x7 METER SUBSONIC TUNNEL.

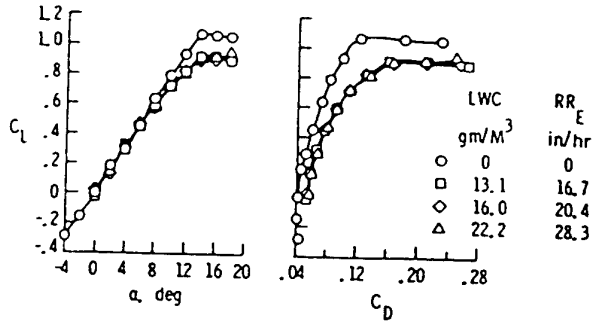

FIG. 38. RAIN EFFECT ON A NACA 0012 WING MODEL.

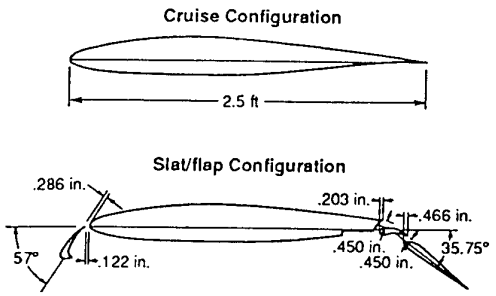

FIG. 41. CROSS SECTION OF 64-210 AIRFOIL.

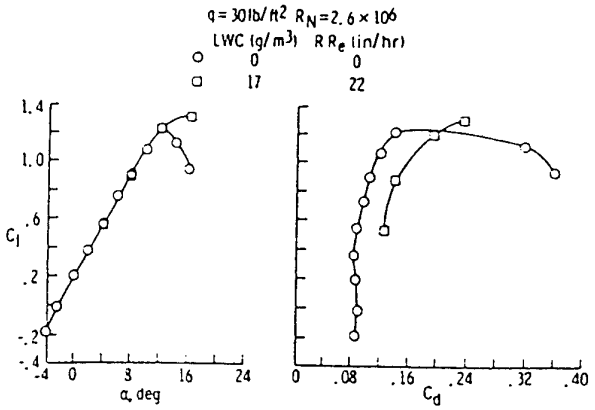

FIG. 42. WATER SPRAY EFFECTS ON LIFT AND DRAG AT DYNAMIC PRESURE OF 30 LB/FT^2 ; CRUISE CONFIGURATION

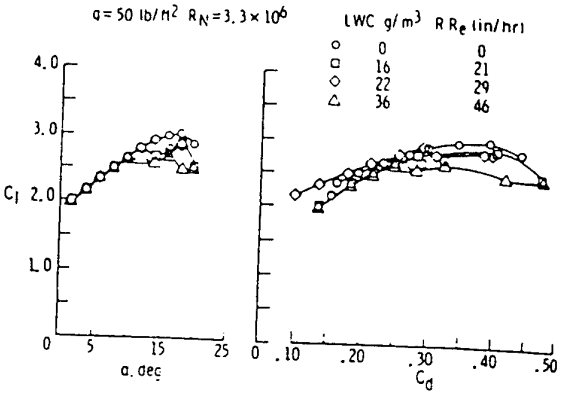

FIG. 45. WATER SPRAY EFFECTS ON LIFT AND DRAG AT DYNAMIC OF 30^{LB}/FT^2 HIGH -LIFT CONFIGURATION.

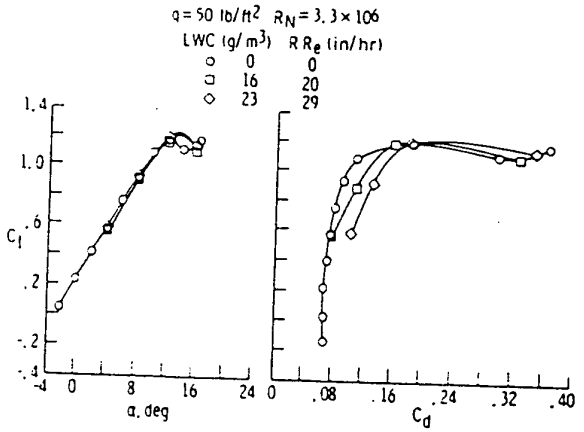

FIG. 43. WATER SPRAY EFFECTS ON LIFT AND DRAG AT DYNAMIC PRESURE 50 LB/FT^2 ; CRUISE CONFIGURATION.

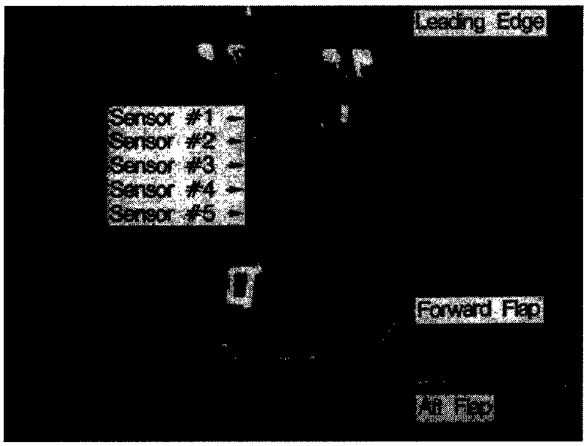

FIG. 46. WATER FILM PATTERN ON UPPER SURFACE. $\alpha = 8^0$; LWC =45 ^{g}/m^3 q_∞ =30 ^{LB}/FT^2 . HIGH -LIFT CONFIGURATION.

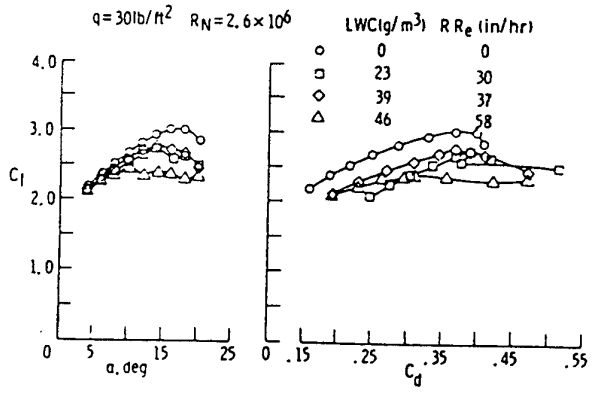

FIG. 44. WATER SPRAY EFFECTS ON LIFT AND DRAG AT DYNAMIC PRESSURE OF 30^{LB}/FT^2 . HIGH -LIFT CONFIGURATION.

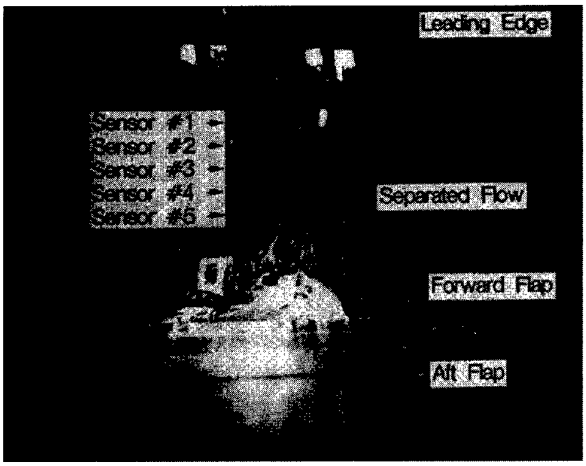

FIG. 47. WATER FILM PATTERN ON UPPER SURFACE.. $\alpha = 20^0$; LWC= 45 ^{g}/m^3; q_∞ = 30 ^{LB}/ FT^2 . HIGH-LIFT CONFIGURATION.

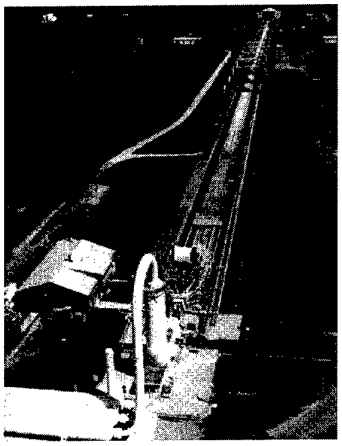

FIG. 48. PHOTOGRAPH OF AIRCRAFT. LANDING DYNAMICS FACILITY AT NASA-LANGLEY.

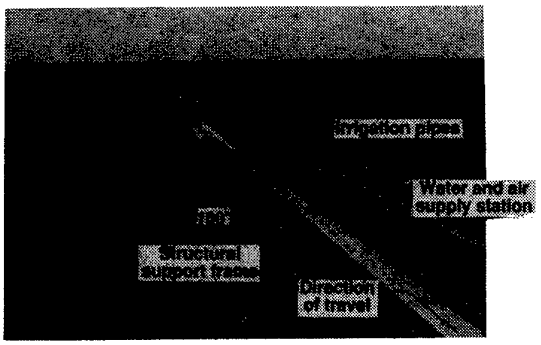

FIG. 51. VIEW OF THE ALDF RAIN SIMULATION SYSTEM.

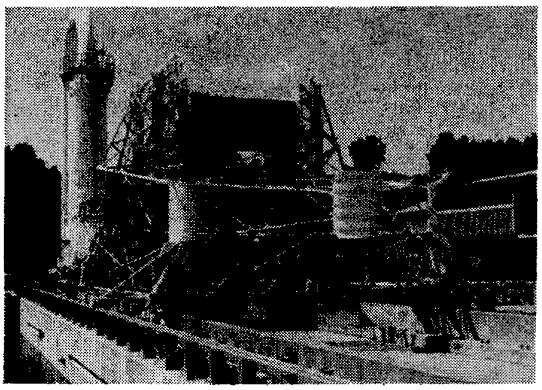

FIG. 49. PHOTOGRAPH OF WING MOUNTED ON THE ALDF CARRIAGE.

fIG. 52. PHOTOGRAPH OF CARRIAGE EXITING THE RSS.

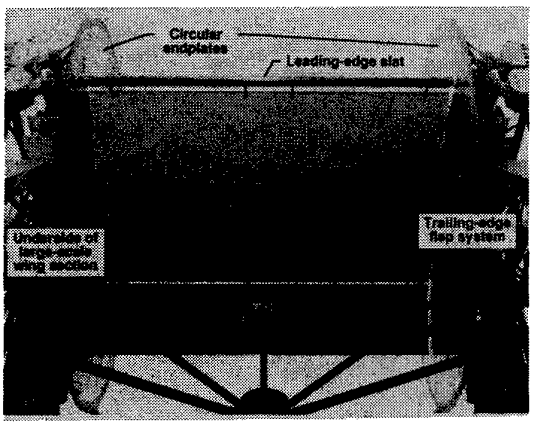

FIG. 50. UNDERSIDE VIEW OF WING AND ENDPLATES INSTALLED ON THE ALDF CARRIAGE.

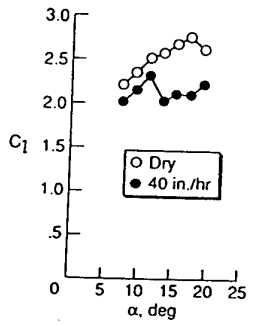

FIG. 53 SIMULATED RAIN EFFECT ON LIFT COEFFICIENT AT LARGE SCALE TESTS.

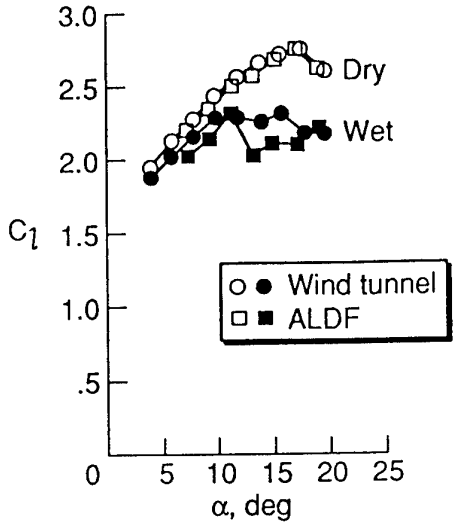

FIG. 54. LIFT COEFFICIENT COMPARISON BETWEEN WIND TUNNEL AND LARGE SCALE TESTS.

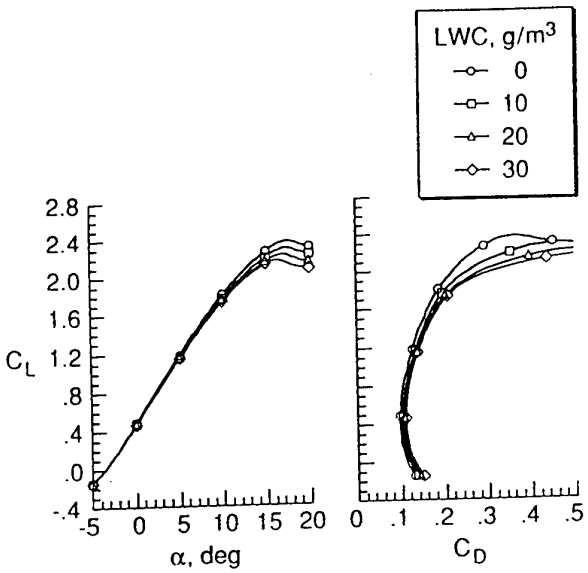

FIG. 57. MODELED RAIN EFFECT ON A BOEING 737-100 IN A LANDING CONFIGURATION (FLAPS 25^0 AND LANDING GEAR DOWN).

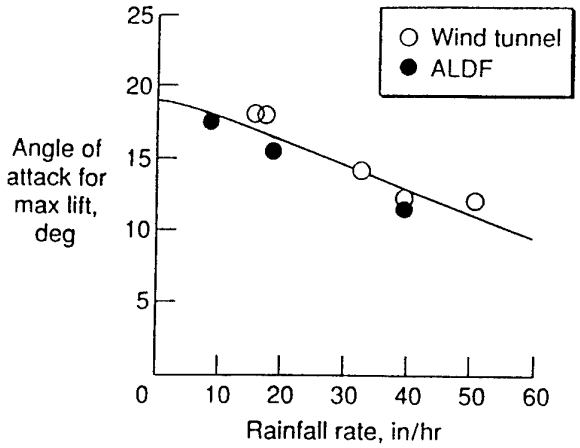

FIG. 55. EFFECT OF RAIN ON STALL ANGLE OF ATTACK.

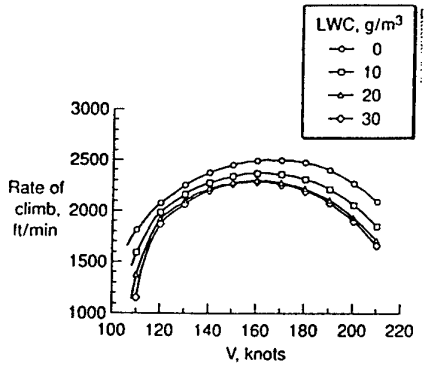

FIG. 58. EFFECT ON RAIN ON CLIMB PERFORMANCE OF A BOEING 737-100.

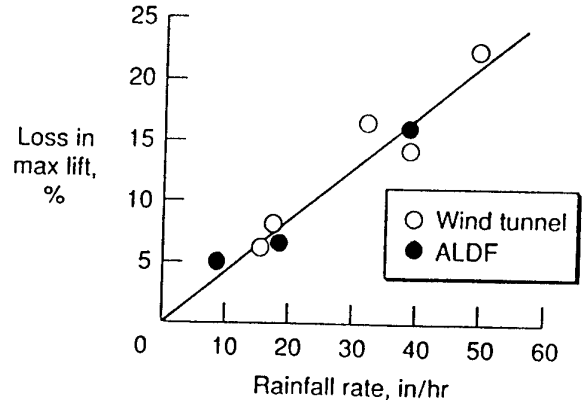

FIG. 56. EFFECT OF RAIN ON MAXIMUN LIFT.

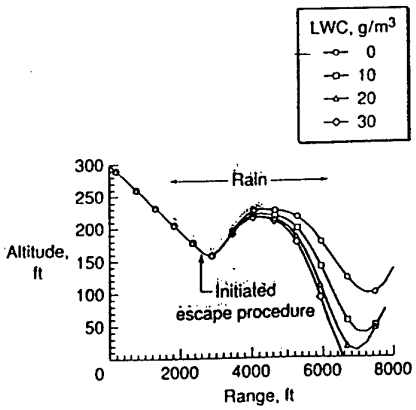

FIG. 59. EFFECT OF RAIN ON A WIND SHEAR ESCAPE PERFORMANCE OF A BOEING 737-100 IN A LANDING CONFIGURATION.

REPORT DOCUMENTATION PAGE

1. Recipient's Reference	2. Originator's Reference	3. Further Reference	4. Security Classification of Document
	AGARD-AR-344	ISBN 92-836-1067-9	UNCLASSIFIED/ UNLIMITED

5. Originator Advisory Group for Aerospace Research and Development
North Atlantic Treaty Organization
7 rue Ancelle, 92200 Neuilly-sur-Seine, France

6. Title
Ice Accretion Simulation

7. Presented at/sponsored by
The Fluid Dynamics Panel Working Group 20.

8. Author(s)/Editor(s)	9. Date
Multiple	December 1997
10. Author's/Editor's Address	**11. Pages**
Multiple	184

12. Distribution Statement There are no restrictions on the distribution of this document. Information about the availability of this and other AGARD unclassified publications is given on the back cover.

13. Keywords/Descriptors

Ice formation
Aviation safety
Ice control
Ice prevention
Flight simulation
Meteorological data
Precipitation (meteorology)
Aircraft
Performance
Degradation
Flight tests
Test facilities
Instruments
Ice forecasting
Aerodynamics

14. Abstract

The results of the AGARD FDP Working Group 20 on Ice Accretion Simulation are presented. This report covers the effect of ice accretion on wings, tail surfaces, engine inlets, and rotary wings. Experimentally, besides the capability of icing wind tunnel facilities, the problems of spray tanker aircraft experiments are considered, the related similarity laws are examined, and the techniques for measuring droplet size and distribution are reviewed. The basic factors influencing computational predictions are also discussed in detail.

AGARD

NATO OTAN

7 RUE ANCELLE • 92200 NEUILLY-SUR-SEINE

FRANCE

Télécopie 0(1)55.61.22.99 • Télex 610 176

DIFFUSION DES PUBLICATIONS

AGARD NON CLASSIFIEES

L'AGARD détient un stock limité de certaines de ses publications récentes. Celles-ci pourront éventuellement être obtenus sous forme de copie papier. Pour de plus amples renseignements concernant l'achat de ces ouvrages, adressez-vous à l'AGARD par lettre ou par télécopie à l'adresse indiquée ci-dessus. *Veuillez ne pas téléphoner.*

Des exemplaires supplémentaires peuvent parfois être obtenus auprès des centres de diffusion nationaux indiqués ci-dessous. Si vous souhaitez recevoir toutes les publications de l'AGARD, ou simplement celles qui concernent certains Panels, vous pouvez demander d'être inclus sur la liste d'envoi de l'un de ces centres.

Les publications de l'AGARD sont en vente auprès des agences de vente indiquées ci-dessous, sous forme de photocopie ou de microfiche. Certains originaux peuvent également être obtenus auprès de CASI.

CENTRES DE DIFFUSION NATIONAUX

ALLEMAGNE
Fachinformationszentrum Karlsruhe
D-76344 Eggenstein-Leopoldshafen 2

BELGIQUE
Coordonnateur AGARD-VSL
Etat-major de la Force aérienne
Quartier Reine Elisabeth
Rue d'Evere, 1140 Bruxelles

CANADA
Directeur - Gestion de l'information
(Recherche et développement) - DRDGI 3
Ministère de la Défense nationale
Ottawa, Ontario K1A 0K2

DANEMARK
Danish Defence Research Establishment
Ryvangs Allé 1
P.O. Box 2715
DK-2100 Copenhagen Ø

ESPAGNE
INTA (AGARD Publications)
Carretera de Torrejón a Ajalvir, Pk.4
28850 Torrejón de Ardoz - Madrid

ETATS-UNIS
NASA Center for AeroSpace Information (CASI)
800 Elkridge Landing Road
Linthicum Heights, MD 21090-2934

FRANCE
O.N.E.R.A. (Direction)
29, Avenue de la Division Leclerc
92322 Châtillon Cedex

GRECE
Hellenic Air Force
Air War College
Scientific and Technical Library
Dekelia Air Force Base
Dekelia, Athens TGA 1010

ISLANDE
Director of Aviation
c/o Flugrad
Reykjavik

ITALIE
Aeronautica Militare
Ufficio del Delegato Nazionale all'AGARD
Aeroporto Pratica di Mare
00040 Pomezia (Roma)

LUXEMBOURG
Voir Belgique

NORVEGE
Norwegian Defence Research Establishment
Attn: Biblioteket
P.O. Box 25
N-2007 Kjeller

PAYS-BAS
Netherlands Delegation to AGARD
National Aerospace Laboratory NLR
P.O. Box 90502
1006 BM Amsterdam

PORTUGAL
Estado Maior da Força Aérea
SDFA - Centro de Documentação
Alfragide
2700 Amadora

ROYAUME-UNI
Defence Research Information Centre
Kentigern House
65 Brown Street
Glasgow G2 8EX

TURQUIE
Millî Savunma Başkanliği (MSB)
ARGE Dairesi Başkanliği (MSB)
06650 Bakanliklar-Ankara

AGENCES DE VENTE

NASA Center for AeroSpace Information (CASI)
800 Elkridge Landing Road
Linthicum Heights, MD 21090-2934
Etats-Unis

The British Library Document Supply Division
Boston Spa, Wetherby
West Yorkshire LS23 7BQ
Royaume-Uni

Les demandes de microfiches ou de photocopies de documents AGARD (y compris les demandes faites auprès du CASI) doivent comporter la dénomination AGARD, ainsi que le numéro de série d'AGARD (par exemple AGARD-AG-315). Des informations analogues, telles que le titre et la date de publication sont souhaitables. Veuiller noter qu'il y a lieu de spécifier AGARD-R-nnn et AGARD-AR-nnn lors de la commande des rapports AGARD et des rapports consultatifs AGARD respectivement. Des références bibliographiques complètes ainsi que des résumés des publications AGARD figurent dans les journaux suivants:

Scientific and Technical Aerospace Reports (STAR)
STAR peut être consulté en ligne au localisateur de ressources uniformes (URL) suivant:
http://www.sti.nasa.gov/Pubs/star/Star.html
STAR est édité par CASI dans le cadre du programme NASA d'information scientifique et technique (STI)
STI Program Office, MS 157A
NASA Langley Research Center
Hampton, Virginia 23681-0001
Etats-Unis

Government Reports Announcements & Index (GRA&I)
publié par le National Technical Information Service
Springfield
Virginia 2216
Etats-Unis
(accessible également en mode interactif dans la base de données bibliographiques en ligne du NTIS, et sur CD-ROM)

Imprimé par le Groupe Communication Canada Inc.
(membre de la Corporation St-Joseph)
45, boul. Sacré-Cœur, Hull (Québec), Canada K1A 0S7

AGARD

NATO OTAN

7 RUE ANCELLE • 92200 NEUILLY-SUR-SEINE

FRANCE

Telefax 0(1)55.61.22.99 • Telex 610 176

DISTRIBUTION OF UNCLASSIFIED

AGARD PUBLICATIONS

AGARD holds limited quantities of some of its recent publications, and these may be available for purchase in hard copy form. For more information, write or send a telefax to the address given above. *Please do not telephone.*

Further copies are sometimes available from the National Distribution Centres listed below. If you wish to receive all AGARD publications, or just those relating to one or more specific AGARD Panels, they may be willing to include you (or your organisation) in their distribution.

AGARD publications may be purchased from the Sales Agencies listed below, in photocopy or microfiche form. Original copies of some publications may be available from CASI.

NATIONAL DISTRIBUTION CENTRES

BELGIUM
Coordonnateur AGARD — VSL
Etat-major de la Force aérienne
Quartier Reine Elisabeth
Rue d'Evere, 1140 Bruxelles

CANADA
Director Research & Development
Information Management - DRDIM 3
Dept of National Defence
Ottawa, Ontario K1A 0K2

DENMARK
Danish Defence Research Establishment
Ryvangs Allé 1
P.O. Box 2715
DK-2100 Copenhagen Ø

FRANCE
O.N.E.R.A. (Direction)
29 Avenue de la Division Leclerc
92322 Châtillon Cedex

GERMANY
Fachinformationszentrum Karlsruhe
D-76344 Eggenstein-Leopoldshafen 2

GREECE
Hellenic Air Force
Air War College
Scientific and Technical Library
Dekelia Air Force Base
Dekelia, Athens TGA 1010

ICELAND
Director of Aviation
c/o Flugrad
Reykjavik

ITALY
Aeronautica Militare
Ufficio del Delegato Nazionale all'AGARD
Aeroporto Pratica di Mare
00040 Pomezia (Roma)

LUXEMBOURG
See Belgium

NETHERLANDS
Netherlands Delegation to AGARD
National Aerospace Laboratory, NLR
P.O. Box 90502
1006 BM Amsterdam

NORWAY
Norwegian Defence Research Establishment
Attn: Biblioteket
P.O. Box 25
N-2007 Kjeller

PORTUGAL
Estado Maior da Força Aérea
SDFA - Centro de Documentação
Alfragide
2700 Amadora

SPAIN
INTA (AGARD Publications)
Carretera de Torrejón a Ajalvir, Pk.4
28850 Torrejón de Ardoz - Madrid

TURKEY
Millî Savunma Başkanliği (MSB)
ARGE Dairesi Başkanliği (MSB)
06650 Bakanliklar-Ankara

UNITED KINGDOM
Defence Research Information Centre
Kentigern House
65 Brown Street
Glasgow G2 8EX

UNITED STATES
NASA Center for AeroSpace Information (CASI)
800 Elkridge Landing Road
Linthicum Heights, MD 21090-2934

SALES AGENCIES

NASA Center for AeroSpace Information (CASI)
800 Elkridge Landing Road
Linthicum Heights, MD 21090-2934
United States

The British Library Document Supply Centre
Boston Spa, Wetherby
West Yorkshire LS23 7BQ
United Kingdom

Requests for microfiches or photocopies of AGARD documents (including requests to CASI) should include the word 'AGARD' and the AGARD serial number (for example AGARD-AG-315). Collateral information such as title and publication date is desirable. Note that AGARD Reports and Advisory Reports should be specified as AGARD-R-nnn and AGARD-AR-nnn, respectively. Full bibliographical references and abstracts of AGARD publications are given in the following journals:

Scientific and Technical Aerospace Reports (STAR)
STAR is available on-line at the following uniform resource locator:
http://www.sti.nasa.gov/Pubs/star/Star.html
STAR is published by CASI for the NASA Scientific and Technical Information (STI) Program
STI Program Office, MS 157A
NASA Langley Research Center
Hampton, Virginia 23681-0001
United States

Government Reports Announcements & Index (GRA&I)
published by the National Technical Information Service
Springfield
Virginia 22161
United States
(also available online in the NTIS Bibliographic Database or on CD-ROM)

Printed by Canada Communication Group Inc.
(A St. Joseph Corporation Company)
45 Sacré-Cœur Blvd., Hull (Québec), Canada K1A 0S7

ISBN 92-836-1067-9